
The University Of Sheffield.

# The Temporal Dynamics of Coordinated Decision-Making in Biological Systems

Ben McGovern

A thesis submitted in partial fulfilment of the requirements for the degree of Doctor of Philosophy

The University of Sheffield
School of Mathematics and Statistics

August 2016

# Abstract

Notch signalling is widely used throughout development in the determination of cell fates and maintenance of progenitors in many developmental systems.
In this thesis, nonlinear ordinary differential equation models and discrete delay differential equation models of the Notch signalling pathway are investigated mathematically to understand the dynamics of cell-fate determination.
We use linear stability analysis to find conditions for when oscillatory dynamics can be observed in bistable systems. We compare how this can be achieved for each type of model, and demonstrate how this affects the temporal dynamics of the decision-making process.
The models are then extrapolated to a larger population scale to understand how the size and geometry of the population can affect the rate at which cells can determine their fate, and the ratio of alternate cell types. We also show conditions for when stable global oscillations can exist without bistability.
Finally, we use vertex-based modelling to introduce Notch signalling into a proliferating population of cells, to demonstrate how the timescales of proliferation and cell-fate determination interact. Specifically, we show that both the rate of proliferation and the presence of oscillatory dynamics can affect the rate of differentiation, supporting results in current literature.

# Acknowledgements

Firstly, I want to say a huge thank you to my supervisor Prof. Nick Monk. His supervision, enthusiasm and patience were constant throughout this work and it would not have been possible without his support. I would also like to thank Dr. Alex Fletcher for his help and ideas for all things Chaste.
Thank you to all of my friends and family for their endless encouragement, and a special thank you to Ella Tainton for getting me to the end.

# Contents


**1 Introduction** **1**

1.1 Feedback loops and associated dynamics . . . . . 2

1.1.1 Positive Feedback . . . . . 2

1.1.2 Negative Feedback . . . . . 3

1.1.3 Using Feedback to Coordinate Population Decision-Making . . . . . 3

1.2 The Notch signalling pathway . . . . . 4

1.2.1 Role of Hes in Notch signalling . . . . . 6

1.3 Existing Models for Patterning via Lateral Inhibition and Motivation for Research . . . . . 7

1.4 Overview and Structure for Thesis . . . . . 11

1.5 Simple Mathematical Model for a Bistable Switch . . . . . 13

1.5.1 Simple Model governed by ODEs . . . . . 13

1.6 Introduction to Delay Differential Equations . . . . . 18

**2 Linear Stability Analysis for systems governed by Delta-Notch signalling 20**

2.1 Two Cells - Ordinary Differential Equations . . . . . 20

2.1.1 Linear Stability Analysis for $n$ components per cell . . . . . 20

2.1.2 Linear stability analysis of the HSS . . . . . 25

2.1.3 Examples . . . . . 30

2.1.4 Summary of ODE Results . . . . . 33

2.2 Two cells - Delay Differential Equations . . . . . 34

2.2.1 One component per cell . . . . . 35

2.2.2 Two components per cell . . . . . 39

2.2.3 Comparison between $m = 1$, $m = 2$ . . . . . 43

2.2.4 Three Components per Cell . . . . . 44

2.2.5 $m$ Components per Cell . . . . . 49

2.2.6 Summary of Results for DDEs . . . . . 52

2.2.7 Analytic Comparison of Models . . . . . 53

2.3 Linear Stability Analysis for a Lattice of Cells . . . . . 55

2.3.1 ODE analysis for $n$ components . . . . . 58

2.3.2 Examples . . . . . 61

2.3.3 Delay Differential Equation Analysis . . . . . 63

2.4 Conclusions and Discussion . . . 67

**3 Global Dynamics of Systems Governed by Lateral Inhibition 71**
3.1 Two cells governed by Ordinary Differential Equations . . . 72
3.1.1 Surface of Equivalence Dynamics . . . 77
3.1.2 Dynamics of the Full System . . . 82
3.2 Results for $n = 2$ . . . 83
3.2.1 Summary of Results . . . 107
3.3 Two cells governed by Delay Differential Equations . . . 108
3.3.1 Surface of Equivalence Dynamics . . . 110
3.3.2 Dynamics of the Full System . . . 112
3.4 Results for $m = 1$ and $m = 2$ . . . 114
3.4.1 Results when using Initial Conditions A . . . 114
3.4.2 Results when using Initial Conditions B . . . 122
3.5 Multicellular Populations . . . 134
3.5.1 Arrangements, model parameters and initial conditions . . . 135
3.5.2 Results . . . 138
3.5.3 Numerical Results for cells on a Hexagonal Array . . . 144
3.6 Discussion . . . 150
3.6.1 Summary of Results . . . 150
3.6.2 Parameter Sensitivity . . . 154
3.6.3 Conclusions . . . 155

**4 Multicellular Pattern Formation in an Adaptive Population 157**
4.1 Model Verification for Simulations Implemented in Chaste . . . 159
4.1.1 Simulation Results . . . 159
4.2 Introducing Cell Proliferation . . . 160
4.2.1 One Division per Cell . . . 161
4.2.2 Multiple Cell Divisions . . . 167
4.3 Including Differentiation for a Spatial Pattern . . . 177
4.3.1 Implementing Differentiation with Delamination . . . 185
4.4 Discussion . . . 194
4.4.1 Summary of Results . . . 194
4.4.2 Model Implementation . . . 196
4.4.3 Conclusions . . . 197

**5 Summary and Conclusions 199**

**6 References 205**

**Appendices 213**

# Chapter 1

# Introduction

For all living organisms, life begins as a single cell. Within this cell, there exists all the necessary information to develop into a functional multicellular organism. The fertilised egg first undergoes a proliferative period, where, through multiple cell divisions, the cell population grows significantly. Then, through cell specialisation and cell-cell interactions, the multitude of cells are able to establish intricate patterns of different cell-types, which form the essential structures during each stage of development [1]. It is through this coordinated cell regulation, whereby individual cells are directed to specific developmental fates at specific times, that allows for these structures and patterns to be formed. It is this tight temporal control which governs the different stages of development, allowing multiple processes to work simultaneously over a variety of time scales, to successfully build a complex multicellular organism [2].

For the successful development and maintenance of such an organism, it is vital that the corresponding cells are capable of both adaptability and robustness. In order for patterns and structures to be formed, cells must be able to adapt to perform different function, whilst remaining robust in their ability to perform such functions when faced with perturbations or conditions of uncertainty. [3] It is the interplay between these two functions which is crucial for both the development and maintenance of such an organism [4].

For example, it is crucial that during development, embryonic stem cells can adapt when necessary to take on more specific roles, which requires cells to make robust cell fate choices. Additionally, there are also high levels of robustness in the remainder of the stem cell population. This ensures that there are the correct proportion of stem and progenitor cells, allowing development to successfully continue [5,6].

In physiology, a clear example of adaptability and robustness is during wound healing. An important step of the healing process is to cover the wound with a new epithelial layer, which is achieved by cells at the edge of wound dividing and migrating to repopulate the wound bed, robust in their new cellular function [7].

## 1.1 Feedback loops and associated dynamics

In order for cells to have these characteristics, cells must be able to communicate with each other, and these interactions are governed via regulatory feedback. [8,9].

Feedback loops play a pivotal role in cell regulation. It is through the interplay of multiple feedback loops operating on different regulatory levels which drives cell diversification during development, and provides continual maintenance of the developed organism.

The concept of feedback has been around for a long time, but the idea of feedback loops in biological systems was first identified by Francois Jacob and Jacques Monod in 1961. In the simplest sense, feedback can either be positive or negative.

In a system with negative feedback, any variation in the output results in changes in the opposite direction of the variation, maintaining a stable output for the system. Conversely, in systems driven by positive feedback, any variation in the output causes this difference to be further amplified [10].

With respect to cell dynamics, negative feedback is a means of stabilisation, or homeostasis, whilst positive feedback is a tool for amplifying deviations, triggering changes to cells' states, and possibly their function [10].

Both positive and negative feedback loops can consist of any number of components. It may be a single component which regulates itself, or there may be a cascade of interactions through several components before an indirect regulation. [11].

Now, when the feedback is more complex than a single component, the overall nature of the feedback is dependent on each regulatory step [12,21].

### 1.1.1 Positive Feedback

Consider a positive feedback loop comprised of two components, A and B, where the levels of their states can either rise or fall.

Positive feedback can be achieved in two different ways. Firstly, A can activate B, and B can activate A, such that the states of A and B will either both rise, or both fall. This is known as mutual activation, or lateral induction, such that A and B are promoting one another. Examples of this are common throughout development, including the formation of the inner ear, angiogenesis and the formation of the lens [13, 14, 15, 16].

Secondly, we can have what is known as a double-negative feedback loop. It is still a positive feedback loop, in that it amplifies any deviations of the original output, but it does so via repression. For example, if A has a small increase from its original output, then this will cause B to have a small decrease. If B then represses A, A will increase further, and B will decrease further. So, where the outcome of the first case would either be both high A and B, or low A and B, a double-negative feedback loop will cause either high A and low B, or low A and high B. This is known as mutual repression, or lateral inhibition, and plays a large role in the determination of different cell types during development [9,11,22]. A key example of this behaviour is neurogenesis, [17,18] and can be found in

other situations, such as cell turnover in the gut [19], and more generally, in root epidermal patterning [20].

If there are more than two components in the feedback loop, mutual activation requires every regulatory step to be positive, whilst mutual inhibition needs an even number of negative regulatory steps.

If we have a population of cells which are initially equivalent, then lateral inhibition between neighbouring cells will amplify any discrepancies, resulting in different cell-types being formed. This is found throughout development, in a vast array of settings, and plays an important role in the partitioning of a population into alternative cell fates [21, 22, 23, 24].

### 1.1.2 Negative Feedback

Negative feedback loops can exist between any number of components, with the requirement that there are an odd number of negative regulatory functions [10].

With regard to biological systems, negative feedback is important for maintaining a state, even when confronted with environmental fluctuations [9,25].

With respect to dynamics, negative feedback relates to stabilisation, but this can come in two distinct forms. Firstly, there may be a single steady state in which the system will return to if perturbed, which is known as homeostasis. It is employed throughout the biological world as a means of keeping an equilibrium state.

An important example of a negative feedback loop is to protect cells from the uncontrolled growth and developmental aberrations that can lead to cancer, following an environmental change [26].

If there exists a negative feedback loop containing three or more components, then alternatively, this can lead to stable oscillatory dynamics.

The first model for a biological oscillator was proposed by Goodwin [27]. It was initially presented as a hypothetical genetic oscillator, in which a protein represses the transcription of its own gene via an inhibitor. This model was subsequently applied in the context of circadian clocks and somitogenesis. There have been many studies into these systems since, with many variations being formulated. [28, 29]

A nice example is the Repressilator; a synthetic biological oscillator. By using three transcriptional repressor systems, they were able to build an oscillating network in *Escherichia coli*. [30].

### 1.1.3 Using Feedback to Coordinate Population Decision-Making

The partitioning of an initially equivalent population of adaptive and robust cells requires cell-cell interactions, and a broadly used molecular mechanism for cells to communicate their fates is the Notch signalling pathway [31].

We will briefly give an overview of the Notch pathway, to highlight its key features throughout development, and how is it relevant to our study.

## 1.2 The Notch signalling pathway

The Notch pathway is an evolutionarily conserved tool used by all metazoans for controlling cell fates via local interactions [32]. It is one of a handful of highly conserved pathways, and is a universal mechanism which regulates cell fate determination, proliferation, differentiation and apoptosis, via lateral inhibition and boundary induction [31, 33].

As mentioned above, lateral inhibition is a means of partitioning a population into alternate cell-types, via juxtacrine (contact-mediated) signalling, and is considered to be controlled by Delta-Notch signalling. In populations of initially equivalent cells who are capable of becoming one of two potential cell types, usually described as primary or secondary fate, there is competition for cells to become primary fate cells, which would be generally be associated with becoming a differentiated cell. These primary fate cells then inhibit direct neighbours from taking on the same fate, resulting in a partitioning of the population, in which all primary fate cells are separated by intermediate secondary fate cells. Nice examples of this type of spatial patterning have been well studied, with one example in particular, the organisation of bristles on *Drosophila*, being a popular model of robust tissue patterning [75].

There are many examples of patterns of alternate cell types found in very different settings. These include photoreceptors in the *Drosophila* eye [76], hair and feather positioning in the epidermis of different species[77], and the sensory cells of the inner ear in vertebrates [78].

The Notch pathway is involved in many stages of embryonic development. Notch is involved in the formation of somites in vertebrates [34,35], neurogenesis [36, 37, 38], and angiogenesis [15,39], to name just a few.

Due to the simplicity of its design, and versatility in function, the Notch pathway is a heavily studied mechanism, with new insights still being discovered [31,40]. As it is known to be involved in so many developmental processes, and its function so varied, it is a continuously growing area of research, from many different areas of biological study.

During Notch signalling, a Notch transmembrane receptor interacts extracellularly by binding to its associated ligands, tethered to the membrane of neighbouring cells [31]. These interactions initiate proteolytic cleavage of the receptor, which leads to the release of the Notch intracellular domain (NICD) of the receptor. The NICD then translocates to the nucleus, where it interacts with a DNA binding protein, initiating the transcription of Notch target genes [31, 41]. The core Notch signalling pathway is illustrated in Figure 1.1.

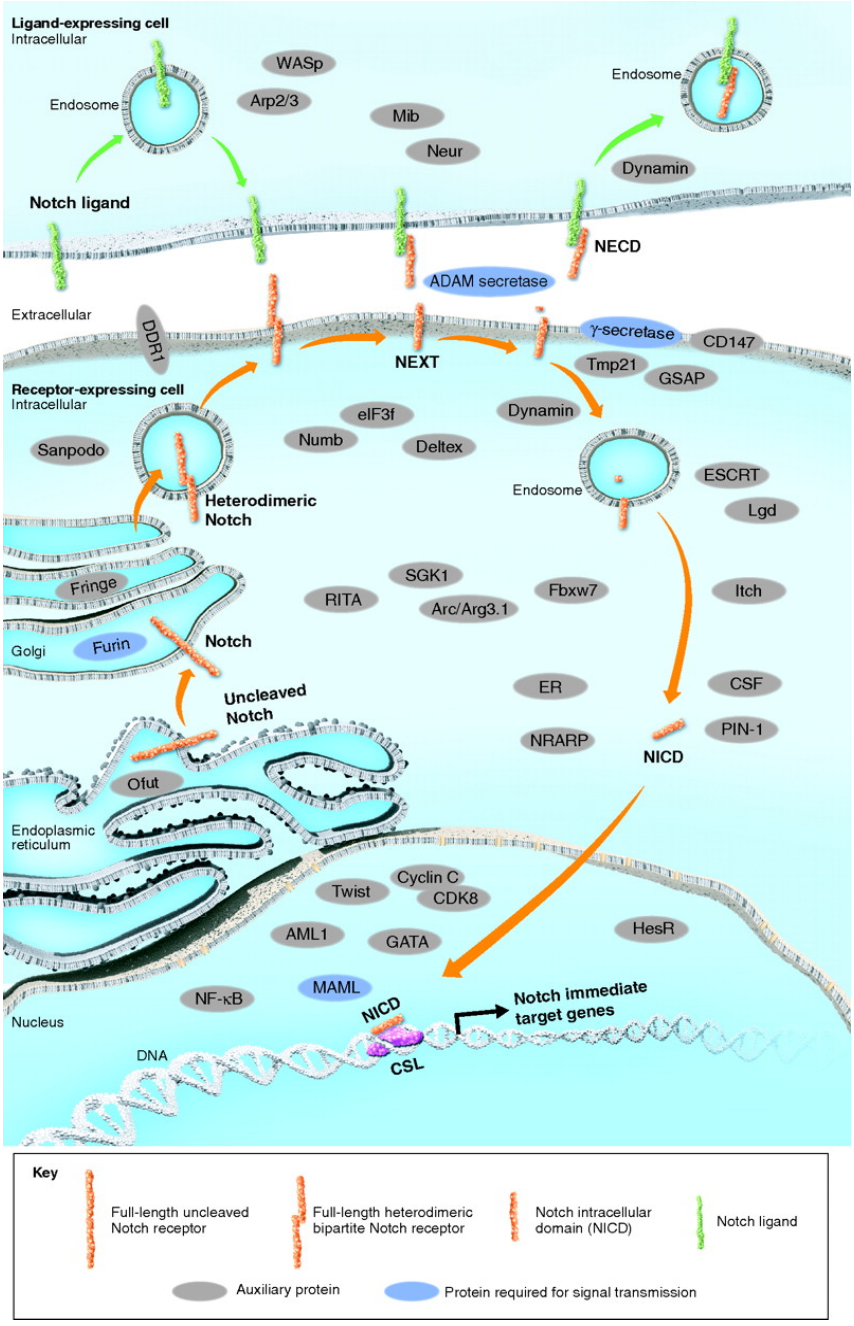


Figure 1.1: An illustration of the core Notch signalling pathway, from [31] to highlight the simplicity of the key process, but also show the underlying complexity of components that play a role in successful Notch signalling.

The Notch receptor has different canonical ligands, depending on the type of animal. In vertebrates, these ligands are Delta and Jagged. These receptor and ligand types can occur as different subtypes, or paralogs [41]. There are four paralogs of the Notch receptor, namely Notch 1-4, and six ligands, four of which are from the Delta family (Delta-like 1-4), and two from the Jagged family (Jag 1, Jag 2) [42]. In comparison, *Drosophila* has just two ligands, Delta and Serrate, the latter being homologous with Jagged.

With respect to cell-fate dynamics, it has been show that the Notch pathway can function in both lateral inhibition and lateral induction, as previously discussed in Section

1.1.1 [24]. There are even some aspects of development where Notch works by induction and then by inhibition. This is the case in the formation of the mammalian inner ear, where Notch is first used for induction to specify presensory domains, and then it is used via inhibition, to single out sensory hair cells [43,44]. Furthermore, it has also been shown that Notch signalling can undergo both synchronous and asynchronous oscillations in the cell, including somitogenesis and the maintenance of neural progenitors [36, 45,46]. A central component in these oscillatory dynamics is the Hes gene, the mammalian homolog of *Drosophila* genes *hairy* and *Enhancer of split*. We will now give a short review of the role of Hes in the Notch pathway.

### 1.2.1 Role of Hes in Notch signalling

The study of the Hes gene family has been well studied due to its biological importance, and a key area of research has been the interplay between Hes and the Notch signalling pathway. A key characteristic that has emerged from studying Hes in the Notch pathway is the associated temporal dynamics, most notably in somitogenesis.

One of the first key papers which suggested the role of Hes was published in 2000 [79], in which it was proposed that there was an element in the presomitic mesoderm [PSM] cells of zebrafish which displayed oscillatory dynamics. It was proposed that the role of Delta-Notch signalling was not to keep individual cells oscillating, but to synchronise oscillations between adjacent PSM cells. This was shown experimentally using zebrafish mutants, and did not refer to Hes specifically, but rather an oscillator in each PSM cell.

It was then proposed by Hirata *et al.* in 2002 via experiments that the oscillatory driver was the protein of the Notch effector Hes1, a basic helix-loop-helix (bHLH) factor with a 2-hour periodicity [68]. In contrast to [79], it was concluded that oscillations are cell-autonomous and depend on the negative autoregulation of hes1 transcription and a degradation of Hes1 protein. Also, because Hes1 oscillations can be seen in many cell types, it was also concluded that this was the key mechanism used to regulate the timing in many biological systems.

In 2003, two modelling papers [69,70] were published, both building on the ideas proposed in [79] and [68]. In [69], Monk presented a model representing a delayed Hes1 negative feedback loop between the hes1 gene, hes1 mRNA and Hes1 protein. He concluded that delays could have a significant impact on the dynamical behaviour of the model, specifically in the processes of somitogenesis and neurogenesis.

In [70], Lewis discussed how the oscillator governing somitogenesis in zebrafish is somehow based on Notch pathway components, and went on to show how oscillations could exist by a simple cell-autonomous, two-component negative feedback loop with a time delay. Furthermore, he was able to show numerically that if two adjacent cells were coupled using the Notch pathway, the synchronicity and stability of the oscillations could be manipulated by the balance of intercellular feedback strength and autonomous regulation.

This idea of synchronising oscillators in the segmentation clock was then beautifully demonstrated experimentally by Riedel-Kruse, Muller and Oates [80]. They analysed the synchrony dynamics of somite formation in zebrafish embryos by varying the strength and timing of Notch signalling. They were able to demonstrate that synchronous oscillations could be induced by simultaneous initiation, independent of Notch signalling, but also demonstrated that out of phase oscillations could indeed be tuned to synchrony via Notch signalling by altering the feedback, or coupling strength between adjacent cells.

This highly active field of research has been extensively reviewed in [81], and is further discussed in a Notch review paper [82].

This gives a clear link between Notch signalling and the Hes gene, but in all of these scenarios, the oscillatory dynamics have been cell-autonomous, with Delta-Notch signalling used as a tool to control synchrony. In later chapters, we explore the existence of oscillations in a model of Delta-Notch mediated lateral inhibition, with additional intracellular components between Notch and Delta. In Chapter 3, we look at models with three components per cell, namely Notch, Hes and Delta, but we are *not* looking at cells which can autonomously oscillate like the models presented in this literature. Instead, we want to explore the possible dynamics when explicitly including an intermediate step between Notch and Delta in systems of coupled cells. We have simply labelled this intermediate component Hes, and this no effect on the behaviours we observe.

## 1.3 Existing Models for Patterning via Lateral Inhibition and Motivation for Research

The first work on formulating a dynamical model for the emergence of pattern formation was proposed by Collier *et al.*, based on the Notch signalling pathway. They were able to show theoretically that different cell fates are spatially regulated via lateral inhibition, where each cell is communicating with each of its direct neighbours via a positive (double-negative) feedback loop [48,49].

They proposed a model consisting of two coupled ordinary differential equations per cell, representing the activity levels of Notch and Delta in each cell. The level of Delta activity was repressed by the level of Notch activity, and in turn, Notch was activated by the mean levels of Delta activity in the neighbouring cells.

With this simple feedback mechanism, they were able to show that for nearly equivalent cells, provided there was sufficiently strong feedback through the pathway, that any perturbations from equivalence between the cells could be amplified, resulting in a population comprised of cells with differing cell-types.

Due to the simplicity of its design, other theoretical models for lateral inhibition were proposed, focusing on different theoretical questions. There has been work which addresses the effect of including time delays in the intercellular signal [50,51], the effect

of adding noise terms [23,53,54], adding extra components into the signalling pathway [51,55], inclusion of the NICD [56], cis-inhibition, such that Notch is also regulated by the level of Delta activity in the same cell [57,58], and the effects of longer-range signalling [54].

Despite the volume and diversity of these models, there are still limitations to these models which we want to address.

In the Collier *et al.* model, only Notch and Delta are included, with no intermediate processes taken into account. In regard to the possible dynamics of the system, there is a distinct partition in parameter space which separates two distinct behaviours. On one hand, the only behaviour is homogeneity (there exists a single, stable steady state in phase space), and the other, a bistable switch (the homogeneous steady states becomes a saddle, and there exist two additional heterogeneous stable steady states).

However, from models of cyclic oscillators, such as the Represillator [30], which are governed by a negative feedback loop, if there are three or more components in the signalling pathway, stable oscillations can exist in the states of each component, as a result of a supercritical Hopf bifurcation [60].

When looking at a 2-cell system each containing two components, where the states of the cells are equivalent, the state of the system can be represented by a 2-component negative feedback loop. Hence, this suggests that by excluding any intermediate steps between Notch and Delta, this simplification restricts the dynamics the system can display. Therefore, a natural extension to the Collier model would be the inclusion of intracellular components between Notch and Delta, to explore possible new dynamics.

One numerical study by Meir *et al.* did use a more sophisticated model for lateral inhibition, in which a host of additional steps were included. But, the focus of this study was not to explore the transient dynamics of the system, but rather the different final patterns which could be achieved, and the associated parameter values [55].

The paper by Veflingstad *et al.* [50] provided an alternative method for overcoming the dynamic restrictions from only having two components per cell by including a discrete time delay in the intercellular signal between cells. The inclusion of a time delay in the governing differential equations revealed a transient competition between patterning and homogeneous oscillations, and showed that although a fine-grained pattern of alternate cell-types still eventually formed across the lattice of cells, the duration of the oscillatory behaviour increased with the time delay.

This highlighted the importance of including known delays in a model, and of studying oscillations, since their presence, depending on the specific role of the pathway, could be problematic or favourable to the decision-making ability of the system.

We saw this system further adapted by Momiji and Monk [51], who included intermediate components between Notch and Delta, namely a Hes-Her protein and a pro neural protein, of which both regulated their own activity via a negative regulatory function, and positive regulatory function, respectively. They then showed how such a system could be

simplified by using time delays as replacements for some steps in the pathway, and the resulting behaviours these models could portray.

However, despite the scope of the dynamics that were observed, only the time delay was varied. Since there is not an obvious 'equivalent' parameter to control if we were to model the full system without delays, it would be useful to have a similar study in which the time delay is not the only varied parameter, and a parameter which affects the feedback strength of a regulatory function is also varied.

It is evident that a variety of research has been carried out for this type of model, but an overall theme from these theoretical models is that the focus is on the dynamics of pattern formation on a fixed lattice of cells, and there has been very little which focuses on the temporal dynamics of patterning, or the consequences of having a temporal restriction for a patterning system. It is addressed in [22] for a simple model of a non-oscillating bistable switch, and it is discussed in [50], who acknowledge that the presence of oscillations during cell-fate determination delays the process, and if there were a temporal restriction to pattern formation, this may prove detrimental to the system's pattern forming potential. However, little else is discussed.

It was justified in Collier *et al.* [48] that the exclusion of proliferation was due to the difference in timescales between cell-fate determination and proliferation, with cell-fate determination happening much quicker. However, as we have mentioned, Veflingstad [50] demonstrates that the time to pattern can increase significantly when oscillatory dynamics are present in the states of the cells, such that there is potential for the timescales of proliferation and patterning to interact.

Since then, it has been shown experimentally that in a proliferating population of neuroepithelial cells, the balance between proliferative and differentiated cells changes when lengthening the G1 phase of the cell cycle, which can lead to premature neurogenesis [62]. Similarly, at least three laboratories have independently proposed a model whereby the length of G1 itself may control the differentiation of embryonic, neural and hematopoietic stem cells [65].

Recently, it has also been shown both experimentally and via a mathematical model, that coordinated control of Delta-Notch signalling and cell-cycle progression drives lateral inhibition-mediated tissue patterning. Specifically, they show how the balance between patterning and proliferation is crucial for the gradual formation of a pattern in which differentiated cells remain in the epithelium, and when this balance is manipulated, such that the rate of patterning quickens, this causes premature decision-making throughout the whole tissue, leading to the formation of excess differentiated cells [83].

Regarding mathematical models which involve the integration of cellular dynamics and signalling dynamics, this is a growing area of research. With advances in computational capability and resources, it is now possible to create multiscale models of complex biological systems which link cellular and subcellular components. We will briefly discuss some

of these models, specifically those which involve Notch signalling.

One recent study has extensively explored the integration of cellular behaviours, such as cell movement, proliferation and differentiation, and subcellular signalling [84]. A particular example specifically looks at the implementation of Notch signalling based on the Collier *et al.* model into a proliferating cell population. They are able to show that for each type of model, including cellular potts and vertex dynamics models, lateral inhibition successfully leads to a pattern of alternate cell-types, and in all cases, patterning capability decreases when increasing the rate of proliferation.

There has been a multi-cellular, multi-scale model for vertebrate segmentation and somite formation. A model was built which integrated a typical clock-and-wavefront model for somite formation, and submodels including the intracellular segmentation clock, intercellular segmentation clock - coupling via Delta-Notch signalling, and cell sorting [85].

This was a rigorous study in which they were able to successfully integrate previous models and present a model which addressed inconsistencies between the models, and how these could be overcome. Also, it was able to highlight the limitations of only considering behaviours at one particular biological level.

There have been several publications which have focused on multiscale modelling of intestinal crypts. In [86], a 3D model of an intestinal crypt was created which incorporated proliferation and differentiation, where cell communication was governed by Notch and Wnt signalling. They showed how cell fates were governed by Notch signalling, and how this was consistent with experimental observations.

Due to the links with carcinogenesis, there is an extensive number of intestinal crypt studies which include multiscale mathematical modelling involving Notch signalling. These have been reviewed in [87, 88].

Although not specific to the Notch pathway, there has been a publication which looks at a multiscale model of juxtacrine EGFR-MAPK signalling [89]. A multiscale computational model was developed which accounted for the emergent heterogeneity from intercellular signalling on individual cells within a population. This was done by coupling an ODE model of juxtacrine signalling and an agent-based representation of individual cells.

This showed that results obtained from a population were very different to what was expected from single-cell findings, highlighting the importance of integrated models over multiple scales for predicting behaviours of a biological system.

With continual technological and computational advances leading to new methods of studying complex biological systems, multiscale mathematical modelling of biological processes is more pivotal now that ever before, and we expect that the use of integrated models will become common practice for progression in the field.

### Motivation for Research

Based on these previous studies for lateral inhibition, to address some of the limitations which we have discussed, and extend this field of research, we propose the following questions:

1. Are oscillatory dynamics in the levels of Notch and Delta activity only possible when there exists a delay in the intercellular signal, or can such dynamics be achieved by including additional steps in the signalling pathway, without a time delay?

2. For systems which can display oscillatory dynamics during the decision-making process, how does this affect the time taken to make this decision?

3. Are the cellular dynamics in a population affected by the geometry and arrangement of the cell population?

4. In a proliferating population of cells governed by lateral inhibition, how do the timescales of proliferation and cell-fate determination interact?

## 1.4 Overview and Structure for Thesis

Now that we have discussed the biological context for the research, reviewed the existing models for pattern formation via lateral inhibition, and discussed how we will be extending this area of research, we will give an overview of what is included in the proceeding chapters, and the aim of each section of research.

Before the main body of research, we use the remainder of this introductory chapter to introduce a simplified model for pattern formation via lateral inhibition, of the form we will be focusing on in the following chapters. This allows some of the recurring results, ideas and definitions which are present throughout all of the models to be introduced immediately, avoiding repetition throughout the thesis. This section is pivotal, since results presented in the main body of research are founded on the framework presented here.

The next three chapters form the main body of research for this thesis.

Chapter 2 introduces the models we are using for cell-fate decision making via lateral inhibition. It focuses on how linear stability analysis provides conditions for when cell populations can partition into alternate cell-fates, the necessary conditions for a system to have a Hopf bifurcation, which is closely related to the existence of oscillatory dynamics, and how these conditions are affected by the geometric arrangement of the population.

The main questions we address here are:

i When can a Hopf bifurcation occur for systems governed by either ordinary differential equations or discrete delay differential equations?

ii Are bifurcation conditions dependent on the geometric arrangement of the population?

Chapter 3 looks numerically at the systems introduced in Chapter 2, exploring the global dynamics of each system. We verify the results obtained from linear stability analysis in Chapter 2 and investigate how they relate to the dynamics observed in the full system. Specifically, we look at how the temporal dynamics of decision-making are dependent on model parameters, initial conditions, population size and arrangement. Additionally, we summarise the similarities and differences observed when using either ordinary differential equations or delay differential equations to govern the systems' dynamics.

The main questions we address here are:

i What are the necessary conditions for oscillatory dynamics during the decision-making process?

ii What is the relationship between patterning time and feedback strength between neighbouring cells, and how does this relationship depend on the specifics of the model used?

iii What is the relationship between patterning time and the geometric arrangement and size of the population?

Chapter 4 looks at models for proliferating populations of cells who are governed by lateral inhibition. We use vertex models to implement Delta-Notch signalling into a population of proliferating cells to explore the interaction of timescales for cell-fate determination and proliferation. We extend the work in previous chapters to see how cell-fate determination is affected for different rates of cell division, how robust oscillatory dynamics are to cell divisions, and how the balance between different cell types is affected by the rate of cell division. By using different methods of implementation for cell differentiation, we consider the conditions needed to create and maintain the optimum balance of cell-types.

The main questions addressed here are:

i Are the behavioural dynamics observed in a static population affected by a spatially changing environment, and if so, to what extent?

ii How do the timescales of cellular signalling kinetics interact with the timescales of cell proliferation and differentiation?

Finally, Chapter 5 summarises the research presented in the thesis. We highlight the main findings from each chapter and how this work has addressed the limitations from previous studies and addressed our proposed questions. We then discuss how this work has progressed this area of research, and give ideas on how this work could be further progressed in the future.

## 1.5 Simple Mathematical Model for a Bistable Switch

The work in Chapters 2 and 3 predominantly revolves around systems of two cells, where each cell has varying numbers of internal components. Regardless of the number of components in the cells however, all components throughout the two cells are connected via a double-negative (positive) feedback loop.

As discussed, positive feedback loops with two negative interactions are the foundation for mutual inhibition, such that the two cells, both capable of reaching one of two distinct outcomes, will inhibit each other from both adopting the same outcome.

The signalling pathway which connects each of the components can be modelled using either a system of non-linear ordinary differential equations (ODEs), or, if a time delay is included, a system of non-linear discrete delay differential equations (DDEs).

In Chapter 2 we present systems with $n$ components per cell, but before we explore these, it will be beneficial to present a simple model first, since the method of analysis is similar for the models we will studying. We can then refer back to this section in the proceeding analysis, rather than present the same results multiple times.

The simplest example of such a system is where each cell has a single component, which are connected via an intercellular regulatory signal. We will formulate a simple model governed by a system of ODEs, and then in the following section we discuss how we will be analysing systems of discrete delay differential equations.

### 1.5.1 Simple Model governed by ODEs

Consider two cells each containing a single component, $A_i$, where each component is regulated by the other via a negative regulatory function. The system can be described by the set of ODEs:

$$\dot{A}_1 = -A_1 + g(A_2), \qquad \dot{A}_2 = -A_2 + g(A_1), \tag{1.5.1}$$

where $g$ is a continuous monotonic decreasing function.
A motif of this system is illustrated in Figure 1.2.

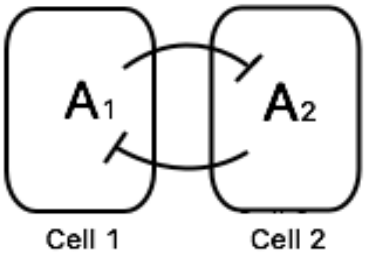


Figure 1.2: A network motif to represent the system described by (1.5.1).
$\dashv$ corresponds to a negative regulatory function.

Steady states of the system are given by:

$$(A_1^*, A_2^*),$$

where $A_1^*$ and $A_2^*$ are fixed points of $g$, with $A_1^* = g(A_2^*)$ and $A_2^* = g(A_1^*)$.

Since $g$ is a monotonic decreasing function, the following lemma can be applied.

**Lemma 1.5.1.** *If $g : [0, \infty) \to [0, \infty)$ is continuous with $g$ monotonic decreasing, then there exists $X_0 \in [0, g(0)]$ such that*

$$X_0 = g(X_0).$$

*Furthermore, $X_0$ is the only fixed point of $g$.*

Proof of Lemma 1.5.1:

*Existence:*

Let $\phi(x) = g(x) - x$, for $x \geq 0$. Since $g : [0, \infty) \to [0, \infty)$ is monotonically decreasing, $g(0) \geq 0$, and hence $g(g(0)) \leq g(0)$. Therefore

$$\phi(0) \geq 0 \geq \phi(g(0)).$$

$\phi$ is continuous on $[0, g(0)]$, so the Intermediate Value Theorem implies that there exists $X_0 \in [0, g(0)]$ such that $\phi(X_0) = 0$; i.e. $X_0 = g(X_0)$.

*Uniqueness:*

Suppose $X_0$, $\hat{X}_0$ are fixed points, with $X_0 \leq \hat{X}_0$. Then, since $g$ is decreasing,

$$X_0 = g(X_0) \geq g(\hat{X}_0) = \hat{X}_0,$$

so $X_0 = \hat{X}_0$. Thus $g$ has exactly one fixed point $X_0$.

Since $X_0 = gg(X_0)$, there is exactly one homogeneous steady state:

$$(A_1^*, A_2^*) = (X_0, X_0).$$

There may also exist one or more pairs of inhomogeneous steady states. If $(X_1, X_2)$ is a period 2 solution of the map $Z_{i+1} = g(Z_i)$, then $X_1 = g(X_2)$, $X_2 = g(X_1)$, $X_1 \neq X_2$, so this gives the pair of inhomogeneous steady states:

$$(A_1^*, A_2^*) = \begin{cases} (X_1, X_2), & \text{or} \\ (X_2, X_1). \end{cases}$$

Note that $(gg)'(X_0) = g'(g(X_0)) \cdot g(X_0) = [g'(X_0)]^2$.

**Lemma 1.5.2.** *Suppose $g : [0, \infty) \to [0, \infty)$ is continuous differentiable, with $g$ monotonic decreasing, and suppose that $X_0$ is the unique point of $g$. Then if $g'(X_0) < -1$ there exists a period 2 solution $(X_1, X_2)$ of the map $Z_{i+1} = g(Z_i)$. Furthermore, if $X_1 < X_0$ then $X_2 > X_0$.*

Proof of Lemma 1.5.2:

Suppose that $g'(X_0) < -1$. Firstly, if $X_0 = 0$ then $g(X) = 0 \ \forall X \geq 0$. Hence $g'(X) \equiv 0$, so $g'(X_0) \not< -1$. Therefore we must have $X_0 > 0$.

We wish to show that there exists $X_1 < X_0$ such that $g(g(X_1)) = X_1$. Then putting $X_2 := g(X_1)$ makes $(X_1, X_2)$ a period 2 solution of the map $Z_{i+1} = g(Z_i)$.

Let $\Psi(X) := gg(X) - X$. Then $\Psi(X_0) \geq 0$, $\Psi(X_0) = 0$, and $\Psi'(X_0) = [g'(X_0)]^2 - 1 > 0$. Since $\Psi$ is differentiable at $X_0$, there exists $\epsilon \in (0, X_0)$ such that whenever $X \in [X_0 - \epsilon, X_0)$,

$$\frac{\Psi(X_0) - \Psi(X)}{X_0 - X} - \Psi'(X_0) > -\frac{1}{2}\Psi'(X_0).$$

Hence, $-\Psi(X) > \frac{1}{2}\Psi'(X_0) \cdot (X_0 - X)$, for $X \in [X_0 - \epsilon, X_0)$. In particular, we have

$$\Psi(X_0 - \epsilon) < 0 \geq \Psi(0).$$

Therefore, the Intermediate Value Theorem tells us that there exists $X_1 \in [0, X_0)$ such that $\Psi(X_1) = 0$; i.e.

$$g(g(X_1)) = X_1,$$

as required.

Since $g$ is decreasing, $X_2 = g(X_1) \geq g(X_0) = X_0 > X_1$, and $X_2 \neq X_0$, so $X_2 > X_0 > X_1$.

## Linear Stability Analysis

We want to know the conditions for which the pair of steady states exist, as these correspond to the two distinct outcomes of the system. To find these conditions, it is standard procedure to use linear stability analysis on the homogeneous steady state, and determine when this fixed point becomes unstable.

However, before doing so we want to establish two definitions.

**Definition 1.5.1.** If we want to make a change of variables from $A_1$ and $A_2$, we define the Mean $[M]$ and Difference $[D]$ variables:

$$M \equiv \frac{A_1 + A_2}{2}, \qquad D \equiv \frac{A_1 - A_2}{2}. \tag{1.5.2}$$

We are using this change of variables as it provides an intuitive means of thinking about the system, especially with regard to how the state of the system moves away from homogeneity to a switched steady state.

**Definition 1.5.2.** For a 2-dimensional system, there exists a 1-dimensional subspace defined as the Surface of Equivalence [SoE], such that

$$SoE \equiv \left\{ \begin{bmatrix} M \\ D \end{bmatrix} \middle| \; D = 0 \right\}. \tag{1.5.3}$$

These definitions also hold for higher-dimension models, when there is more than just a single component per cell. If each cell has $n$ components $A_{i,j}$, for $i = 1, 2, \ldots, n$ and $j = 1, 2$, then

$$M_i \equiv \frac{A_{i,1} + A_{i,2}}{2}, \qquad D_i \equiv \frac{A_{i,1} - A_{i,2}}{2}, \qquad \text{for } i = 1, 2, \ldots, n. \tag{1.5.4}$$

Similarly, for this $2n$-dimensional system, there exists an $n$-dimensional subspace [SoE], where

$$SoE \equiv \left\{ \begin{bmatrix} M_1 \\ M_2 \\ \vdots \\ M_n \\ D_1 \\ D_2 \\ \vdots \\ D_n \end{bmatrix} \middle| \; D_i = 0, \; i = 1, 2, \ldots, n \right\}. \tag{1.5.5}$$

The Surface of Equivalence is the set of states in which the states of the two cells are identical. In Chapter 2 we also look at systems comprised of more than two cells. These systems also have a Surface of Equivalence subspace, but we have defined that in the corresponding section, given by Definition 2.3.1.

### Linear Stability Analysis of the HSS

Consider perturbations about the HSS for the system (1.5.1), such that $A_1 = X_0 + a_1$, $A_2 = X_0 + a_2$, and

$$g(A_1) = g(X_0) - \gamma a_1 + O(a_1^2),$$
$$g(A_2) = g(X_0) - \gamma a_2 + O(a_2^2),$$

where

$$\gamma \equiv -\frac{\partial g}{\partial A_1}\Big|_{X_0} \equiv -\frac{\partial g}{\partial A_2}\Big|_{X_0} > 0.$$

This gives the linearised system

$$\dot{a_1} = -a_1 - \gamma\, a_2, \qquad \dot{a_2} = -a_2 - \gamma\, a_1, \tag{1.5.6}$$

We can make a change of variables to the mean and difference here, where

$$m = \frac{a_1 + a_2}{2}, \qquad d = \frac{a_1 - a_2}{2},$$

which gives

$$\dot{m} = -m - \gamma\, m, \qquad \dot{d} = -d + \gamma\, d. \tag{1.5.7}$$

Since we want to know when there exists a pair of inhomogeneous steady states, which corresponds to the difference variable being able to grow, let us look at the difference equation of 1.5.7. We seek solutions of the form $d = Ce^{\lambda t}$, where $C$, $\lambda$ are constant.

Substituting this into the difference equation of 1.5.7 gives

$$\lambda C e^{\lambda t} = -C e^{\lambda t} + \gamma C e^{\lambda t}. \tag{1.5.8}$$

The condition for a non-trivial solution is therefore

$$\lambda = \gamma - 1. \tag{1.5.9}$$

Now, the HSS is stable if $\mathrm{Re}(\lambda) < 0$ and unstable if $\mathrm{Re}(\lambda) > 0$. It is clear that $\lambda \in \mathbb{R}$, and therefore, the HSS is unstable to perturbations out of the SoE when

$$\gamma > 1. \tag{1.5.10}$$

Since this parameter also corresponds to the existence of a pair of inhomogeneous steady states, the system therefore has a bifurcation at $\gamma = 1$.

This bifurcation exists in all of the models we will analyse, and it introduces bistability into the system. Since the HSS is the only steady state for $\gamma < 1$, we may refer to this bifurcation as the point at which *switching* becomes possible, i.e. When the system switches from only being able to reach homogeneity to being able to diverge away from the SoE to one of the two distinct steady states.

## 1.6 Introduction to Delay Differential Equations

Throughout this thesis we are studying the dynamics of systems governed by differential equations with the inclusion of a discrete time delay. However, the analysis for these systems is different from the analysis for systems of ordinary differential equations, so we provide a section here to explain how we will be analysing these systems.

Firstly, consider the single differential equation

$$\dot{X} = f(X(t),\ X(t-\tau)). \tag{1.6.1}$$

To generate a unique solution of (1.6.1) for $t > 0$, we must specify

$$X(t) = \Phi(t), \quad \text{for } t \in [-\tau, 0], \tag{1.6.2}$$

where $\Phi(t) : [-\tau, 0] \to \mathbb{R}$ is continuous.

It must be addressed that a delay differential equation (DDE) system has the same steady states as the corresponding ODE system, since these are time-independent. Therefore, if we were to include a discrete time delay in the equations (1.5.1), Lemma 1.5.1 and Lemma 1.5.2 would still be true. This will be used throughout the thesis, so it worth explicitly stating this result here.

### Stability of a Steady State

We will refer to the stability of steady states for systems with a delay regularly, so we want to clarify exactly what is meant when we refer to this.

Given a steady state of (1.6.1):

$$f(X^*,\ X^*) = 0.$$

If we assume $X^* = 0$ is asymptotically stable for any $\Phi(t)$, such that $\sup \Phi(t) \leq \epsilon$, then

$$X(t) \to 0 \text{ as } t \to \infty. \tag{1.6.3}$$

If $f$ is linear in both arguments, then (1.6.3) is true if and only if the roots of the characteristic equation all have negative real parts.

To determine if this is true, we must first linearise the system about the HSS, as we do for ordinary differential equations. Then, we seek solutions for the linearised system of the form

$$X(t) \sim \mathrm{e}^{\lambda t}, \quad \text{for } -\infty < t < \infty.$$

We can show that these exist if and only if $\lambda$ is a root of the characteristic equation. Note that these are transcendental equations, such that they have an infinite number of solutions.

Then, $X^*$ is asymptotically stable if and only if $\mathrm{Re}(\lambda) < 0$ for *all* roots of the characteristic equation, and therefore, if $\mathrm{Re}(\lambda) > 0$ for *any* root of the characteristic equation, then $X^*$ is unstable. This is explained in further detail in [90].

Throughout Chapter 2, in which we consider the stability of models governed by delay differential equations, we will be using this framework frequently. We know that unique solutions can only be found when specifying the history in $[-\tau, 0]$, and we are picking out one of many solutions in the proceeding analysis, but this is a negligible limitation.

To provide evidence for this claim, we have numerically solved a delay differential equation system for various forms of $\Phi(t)$, and have found that all solutions quickly tend to $X(t) \to k\mathrm{e}^{\lambda t}$ for large $t$. Simulation results are presented in Appendix A.

# Chapter 2

# Linear Stability Analysis for systems governed by Delta-Notch signalling

In this chapter we are using linear stability analysis to analyse models of dynamical systems which can be used to represent Delta-Notch mediated lateral inhibition between cells. We will be considering systems governed by ordinary differential equations [ODEs] and discrete delay differential equations [DDEs]. Before simulating these models numerically, we want to use linear stability analysis to gain insight into the certain behaviours these systems are capable of displaying.

The majority of this chapter focuses on the dynamics of a two-cell system, driven by a positive feedback loop. In Section 2.1 we analyse a $2n$-component system governed by ODEs, and show which bifurcations are possible, and how this is dependent on $n$.

In Section 2.2 we carry out similar analysis on a $2m$-component system governed by DDEs. We show when the same type of bifurcations are possible for this type of model, and give an analytic comparison between the bifurcation conditions of each model.

In Section 2.3 we move on to a larger population of cells governed by the same form of differential equations. We introduce an idea of modelling a population of cells in which we know what the final pattern of different cell-states are, allowing us to reduce the dimensionality of the system, and then show how the bifurcation conditions are affected for different arrangements and geometries of the population.

The results are summarised in Section (2.4).

## 2.1 Two Cells - Ordinary Differential Equations

### 2.1.1 Linear Stability Analysis for $n$ components per cell

Consider a system of two neighbouring cells, each containing $n$ components. The total $2n$ components are connected via a signalling pathway, with each component being regulated only by the component immediately upstream of it. The $n^{th}$ component of each cell then regulates the first component in the neighbouring cell, and the signal continues, forming

a closed cyclic network.

Such a model can be represented by the set of $2n$ ordinary differential equations:

$$\begin{aligned}
\dot{X}_{1,1} &= -\mu_1 X_{1,1} + f_1(X_{n,2}), & \dot{X}_{1,2} &= -\mu_1 X_{1,2} + f_1(X_{n,1}),\\
\dot{X}_{2,1} &= -\mu_2 X_{2,1} + f_2(X_{1,1}), & \dot{X}_{2,2} &= -\mu_2 X_{2,2} + f_2(X_{1,2}),\\
&\vdots & &\vdots\\
\dot{X}_{n,1} &= -\mu_n X_{n,1} + f_n(X_{n-1,1}), & \dot{X}_{n,2} &= -\mu_n X_{n,2} + f_n(X_{n-1,2});
\end{aligned} \tag{2.1.1}$$

where $X_{i,j}$ refers to the $i^{th}$ component in cell $j$, for $i = 1, 2, \ldots, n$, and $\mu_i$ is its associated degradation rate. The functions $f_i : [0, \infty) \to [0, \infty)$ are all continuous monotonic functions, and as discussed in Chapter 1, for the system to display inhibitory dynamics, there must be an odd number of $f_i$ which are continuous decreasing functions. Additionally, we are interested in functions which are bounded above by a finite value, to represent saturating production rates. Therefore, we can represent our model by the ODEs:

$$\begin{aligned}
\dot{X}_{1,j} &= -\mu_1 X_{1,j} + f_s(\bar{X}_{n,j}),\\
\dot{X}_{p,j} &= -\mu_p X_{p,j} + f_p(X_{p-1,j}),\\
\dot{X}_{n,j} &= -\mu_n X_{n,j} + g(X_{n-1,j});
\end{aligned} \tag{2.1.2}$$

where $\bar{X}_{n,j}$ refers to the $n^{th}$ component in the neighbouring cell and $\mu_i$ are the associated degradation rates for the $i^{th}$ component, for $i \in \{1, p, n\}$, where $p = 2, 3, \ldots, n-1$. A motif of this system is illustrated in Figure 2.1.

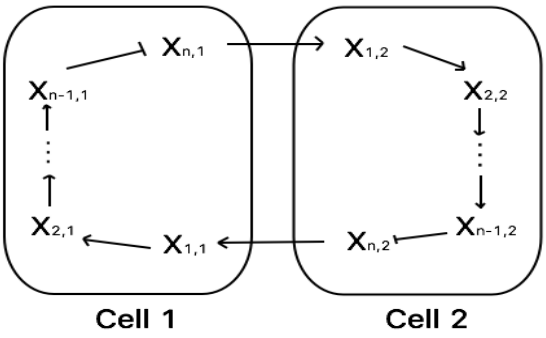


Figure 2.1: A network motif to represent the system described by (2.1.2).
→ corresponds to a positive regulatory function;
⊣ corresponds to a negative regulatory function.

The functions $f_s$, $f_p : [0, \infty) \to [0, F_{\max})$ are bounded continuous monotonic increasing functions, whilst $g : [0, \infty) \to [0, G_{\max})$ is a bounded continuous monotonic decreasing function. Examples of each are shown in Figure 2.2.

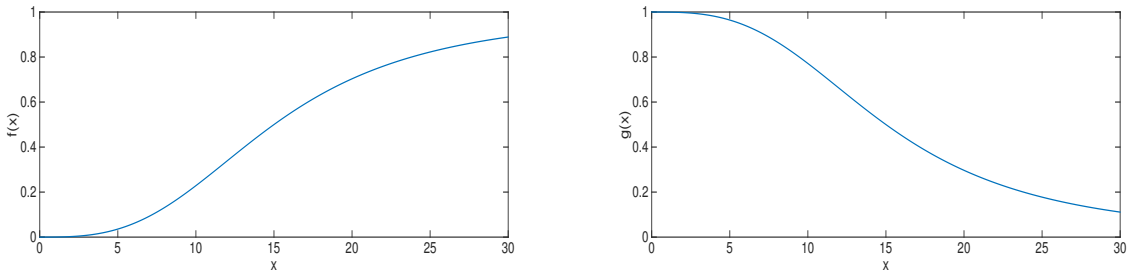


(a) (b)

Figure 2.2: Examples of positive and negative regulatory functions. (a) Increasing regulatory function $f(x) : [0, \infty) \to [0, F_{\max})$; (b) Decreasing regulatory function $g(x) : [0, \infty) \to [0, G_{\max})$.

The forms of $f_s$, $f_p$ and $g$ are unspecified, but provided they are sufficiently smooth then all results in this chapter hold, unless stated otherwise.

## Steady States and Linear Stability

Our system 2.1.1 has steady states given by

$$\underline{X}^*_{i,j} = (X^*_{1,1}, X^*_{2,1}, \ldots, X^*_{n,1}, X^*_{1,2}, X^*_{2,2}, \ldots, X^*_{n,2})$$

$$= \left( X^*_{1,1}, \frac{1}{\mu_2} f_2(X^*_{1,1}), \ldots, \frac{1}{\mu_n} g\left( \frac{1}{\mu_{n-1}} f_{n-1}\left( \ldots \left( \frac{1}{\mu_2} f_2(X^*_{1,1}) \right) \ldots \right) \right), \right. \tag{2.1.3}$$
$$\left. X^*_{1,2}, \frac{1}{\mu_2} f_2(X^*_{1,2}), \ldots, \frac{1}{\mu_n} g\left( \frac{1}{\mu_{n-1}} f_{n-1}\left( \ldots \left( \frac{1}{\mu_2} f_2(X^*_{1,2}) \right) \ldots \right) \right) \right).$$

Since all of the functions are continuous and $f_s \circ f_2 \circ \cdots \circ f_{n-1} \circ g$ is monotonic decreasing, there exists exactly one homogeneous steady state [HSS]. If we denote $X^*_i \equiv X^*_{i,j} = \bar{X}^*_{i,j}$, then the HSS can be expressed as

$$\underline{X}^*_{i,j} = (X^*_1, X^*_2, \ldots, X^*_n, X^*_1, X^*_2, \ldots, X^*_n). \tag{2.1.4}$$

As established in the simple model in Chapter 1, the HSS exists in an $n$-dimensional subspace of the full system, the Surface of Equivalence [SoE], in which $\underline{X}_{i,j} = \underline{\bar{X}}_{i,j}$. If the state of the system starts in this subspace then it will remain there, since there are no differences between the states of the two cells to amplify.

To evaluate the stability of the HSS, we can make a perturbation from this point by letting

$$X_{i,j} = X^*_i + x_{i,j}, \tag{2.1.5}$$

for $i = 1, 2, \ldots, n$, where $x_{i,j}$ are small. We then obtain the linearised system

$$\dot{\underline{x}} = A\underline{x}, \tag{2.1.6}$$

where

$$\underline{x} = \begin{pmatrix} x_{1,1} \\ x_{1,2} \\ x_{2,1} \\ x_{2,2} \\ \vdots \\ x_{n,1} \\ x_{n,2} \end{pmatrix}, \tag{2.1.7}$$

$$A = \begin{bmatrix} -\mu_1 & 0 & 0 & 0 & \dots & 0 & 0 & 0 & \phi_s \\ 0 & -\mu_1 & 0 & 0 & \dots & 0 & 0 & \phi_s & 0 \\ \phi_2 & 0 & -\mu_2 & 0 & \dots & 0 & 0 & 0 & 0 \\ 0 & \phi_2 & 0 & -\mu_2 & \dots & 0 & 0 & 0 & 0 \\ \vdots & \vdots & \vdots & \vdots & \ddots & \vdots & \vdots & \vdots & \vdots \\ \vdots & \vdots & \vdots & \vdots & \ddots & \vdots & \vdots & \vdots & \vdots \\ 0 & 0 & 0 & 0 & \dots & -\gamma & 0 & -\mu_n & 0 \\ 0 & 0 & 0 & 0 & \dots & 0 & -\gamma & 0 & -\mu_n \end{bmatrix}, \tag{2.1.8}$$

where

$$\phi_s \equiv \frac{\partial f_s}{\partial X_n}\Big|_{X_n^*} > 0, \qquad \phi_2 \equiv \frac{\partial f_2}{\partial X_2}\Big|_{X_2^*} > 0, \qquad \gamma \equiv -\frac{\partial g}{\partial X_{n-1}}\Big|_{X_{n-1}^*} > 0.$$

This is true for all values of $p$, such that

$$\phi_p \equiv \frac{\partial f_p}{\partial X_{p-1}}\Big|_{X_{p-1}^*} > 0.$$

Now, we can evaluate the full linearised version of the system in this way, but it is also possible to make a change of variables. If we let

$$M_i \equiv \frac{x_{i,1} + x_{i,2}}{2} \quad \text{and} \quad D_i \equiv \frac{x_{i,1} - x_{i,2}}{2},$$

where $M_i$ are the Mean variables and $D_i$ are the Difference variables of the linearised system (2.1.6). This then allows the $2n \times 2n$ Jacobian $A$ to be written in block-diagonal form. This can be thought of as writing the system as two uncoupled sets of $n$ linear differential equations.

The sets of linear differential equations are:

$$\dot{\underline{M}} = J_M \, \underline{M} \tag{2.1.9}$$

where

$$\underline{M} = \begin{pmatrix} M_1 \\ M_2 \\ \vdots \\ M_n \end{pmatrix}, \tag{2.1.10}$$

and

$$J_M = \begin{bmatrix} -\mu_1 & 0 & \dots & 0 & 0 & \phi_s \\ \phi_2 & -\mu_2 & \dots & 0 & 0 & 0 \\ \vdots & \vdots & \ddots & \vdots & \vdots & \vdots \\ \vdots & \vdots & \ddots & \vdots & \vdots & \vdots \\ 0 & 0 & \dots & \phi_{n-1} & -\mu_{n-1} & 0 \\ 0 & 0 & \dots & 0 & -\gamma & -\mu_n \end{bmatrix}, \tag{2.1.11}$$

and

$$\underline{\dot{D}} = J_D \, \underline{D}, \tag{2.1.12}$$

where

$$\underline{D} = \begin{pmatrix} D_1 \\ D_2 \\ \vdots \\ D_n \end{pmatrix}, \tag{2.1.13}$$

and

$$J_D = \begin{bmatrix} -\mu_1 & 0 & \dots & 0 & 0 & -\phi_s \\ \phi_2 & -\mu_2 & \dots & 0 & 0 & 0 \\ \vdots & \vdots & \ddots & \vdots & \vdots & \vdots \\ \vdots & \vdots & \ddots & \vdots & \vdots & \vdots \\ 0 & 0 & \dots & \phi_{n-1} & -\mu_{n-1} & 0 \\ 0 & 0 & \dots & 0 & -\gamma & -\mu_n \end{bmatrix}. \tag{2.1.14}$$

The associated characteristic equations of (2.1.9) and (2.1.12) are

$$|J_M - \lambda_M I| = 0, \qquad |J_D - \lambda_D I| = 0,$$

which take the form

$$(-1)^n \prod_{i=1}^{n} (\mu_i + \lambda_M) + (-1)^n \, \phi_s \gamma \prod_{p=2}^{n-1} \phi_p = 0, \tag{2.1.15}$$

and

$$(-1)^n \prod_{i=1}^{n} (\mu_i + \lambda_D) + (-1)^{n+1} \, \phi_s \gamma \prod_{p=2}^{n-1} \phi_p = 0, \tag{2.1.16}$$

respectively.

If $\mu_1 = \mu_2 = \cdots = \mu_n = \mu$, then these expressions simplify to

$$(\mu + \lambda_M)^n + \chi^n = 0, \tag{2.1.17}$$

and

$$(\mu + \lambda_D)^n - \chi^n = 0, \tag{2.1.18}$$

where

$$\chi^n \equiv \phi_s \gamma \prod_{p=2}^{n-1} \phi_p,$$

which is just the product of the gradients of the regulatory functions evaluated at the HSS.

Since this is a linear transformation $\underline{x} \to \underline{\tilde{x}}$, where

$$\underline{x} = \begin{pmatrix} x_{1,1} \\ x_{1,2} \\ x_{2,1} \\ x_{2,2} \\ \vdots \\ \vdots \\ x_{n,1} \\ x_{n,2} \end{pmatrix}, \qquad \underline{\tilde{x}} = \begin{pmatrix} M_1 \\ M_2 \\ \vdots \\ M_n \\ D_1 \\ D_2 \\ \vdots \\ D_n \end{pmatrix},$$

the eigenvalues of $J_M$ and $J_D$ are collectively the same as those of $A$. However, being able to evaluate the Mean and Difference dynamics separately is most valuable for an intuitive understanding of the global dynamics of the system.

We know that the HSS of a system changes stability as the eigenvalue $\lambda_{MAX}$ (i.e. the eigenvalue with the largest real part) crosses the Real axis. If $Re(\lambda_{MAX})$ changes from negative to positive, this signifies when the HSS changes from a stable point to an unstable saddle, and the two opposite heterogeneous steady states are created. This change in stability signifies when the feedback in the system's signalling pathway can now amplify small differences between $x_{i,j}$ and $\bar{x}_{i,j}$, resulting in the states of the cells moving away from the SoE to one of the heterogeneous steady states.

### 2.1.2 Linear stability analysis of the HSS

To assess the changes in stability the system can undertake, we will look at the linear systems for the Mean and Difference variables individually. The bifurcation conditions will be expressed in terms of $\chi$ where possible. As $\chi$ is the geometric mean of the gradients of the regulatory functions at the HSS, $\chi$ can be modulated using any of the parameters in the regulatory functions, which allows for the following conditions to be achieved in a multitude of ways.

Since we are interested in how the two cells become different when starting nearly equivalent, let us first evaluate the eigenvalues for the linear system of the Difference

variables (2.1.12). The associated characteristic equation is given by (2.1.16), which we can express as

$$\prod_{j=1}^{n}(\mu_j + \lambda_D) = \chi^n, \qquad \mu_j,\ \chi^n \in \mathbb{R}^+. \tag{2.1.19}$$

Let

$$P(\lambda_D) = (\mu_1 + \lambda_D)(\mu_2 + \lambda_D)\dots(\mu_n + \lambda_D), \tag{2.1.20}$$

such that $P(\lambda_D) = \chi^n$.

- If $\chi^n > \prod_{j=1}^{n} \mu_j$, there exists a solution $\lambda$ of $P(\lambda_D)$, such that $\lambda \in \mathbb{R}^+$.

Consider $\lambda$ is a solution of $P(\lambda_D) = \chi^n$, where $\lambda \in \mathbb{R}$, and $P(\lambda)$ is continuous. Since $P(0) = \prod_{j=1}^{n} \mu_j$, this implies

$$P(\lambda) \in \mathbb{R}^+;$$
$$P'(\lambda) \in \mathbb{R}^+;$$
$$P(\lambda) \to \infty \text{ as } \lambda \to \infty.$$

Therefore, $P(\lambda) > \prod_{j=1}^{n} \mu_j$ for $\lambda > 0$, and so, if

$$\prod_{j=1}^{n} \mu_j < \chi^n < \infty,$$

$\exists \lambda \in \mathbb{R}^+$, such that $P(\lambda) = \chi^n$.

- If $\chi^n < \prod_{j=1}^{n} \mu_j$, then $P(\lambda_D) = \chi^n$ only has solutions $\lambda$ with $\mathrm{Re}(\lambda) < 0$, $\lambda \in \mathbb{C}$.

Let $\mu_j + \lambda_D = r_j e^{i\theta_j}$, where $r_j \in \mathbb{R}^+$, $\theta_j \in [0, 2\pi)$, for $j = 1, 2, \dots, n$. Then

$$\lambda_D = -\mu_j + r_j e^{i\theta_j}. \tag{2.1.21}$$

For $\mathrm{Re}(\lambda) > 0$, it is necessary that $r_j > \mu_j\ \forall j$, and therefore,

$$\prod_{j=1}^{n} r_j > \prod_{j=1}^{n} \mu_j. \tag{2.1.22}$$

Now,

$$P(\lambda_D) = \prod_{j=1}^{n} r_j e^{i\sum_{j=1}^{n}\theta_j} = \chi^n. \tag{2.1.23}$$

Equating real and imaginary terms, this tells us

$$\prod_{j=1}^{n} r_j = \chi^n, \qquad \sum_{j=1}^{n} \theta_j = 2k\pi \quad \text{for } k = 0, 1, 2, \dots, n-1. \tag{2.1.24}$$

But $\mathrm{Re}(\lambda) > 0$ only if $\prod_{j=1}^{n} r_j > \prod_{j=1}^{n} \mu_j$, and therefore, if $\chi^n < \prod_{j=1}^{n} \mu_j$, there cannot be solutions with $\mathrm{Re}(\lambda) > 0$.

Hence, if $\chi^n > \prod_{j=1}^{n} \mu_j$, $\exists\ \lambda \in \mathbb{R}^+$ such that $P(\lambda) = \chi^n$, and if $\chi^n < \prod_{j=1}^{n} \mu_j$, $\exists \lambda \in \mathbb{C}$, $\mathrm{Re}(\lambda) < 0$ such that $P(\lambda) = \chi^n$.

Therefore, the system will undergo a bifurcation when $\chi^n = \prod_{j=1}^{n} \mu_j$, and the HSS becomes unstable to perturbations out of the SoE if

$$\chi > \sqrt[n]{\prod_{j=1}^{n} \mu_j} \qquad \forall\ n. \tag{2.1.25}$$

The eigenvalues of the Jacobian of the Mean variables (2.1.11) can be similarly expressed. The characteristic equation, (2.1.15) can be written in the form

$$\prod_{j=1}^{n} (\mu_j + \lambda_M) = -\chi^n.$$

Again, let

$$P(\lambda_M) = (\mu_1 + \lambda_M)(\mu_2 + \lambda_M) \dots (\mu_n + \lambda_M), \tag{2.1.26}$$

and

$$\mu_j + \lambda_M = r_j e^{i\theta_j}, \tag{2.1.27}$$

where $r_j \in \mathbb{R}^+$, $\theta_j \in [0, 2\pi)$, for $j = 1, 2, \dots, n$.

Therefore,

$$P(\lambda_M) = \prod_{j=1}^{n} r_j e^{i \sum_{j=1}^{n} \theta_j} = \chi^n e^{i(\pi + 2k\pi)}, \quad \text{for } k = 0, 1, 2, \dots, n-1. \tag{2.1.28}$$

Hence,

$$\prod_{j=1}^{n} r_j = \chi^n, \qquad \sum_{j=1}^{n} \theta_j = \pi + 2k\pi \quad \text{for } k = 0, 1, 2, \dots, n-1.$$

From the previous case for $\lambda_D$ we know there are no solutions $\lambda_M \in \mathbb{R}^+$, so is it possible to have a pure imaginary solution?

Let us assume this is true, and $\lambda_M = i\omega$, $\omega \in \mathbb{R}$. We now have

$$(\mu_1 + i\omega)(\mu_2 + i\omega) \dots (\mu_n + i\omega) = -\chi^n,$$

where

$$\mu_j + i\omega = r_j e^{i\theta_j}.$$

We now want to equate moduli and arguments.

Equating moduli:

$$r_j = \sqrt{\mu_j^2 + \omega^2}\ , \text{and}\ \prod_{j=1}^{n} r_j = \chi^n,$$

and so,

$$(\mu_1^2 + \omega^2)(\mu_2^2 + \omega^2)\ldots(\mu_n^2 + \omega^2) = \chi^{2n}.$$

Therefore,

$$\prod_{j=1}^{n} \mu_j^2 \leq \chi^{2n},$$

with equality when $\omega = 0$.

So, if $\omega \neq 0$, $\lambda_M = i\omega$, and $\chi^n > \prod_{j=1}^{n} \mu_j$.

Hence, a necessary conditions for the existence of a pure imaginary solution is

$$\chi > \sqrt[n]{\prod_{j=1}^{n} \mu_j} \qquad \forall\ n. \tag{2.1.29}$$

Equating arguments:

$$\sum_{j=1}^{n} \theta_j = \pi + 2k\pi\ , \qquad \text{for } k = 0, 1, 2, \ldots, n-1,$$

but

$$\begin{aligned} \theta_j = \text{Arg}(\mu_j + \lambda_M) &= \text{Arg}(\mu_j + i\omega), \qquad \text{if } \lambda_M = i\omega \\ &= \tan^{-1}\left(\frac{\omega}{\mu_j}\right). \end{aligned}$$

$$\therefore \sum_{j=1}^{n} \tan^{-1}\left(\frac{\omega}{\mu_j}\right) = \pi + 2k\pi \quad \text{for } k = 0, 1, 2, \ldots, n-1$$

As $\omega$ is an increasing function of $\chi$ and $\tan^{-1}(\omega/\mu_j)$ is an increasing function of $\omega$, then $\tan^{-1}(\omega/\mu_j)$ is an increasing function of $\chi$, assuming $\omega > 0$.

Therefore, $\lambda_M = i\omega$ occurs for the lowest value of $\chi$, and there exists a purely imaginary solution when

$$\sum_{j=1}^{n} \tan^{-1}\left(\frac{\omega}{\mu_j}\right) = \pi. \tag{2.1.30}$$

**Bifurcation conditions when $\mu_j = \mu \ \forall j$**

If $\mu_j = \mu \ \forall j$, then these conditions become simplified.

For the condition obtained from evaluating the Difference variables (2.1.25), the system will now go through a bifurcation when $\chi = \mu$, and the HSS becomes unstable to perturbations out of the SoE if

$$\chi > \mu. \tag{2.1.31}$$

For the conditions from evaluating the Mean variables, it is simpler to start from (2.1.17),

$$(\mu + \lambda_M)^n = -\chi^n.$$

Rearranging with respect to $\lambda_M$:

$$\begin{aligned} \lambda_M &= -\mu + (-1)^{1/n}\chi \\ &= -\mu + \mathrm{e}^{\frac{\pi i + 2k\pi i}{n}}\chi, \quad = -\mu + \chi\left(\cos\left(\frac{\pi + 2k\pi}{n}\right) + i\sin\left(\frac{\pi + 2k\pi}{n}\right)\right), \end{aligned} \tag{2.1.32}$$

for $k = 0, 1, \ldots, n-1$.

The eigenvalues with the largest real part are when $k = 0$ and $k = n-1$;

$$\lambda_M = -\mu + \chi\cos\left(\frac{\pi}{n}\right) \pm i\chi\sin\left(\frac{\pi}{n}\right), \tag{2.1.33}$$

$$\implies Re(\lambda_M) = -\mu + \chi\cos\left(\frac{\pi}{n}\right).$$

This tells us that the system will undergo a Hopf bifurcation when $\lambda_M = i\omega$, which is met when

$$\chi = \frac{\mu}{\cos(\frac{\pi}{n})}. \tag{2.1.34}$$

It is important to note that this is only possible when $n > 2$, since

$$\cos(\pi) = -1, \qquad \text{and} \qquad \cos\left(\frac{\pi}{2}\right) = 0,$$

making it impossible for $\mathrm{Re}(\lambda_M) \geq 0$.

Furthermore, if the Difference variables equal zero, the state of the system lies in the SoE, with the eigenvalues of the Mean variables determining the dynamics. This tells us that when the system undergoes a Hopf bifurcation it causes the HSS to change from a stable spiral to an unstable spiral surrounded by a stable periodic orbit within the SoE. The imaginary parts of $\lambda_M$ provide the angular frequency $\omega$ at which trajectories are spiralling towards, or away from, the HSS.

So, evaluating the imaginary part of $\lambda_M$ at a Hopf bifurcation, we obtain the angular frequency of the stable periodic orbit surrounding the HSS, from which we can easily

obtain the period of oscillation $T$ for the variables of the cells, since they are simply connected by

$$\omega = \frac{2\pi}{T}.$$

Therefore, this analysis tells us not only when a Hopf bifurcation will happen, but allows us to calculate the frequency and period of the resulting oscillations.

Hence, for a system of two cells each containing $n$ components ($n > 2$), a Hopf bifurcation occurs when

$$\chi = \frac{\mu}{\cos(\frac{\pi}{n})}, \tag{2.1.35}$$

generating a stable periodic orbit in the SoE with angular frequency

$$\omega = \chi \sin\left(\frac{\pi}{n}\right) = \mu \tan\left(\frac{\pi}{n}\right), \tag{2.1.36}$$

and period of oscillation

$$T = \frac{2\pi}{\omega} = \frac{2\pi}{\mu} \cot\left(\frac{\pi}{n}\right). \tag{2.1.37}$$

### 2.1.3 Examples

$\underline{n = 2}$

When $n = 2$ we have the set of ODEs:

$$\begin{aligned} \dot{X}_{1,j} &= -\mu_1 X_{1,j} + f_s(\bar{X}_{2,j}) \\ \dot{X}_{2,j} &= -\mu_2 X_{2,j} + g(X_{1,j}), \qquad j = 1, 2. \end{aligned} \tag{2.1.38}$$

Linearising about the HSS gives the linearised system

$$\begin{aligned} \dot{x}_{1,j} &= -\mu_1 x_{1,j} + \phi_s \bar{x}_{2,j} \\ \dot{x}_{2,j} &= -\mu_2 x_{2,j} - \gamma x_{1,j}, \qquad j = 1, 2. \end{aligned} \tag{2.1.39}$$

Making the linear transformation to Mean and Difference variables, we have the uncoupled linear systems

$$\begin{aligned} \dot{M}_1 &= -\mu_1 M_1 + \phi_s M_2, & \dot{D}_1 &= -\mu_1 D_1 - \phi_s D_2, \\ \dot{M}_2 &= -\mu_2 M_2 - \gamma M_1, & \dot{D}_2 &= -\mu_2 D_2 - \gamma D_1, \end{aligned} \tag{2.1.40}$$

which have corresponding Jacobian matrices

$$J_M = \begin{bmatrix} -\mu_1 & \phi_s \\ -\gamma & -\mu_2 \end{bmatrix}, \qquad J_D = \begin{bmatrix} -\mu_1 & -\phi_s \\ -\gamma & -\mu_2 \end{bmatrix}. \tag{2.1.41}$$

The characteristic equation for $J_M$, and resulting eigenvalues are

$$(\mu_1 + \lambda_M)(\mu_2 + \lambda_M) + \phi_s \gamma = 0$$

$$\implies \lambda_M^2 + (\mu_1+\mu_2)\lambda + (\mu_1\mu_2+\chi^2) = 0$$

$$\begin{aligned}\implies \lambda_M &= -\frac{(\mu_1+\mu_2)}{2} \pm \frac{\sqrt{(\mu_1+\mu_2)^2 - 4\mu_1\mu_2 - 4\chi^2}}{2} \\ &= -\frac{(\mu_1+\mu_2)}{2} \pm \frac{\sqrt{(\mu_1-\mu_2)^2 - 4\chi^2}}{2},\end{aligned} \tag{2.1.42}$$

and similarly for $J_D$, the characteristic equation and resulting eigenvalues are

$$(\mu_1+\lambda_D)(\mu_2+\lambda_D) - \phi_s\gamma = 0$$
$$\implies \lambda_D^2 + (\mu_1+\mu_2)\lambda + (\mu_1\mu_2-\chi^2) = 0$$

$$\begin{aligned}\implies \lambda_D &= -\frac{(\mu_1+\mu_2)}{2} \pm \frac{\sqrt{(\mu_1+\mu_2)^2 - 4\mu_1\mu_2 + 4\chi^2}}{2} \\ &= -\frac{(\mu_1+\mu_2)}{2} \pm \frac{\sqrt{(\mu_1-\mu_2)^2 + 4\chi^2}}{2},\end{aligned} \tag{2.1.43}$$

where $\chi^2 = \phi_s\gamma$, $\chi \in \mathbb{R}^+$.

We know $Re(\lambda_M) < 0$ for all $\mu_1$, $\mu_2$, $\phi_s$, $\gamma > 0$, so this system is unable to go through a Hopf bifurcation. However, the nature of the steady state can still change:

- If $(\mu_1 - \mu_2) < 2\chi$ there exists a stable spiral,
- If $(\mu_1 - \mu_2) \geq 2\chi$ there exists a stable node.

We know perturbations from the HSS out of the SoE can grow when $Re(\lambda_{D+}) > 0$, which is satisfied when $4\chi^2 > 4\mu_1\mu_2$. Hence, the system goes through a bifurcation when $\chi = \sqrt{\mu_1\mu_2}$. If $\mu_1 = \mu_2$, this condition becomes $\chi = \mu$, as we have already shown.

## $n = 3$

When $n = 3$ we have the set of ODEs:

$$\begin{aligned}\dot{X}_{1,j} &= -\mu X_{1,1} + f_s(\bar{X}_{3,j}), \\ \dot{X}_{2,j} &= -\mu X_{2,j} + f_2(X_{1,j}), \\ \dot{X}_{3,j} &= -\mu X_{3,j} + g(X_{2,j}), \qquad j = 1, 2,\end{aligned} \tag{2.1.44}$$

where we have assumed that each variable has the same degradation rate $\mu$ for simplicity.

Linearising about the HSS gives the linearised system

$$\begin{aligned}
\dot{x}_{1,j} &= -\mu x_{1,1} + \phi_s \bar{X}_{3,j}, \\
\dot{x}_{2,j} &= -\mu x_{2,j} + \phi_2 X_{1,j}, \\
\dot{x}_{3,j} &= -\mu x_{3,j} - \gamma X_{2,j}, \qquad j = 1, 2.
\end{aligned} \tag{2.1.45}$$

Making a change of variables to Mean and Difference variables, we have the linear systems

$$\begin{aligned}
\dot{M}_1 &= -\mu M_1 + \phi_s M_3, & \dot{D}_1 &= -\mu D_1 - \phi_s D_3, \\
\dot{M}_2 &= -\mu M_2 - \phi_2 M_1, & \dot{D}_2 &= -\mu D_2 + \phi_2 D_1, \\
\dot{M}_3 &= -\mu M_3 - \gamma M_2, & \dot{D}_3 &= -\mu D_3 - \gamma D_2,
\end{aligned} \tag{2.1.46}$$

which have corresponding Jacobian matrices

$$J_M = \begin{bmatrix} -\mu & 0 & \phi_s \\ \phi_2 & -\mu & 0 \\ 0 & -\gamma & -\mu \end{bmatrix}, \qquad J_D = \begin{bmatrix} -\mu & 0 & -\phi_s \\ \phi_2 & -\mu & 0 \\ 0 & -\gamma & -\mu \end{bmatrix}. \tag{2.1.47}$$

The characteristic equation and resulting eigenvalues of $J_M$ are

$$-(\mu + \lambda_M)^3 - \phi_s \phi_2 \gamma = 0, \tag{2.1.48}$$

$$\begin{aligned}
&\implies (\mu + \lambda_M)^3 = -\chi^3, \\
&\implies \lambda_M = -\mu + (-1)^{1/3} \chi \\
&\qquad\quad = -\mu + \mathrm{e}^{\frac{\pi i + k\pi i}{3}} \chi, \qquad \text{for } k = 0, 1, 2,
\end{aligned} \tag{2.1.49}$$

and the characteristic equation and resulting eigenvalues of $J_D$ are

$$-(\mu + \lambda_D)^3 + \phi_s \phi_2 \gamma = 0, \tag{2.1.50}$$

$$\begin{aligned}
&\implies (\mu + \lambda_D)^3 = \chi^3, \\
&\implies \lambda_D = -\mu + (1)^{1/3} \chi \\
&\qquad\quad = -\mu + e^{\frac{k\pi i}{2}} \chi, \qquad \text{for } k = 0, 1, 2,
\end{aligned} \tag{2.1.51}$$

where $\chi^3 = \phi_s \phi_2 \gamma$.

Again, the HSS becomes unstable to perturbations out of the SoE when $\chi > \mu$, confirmed when $k = 0$ in (2.1.51). From (2.1.49), the eigenvalue with largest real part corresponds to $k = 0$ or $k = 2$, which have the form

$$\begin{aligned}
\lambda_M &= -\mu + \chi \cos\left(\frac{\pi}{3}\right) \pm i\chi \sin\left(\frac{\pi}{3}\right) \\
&= -\mu + \frac{\chi}{2} \pm i\frac{\sqrt{3}\,\chi}{2}.
\end{aligned} \tag{2.1.52}$$

Therefore, a Hopf bifurcation occurs when

$$\chi = 2\,\mu, \tag{2.1.53}$$

generating a periodic orbit in the SoE with angular frequency

$$\begin{aligned}\omega &= \chi \sin\left(\frac{\pi}{3}\right) \\ &= \sqrt{3}\,\mu,\end{aligned} \tag{2.1.54}$$

and a period of oscillation

$$T = \frac{2\pi}{\sqrt{3}\,\mu}. \tag{2.1.55}$$

### 2.1.4 Summary of ODE Results

For a system of two cells each containing $n$ components, the following results hold:

- There is always a homogeneous steady state where $X^*_{i,j} = \bar{X}^*_{i,j} \equiv X^*_i$. This is an element of the $n$-dimensional subspace, the Surface of Equivalence, in which $X_{i,j} = \bar{X}_{i,j}$.
- If we consider initial conditions in the SoE, then $X_{i,j}(t) = \bar{X}_{i,j}(t)\ \forall t$. If the states of the cells are identical, the system will remain in the SoE.

  Simply, if $X(0) \in$ SoE, and $X(t)$ is the solution of the Initial Value Problem

  $$\dot{X} = f(X), \qquad X(0) = X_0,$$

  then $X(t) \in$ SoE, $t > 0$.
- The HSS is either stable or unstable to perturbations out of the SoE. If it is stable then this is the only steady state of the system and will be the final state of both cells. If it is unstable then it behaves as a saddle point, causing solution trajectories to asymptotically approach one of the two heterogeneous steady states.
- For all $n$, the system undergoes a bifurcation when $\chi$, the product of the gradients of the regulatory functions evaluated at the HSS, is equal to the geometric mean of the degradation rates of the cells' variables. Hence, the HSS is unstable to perturbations out of the SoE when

  $$\chi > \sqrt[n]{\prod_{i=1}^{n} \mu_i},$$

  and when all degradation rates are equal, this simplifies to

  $$\chi > \mu.$$

- For $n > 2$, the system can also undergo a Hopf bifurcation. This causes a change to the dynamics in the SoE, where the HSS changes from a stable spiral to an unstable spiral surrounded by a stable periodic orbit. This has been proved in the case of the n-component Repressilator, both with and without time delays [66,67], using the Poincare-Bendixson theorem.
  A Hopf bifurcation will occur provided

$$\chi > \sqrt[n]{\prod_{i=1}^{n} \mu_i}, \text{ and } \sum_{i=1}^{n} \tan^{-1}\left(\frac{\omega}{\mu_i}\right) = \pi,$$

  and when all degradation rates are equal, this simplifies to

$$\chi = \frac{\mu}{\cos(\pi/n)}.$$

  For initial conditions in the SoE, solution trajectories are now attracted onto the periodic orbit surrounding the HSS, corresponding to oscillatory dynamics in each of the cells' variables.

## 2.2 Two cells - Delay Differential Equations

As discussed in Chapter 1, models of Delta-Notch mediated lateral inhibition with delays have been studied in detail [50,51,52]. This section is not to restate these previous results, but to show the similarities and differences between systems which do, and do not have time delays.

The key difference between these types of models is the time taken for the signal to be passed on; systems described by ordinary differential equations do this immediately from component to component, whilst delay differential equations systems can include a time delay in each step, representing the duration it would take between the signal being sent and received.

Delay differential equations are being used more frequently in modelling biological systems. The delay, or lag, can represent any biological process, such as transcription and translation times, maturation time of circulating red blood cells, reflex time of the pupil to light, [59], neural transmission times; virus reproduction times, and many more.

The analysis for the delay systems closely follows that of the non-delay models, except we look for solutions of a particular form, as opposed to calculating eigenvalues from a Jacobian matrix, as we have explained in Section 1.6.

Instead of initially studying the general $m$-component model, we will carry out analysis for the cases of $m = 1$ and $m = 2$. These provide the appropriate foundations to then extend the analysis to $m = 3$, before finally analysing the general $m$-component system.

### 2.2.1 One component per cell

Systems of delay differential equations can be simpler than their ODE-counterparts, since several steps of the pathway can be reduced to fewer steps with time delays. The biggest simplification that can made is each cell only having one component; we no longer require the cells to have a separate component for sending and receiving the signal, and all internal processes have been reduced to a time-delay when sending the signal from one cell to the other. Cell-fates are still determined by the level of this variable once the system has diverged from homogeneity.

When $m = 1$, the system is described by the delay differential equations (DDEs):

$$\begin{aligned} \dot{Y}_1 &= -\mu Y_1 + g\left(Y_2(t-\tau)\right) \\ \dot{Y}_2 &= -\mu Y_2 + g\left(Y_1(t-\tau)\right), \end{aligned} \tag{2.2.1}$$

where $Y_j$ represents the variable level in cell $j$, $\tau$ is the time delay in the signal and $g$ is a bounded continuous monotonic decreasing function, as before.

The system has steady states $(Y_1^*, Y_2^*)$, such that

$$\mu Y_1^* = g(Y_2^*), \qquad \mu Y_2^* = g(Y_1^*),$$

and therefore a unique spatially-uniform, time-independent homogeneous steady state [HSS]

$$(Y_1^*, Y_2^*) = (Y^*, Y^*), \tag{2.2.2}$$

where $Y^* = \frac{1}{\mu} g(Y^*)$.

Consider small perturbations about the HSS:

$$Y_1 = Y^* + y_1, \qquad Y_2 = Y^* + y_2$$

and

$$\begin{aligned} g\left(Y_i(t-\tau)\right) &= g\left(Y^* + y_i(t-\tau)\right) \\ &= g(Y^*) - \gamma y_i(t-\tau) + O(y_i^2(t-\tau)) \end{aligned} \tag{2.2.3}$$

using a first order Taylor expansion, where

$$\gamma \equiv -\frac{\partial g}{\partial Y}\Big|_{Y^*} > 0.$$

The linearised system is therefore given by

$$\begin{aligned} \dot{y}_1 &= -\mu y_1 - \gamma y_2(t-\tau) \\ \dot{y}_2 &= -\mu y_2 - \gamma y_1(t-\tau). \end{aligned} \tag{2.2.4}$$

Using the same technique to uncouple the linearised system, we will again make a change of variables to the Mean and Difference variables, defined by

$$M \equiv \frac{y_1 + y_2}{2}, \qquad D \equiv \frac{y_1 - y_2}{2}.$$

This gives

$$\begin{aligned} \dot{M} &= -\mu M - \gamma M(t-\tau) \\ \dot{D} &= -\mu D + \gamma D(t-\tau). \end{aligned} \tag{2.2.5}$$

Considering the $M$ equation, we seek solutions of the form

$$M(t) = C_1 e^{\lambda_M t}, \qquad C_1 \neq 0.$$

This gives

$$\begin{aligned} M(t-\tau) &= C_1 e^{\lambda_M (t-\tau)} \\ &= C_1 e^{-\lambda_M \tau} e^{\lambda_M t}, \end{aligned}$$

and

$$\dot{M} = C_1 \lambda_M e^{\lambda_M t}.$$

Substituting these into the first equation of (2.2.5) gives

$$C_1 \lambda_M e^{\lambda_M t} = -\mu C_1 e^{\lambda_M (t)} - \gamma C_1 e^{-\lambda_M \tau} e^{\lambda_M t}. \tag{2.2.6}$$

The condition for non-trivial solution of (2.2.5 i) is therefore

$$\mu + \lambda_M = -\gamma e^{-\lambda_M \tau}. \tag{2.2.7}$$

Similarly, the condition for the non-trivial solution of (2.2.5 ii) (using $D(t) = C_2 e^{\lambda_D t}$), gives

$$\mu + \lambda_D = \gamma e^{-\lambda_D \tau}. \tag{2.2.8}$$

Firstly, let us consider the equation (2.2.8), the equation governing $D(t)$. From the ODE models, we know that a bifurcation related to switching can occur when $Re(\lambda_D) = 0$, generating two additional non-homogeneous steady states and changing the HSS from a stable node to an unstable saddle point.

If we let $\lambda_D = k + i\omega_D$, where $k$, $\omega_D \in \mathbb{R}$, (2.2.8) becomes

$$\begin{aligned} \mu + k + i\omega_D &= \gamma e^{-(k+i\omega_D)\tau} \\ &= \gamma e^{-k\tau} \left( \cos(\omega_D \tau) - i \sin(\omega_D \tau) \right). \end{aligned} \tag{2.2.9}$$

Separating into its real and imaginary parts:

$$\begin{aligned} \text{Re}: &\quad k + \mu = \gamma e^{-k\tau} \cos(\omega_D \tau), \\ \text{Im}: &\quad \omega_D = -\gamma e^{-k\tau} \sin(\omega_D \tau). \end{aligned} \tag{2.2.10}$$

It is clear that $\max(\mathrm{Re}(\lambda_D))$ occurs when $\cos(\omega_D\tau) = 1$, implying $\omega_D\tau = 2n\pi$ for $n = 0, 1, 2, \ldots$. However, this means that $\sin(\omega_D\tau) = 0$, and since $\tau > 0$, then $\omega_D = 0$. Therefore, $\lambda_D \in \mathbb{R}$.

The system will have a bifurcation when $\lambda_D = 0$, so with respect to $\gamma$, the HSS is unstable to perturbations out of the SoE when

$$\gamma > \mu. \tag{2.2.11}$$

Secondly, we want to assess the conditions for when the system has a Hopf bifrucation. In this case, let us consider uniform perturbations, such that $y_1 = y_2$. This implies $D = 0$, and only the $\lambda_M$ equation (2.2.7) is relevant.

For a Hopf bifurcation, we assume a pure imaginary eigenvalue, such that $\lambda_M = i\omega_M$, $\omega_M \in \mathbb{R}$. Now (2.2.7) becomes

$$\begin{aligned} \mu + i\omega_M &= -\gamma \mathrm{e}^{-i\omega_M\tau} \\ &= -\gamma\left(\cos(\omega_M\tau) - i\sin(\omega_M\tau)\right). \end{aligned} \tag{2.2.12}$$

Separating into its real and imaginary parts:

$$\begin{aligned} &\mathrm{Re}: \quad \mu = -\gamma\cos(\omega_M\tau), \\ &\mathrm{Im}: \quad \omega_M = \gamma\sin(\omega_M\tau). \end{aligned} \tag{2.2.13}$$

By finding the modulus and argument of (2.2.12), we find

$$\begin{aligned} &\mu^2 + \omega_M^2 = \gamma^2, \\ &\implies \omega_M = \sqrt{\gamma^2 - \mu^2}, \end{aligned} \tag{2.2.14}$$

provided $\gamma > \mu$, and

$$\begin{aligned} &\frac{\omega_M}{\mu} = -\tan(\omega_M\tau) = \tan(\pi - \omega_M\tau), \\ &\implies \tau = \frac{1}{\omega_M}\left(\pi - \tan^{-1}\left(\frac{\omega_M}{\mu}\right)\right). \end{aligned} \tag{2.2.15}$$

Hence, this system is capable of having a Hopf bifurcation, provided

$$\gamma > \mu,$$

and the bifurcation occurs when the delay is

$$\tau = \frac{1}{\omega_M}\left(\pi - \tan^{-1}\left(\frac{\omega_M}{\mu}\right)\right), \tag{2.2.16}$$

where $\omega_M = \sqrt{\gamma^2 - \mu^2}$.

Rewriting (2.2.16) with respect to $\gamma$:

$$\tau = \frac{1}{\sqrt{\gamma^2 - \mu^2}} \left( \pi - \tan^{-1} \left( \frac{\sqrt{\gamma^2 - \mu^2}}{\mu} \right) \right). \tag{2.2.17}$$

illustrated graphically in Figure 2.3.

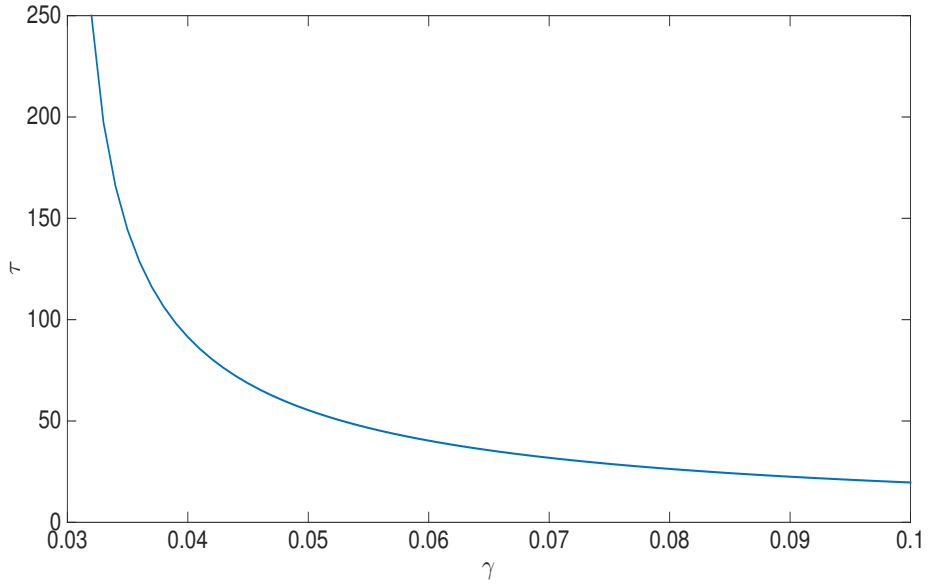


Figure 2.3: Relationship between $\gamma$ and $\tau$ for the existence of a Hopf bifurcation, as described by equation (2.2.17), when $\mu = 0.03$. As $\gamma \to \infty$, $\tau \to 0$, and as $\gamma \to \mu$, $\tau \to \infty$. Therefore, provided $\gamma > \mu$, a Hopf bifurcation is always possible.

To show that $\mathrm{Re}(\lambda_M)$ becomes positive as $\tau$ surpasses (2.2.16), which we will refer to as $\tau*$, we want to differentiate (2.2.7) with respect to $\tau$:

$$\frac{d\lambda_M}{d\tau} = \lambda_M \gamma e^{-\lambda_M \tau} + \tau \frac{d\lambda_M}{d\tau} \gamma e^{-\lambda_M \tau} \tag{2.2.18}$$

$$\implies \frac{d\lambda_M}{d\tau} \left( 1 - \gamma \tau e^{-\lambda_M \tau} \right) = \lambda_M \gamma e^{-\lambda_M \tau} \tag{2.2.19}$$

$$\begin{aligned} \implies \frac{d\lambda_M}{d\tau} &= \frac{\lambda_M \gamma e^{-\lambda_M \tau}}{1 - \gamma \tau e^{-\lambda_M \tau}} \\ &= \frac{\lambda_M \gamma}{e^{\lambda_M \tau} - \gamma \tau}. \end{aligned} \tag{2.2.20}$$

Therefore, when $\tau = \tau*$ (and $\lambda_M = i\omega_M$),

$$\frac{d\lambda_M}{d\tau} = \frac{i\gamma\omega_M}{e^{i\omega_M \tau*} - \gamma\tau*}, \tag{2.2.21}$$

which has real part

$$\mathrm{Re}\left(\frac{d\lambda_M}{d\tau}\right) = \frac{d\mathrm{Re}(\lambda_M)}{d\tau} = \frac{\gamma\omega_M \sin(\omega\tau*)}{\psi^2} \tag{2.2.22}$$

where $\psi^2 = (\cos(\omega_M\tau*) - \gamma\tau*)^2 + \sin^2(\omega_M\tau*) > 0$.

Substituting the imaginary expression of (2.2.13) gives

$$\frac{d\mathrm{Re}(\lambda_M)}{d\tau} = \frac{\omega_M^2}{\psi^2} > 0. \tag{2.2.23}$$

Therefore, $\mathrm{Re}(\lambda_M)$ increases from negative to positive as $\tau$ surpasses $\tau*$.

### 2.2.2 Two components per cell

As mentioned, when using multiple delay differential equations to model a signalling pathway, delays can be included throughout the pathway in several different ways, depending on the purpose of the model. It may be that there is only a single delay at a specified step and the rest of the signals are instantaneous; or every step has some associated delay; or some intermediate of these cases.

In principle, it is only the total delay $\tau$ which is of major importance regarding the local dynamics about the system's HSS and bifurcation conditions. The individual $\tau_i$ do play a part in the dynamics, and their position in the cycle can affect local behaviours, such as phase differences between different components, but it is the total which dictates the system's overall global behaviour.

The analysis differs slightly from $m = 1$, introducing a technique which will be further used for $m = 3$ and the generalised $m$-component case.

Similarly to the ODE model where $n = 2$, each cell in this model has a transmitter and receiver for the signal, denoted by $Y_{1,j}$ and $Y_{2,j}$, respectively, where $j$ refers to the cell number. There are also delays present in the signals, whereby the total delay between $Y_{i,j}$ and $\bar{Y}_{i,j}$ (any variable in one of the cells, and the equivalent variable in the neighbouring cell) is $\tau$. The delays have been distributed such that there is a delay in the signal between cell-cell interactions, $\tau_s$, and a delay in the internal signal between receiver and transmitter, $\tau_1$.

This is represented by the system of DDEs:

$$\begin{aligned} \dot{Y}_{1,j} &= -\mu Y_{1,j} + f_s(\bar{Y}_{2,j}(t-\tau_s)) \\ \dot{Y}_{2,j} &= -\mu Y_{2,j} + g(Y_{1,j}(t-\tau_1)), \qquad j = 1,2, \end{aligned} \tag{2.2.24}$$

where $f_s$ and $g$ are the same regulatory functions as previously defined. For simplicity, we have chosen the degradation rates of the cells' components to be equal.

There are steady states when

$$\mu Y_{1,j}^* = f_s(\bar{Y}_{2,j}^*), \qquad \mu Y_{2,j}^* = g(Y_{1,j}^*),$$

and a homogeneous steady state [HSS] $(Y_1^*, Y_2^*, Y_1^*, Y_2^*)$, where $Y_{i,j} = Y_i^*$,

$$Y_1^* = \frac{1}{\mu} f_s(Y^*), \qquad Y_2^* = \frac{1}{\mu} g(Y_1^*) \tag{2.2.25}$$

Considering small perturbations about the HSS, such that

$$Y_{i,j} = Y_i^* + y_{i,j}$$

and

$$\begin{aligned} f_s\left(Y_{2,1}(t-\tau_s)\right) &= f_s\left(Y_2^* + y_{2,j}(t-\tau_s)\right), \\ &= f_s(Y_2^*) + \phi_s y_{2,j}(t-\tau_s) + O(y_{2,j}^2(t-\tau_s)), \end{aligned}$$

$$\begin{aligned} g\left(Y_{1,j}(t-\tau_i)\right) &= g\left(Y_1^* + y_{1,j}(t-\tau_i)\right) \\ &= g(Y_1^*) - \gamma y_{1,j}(t-\tau_i) + O(y_{1,j}^2(t-\tau_1)), \end{aligned}$$

using a first order Taylor expansion, where

$$\phi_s \equiv \frac{\partial f_s}{\partial Y_2}\Big|_{Y_2^*} > 0, \qquad \gamma \equiv -\frac{\partial g}{\partial Y_1}\Big|_{Y_1^*} > 0.$$

The linearised system is therefore given by

$$\begin{aligned} \dot{y}_{1,j} &= -\mu y_{1,j} + \phi_s \bar{y}_{2,j}(t-\tau_s) \\ \dot{y}_{2,j} &= -\mu y_{2,j} - \gamma y_{1,j}(t-\tau_1), \qquad j = 1, 2. \end{aligned} \tag{2.2.26}$$

If we want to make a change of variables to separate the linearised system into uncoupled equations, we want to form two second-order differential equations for $y_{1,j}$ and $y_{2,j}$.

Firstly with respect to $y_{1,j}$ :

$$\ddot{y}_{1,j} = -\mu \dot{y}_{1,j} + \phi_s \dot{\bar{y}}_{2,j}(t-\tau_s). \tag{2.2.27}$$

Substituting in (2.2.26 ii), evaluated at $t - \tau_s$;

$$\begin{aligned} \ddot{y}_{1,j} &= -\mu \dot{y}_{1,j} + \phi_s \left(-\mu \bar{y}_{2,j}(t-\tau_s) - \gamma \bar{y}_{1,j}(t-\tau_1-\tau_s)\right) \\ &\quad - \mu \dot{y}_{1,j} + \left(-\mu \dot{y}_{1,j} - \mu^2 y_{1,j}\right) - \phi_s \gamma \bar{y}_{1,j}(t-\tau). \end{aligned} \tag{2.2.28}$$

This gives

$$\ddot{y}_{1,j} + 2\mu \dot{y}_{1,j} + \mu^2 y_{1,j} = -\chi^2 \bar{y}_{1,j}(t-\tau), \tag{2.2.29}$$

where $\chi^2 \equiv \gamma \phi_s$, and $\tau = \tau_s + \tau_1$.

Secondly with respect to $y_{2,j}$:

$$\ddot{y}_{2,j} = -\mu \dot{y}_{2,j} - \gamma \dot{y}_{1,j}(t-\tau_1). \tag{2.2.30}$$

Substituting in (2.2.26 i), evaluated at $t-\tau_1$;

$$\begin{aligned}\ddot{y}_{2,j} &= -\mu\dot{y}_{2,j} - \gamma\left(-\mu y_{1,j}(t-\tau_1) + \phi\bar{y}_{2,j}(t-\tau_s-\tau_1)\right)\\ &\quad - \mu\dot{y}_{2,j} - \left(\mu\dot{y}_{2,j} + \mu^2 y_{1,j}\right) - \phi_s\gamma\bar{y}_{2,j}(t-\tau).\end{aligned} \tag{2.2.31}$$

This gives

$$\ddot{y}_{2,j} + 2\mu\dot{y}_{2,j} + \mu^2 y_{2,j} = -\chi^2\bar{y}_{1,j}(t-\tau). \tag{2.2.32}$$

We then want to make a change of variables to the Mean and Difference variables for each of (2.2.29) and (2.2.32) to give conditions for when the differences between $y_{i,j}$ and $\bar{y}_{i.j}$ will grow.

Since (2.2.29) and (2.2.32) have the same form, the conditions for growth in the Difference variables will the the same in both cases. Therefore, we only need to find conditions for when the difference between $y_{2,j}$ and $\bar{y}_{2,j}$ is able to grow, and the same conditions will hold for the difference between $y_{1,j}$ and $\bar{y}_{1,j}$.

We can now make the change of variables to the Mean and Difference variables using

$$M \equiv \frac{y_{2,1}+y_{2,2}}{2}, \qquad D \equiv \frac{y_{2,1}-y_{2,2}}{2},$$

we have the uncoupled second-order equations

$$\begin{aligned}\ddot{M} + 2\mu\dot{M} + \mu^2 M &= -\chi^2 M(t-\tau),\\ \ddot{D} + 2\mu\dot{D} + \mu^2 D &= \chi^2 D(t-\tau).\end{aligned} \tag{2.2.33}$$

Firstly looking at the $M$ equation, when we use $M(t) = C_1 e^{\lambda_M t}$, (2.2.33 i) becomes

$$\begin{aligned}\lambda_M^2 C_1 e^{\lambda_M t} + 2\mu\lambda_M C_1 e^{\lambda_M t} + \mu^2 C_1 e^{\lambda_M t} &= -\chi^2 C_1 e^{\lambda_M(t-\tau)}\\ &= -\chi^2 C_1 e^{\lambda_M t} e^{-\lambda_M\tau}.\end{aligned} \tag{2.2.34}$$

Assuming $C_1 e^{\lambda_M t} \neq 0$, (2.2.34) reduces to

$$\begin{aligned}\lambda_M^2 + 2\mu\lambda_M + \mu^2 &= -\chi^2 e^{-\lambda_M\tau},\\ (\lambda_M+\mu)^2 &= -\chi^2 e^{-\lambda_M\tau}.\end{aligned} \tag{2.2.35}$$

Similarly, substituting $D(t) = C_2 e^{\lambda_D t}$ into the $D$ part of (2.2.33) gives

$$(\lambda_D+\mu)^2 = \chi^2 e^{-\lambda_D\tau}, \tag{2.2.36}$$

and hence, $\lambda_M$ and $\lambda_D$ satisfy the expressions

$$\lambda_M = -\mu \pm i\chi e^{-\lambda_M\tau/2}, \qquad \lambda_D = -\mu \pm \chi e^{-\lambda_D\tau/2}. \tag{2.2.37}$$

As usual, a bifurcation which allows for switching will occur when $\mathrm{Re}(\lambda_D) = 0$, where we assume $\lambda_D \in \mathbb{R}$, following the same argument as the $m = 1$ case.

When $\lambda_D = 0$, (2.2.37ii) becomes

$$0 = -\mu \pm \chi,$$

which implies $\lambda_{D+} = 0$ (the positive branch of (2.2.37 ii)) when $\chi = \mu$.

Therefore, switching is possible once $\chi > \mu$, enabling the difference between $y_{i,1}$ and $y_{i,2}$ for $i = 1, 2$ to grow.

To determine the conditions necessary for a Hopf bifurcation, let us first consider the two possible solutions for $\lambda_M$. We can rewrite (2.2.37i) in the following form:

$$\lambda_{M1} = -\mu + \mathrm{e}^{i\pi/2}\chi \mathrm{e}^{-\lambda_{M1}\tau/2}; \tag{2.2.38}$$

and

$$\lambda_{M2} = -\mu + \mathrm{e}^{-i\pi/2}\chi \mathrm{e}^{-\lambda_{M2}\tau/2}. \tag{2.2.39}$$

Since these equations are complex conjugates of each other, if $\lambda$ is a solution of (2.2.38), then $\bar{\lambda}$ is a solution of (2.2.39). Therefore, we only need to consider solutions with $\mathrm{Im}(\lambda) \geq 0$. Let us consider $\lambda_M = i\omega_M$, where $\omega_M \geq 0$.

Separating each into their real and imaginary parts, (2.2.38) becomes

$$\begin{aligned} &\text{Re: } \mu = \chi \cos\left(\frac{\pi}{2} - \frac{\omega_M \tau}{2}\right) \\ &\text{Im: } \omega_M = \chi \sin\left(\frac{\pi}{2} - \frac{\omega_M \tau}{2}\right). \end{aligned} \tag{2.2.40}$$

Finding the modulus and argument:

$$\begin{aligned} &\mu^2 + \omega_M^2 = \chi^2, \\ &\implies \omega_M = \sqrt{\chi^2 - \mu^2}, \end{aligned} \tag{2.2.41}$$

provided $\chi > \mu$.

For finding the argument, we know that $\dfrac{\pi - \omega_M \tau}{2}$ is in the first quadrant of the complex plane, and since

$$\frac{\pi - \omega_M \tau}{2} = \tan^{-1}\left(\frac{\omega_M}{\mu}\right), \tag{2.2.42}$$

then

$$\begin{aligned} &\frac{\pi}{2} - \frac{\omega_M \tau}{2} \in \left(0, \frac{\pi}{2}\right) + 2n\pi \\ &\implies \omega_M \tau \in (0, \pi) \qquad (n = 0). \end{aligned} \tag{2.2.43}$$

Similarly, (2.2.39) becomes

$$\begin{aligned} &\text{Re: } \mu = \chi \cos\left(\frac{\pi}{2} + \frac{\omega_M \tau}{2}\right) \\ &\text{Im: } \omega_M = -\chi \sin\left(\frac{\pi}{2} + \frac{\omega_M \tau}{2}\right). \end{aligned} \tag{2.2.44}$$

Finding the modulus and argument:

$$\begin{aligned} &\mu^2 + \omega_M^2 = \chi^2, \\ &\implies \omega_M = \sqrt{\chi^2 - \mu^2}, \end{aligned} \tag{2.2.45}$$

provided $\chi > \mu$.

For finding the argument, we know that $\dfrac{\pi + \omega_M \tau}{2}$ is in the fourth quadrant of the complex plane, and since

$$\frac{\pi + \omega_M \tau}{2} = \tan^{-1}\left(\frac{\omega_M}{\mu}\right), \tag{2.2.46}$$

then

$$\begin{aligned} &\frac{\pi}{2} + \frac{\omega_M \tau}{2} \in \left(\frac{3\pi}{2}, 2\pi\right) + 2n\pi \\ &\implies \omega_M \tau \in (2\pi, 3\pi) \qquad (n = 0). \end{aligned} \tag{2.2.47}$$

Therefore, since the possible range for $\omega_M \tau$ is smaller for equation (2.2.38), the necessary conditions for a Hopf bifurcation are

$$\chi > \mu, \qquad \tau = \frac{\pi - 2\tan^{-1}\left(\frac{\omega_M}{\mu}\right)}{\omega_M}. \tag{2.2.48}$$

.

### 2.2.3 Comparison between $m = 1$, $m = 2$

Now that we have explicit conditions for when there exists a Hopf bifurcation in the cases of $m = 1$ and $m = 2$, we can show how the necessary delays are related, such that both systems have a Hopf bifurcation for the same value of $\chi$ and $\mu$, and consequently, $\omega_M$.

Denoting the corresponding delays of $\tau_1$ and $\tau_2$, we can equate the delay expressions easily:

$$\tau_1 = \frac{\pi - \tan^{-1}\left(\frac{\omega_M}{\mu}\right)}{\omega_M}, \qquad \tau_2 = \frac{\pi - 2\tan^{-1}\left(\frac{\omega_M}{\mu}\right)}{\omega_M},$$

hence

$$\pi - \omega_M \tau_1 = \frac{\pi - \omega_M \tau_2}{2},$$

and so,

$$\tau_2 = 2\tau_1 - \frac{\pi}{\omega_M}. \tag{2.2.49}$$

Therefore, provided the above relation holds, it is possible for both systems $m = 1$ and $m = 2$ to have a Hopf bifurcation for equal values of $\chi$ and $\mu$.

### 2.2.4 Three Components per Cell

For $m = 3$, we have the system of DDEs:

$$\begin{aligned}
\dot{Y}_{1,j} &= -\mu Y_{1,j} + f_s(\bar{Y}_{3,j}(t-\tau_s)) \\
\dot{Y}_{2,j} &= -\mu Y_{2,j} + f_2(Y_{1,j}(t-\tau_1)) \\
\dot{Y}_{3,j} &= -\mu Y_{3,j} + g(Y_{2,j}(t-\tau_2)), \qquad j = 1, 2,
\end{aligned} \tag{2.2.50}$$

where the regulatory functions are the same as those defined in Section (2.1). There are steady states when

$$\mu Y^*_{1,j} = f_s(Y^*_{3,j}), \qquad \mu Y^*_{2,j} = f_2(Y^*_{1,j}), \qquad \mu Y^*_{3,j} = g(Y^*_{1,j}),$$

and a homogeneous steady state [HSS] when

$$Y^*_1 = \frac{1}{\mu} f_s(Y^*_3), \qquad Y^*_2 = \frac{1}{\mu} f_2(Y^*_1), \qquad Y^*_3 = \frac{1}{\mu} g(Y^*_2) \tag{2.2.51}$$

Considering small perturbations about the HSS, such that

$$Y_{i,j} = Y^*_i + y_{i,j}$$

and

$$\begin{aligned}
f_s\left(Y_{3,1}(t-\tau_s)\right) &= f_s\left(Y^*_3 + y_{3,j}(t-\tau_s)\right), \\
&= f_s(Y^*_3) + \phi_s y_{3,j}(t-\tau_s) + O(y^2_{3,j}(t-\tau_s)),
\end{aligned}$$

$$\begin{aligned}
f_2\left(Y_{1,1}(t-\tau_s)\right) &= f_s\left(Y^*_1 + y_{1,j}(t-\tau_1)\right), \\
&= f_s(Y^*_1) + \phi_2 y_{1,j}(t-\tau_1) + O(y^2_{1,j}(t-\tau_1)),
\end{aligned}$$

$$\begin{aligned}
g\left(Y_{2,j}(t-\tau_i)\right) &= g\left(Y^*_2 + y_{2,j}(t-\tau_2)\right), \\
&= g(Y^*_2) - \gamma y_{2,j}(t-\tau_2) + O(y^2_{2,j}(t-\tau_2)),
\end{aligned}$$

using first order Taylor expansions, where

$$\phi_s \equiv \left.\frac{\partial f_s}{\partial Y_3}\right|_{Y^*_3} > 0, \qquad \phi_2 \equiv \left.\frac{\partial f_2}{\partial Y_1}\right|_{Y^*_1} > 0, \qquad \gamma \equiv -\left.\frac{\partial g}{\partial Y_2}\right|_{Y^*_2} > 0.$$

The linearised system is therefore given by:

$$\begin{aligned}
\dot{y}_{1,j} &= -\mu y_{1,j} + \phi_s \bar{y}_{3,j}(t-\tau_s) \\
\dot{y}_{2,j} &= -\mu y_{2,j} + \phi_2 y_{1,j}(t-\tau_1) \\
\dot{y}_{3,j} &= -\mu y_{3,j} - \gamma y_{2,j}(t-\tau_2), \qquad j = 1, 2.
\end{aligned} \tag{2.2.52}$$

Similarly to $m = 2$, if we want to make a change of variables to separate the linearised system into uncoupled equations, we want to form three third-order differential equations, for each of $y_{1,j}$, $y_{2,j}$ and $y_{3,j}$. However, as we saw in the $m = 2$ case, the form of each

of the third-order equations will be the same, and therefore the conditions for when the difference between $y_{i,1}$ and $\bar{y}_{i,1}$ will hold for each $i = 1, 2, 3$.

Hence we only need to form one third-order differential equation for $y_{3,j}$ say, and the same conditions will hold for both $y_{1,j}$ and $y_{2,j}$.

If we take the third derivative of $y_{3,j}$;

$$\dddot{y}_{3,j} = -\mu\ddot{y}_{3,j} - \gamma\ddot{y}_{2,j}(t-\tau_2), \tag{2.2.53}$$

then, substituting equations $(i, ii)$ of (2.2.52) and their derivatives into (2.2.53):

$$\begin{aligned}
\dddot{y}_{3,j} &= -\mu\ddot{y}_{3,j} - \gamma\left[-\mu\dot{y}_{2,j}(t-\tau_2) + \phi_2\dot{y}_{1,j}(t-\tau_1-\tau_2)\right] \\
&= -\mu\ddot{y}_{3,j} + \gamma\mu\dot{y}_{2,j}(t-\tau_2) - \gamma\phi_2\dot{y}_{1,j}(t-\tau_1-\tau_2) \\
&= -\mu\ddot{y}_{3,j} + \gamma\mu\left[-\mu y_{2,j}(t-\tau_2) + \phi_2 y_{1,j}(t-\tau_1-\tau_2)\right] \\
&\quad - \gamma\phi_2\left[-\mu y_{1,j}(t-\tau_1-\tau_2) + \phi_s\bar{y}_{3,j}(t-\tau_s-\tau_1-\tau_2)\right] \\
&= -\mu\ddot{y}_{3,j} + \gamma\mu\left[\frac{\mu\dot{y}_{3,j} + \mu^2 y_{3,j}}{\gamma}\right] + \gamma\mu\left[\dot{y}_{2,j}(t-\tau_2) + \mu y_{2,j}(t-\tau_2)\right] \\
&\quad + \gamma\mu\left[\dot{y}_{2,j}(t-\tau_2) + \mu y_{2,j}(t-\tau_2)\right] - \gamma\phi_s\phi_2\bar{y}_{3,j}(t-\tau_s-\tau_1-\tau_2) \\
&= -\mu\ddot{y}_{3,j} + \mu^2\dot{y}_{3,j} + \mu^3 y_{3,j} + 2\mu[-\ddot{y}_{3,j} - \mu\dot{y}_{3,j}] + 2\mu^2[-\ddot{y}_{3,j} - \mu\dot{y}_{3,j}] \\
&\quad - \gamma\phi_s\phi_2\bar{y}_{3,j}(t-\tau_s-\tau_1-\tau_2) \\
&= -3\mu\ddot{y}_{3,j} - 3\mu^2\dot{y}_{3,j} - \mu^3 y_{3,j} - \gamma\phi_s\phi_2\bar{y}_{3,j}(t-\tau_s-\tau_1-\tau_2).
\end{aligned} \tag{2.2.54}$$

We now have an equation in terms of $y_{3,j}$ and its derivatives only;

$$\dddot{y}_{3,j} + 3\mu\ddot{y}_{3,j} + 3\mu^2\dot{y}_{3,j} + \mu^3 y_{3,j} = -\chi^3\bar{y}_{3,j}(t-\tau), \tag{2.2.55}$$

where $\chi^3 = \gamma\phi_s\phi_2$ and $\tau = \tau_s + \tau_1 + \tau_2$.

We are now able to change to the Mean and Difference variables, where

$$M_3 \equiv \frac{y_{3,1} + y_{3,2}}{2}, \qquad D_3 \equiv \frac{y_{3,1} - y_{3,2}}{2},$$

such that

$$\begin{aligned}
\dddot{M}_3 + 3\mu\ddot{M}_3 + 3\mu^2\dot{M}_3 + \mu^3 M_3 &= -\chi^3 M_3(t-\tau), \\
\dddot{D}_3 + 3\mu\ddot{D}_3 + 3\mu^2\dot{D}_3 + \mu^3 D_3 &= \chi^3 D_3(t-\tau).
\end{aligned} \tag{2.2.56}$$

The analysis now follows from $m = 1$ and $m = 2$. Substituting $M_3(t) = C_1 e^{\lambda_M t}$, $D_3(t) = C_2 e^{\lambda_D t}$ and their derivatives into (2.2.56), these become

$$\begin{aligned} &\lambda_M^3 C_1 e^{\lambda_M t} + 3\mu\lambda_M^2 C_1 e^{\lambda_M t} + 3\mu^2\lambda_M C_1 e^{\lambda_M t} + \mu^3 C_1 e^{\lambda_M t} = -\chi^3 C_1 e^{\lambda_M t} e^{-\lambda_M \tau}, \\ &\lambda_D^3 C_2 e^{\lambda_D t} + 3\mu\lambda_D^2 C_2 e^{\lambda_D t} + 3\mu^2\lambda_D C_2 e^{\lambda_D t} + \mu^3 C_2 e^{\lambda_D t} = \chi^3 C_2 e^{\lambda_D t} e^{-\lambda_D \tau}. \end{aligned} \tag{2.2.57}$$

Dividing by $C_1 e^{\lambda_M t}$ and $C_2 e^{\lambda_D t}$, respectively, (2.2.57) reduces to

$$\begin{aligned} &(\lambda_M + \mu)^3 = -\chi^3 e^{-\lambda_M \tau}, \\ &(\lambda_D + \mu)^3 = \chi^3 e^{-\lambda_D \tau}. \end{aligned} \tag{2.2.58}$$

Hence, we obtain the expressions

$$\begin{aligned} \lambda_M &= -\mu + (-1)^{1/3}\chi e^{-\lambda_M \tau/3} \\ &= -\mu + e^{\frac{i(2\pi k+\pi)}{3}}\chi e^{-\lambda_M \tau/3}, \qquad k = 0, 1, 2, \end{aligned} \tag{2.2.59}$$

and

$$\begin{aligned} \lambda_D &= -\mu + 1^{1/3}\chi e^{-\lambda_D \tau/3} \\ &= -\mu + e^{\frac{2\pi k i}{3}}\chi e^{-\lambda_D \tau/3} \qquad k = 0, 1, 2. \end{aligned} \tag{2.2.60}$$

**Bifurcation parameters**

We now want to evaluate when switching from homogeneity can occur, and when there exists and Hopf bifurcation.

Again, a bifurcation allowing for switching occurs when $\max(\mathrm{Re}(\lambda_D) = 0)$, and following the analysis from the $m = 1$ case, we can assume that this $\lambda_D \in \mathbb{R}$. The $\lambda_D$ with the largest real part exists when $k = 0$ in (2.2.60), such that

$$\lambda_D = -\mu + \chi e^{-\lambda_D \tau}. \tag{2.2.61}$$

Since this $\lambda_D \in \mathbb{R}$, this implies that the bifurcation exists when $\lambda_D = 0$, and (2.2.61) becomes

$$0 = -\mu + \chi.$$

Therefore, in terms of $\chi$, the HSS is unstable to perturbations out of the SoE when

$$\chi > \mu. \tag{2.2.62}$$

For a Hopf bifurcation, we assume a pure imaginary eigenvalue $\lambda_M = i\omega_M$, where $\omega_M \in \mathbb{R}$. Firstly, however, we need to know which cube root of $-1$ corresponds to the smallest $\tau$ needed for a Hopf bifurcation, which corresponds to the $\lambda_M$ expression with the largest real part.

From (2.2.59), the three possible $\lambda_M$ are given by

$$\begin{aligned}
\lambda_{M1} &= -\mu + \mathrm{e}^{i\pi/3}\chi\mathrm{e}^{-\lambda_M\tau/3} \\
\lambda_{M2} &= -\mu + \mathrm{e}^{-i\pi/3}\chi\mathrm{e}^{-\lambda_M\tau/3} \\
\lambda_{M3} &= -\mu + \mathrm{e}^{i\pi}\chi\mathrm{e}^{-\lambda_M\tau/3}
\end{aligned} \tag{2.2.63}$$

Similarly to the $m = 2$ case, the first two equations of (2.2.63) are complex conjugates of each other, so if $\lambda_M$ is a solution to the first, then $\bar{\lambda}_M$ is a solution to the second. Additionally the third equation is its own conjugate, and we can therefore consider only solutions with $\mathrm{Im}(\lambda) \geq 0$. Let $\lambda_M = i\omega_M$, where $\omega_M \geq 0$.

Evaluating each of (2.2.63) in terms of its real and imaginary parts:

- $\lambda_{M1} = i\omega_M$ :

$$\begin{aligned}
&\text{Re: } \mu = \chi\cos\left(\frac{\pi - \omega_M\tau}{3}\right), \\
&\text{Im: } \omega_M = \chi\sin\left(\frac{\pi - \omega_M\tau}{3}\right).
\end{aligned} \tag{2.2.64}$$

Finding the modulus and argument:

$$\begin{aligned}
&\mu^2 + \omega_M^2 = \chi^2, \\
&\implies \omega_M = \sqrt{\chi^2 - \mu^2}
\end{aligned} \tag{2.2.65}$$

provided $\chi > \mu$.

For finding the argument, we know that $\dfrac{\pi - \omega_M\tau}{3}$ is in the first quadrant of the complex plane, and since

$$\frac{\pi - \omega_M\tau}{3} = \tan^{-1}\left(\frac{\omega_M}{\mu}\right), \tag{2.2.66}$$

then

$$\begin{aligned}
&\frac{\pi}{3} + \frac{\omega_M\tau}{3} \in \left(0, \frac{\pi}{2}\right) + 2n\pi \\
&\implies \frac{\omega_M\tau}{3} \in (2\pi, 3\pi) \qquad (n = 0) \\
&\implies \omega_M\tau \in (0, \pi)
\end{aligned} \tag{2.2.67}$$

- $\lambda_{M2} = i\omega_M$ :

$$\begin{aligned} &\text{Re: } \mu = \chi \cos\left(\frac{\pi + \omega_M \tau}{3}\right), \\ &\text{Im: } \omega_M = -\chi \sin\left(\frac{\pi + \omega_M \tau}{3}\right). \end{aligned} \tag{2.2.68}$$

Finding the modulus and argument:

$$\begin{aligned} &\mu^2 + \omega_M^2 = \chi^2, \\ &\implies \omega_M = \sqrt{\chi^2 - \mu^2} \end{aligned} \tag{2.2.69}$$

provided $\chi > \mu$.

For finding the argument, we know that $\frac{\pi + \omega_M \tau}{3}$ is in the fourth quadrant of the complex plane, and since

$$\frac{\pi + \omega_M \tau}{3} = \tan^{-1}\left(\frac{\omega_M}{\mu}\right), \tag{2.2.70}$$

then

$$\begin{aligned} &\frac{\pi}{3} + \frac{\omega_M \tau}{3} \in \left(\frac{3\pi}{2}, 2\pi\right) + 2n\pi \\ &\implies \omega_M \tau \in \left(\frac{9\pi}{2}, 6\pi\right) - \pi, \qquad (n = 0) \\ &\implies \omega_M \tau \in \left(\frac{7\pi}{2}, 5\pi\right) \end{aligned} \tag{2.2.71}$$

- $\lambda_{M3} = i\omega_M$ :

$$\begin{aligned} &\text{Re: } \mu = \chi \cos\left(\pi - \frac{\omega_M \tau}{3}\right), \\ &\text{Im: } \omega_M = \chi \sin\left(\pi - \frac{\omega_M \tau}{3}\right). \end{aligned} \tag{2.2.72}$$

Finding the modulus and argument:

$$\begin{aligned} &\mu^2 + \omega_M^2 = \chi^2, \\ &\implies \omega_M = \sqrt{\chi^2 - \mu^2} \end{aligned} \tag{2.2.73}$$

provided $\chi > \mu$.

For finding the argument, we know that $\pi - \frac{\omega_M \tau}{3}$ is in the first quadrant of the complex plane, and since

$$\pi - \frac{\omega_M \tau}{3} = \tan^{-1}\left(\frac{\omega_M}{\mu}\right), \tag{2.2.74}$$

then

$$\pi - \frac{\omega_M \tau}{3} \in \left(0, \frac{\pi}{2}\right) + 2n\pi$$

$$\implies \frac{\omega_M \tau}{3} \in \left(\frac{\pi}{2}, \pi\right) \qquad (n = 0) \tag{2.2.75}$$

$$\implies \omega_M \tau \in \left(\frac{3\pi}{2}, 3\pi\right)$$

Therefore, since the possible range for $\omega_M \tau$ is smallest for the $\lambda_{M1}$ equation of (2.2.63), the necessary conditions for a Hopf bifurcation obtained from (2.2.65) and (2.2.66):

$$\chi > \mu, \qquad \tau = \frac{\pi - 3\tan^{-1}\left(\frac{\omega_M}{\mu}\right)}{\omega_M}. \tag{2.2.76}$$

However, this expression for $\tau$ is now capable of becoming negative, which is physically unrealistic. From the linear stability analysis of the ODE system with $n = 3$, there exists a Hopf bifurcation when

$$\chi = \frac{\mu}{\cos\left(\frac{\pi}{3}\right)} = 2\mu. \tag{2.2.77}$$

When evaluating $\tau$ at $\chi = 2\mu$, such that $\omega_M = \sqrt{3}\mu$, we find $\tau = 0$. Therefore, for $m = 3$, the conditions for a Hopf bifurcation are

$$\mu < \chi < \frac{\mu}{\cos\left(\frac{\pi}{3}\right)}, \qquad \tau = \frac{\pi - 3\tan^{-1}\left(\frac{\omega_M}{\mu}\right)}{\omega_M}, \tag{2.2.78}$$

and there exists a Hopf bifurcation without the need for a delay when

$$\chi = \frac{\mu}{\cos\left(\frac{\pi}{3}\right)}.$$

### 2.2.5 $m$ Components per Cell

For the general $m$-component model, the analytic steps closely follow those of when $m = 3$. However, rather than carry out the analysis explicitly, we will give an outline of the steps and highlight the key results regarding stability and bifurcation conditions.

As always, we start with the full system of $2m$ DDEs:

$$\begin{aligned}
\dot{Y}_{1,j} &= -\mu Y_{1,j} + f_s(\bar{Y}_{m,j}(t - \tau_s)), \\
\dot{Y}_{p,j} &= -\mu Y_{p,j} + f_p(Y_{p-1,j}(t - \tau_{p-1})), \\
\dot{Y}_{m,j} &= -\mu Y_{m,j} + g(Y_{n-1,j}(t - \tau_{m-1}));
\end{aligned} \tag{2.2.79}$$

for $p = 2, \ldots, m-1$ and $j = 1, 2$.

There exists a homogeneous steady state where $Y^*_{i,j} = \bar{Y}^*_{i,j} = Y^*_i \ \forall i$, and we can linearise about this point using small perturbations $y_{i,j}$, such that

$$Y_{i,j} = Y^*_i + y_{i,j}.$$

This gives the linearised system

$$\begin{aligned}
\dot{y}_{1,j} &= -\mu y_{1,j} + \phi_s \bar{y}_{m,j}(t-\tau_s), \\
\dot{y}_{i,j} &= -\mu y_{i,j} + \phi_i y_{i-1,j}(t-\tau_{i-1}), \\
\dot{y}_{m,j} &= -\mu y_{m,j} - \gamma y_{m-1,j}(t-\tau_{m-1});
\end{aligned} \tag{2.2.80}$$

for $i = 2, \ldots, m-1,\ j = 1, 2$.

As shown for $m = 2$, to make a change of variables to separate the linearised system into uncoupled equations we want to form $m$ $m^{th}$-order differential equations for each $y_{i,j}$, $i, 1, 2, \ldots, m,\ j = 1, 2$.

Using the same reasoning as the $m = 3$ case, we only need to do this for one of the $y_{i,j}$, and the form of the other $m-1$ equations will be the same. Therefore, any bifurcation conditions will hold for all variables.

Hence, in this general case we find the $m^{th}$ derivate of $y_{m,j}$, say, and then make a change of variables to the Mean and Difference variables using

$$M \equiv \frac{y_{m,1} + y_{m,2}}{2}, \qquad D \equiv \frac{y_{m,1} - y_{m,2}}{2}, \tag{2.2.81}$$

and obtain $m^{th}$-order equations for $M$ and $D$. These are given by

$$\sum_{i=0}^{m} \binom{m}{i} M^{(m-i)} \mu^i = -\chi^m M(t-\tau), \tag{2.2.82}$$

and

$$\sum_{i=0}^{m} \binom{m}{i} D^{(m-i)} \mu^i = \chi^m D(t-\tau), \tag{2.2.83}$$

where $M^{(m-i)}$ and $D^{(m-i)}$ refer to the $(m-i)^{th}$ derivatives of $M$ and $D$, and $\tau$ is the total delay in each cell.

Substituting $M(t) = C_M e^{\lambda_M t}$ and $D(t) = C_D e^{\lambda_D t}$ into (2.2.82) and (2.2.83) gives

$$C_M e^{\lambda_M t} \sum_{i=0}^{m} \binom{m}{i} \lambda_M^{m-i} \mu^i = -\chi^m C_M e^{\lambda_M t} e^{-\lambda_M \tau} \tag{2.2.84}$$

and

$$C_D e^{\lambda_D t} \sum_{i=0}^{m} \binom{m}{i} \lambda_D^{m-i} \mu^i = \chi^m C_D e^{\lambda_D t} e^{-\lambda_D \tau} \tag{2.2.85}$$

Assuming $C_M e^{\lambda_M t} \neq 0$ and $C_D e^{\lambda_D t} \neq 0$, these reduce to

$$\begin{aligned}(\lambda_M + \mu)^m &= -\chi^m e^{-\lambda_M \tau}, \\ (\lambda_D + \mu)^m &= \chi^m e^{-\lambda_D \tau},\end{aligned} \tag{2.2.86}$$

respectively. In terms of $\lambda_M$ and $\lambda_D$;

$$\begin{aligned}\lambda_M &= -\mu + (-1)^{1/m} \chi e^{-\lambda_M \tau/m}, \\ \lambda_D &= -\mu + 1^{1/m} \chi e^{-\lambda_D \tau/m}.\end{aligned} \tag{2.2.87}$$

As we have shown explicitly for $m = 2$ and $m = 3$, the $m^{th}$ roots of $-1$ and $1$ which give the necessary bifurcation conditions are $e^{i\pi/m}$ and $1$, respectively. (2.2.87) then becomes

$$\lambda_M = -\mu + \chi e^{(i\pi - \lambda_M \tau)/m}, \tag{2.2.88}$$

and

$$\lambda_D = -\mu + \chi e^{-\lambda_D \tau/m}. \tag{2.2.89}$$

The system has a bifurcation associated with switching when $\mathrm{Re}(\lambda_D) = 0$ where we assume $\lambda_D \in \mathbb{R}$. When $\lambda_D = 0$, (2.2.89) is simply

$$0 = -\mu + \chi,$$

stating the HSS becomes unstable to perturbations out of the SoE, and is able to switch when

$$\chi > \mu. \tag{2.2.90}$$

A Hopf bifurcation exists when $\lambda_M$ is purely imaginary. Let $\lambda_M = i\omega_M, \omega_M \in \mathbb{R}$, (2.2.88) then becomes

$$\begin{aligned}i\omega_M &= -\mu + \chi e^{i(\pi - \omega_M \tau)/m} \\ &= -\mu + \chi \left( \cos\left( \frac{\pi - \omega_M \tau}{m} \right) + i \sin\left( \frac{\pi - \omega_M \tau}{m} \right) \right);\end{aligned} \tag{2.2.91}$$

Rewriting (2.2.91) in terms of its Real and Imaginary parts;

$$\begin{aligned}\mathrm{Re}: &\quad \mu = \chi \cos\left( \frac{\pi - \omega_M \tau}{m} \right), \\ \mathrm{Im}: &\quad \omega_M = \chi \sin\left( \frac{\pi - \omega_M \tau}{m} \right).\end{aligned} \tag{2.2.92}$$

Finding the modulus and the argument:

$$\begin{aligned} &\mu^2 + \omega_M^2 = \chi^2, \\ &\implies \omega = \sqrt{\chi^2 - \mu^2}, \end{aligned} \tag{2.2.93}$$

provided $\chi > \mu$, and

$$\begin{aligned} &\frac{\omega_M}{\mu} = \tan\left(\frac{\pi - \omega_M \tau}{m}\right), \\ &\implies \tau = \frac{\pi - m\tan^{-1}\left(\frac{\omega_M}{\mu}\right)}{\omega_M}. \end{aligned} \tag{2.2.94}$$

Therefore, for any 2-cell system with $m$ components in each cell and a total delay of $\tau$, the system is capable of bistability when

$$\chi > \mu,$$

and a Hopf bifurcation occurs when

$$\chi > \mu, \qquad \tau = \frac{\pi - m\tan^{-1}\left(\frac{\omega_M}{\mu}\right)}{\omega_M}. \tag{2.2.95}$$

However, if $m > 2$, then the conditions for a Hopf bifurcation are either

$$\mu < \chi < \frac{\mu}{\cos\left(\frac{\pi}{m}\right)}, \qquad \tau = \frac{\pi - m\tan^{-1}\left(\frac{\omega_M}{\mu}\right)}{\omega_M}, \tag{2.2.96}$$

or

$$\chi = \frac{\mu}{\cos\left(\frac{\pi}{m}\right)},$$

which will give a Hopf bifurcation without a delay.

### 2.2.6 Summary of Results for DDEs

For a system of 2 cells each containing $m$ components, the following results hold:

- There is always a homogeneous steady state where $Y_{i,j}^* = Y_i^*$. This exists in the $m$-dimensional subspace, the Surface of Equivalence, in which $Y_{i,j} = \bar{Y}_{i,j}$.
- If we consider initial conditions on the SoE, then $Y_{i,j}(t) = \bar{Y}_{i,j}(t)$, $t > 0$, and the system will remain on the SoE.

- The HSS is either stable or unstable; if it is stable then this is the only steady state of the system, resulting in both cells having the same final state. If it is unstable, the HSS becomes a saddle-type point and there also exists a pair of inhomogeneous steady states.

- For all $m$, the system has a bifurcation related to the possibility of switching when the product of the gradients of the regulatory functions evaluated at the HSS is equal to the geometric mean of the variables' degradation rates. Therefore, the HSS is unstable to perturbations out of the SoE when

$$\chi > \sqrt[m]{\prod_{i=1}^{m} \mu_i},$$

and when all degradation rates are equal, this simplifies to

$$\chi > \mu.$$

- The HSS also becomes unstable in the SoE when a Hopf bifurcation occurs, and this is possible for all values of $m$. Assuming that all degradation rates are equal, for $m = 1$, $m = 2$, a Hopf bifurcation occurs when

$$\chi > \mu, \qquad \tau = \frac{\pi - m\tan^{-1}\left(\frac{\omega_M}{\mu}\right)}{\omega_M},$$

and for $m \geq 3$, a Hopf bifurcation occurs when

$$\mu < \chi < \frac{\mu}{\cos\left(\frac{\pi}{m}\right)}, \qquad \tau = \frac{\pi - m\tan^{-1}\left(\frac{\omega_M}{\mu}\right)}{\omega_M},$$

or

$$\chi = \frac{\mu}{\cos\left(\frac{\pi}{m}\right)}.$$

### 2.2.7 Analytic Comparison of Models

It is clear from this analysis that both types of models are capable of similar dynamics, but what conditions do we need to make them quantitatively equivalent?

If we compare the results of the linear stability analysis for the $n$-component ODE system and $m$-component DDE system, we know that there can exist a bifurcation associated with switching and a Hopf bifurcation in both cases.

Comparing the conditions for the bifurcations allowing for switching, they exist when $\chi = \sqrt[n]{\prod_{i=1}^{n} \mu_i}$ and $\chi = \sqrt[m]{\prod_{k=1}^{m} \mu_k}$. Therefore, both systems will have the capability to switch from homogeneity for the same value of $\chi$ when

$$\sqrt[n]{\prod_{i=1}^{n} \mu_i} = \sqrt[m]{\prod_{k=1}^{m} \mu_k}. \tag{2.2.97}$$

To compare the conditions for Hopf bifurcations, let us assume that all degradation rates are equal for simplicity. The Hopf bifurcation conditions are

$$\chi = \frac{\mu}{\cos(\pi/n)},$$

provided $n > 2$, and for the delay system, it is

$$\chi > \mu, \qquad \tau = \frac{\pi - m \tan^{-1}(\omega_M/\mu)}{\omega_M}$$

for $m < 3$, and if $m \geq 3$, they are either

$$\mu < \chi < \frac{\mu}{\cos(\pi/m)}, \qquad \tau = \frac{\pi - m \tan^{-1}(\omega_M/\mu)}{\omega_M},$$

or

$$\chi = \frac{\mu}{\cos(\pi/m)}.$$

If an $n$-component ODE system ($n \geq 3$) and $m$-component DDE system have an equal value of $\chi$, where $n > m$, they will also have an equivalent value of $\omega_M$, which, at the Hopf bifurcation is

$$\omega_M = \chi \sin\left(\frac{\pi}{n}\right), \qquad \omega_M = \chi \sin\left(\frac{\pi - \omega_M \tau}{m}\right),$$

which implies

$$\frac{\pi}{n} = \frac{\pi - \omega_M \tau}{m}. \tag{2.2.98}$$

Therefore, if $\chi = \dfrac{\mu}{\cos(\pi/n)}$, both systems will have a Hopf bifurcation for this value, provided the the DDE system has a delay of

$$\tau = \frac{(n-m)\pi}{n\,\omega_M}. \tag{2.2.99}$$

Additionally, an $m$-component DDE system and a $k$-component DDE system ($k > m$) can both have a Hopf bifurcation for equal values of $\chi$.

Case i : $k, m < 3$, $\chi > \mu$.

This case has been addressed in Section 2.2.3. If $m = 1$ and $k = 2$, then the necessary delays for the existence of a Hopf bifurcation are

$$\tau_m = \frac{\pi - \tan^{-1}(\omega_M/\mu)}{\omega_M}, \qquad \tau_k = \frac{\pi - 2\tan^{-1}(\omega_M/\mu)}{\omega_M}.$$

Therefore, both will have a Hopf bifurcation for the same value of $\chi$, provided

$$\tau_2* = 2\tau_1 * - \frac{\pi}{\omega_M}. \tag{2.2.100}$$

Case ii : $k \geq 3$, $\mu < \chi < \frac{\mu}{\cos(\pi/k)}$.

In this case, the necessary delays needed for a Hopf bifurcation are

$$\tau_k = \frac{\pi - k\tan^{-1}(\omega_M/\mu)}{\omega_M}, \qquad \tau_m = \frac{\pi - m\tan^{-1}(\omega_M/\mu)}{\omega_M}, \tag{2.2.101}$$

Therefore, both will have a Hopf bifurcation for the same value of $\chi$, provided

$$\tau_k = \left(\frac{k}{m}\right)\tau_m - \frac{(k-m)\pi}{m\omega_M}. \tag{2.2.102}$$

## 2.3 Linear Stability Analysis for a Lattice of Cells

The work in this chapter so far has only investigated the local dynamics of 2-cell systems. Every variable is connected via a single pathway, with no additional complexities, such as back-reactions or self-regulation.

However, developing multicellular systems do not have the luxury of cells determining their fates in these undisturbed pairs. Instead, cells are continuously sending and receiving signals to and from multiple cells, and must collectively decide on their fates to form a coherent pattern of different cell types for development to continue successfully.

We therefore want to extend this work to look at larger populations of cells who interact via multiple pathways. By considering cell populations arranged in different ways, we can explore how geometry and signalling coherence can affect the previous sections' results.

### Cell-type dynamics

As discussed in Chapter 1, patterning via lateral inhibition relies on each cell sending and receiving signals to and from all of their neighbours simultaneously. With such an increase in the overall complexity of the system, it becomes unfeasible to analyse the dynamics of each variable of each cell.

However, if it is understood how the system's final pattern will form with respect to the ratios and distribution of the different cell types, it is possible to model the dynamics of each cell-type, rather than each cell.

For example, consider the system equivalent to that defined in Chapter 1:

$$\dot{X} = -\mu X + g(Y), \qquad \dot{Y} = -\mu Y + g(X). \tag{2.3.1}$$

When the system is bistable, then the final values of X and Y will be such that $X > Y$ or $Y > X$. Let us assume $X > Y$ is the outcome, and this represents cell 1 becoming type A, and cell 2 becoming type B, for example. Therefore, let us rewrite (2.3.1) in terms of $A$ and $B$:

$$\dot{A} = -\mu A + g(B), \qquad \dot{B} = -\mu B + g(A). \tag{2.3.2}$$

We can now think of this as representing a system in which cells who become type A are regulated by cells who become type B, and cells who become type B are regulated by cells who become type A. So we now have two ODEs which describe how two cells interact, but they can also describe the dynamics of all type A cells and all type B cells in a multicellular system, provided A only signals to B, and B only signals to A.

Therefore, these systems can describe any multicellular system which displays a period-2 pattern. An example of a perfect period-2 pattern on a square lattice of cells is shown in Figure 2.4

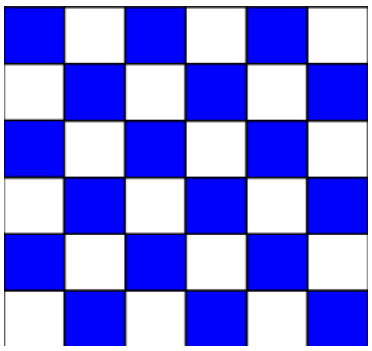

Figure 2.4: Example of a period-2 pattern of cell-types on a $6 \times 6$ square lattice, such that there is an even ratio of cell-types. White represents cells of type A, and blue represents cells of type B.

Consequently, assuming that a perfect pattern is formed free from any defects, the exact number of neighbours a cell sends information to, and receives information from, is no longer important.

So, for a system adopting a perfect period-2 pattern, the linear stability analysis holds exactly from the previous sections, regardless of geometry or the size of the population. However, due to the necessity of a final perfect pattern, this technique does not take defects into account.

This method holds for any number of variables per cell, and can be used in analysis for systems of ODEs or DDEs. We will demonstrate this in the following subsections.

Firstly, we must redefine the Surface of Equivalence for populations of more that two cells.

**Definition 2.3.1.** For a system of $k$ cells, if each cell is described by the state vector $\underline{X}_j$, where $\underline{X}_j = (X_1, X_2, \ldots, X_n)$ for $j = 1, 2, \ldots, k$, the Surface of Equivalence [SoE] is the subspace in which the state vector for each cell is equivalent, such that

$$SoE \equiv \left\{ \underline{X} = \underline{X}_j \quad \text{for } j = 1, 2, \ldots, k. \right\}$$

## Hexagonal Lattice of Cells

A hexagonal lattice of cells allows the population to be regularly arranged, such that each cell, except for those on the boundary, has 6 neighbours. There are no voids in the array, and every cell is the same shape and size.

If the lattice has toroidal periodic boundary conditions and each pair of neighbouring cells is connected via a double-negative (positive) feedback loop, the system is capable of producing patterns of cell-type arrangements with periodicities of 3, 4 and even 7, provided a large enough population [47].

However, unless initial conditions are chosen specifically to favour a particular pattern, the pattern with the fastest growing mode, and therefore the greatest likelihood, is period-3. If cells can become either type A or B, then the ratio of cell-types between A and B will be $1:2$, as shown in Figure 2.5.

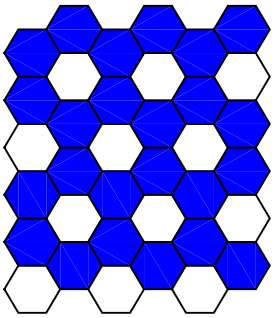

Figure 2.5: Example of a period-3 pattern of cell-types on a $6 \times 6$ hexagonal lattice, such that the ratio of cell-types is 1:2. White represents cells of type A, and blue represents cells of type B.

We can see that if a cell adopts type A, this inhibits the 6 neighbouring cells from doing the same, and they adopt fate B. If we then look at a B cell, we find that they have 3 neighbours of each type A and B.

If each cell had just a single variable (simply denoted as A or B), then the governing ordinary differential equations of this system would be

$$\dot{A} = -\mu A + g(B), \qquad \dot{B} = -\mu B + g\left(\frac{A}{2} + \frac{B}{2}\right). \tag{2.3.3}$$

For the remainder of this chapter we will be analysing this type of multicellular system for both ODEs and DDEs with varying numbers of variables per cell.

Once the main results have been shown, and how they differ from the 2-cell models, we will consider how this method can be extended to more complex arrays, or populations with less uniformity to their final pattern of cell-types.

### 2.3.1 ODE analysis for $n$ components

For an array of cells with periodic boundary conditions, each containing $n$ components, we can describe the dynamics of the whole population using the system of $2n$ ordinary differential equations:

$$\begin{aligned}
\dot{X}_{1,1} &= -\mu_1 X_{1,1} + f_s(X_{n,2}), & \dot{X}_{1,2} &= -\mu_1 X_{1,2} + f_s\left(\frac{X_{n,1}}{2} + \frac{X_{n,2}}{2}\right),\\
\dot{X}_{2,1} &= -\mu_2 X_{2,1} + f_2(X_{1,1}), & \dot{X}_{2,2} &= -\mu_2 X_{2,2} + f_2(X_{1,2}),\\
&\vdots & &\vdots\\
\dot{X}_{n,1} &= -\mu_n X_{n,1} + g(X_{n-1,1}), & \dot{X}_{n,2} &= -\mu_n X_{n,2} + g(X_{n-1,2});
\end{aligned} \tag{2.3.4}$$

where $X_{i,j}$ refers to the $i^{th}$ component of a cell who is adopting fate $j$.

The only term which is different to (2.1.1) is the $X_{1,2}$ equation. Since any cell adopting fate 2 has an equal number of neighbours of each fate, the accumulative signal received is half from cell-type 1 and half from cell-type 2. The remainder of the terms remain the same; $X_{1,1}$ only receives signals from cells of fate 2, and all internal signalling is conserved.

#### Steady States and Linear Stability Analysis

Similarly to the system of 2 cells with $n$ components, this multicellular system (2.3.4) has steady states given by

$$\begin{aligned}
\underline{X}^*_{i,j} &= (X^*_{1,1}, X^*_{2,1}, \dots, X^*_{n,1}, X^*_{1,2}, X^*_{2,2}, \dots, X^*_{n,2})\\
&= \left(X^*_{1,1}, \frac{1}{\mu_2} f_2(X^*_{1,1}), \dots, \frac{1}{\mu_n} g\left(\frac{1}{\mu_{n-1}} f_{n-1}\Big(\dots\Big(\frac{1}{\mu_2} f_2(X^*_{1,1})\Big)\dots\Big)\right),\right.\\
&\qquad \left. X^*_{1,2}, \frac{1}{\mu_2} f_2(X^*_{1,2}), \dots, \frac{1}{\mu_n} g\left(\frac{1}{\mu_{n-1}} f_{n-1}\Big(\dots\Big(\frac{1}{\mu_2} f_2(X^*_{1,2})\Big)\dots\Big)\right)\right).
\end{aligned} \tag{2.3.5}$$

and because $f_s \circ f_2 \circ \dots \circ f_{n-1} \circ g$ is a continuous monotonic decreasing function, there exists a single homogeneous steady state [HSS] when $X^*_{i,j} = X^*_{i,j} \equiv X^*_i$ for all $i$.

Consider perturbations to the HSS, such that $X_{i,j} = X^*_i + x_{i,j}$, for $i = 1, 2, \dots, n$, where $x_{i,j}$ are small. We then obtain the linearised system

$$\dot{\mathbf{x}} = A\mathbf{x},$$

where

$$\underline{x} = \begin{pmatrix} x_{1,1} \\ x_{1,2} \\ x_{2,1} \\ x_{2,2} \\ \vdots \\ x_{n,1} \\ x_{n,2} \end{pmatrix}, \tag{2.3.6}$$

$$A = \begin{bmatrix} -\mu_1 & 0 & 0 & 0 & \dots & 0 & 0 & 0 & \phi_s \\ 0 & -\mu_1 & 0 & 0 & \dots & 0 & 0 & \frac{\phi_s}{2} & \frac{\phi_s}{2} \\ \phi_2 & 0 & -\mu_2 & 0 & \dots & 0 & 0 & 0 & 0 \\ 0 & \phi_2 & 0 & -\mu_2 & \dots & 0 & 0 & 0 & 0 \\ \vdots & \vdots & \vdots & \vdots & \ddots & \vdots & \vdots & \vdots & \vdots \\ \vdots & \vdots & \vdots & \vdots & \ddots & \vdots & \vdots & \vdots & \vdots \\ 0 & 0 & 0 & 0 & \dots & -\gamma & 0 & -\mu_n & 0 \\ 0 & 0 & 0 & 0 & \dots & 0 & -\gamma & 0 & -\mu_n \end{bmatrix}, \tag{2.3.7}$$

where $\phi_s$, $\phi_p$ and $\gamma$ are previously defined in Section (2.1.1)

We again want to make a change of variables to the Mean and Difference variables, such that we can express the full $2n$-dimensional linearised system as two $n$-dimensional uncoupled systems. If we let

$$M_i \equiv x_{i,1} + 2x_{i,2}, \qquad D_i \equiv x_{i,2} - x_{i,2}.$$

This gives two sets of uncoupled equations:

$$\dot{\underline{M}} = J_M \, \underline{M} \tag{2.3.8}$$

where

$$\underline{M} = \begin{pmatrix} M_1 \\ M_2 \\ \vdots \\ M_n \end{pmatrix}, \tag{2.3.9}$$

and

$$J_M = \begin{bmatrix} -\mu_1 & 0 & \dots & 0 & 0 & \phi_s \\ \phi_2 & -\mu_2 & \dots & 0 & 0 & 0 \\ \vdots & \vdots & \ddots & \vdots & \vdots & \vdots \\ \vdots & \vdots & \ddots & \vdots & \vdots & \vdots \\ 0 & 0 & \dots & \phi_{n-1} & -\mu_{n-1} & 0 \\ 0 & 0 & \dots & 0 & -\gamma & -\mu_n \end{bmatrix}, \tag{2.3.10}$$

and

$$\underline{\dot{D}} = J_D \, \underline{D}, \tag{2.3.11}$$

where

$$\underline{D} = \begin{pmatrix} D_1 \\ D_2 \\ \vdots \\ D_n \end{pmatrix}, \tag{2.3.12}$$

and

$$J_D = \begin{bmatrix} -\mu_1 & 0 & \dots & 0 & 0 & -\frac{\phi_s}{2} \\ \phi_2 & -\mu_2 & \dots & 0 & 0 & 0 \\ \vdots & \vdots & \ddots & \vdots & \vdots & \vdots \\ \vdots & \vdots & \ddots & \vdots & \vdots & \vdots \\ 0 & 0 & \dots & \phi_{n-1} & -\mu_{n-1} & 0 \\ 0 & 0 & \dots & 0 & -\gamma & -\mu_n \end{bmatrix}. \tag{2.3.13}$$

The associated characteristic equations of (2.3.8) and (2.3.11) are

$$|J_M - \lambda_M I| = 0, \qquad |J_D - \lambda_D I| = 0,$$

which take the form

$$(-1)^n \prod_{i=1}^{n} (\mu_i + \lambda_M) + (-1)^n \, \phi_s \gamma \prod_{p=2}^{n-1} \phi_p = 0, \tag{2.3.14}$$

and

$$(-1)^n \prod_{i=1}^{n} (\mu_i + \lambda_D) + (-1)^{n+1} \frac{1}{2} \, \phi_s \gamma \prod_{p=2}^{n-1} \phi_p = 0, \tag{2.3.15}$$

respectively.

If $\mu_1 = \mu_2 = \cdots = \mu_n = \mu$, then these expressions simplify to

$$(\mu + \lambda_M)^n + \chi^n = 0, \tag{2.3.16}$$

and

$$(\mu + \lambda_D)^n - \frac{1}{2}\chi^n = 0, \tag{2.3.17}$$

where

$$\chi^n \equiv \phi_s \gamma \prod_{p=2}^{n-1} \phi_p.$$

**Bifurcation Conditions**

When comparing the characteristic equations for the Mean and Difference differential equations for 2 cells and this system, we find that for $\lambda_M$ these are identical ((2.1.15) and (2.3.14)), and for $\lambda_D$, the only difference is a multiple of 1/2 in the product of the gradients of the regulatory functions. Consequently, this makes finding the bifurcation conditions very straightforward. We will therefore just state the conditions for when both occur, with proofs being omitted.

There is a bifurcation which allows for switching when $\chi^n = 2\prod_{i=1}^{n}\mu_i$, and the HSS becomes unstable to perturbations out of the SoE if

$$\chi > \sqrt[n]{2\prod_{i=1}^{n}\mu_i}, \qquad \forall n, \tag{2.3.18}$$

and a Hopf bifurcation when

$$\chi > \sqrt[n]{\prod_{i=1}^{n}\mu_i} \qquad \forall\, n, \tag{2.3.19}$$

and

$$\sum_{i=1}^{n}\tan^{-1}\left(\frac{\omega}{\mu_i}\right) = \pi. \tag{2.3.20}$$

.

Similarly, if all degradation rates are the same, such that $\mu_i = \mu$, then these conditions simplify to

$$\chi > 2^{1/n}\mu, \tag{2.3.21}$$

and

$$\chi = \frac{\mu}{\cos(\frac{\pi}{n})}, \tag{2.3.22}$$

respectively.

Hence, the bifurcation for switching requires a greater $\chi$ for this system in comparison to the 2-cell case, but the Hopf bifurcation requires the same conditions.

### 2.3.2 Examples

$\underline{n = 3}$

When there are three components in each cell with equal degradation rates $\mu$, the whole array can be described using the system of equations

$$\begin{aligned}
\dot{X}_{1,1} &= -\mu X_{1,1} + f_s(X_{3,2}), & \dot{X}_{1,2} &= -\mu X_{1,2} + f_s\left(\frac{X_{3,1}}{2} + \frac{X_{3,2}}{2}\right),\\
\dot{X}_{2,1} &= -\mu X_{2,1} + f_2(X_{1,1}), & \dot{X}_{2,2} &= -\mu X_{2,2} + f_2(X_{1,2}),\\
\dot{X}_{3,1} &= -\mu X_{3,1} + g(X_{2,1}), & \dot{X}_{3,2} &= -\mu X_{3,2} + g(X_{2,2}).
\end{aligned} \tag{2.3.23}$$

Following linearisation about the HSS and making a change of variables, the uncoupled equations are

$$\begin{aligned} \dot{M}_1 &= -\mu M_1 + \phi_s M_3, & \dot{D}_1 &= -\mu D_1 - \frac{1}{2}\phi_s D_3, \\ \dot{M}_2 &= -\mu M_2 + \phi_2 M_1, & \dot{D}_2 &= -\mu D_2 + \phi_2 D_1, \\ \dot{M}_3 &= -\mu M_3 - \gamma M_2, & \dot{D}_3 &= -\mu D_3 - \gamma D_2, \end{aligned} \tag{2.3.24}$$

which have corresponding Jacobian matrices

$$J_M = \begin{bmatrix} -\mu & 0 & \phi_s \\ \phi_2 & -\mu & 0 \\ 0 & -\gamma & -\mu \end{bmatrix}, \qquad J_D = \begin{bmatrix} -\mu & 0 & -\frac{\phi_s}{2} \\ \phi_2 & -\mu & 0 \\ 0 & -\gamma & -\mu \end{bmatrix}. \tag{2.3.25}$$

The characteristic equation and resulting eigenvalues of $J_M$ are

$$-(\mu + \lambda_M)^3 - \phi_s \phi_2 \gamma = 0, \tag{2.3.26}$$

$$\begin{aligned} &\implies (\mu + \lambda_M)^3 = -\chi^3, \\ &\implies \lambda_M = -\mu + (-1)^{1/3}\chi \\ &\qquad\quad = -\mu + \mathrm{e}^{\frac{\pi i + k\pi i}{3}}\chi, \qquad \text{for } k = 0, 1, 2, \end{aligned} \tag{2.3.27}$$

and the characteristic equation and resulting eigenvalues of $J_D$ are

$$-(\mu + \lambda_D)^3 + \frac{1}{2}\phi_s \phi_2 \gamma = 0, \tag{2.3.28}$$

$$\begin{aligned} &\implies (\mu + \lambda_D)^3 = \frac{\chi^3}{2}, \\ &\implies \lambda_D = -\mu + 1^{1/3}\frac{\chi}{\sqrt[3]{2}} \\ &\qquad\quad = -\mu + e^{\frac{k\pi i}{3}}\frac{\chi}{\sqrt[3]{2}} \qquad \text{for } k = 0, 1, 2, \end{aligned} \tag{2.3.29}$$

where $\chi^3 = \phi_s \phi_2 \gamma$.

From (2.3.29), the $\lambda_D$ with the largest real part corresponds to $k = 0$;

$$\lambda_D = -\mu + \frac{\chi}{\sqrt[3]{2}}. \tag{2.3.30}$$

Therefore, the system will have a bifurcation which allows for switching when $\chi = \sqrt[3]{2}\,\mu$, and the HSS becomes unstable to perturbations out of the SoE when

$$\chi > \sqrt[3]{2}\,\mu. \tag{2.3.31}$$

### 2.3.3 Delay Differential Equation Analysis

#### $m$ Components per cell

For an array of cells with periodic boundary conditions, each containing $m$ components, we can describe the dynamics of the whole population using the system of $2m$ delay differential equations:

$$\begin{aligned}
&\dot{Y}_{1,1} = -\mu_1 Y_{1,1} + f_s(Y_{m,2}(t-\tau_s)), && \dot{Y}_{1,2} = -\mu_1 Y_{1,2} + f_s\left(\frac{1}{2}\left(Y_{m,1}(t-\tau_s) + Y_{m,2}(t-\tau_s)\right)\right),\\
&\dot{Y}_{2,1} = -\mu_2 Y_{2,1} + f_2(Y_{1,1}(t-\tau_1)), && \dot{Y}_{2,2} = -\mu_2 Y_{2,2} + f_2(Y_{1,2}(t-\tau_1)),\\
&\quad\vdots && \quad\vdots\\
&\dot{Y}_{m,1} = -\mu_n X_{m,1} + g(Y_{m-1,1}(t-\tau_{m-1})), && \dot{Y}_{m,2} = -\mu_m Y_{m,2} + g(Y_{m-1,2}(t-\tau_{m-1}));
\end{aligned} \tag{2.3.32}$$

There exists a homogeneous steady state where $Y^*_{i,j} = \bar{Y}^*_{i,j} = Y^*_i \ \forall i$, and we can linearise about this point using small perturbations $y_{i,j}$, such that

$$Y_{i,j} = Y^*_i + y_{i,j}.$$

This gives the linearised system

$$\begin{aligned}
&\dot{y}_{1,1} = -\mu y_{1,1} + \phi_s y_{m,2}(t-\tau_s), && \dot{y}_{1,2} = -\mu y_{1,2} + \frac{1}{2}\phi_s(y_{m,1}(t-\tau_s) + y_{m,2}(t-\tau_s)),\\
&\dot{y}_{p,1} = -\mu y_{p,1} + \phi_p y_{p-1,1}(t-\tau_{p-1}), && \dot{y}_{p,2} = -\mu y_{p,2} + \phi_p y_{p-1,2}(t-\tau_{p-1}),\\
&\dot{y}_{m,1} = -\mu y_{m,1} - \gamma y_{m-1,1}(t-\tau_{m-1}), && \dot{y}_{m,2} = -\mu y_{m,2} - \gamma y_{m-1,2}(t-\tau_{m-1});
\end{aligned} \tag{2.3.33}$$

where $p = 2, 3, \ldots, m-1$.

Using the same method as the 2-cell model in Section 2.2.5, we must find the $m^{th}$ derivative for $y_{m,1}$ and $y_{m,2}$ (or any other pair of corresponding variables), and substitute the other equations of (2.3.33) into this $m^{th}$-order delay differential equation. We can then making a change of variables to the Mean and Difference variables, where

$$M \equiv y_{m,1} + 2y_{m,2}\ , \qquad D \equiv y_{m,1} - y_{m,2}, \tag{2.3.34}$$

and obtain $m^{th}$-order differential equations for $M$ and $D$. These are given by

$$\sum_{i=0}^{m} \binom{m}{i} M^{(m-i)} \mu^i = -\chi^m M(t-\tau), \tag{2.3.35}$$

and

$$\sum_{i=0}^{m} \binom{m}{i} D^{(m-i)} \mu^i = \frac{1}{2}\chi^m D(t-\tau), \tag{2.3.36}$$

where $M^{(m-i)}$ and $D^{(m-i)}$ refer to the $(m-i)^{th}$ derivatives of $M$ and $D$, and $\tau$ is the total delay in each cell.

We now look for solutions of the form $M(t) = C_M e^{\lambda_M t}$ and $D(t) = C_D e^{\lambda_D t}$. Substituting these expressions into (2.3.35) and (2.3.36) gives

$$C_M e^{\lambda_M t} \sum_{i=0}^{m} \binom{m}{i} \lambda_M^{m-i} \mu^i = -\chi^m C_M e^{\lambda_M t} e^{-\lambda_M \tau} \tag{2.3.37}$$

and

$$C_D e^{\lambda_D t} \sum_{i=0}^{m} \binom{m}{i} \lambda_D^{m-i} \mu^i = \frac{1}{2} \chi^m C_D e^{\lambda_D t} e^{-\lambda_D \tau} \tag{2.3.38}$$

Assuming $C_M e^{\lambda_M t} \neq 0$ and $C_D e^{\lambda_D t} \neq 0$, these reduce to

$$\begin{aligned} (\lambda_M + \mu)^m &= -\chi^m e^{-\lambda_M \tau}, \\ (\lambda_D + \mu)^m &= \frac{1}{2} \chi^m e^{-\lambda_D \tau}, \end{aligned} \tag{2.3.39}$$

respectively. In terms of $\lambda_M$ and $\lambda_D$;

$$\begin{aligned} \lambda_M &= -\mu + (-1)^{1/m} \chi e^{-\lambda_M \tau / m}, \\ \lambda_D &= -\mu + \left(\frac{1}{2}\right)^{1/m} \chi e^{-\lambda_D \tau / m}. \end{aligned} \tag{2.3.40}$$

Following the justification from previous analysis in Section (2.2.5), we want to take the $m^{th}$ root of $-1$ and $1/2$ which give the largest real parts. These are given by

$$\lambda_M = -\mu + \chi e^{(i\pi - \lambda_M \tau)/m}, \tag{2.3.41}$$

and

$$\lambda_D = -\mu + \frac{1}{\sqrt[m]{2}} \chi e^{-\lambda_D \tau / m}. \tag{2.3.42}$$

The system has a bifurcation which allows for switching when $\mathrm{Re}(\lambda_D) = 0$, where we assume $\lambda_D \in \mathbb{R}$. When $\lambda_D = 0$, (2.3.42) is simply

$$0 = -\mu + \frac{1}{\sqrt[m]{2}} \chi,$$

stating the HSS becomes unstable to perturbations out of the SoE when

$$\chi > \sqrt[m]{2}\, \mu. \tag{2.3.43}$$

A Hopf bifurcation can happen when $\lambda_M$ is purely imaginary; $\lambda_M = i\omega_M, \omega_M \in \mathbb{R}$. As we saw in the $n$-component ODE model, the conditions for a Hopf bifurcation remain the same as those in the 2-cell case, and therefore, we know that the system is capable of going through a Hopf bifurcation when

$$\chi > \mu, \tag{2.3.44}$$

and

$$\tau = \frac{\pi - m\tan^{-1}\left(\frac{\omega_M}{\mu}\right)}{\omega_M}. \tag{2.3.45}$$

However, if $m > 2$, then the conditions change, as they did for the 2-cell system. There exists a Hopf bifurcation for $m > 2$ if

$$\mu < \chi < \frac{\mu}{\cos\left(\frac{\pi}{m}\right)}, \tag{2.3.46}$$

and

$$\tau = \frac{\pi - m\tan^{-1}\left(\frac{\omega_M}{\mu}\right)}{\omega_M}, \tag{2.3.47}$$

or, when

$$\chi = \frac{\mu}{\cos\left(\frac{\pi}{m}\right)}. \tag{2.3.48}$$

## Example

### $m = 1$

We will not go through the analysis explicitly for this example, but just give the conditions for both the bifurcation for switching and a Hopf bifurcation.

Since there is only a single variable in each cell, from (2.3.43) we know that this system has a bifurcation which allows for switching when $\chi = \sqrt{2}\,\mu$, and the HSS is therefore unstable to perturbations out of the SoE when

$$\chi > \sqrt{2}\,\mu. \tag{2.3.49}$$

Similarly to the 2-cell case, the conditions for a Hopf bifurcation do not change, and they are therefore given by

$$\chi > \mu, \qquad \tau = \frac{\pi - \tan^{-1}\left(\frac{\omega_M}{\mu}\right)}{\omega_M}. \tag{2.3.50}$$

.

## Summary of Results for Cells on a Hexagonal Lattice

For a hexagonal array of cells each containing $k$ components, the system is capable of switching from homogeneity when

$$\chi > \sqrt[k]{2\prod_{i=1}^{k}\mu_i}, \tag{2.3.51}$$

where $\mu_i$ is the degradation rate of the $i^{th}$ component in each cell.

This result holds for both ODEs and DDEs and introduces the key difference between a 2-cell (or period-2) model and cells in a hexagonal lattice with a period-3 pattern.

With respect to Hopf bifurcations, the conditions are the same as for 2 cells in both ODE and DDE cases.

For ODEs, the system will go through a Hopf bifurcation when

$$\chi = \frac{\mu}{\cos(\pi/k)}, \tag{2.3.52}$$

for $k > 2$, where $\mu_i = \mu \forall\ i$.

For DDEs, the system will go through a Hopf bifurcation when

$$\chi \in \left(\mu, \frac{\mu}{\cos(\pi/k)}\right) \text{ and } \quad \tau = \frac{\pi - k\tan^{-1}\left(\frac{\omega_M}{\mu}\right)}{\omega_M}, \tag{2.3.53}$$

or, when

$$\chi = \frac{\mu}{\cos(\pi/k)}.$$

For both the ODE and DDE models, the bifurcation associated with switching is now dependent on the number of components per cell. The presence of $2^{1/k}$ in (2.3.51) now causes this bifurcation to move, which was always fixed at $\mu$ for a system of two cells (provided $\mu_i = \mu \forall\ i$). $\chi$ must be now be a factor of $2^{1/k}$ larger for a hexagonal lattice of cells with a period-3 pattern, than for two cells (or any system with period-2 patterning).

Assuming $\mu_i = \mu\ \forall i$, the two bifurcations for the ODE system are

$$\chi = \sqrt[k]{2}\mu\ , \qquad \chi = \frac{\mu}{\cos(\pi/k)}.$$

For two cells we found that the Hopf bifurcation tended towards the bifurcation for switching as $k \to \infty$. Now, however, we find that both tend towards $\mu$ as $k \to \infty$. Interestingly, $\frac{\mu}{\cos(\pi/k)} \to \mu$ faster than $\sqrt[k]{2}\mu \to \mu$, so for a large enough $k$ ($k \geq 8$), there can be

$$\chi \in \left(\frac{\mu}{\cos(\pi/k)}, \sqrt[k]{2}\,\mu\right), \tag{2.3.54}$$

such that the system has a Hopf bifurcation *before* switching from homogeneity is possible. This implies that the HSS remains stable to perturbations out of the SoE, but is now unstable to perturbations within the SoE.

For such parameters these systems are only capable of homogeneous dynamics. No matter how different the initial conditions may be, there only exists the one HSS fixed point surrounded by a stable periodic orbit in the SoE. Therefore, the states of all of the cells will all display stable, in-phase oscillations indefinitely.

For DDEs, we again have two bifurcations, given by (2.3.51) and (2.3.53). Due to the dependence of $\tau$ for a Hopf bifurcation, a large $k$ is no longer needed to change the order of bifurcations.

For example, let $k = 1$. Switching is now possible when $\chi > \sqrt{2}\,\mu$. If we let $\chi = \sqrt[4]{2}\,\mu$, then the bifurcation for switching does not exist, $\omega = (\sqrt{2}-1)^{1/2}\,\mu$. This implies

$$\begin{aligned}\tau &= \frac{\pi - \tan^{-1}\left((\sqrt{2}-1)^{1/2}\right)}{(\sqrt{2}-1)^{1/2}\,\mu} \\ &\simeq \frac{4}{\mu}.\end{aligned} \tag{2.3.55}$$

Therefore, provided there is a total delay of approximately $4/\mu$ per cell, A Hopf bifurcation can be achieved before switching is possible when there is only a single component per cell. Furthermore, this will hold for any $k$, with the required $\tau \to 0$ as $k \to \infty$.

## 2.4 Conclusions and Discussion

In this chapter, we have presented models for Delta-Notch mediated lateral inhibition for systems of two cells and for larger populations. We have provided an analytic comparison for the bifurcation conditions for systems governed by ordinary differential equations, and those governed by delay differential equations, highlighting the similarities and differences between each type of model.

For systems of two cells, or any larger population which can form a period-2 pattern of alternate cell-types, there always exists a bifurcation which allows for switching when $\chi$, the product of the gradients of the regulatory functions evaluated at the HSS is equal to the geometric mean of the cells' components' degradation rates. Therefore, the HSS is unstable to perturbations out of the SoE when

$$\chi > \sqrt[n]{\prod_{i=1}^{n} \mu_i}.$$

This holds for all systems who can exhibit a period-2 pattern, independent of whether there is a time delay in the governing equations.

For a population of cells on a hexagonal lattice, this system has the potential to form a period-3 pattern of alternate cell-types, such that the ratio between the two possible fates is $1:2$.

By using a method of reduction to model the dynamics of each cell-fate rather than each cell individually, assuming a spatially perfect pattern is formed across the whole lattice, the condition for when the system is capable of switching from homogeneity is now given by

$$\chi > \sqrt[n]{2\prod_{i=1}^{n}\mu_i},$$

where $\mu_i$ is the degradation rate for the $i_{th}$ component in each cell.

Again, this holds for all systems who can exhibit a period-3 pattern, independent of whether there is a time delay in the governing equations.

This therefore clearly demonstrates that the conditions for when switching is possible is dependent on the geometric structure and arrangement of the population. Additionally, it also shows that for any pattern of cell types with a ratio other that $1:1$, the condition for switching also depends on the number of components per cell.

To show how this idea could be extended to systems which show less, or no periodicity in the final pattern of cell types, whether due to an irregular lattice of cells or if cell movement is incorporated, we could use a mean field approach for formulating the governing differential equations.

From the conditions for lateral inhibition, we know that any type-1 cell will always only have type-2 cells as direct neighbours, and if the ratio of neighbouring cell types varies for type-2 cells throughout the array, then we can find the mean cell type neighbour ratio for type-2 cells to use in the governing equations.

So, for a population of cells each with $n$ components, where type-2 cells have neighbours of each cell type with a ratio of $\alpha:(1-\alpha)$, where $\alpha \in [0,1]$, the generalised form of the differential equations governing the cell-type dynamics are given by

$$\begin{aligned}
\dot{X}_{1,1} &= -\mu X_{1,1} + f_s(X_{n,2}), & \dot{X}_{1,2} &= -\mu X_{1,2} + f_s\left(\alpha X_{n,1} + (1-\alpha)X_{n,2}\right),\\
\dot{X}_{2,1} &= -\mu X_{2,1} + f_2(X_{1,1}), & \dot{X}_{2,2} &= -\mu X_{2,2} + f_2(X_{1,2}),\\
&\vdots & &\vdots\\
\dot{X}_{n,1} &= -\mu X_{n,1} + g(X_{n-1,1}), & \dot{X}_{n,2} &= -\mu X_{n,2} + g(X_{n-1,2}).
\end{aligned} \tag{2.4.1}$$

Following the same analysis as in Section 2.3.1, we find that this generalised model will be able to form a pattern of alternate cell types when

$$\chi > \sqrt[n]{\frac{1}{\alpha}\prod_{i=1}^{n}\mu_i}. \tag{2.4.2}$$

Hence, when the proportion of type-1 cells decreases, or we include fewer components per cell, this causes either $\alpha$ or $n$ to decrease, and a greater $\chi$ is required to satisfy this result.

For systems of $k$ cells with $n$ components per cell ($n \geq 3$), arranged in any geometry and governed by ordinary differential equations, the system will have a Hopf bifurcation when

$$\chi > \sqrt[n]{\prod_{i=1}^{n} \mu_i} \qquad \text{and} \qquad \sum_{i=1}^{n} \tan^{-1}\left(\frac{\omega}{\mu_j}\right) = \pi,$$

and if all degradation rates are equal. this condition simplifies to

$$\chi = \frac{\mu}{\cos(\pi/n)}.$$

If the system is governed by delay differential equations and there are either one or two components per cell, the conditions for a Hopf bifurcation are

$$\chi > \sqrt[n]{\prod_{i=1}^{n} \mu_i} \qquad \text{and} \qquad \tau = \frac{\pi - \sum_{i=1}^{n} \tan^{-1}\left(\frac{\omega}{\mu_j}\right)}{\omega},$$

and if $n \geq 3$, where the degradation rates are all equal, the conditions for a Hopf are either

$$\mu < \chi < \frac{\mu}{\cos(\pi/n)}, \qquad \tau = \frac{\pi - n\tan^{-1}\left(\frac{\omega}{\mu}\right)}{\omega},$$

or

$$\chi = \frac{\mu}{\cos(\pi/n)},$$

and a time delay is no longer required.

Hence, the conditions for a Hopf bifurcation are independent of the geometric structure of the system. Since the Hopf bifurcation is related to homogeneous dynamics and the stability of the HSS *in* the SoE, it is understandable that the conditions for a Hopf bifurcation are independent of geometry.

As previously discussed in the summary of results for cells on a hexagonal lattice, there is now a potential section of parameter space in which conditions for a Hopf bifurcation are met, but not for the bifurcation associated with switching. This suggests that the SoE is now a stable manifold and any perturbations out of the SoE will only result in the states of the cells returning to homogeneity. However, the HSS is now unstable within the

SoE, with the state of the system now being attracted by the surrounding stable periodic orbit.

Since this result has been assumed only from linear stability analysis of the HSS, we will check this claim numerically in the next chapter.

If we consider the system given by equations (2.4.1), where $n \geq 3$, the conditions for switching and a Hopf bifurcation are given by

$$\chi = \sqrt[n]{\frac{1}{\alpha}}\mu\,, \qquad \chi = \frac{\mu}{\cos(\pi/n)}.$$

Therefore, the conditions for a Hopf bifurcation can be met before the conditions for switching (with respect to $\chi$) if

$$\sqrt[n]{\frac{1}{\alpha}} > \frac{1}{\cos(\pi/n)}. \tag{2.4.3}$$

So, as the ratio of type-1 cells decrease, this causes $\alpha$ to decrease, and fewer components are needed to meet this condition.

The same claim can be made for delay differential equations, with an example given in the results for Section 2.3.3 . For a delay system, a large number of components is not required, due to the conditions for a Hopf bifurcation depending on both $\chi$ and $\tau$.

This chapter has provided a strong foundation for understanding not just the local dynamics of these systems, but also specifies the topology of phase space for each system.

Although this provides clear conditions for when different dynamics are possible in the full systems, this analysis cannot reliably tell us anything about the systems' temporal dynamics. This is something which we will address in the following chapter, in which we model these systems numerically.

In terms of the questions we proposed for this chapter specifically, we have shown that a Hopf bifurcation can indeed occur for systems governed by both ODEs and DDEs, but for the possibility of a Hopf bifurcation *without* a time delay, there must be at least three components per cell.

We have also shown that the bifurcation conditions for switching are dependent on the geometry of the system. However, the conditions for a Hopf bifurcation are independent of the geometry, and in some scenarios, there exists a section of parameter space in which the conditions for a Hopf bifurcation are met before those for switching (with respect to $\chi$). This is a unique result for lateral inhibition models, which we will explore further in the proceeding chapter.

# Chapter 3

# Global Dynamics of Systems Governed by Lateral Inhibition

The main focus of this chapter is to establish the global dynamics of the systems analysed in Chapter 2. We will simulate the systems governed by the sets of ODEs (2.1.38) and (2.1.44) in which each cell has either 2 or 3 variables, as well as the systems governed by the sets of DDEs (2.2.1) and (2.2.24), corresponding to each cell having either 1 or 2 variables.

In each case we will first confirm the results of the linear stability analysis from the previous chapter, and then investigate how the linear stability analysis can help predict the global dynamics of the systems, and how these dynamics depend on both the model parameters and the initial conditions of the system.

In Sections 3.1 and 3.2 we simulate systems of two cells governed by ODEs. We establish the dynamics in the SoE to verify the results from the previous chapter, before dissecting each model extensively. We are able to determine when these models behave the same, and more importantly, when they become different.

In Sections 3.3 and 3.4 we then simulate systems of two cells governed by DDEs. Following the same format, we show how the systems behave when in the SoE to verify the previous chapter's results. The focus of this section is to compare the dynamics of a system with a time delay and one without, to confirm that both are capable of displaying equivalent dynamics.

In Section 3.5 we will then study simulations for the multicellular systems. We will confirm the results from linear stability analysis, and then explore how different geometries and population sizes affect the pattern, and patterning times of the system.

We will begin with the systems governed by the ODEs (2.1.38) and (2.1.44).

## 3.1 Two cells governed by Ordinary Differential Equations

In Section 2.1 we found that there always exists a homogeneous steady state [HSS] in the Surface of Equivalence [SoE], and depending on the system's parameters, the HSS is either stable or unstable.

As discussed in Section 1.5, and demonstrated throughout Chapter 2, we know that when the HSS is unstable to perturbations out of the SoE, there exists a pair of inhomogeneous steady states, and for initial conditions out of the SoE, such that there exists an initial difference between the cells, the solution trajectory of the system will reach one of these two steady states.

If initial conditions are chosen such that the system starts on the SoE however, then the system will remain on the SoE for all time. Although this case cannot lead to switching, we do want to know if the dynamics observed on the SoE can affect the system's dynamics when using initial conditions very close to the SoE.

We want to therefore start by simulating the system with initial conditions on the SoE, illustrate the results of the linear stability analysis, and show how the number of variables per cell can affect the possible dynamics on the SoE.

### Notation and Parameters

As the primary motivation for this work is the Notch signalling pathway, we will change the notation from Chapter 2.

In the case of $n = 2$, where there are 4 variables $x_{1,1}$, $x_{1,2}$, $x_{2,1}$ and $x_{2,2}$ in total, we will refer to $x_{1,1}$, $x_{1,2}$ as $N_1$ and $N_2$ to represent the corresponding level of the cells' Notch activity, and $x_{2,1}$, $x_{2,2}$ as $D_1$ and $D_2$, to represent the corresponding levels of the cells' Delta activity.

The $n = 2$ system is now represented by the ODEs:

$$\begin{aligned} \dot{N}_1 &= -\mu_N N_1 + f_s(D_2), & \dot{N}_2 &= -\mu_N N_2 + f_s(D_1) \\ \dot{D}_1 &= -\mu_D D_1 + g(N_1), & \dot{D}_2 &= -\mu_D D_2 + g(N_2). \end{aligned} \tag{3.1.1}$$

A motif of this system is illustrated in Figure 3.1.

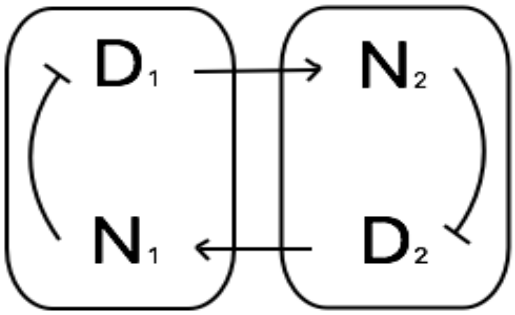


Figure 3.1: A network motif to represent the system described by (3.1.1).
→ corresponds to a positive regulatory function;
⊣ corresponds to a negative regulatory function.

Similarly for $n = 3$, we now have 6 variables in total. In this case we want the first and last variables in each cell to represent Notch and Delta, and we now want the middle variable to represent the level of the cells' Hes activity. Hence, we will use $N_1$ and $N_2$ instead of $x_{1,1}$ and $x_{1,2}$, $H_1$ and $H_2$ instead of $x_{2,1}$ and $x_{2,2}$, and $D_1$ and $D_2$ instead of $x_{3,1}$ and $x_{3,2}$.

The $n = 3$ system is now represented by the ODEs:

$$\begin{aligned} \dot{N}_1 &= -\mu_N N_1 + f_s(D_2), & \dot{N}_2 &= -\mu_N N_2 + f_s(D_1) \\ \dot{H}_1 &= -\mu_H H_1 + f_2(N_1), & \dot{H}_2 &= -\mu_H H_2 + f_2(N_2) \\ \dot{D}_1 &= -\mu_D D_1 + g(H_1), & \dot{D}_2 &= -\mu_D D_2 + g(H_2). \end{aligned} \tag{3.1.2}$$

A motif of this system is illustrated in Figure 3.2.

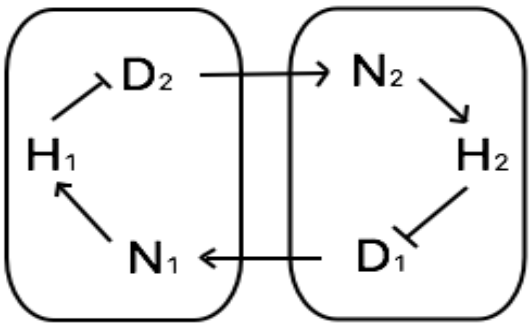


Figure 3.2: A network motif to represent the system described by (3.1.2).
→ corresponds to a positive regulatory function;
⊣ corresponds to a negative regulatory function.

**Definition 3.1.1.** For both systems, where applicable, we can make a change of variables

to the Mean and Difference variables $\underline{M}$ and $\underline{\Delta}$, where

$$M_N \equiv \frac{N_1 + N_2}{2}, \qquad M_H \equiv \frac{H_1 + H_2}{2}, \qquad M_D \equiv \frac{D_1 + D_2}{2} \tag{3.1.3}$$

and

$$\Delta_N \equiv \frac{N_1 - N_2}{2}, \qquad \Delta_H \equiv \frac{H_1 - H_2}{2}, \qquad \Delta_D \equiv \frac{D_1 - D_2}{2}. \tag{3.1.4}$$

For the regulation functions $f_s$, $f_2$ and $g$, we will be using the Hill functions

$$f_s(x) = \frac{x^{n_s}}{\theta_s^{n_s} + x^{n_s}}, \qquad f_2(x) = \frac{x^{n_2}}{\theta_2^{n_2} + x^{n_2}}, \qquad g(x) = \frac{1}{1 + (x/\theta_g)^{n_g}}, \tag{3.1.5}$$

where $n_s$, $n_2$, $n_g \geq 1$ are the 'sensitivities' or Hill coefficients of the functions, and $\theta_s$, $\theta_2$, $\theta_g > 0$ are the thresholds of the functions.

Typical $f$ and $g$ functions are shown in Figure 3.3, demonstrating how $n$ and $\theta$ change the form of the function.

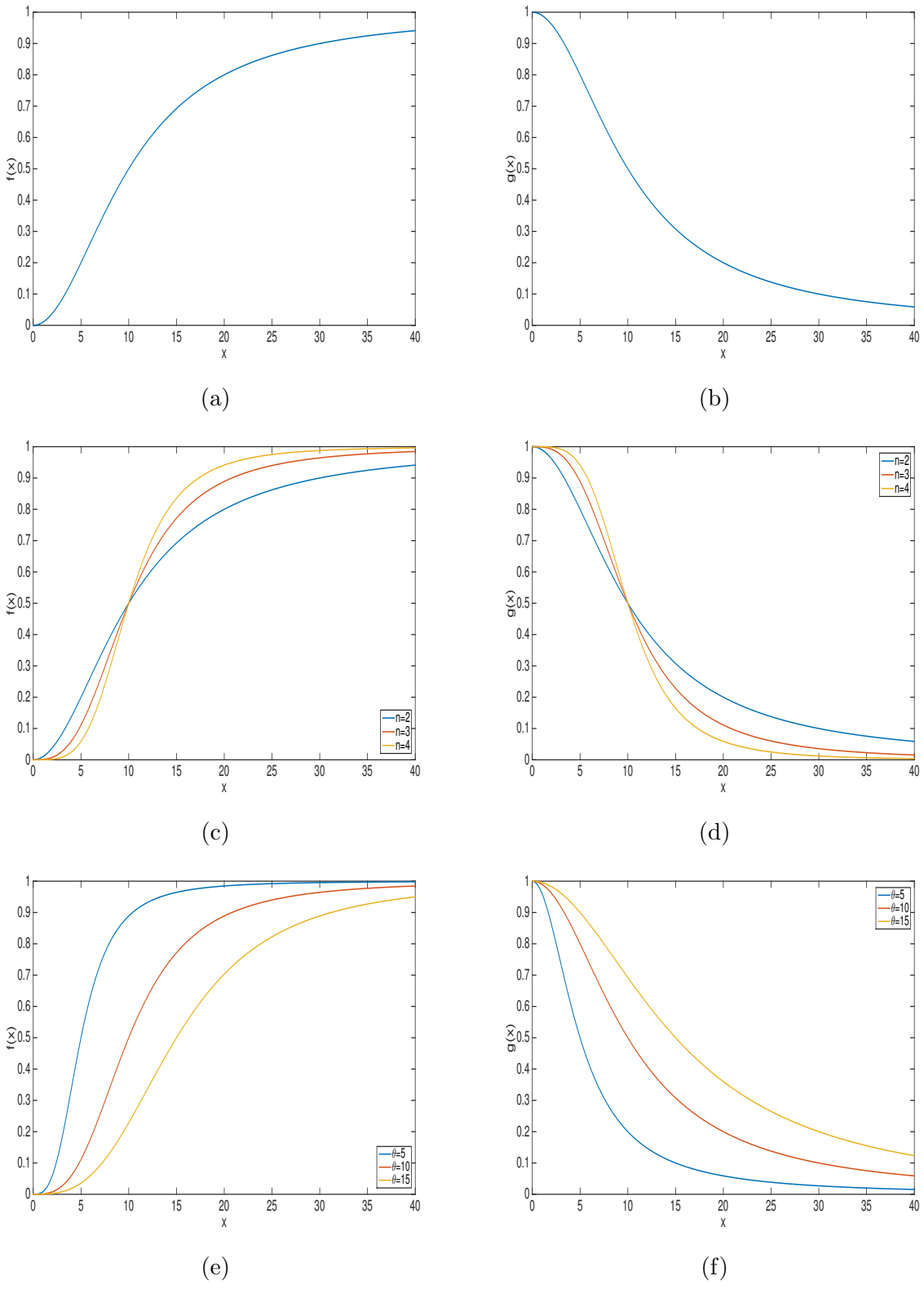


Figure 3.3: Examples of positive and negative regulatory functions described by (3.1.5), showing the effects of changing the parameters $n$ and $\theta$. (a) f(x), $n = 2$, $\theta = 10$; (b) g(x), $n = 2$, $\theta = 10$; (c) f(x), $n = 2, 3, 4$, $\theta = 10$; (d) g(x), $n = 2, 3, 4$, $\theta = 10$; (e) f(x), $n = 2$, $\theta = 5, 10, 15$; (f) g(x), $n = 2$, $\theta = 5, 10, 15$.

**Simulation Parameters**

The results in the remainder of this Section were obtained using the parameters

$$\begin{aligned}
&\mu_N = \mu_D = \mu = 0.03\text{min}^{-1}, \\
&\theta_s = \theta_g = \frac{0.2}{\mu}\text{min}, \\
&n_g = 2,
\end{aligned} \tag{3.1.6}$$

for $n = 2$, and

$$\begin{aligned}
&\mu_N = \mu_H = \mu_D = \mu = 0.03\text{min}^{-1}, \\
&\theta_s = \theta_2 = \theta_g = \frac{0.2}{\mu}\text{min}, \\
&n_2 = 2,\ n_g = 3,
\end{aligned} \tag{3.1.7}$$

for $n = 3$.

The time units are in minutes and degradation rates of $0.03\text{min}^{-1}$ correspond to half-lives of $\sim$ 22 minutes. Here, half-life does not refer to the molecular half-life in the conventional sense, but rather the half-lives of the level of activity for each variable in the cell. These have been inspired by the work in Hes1 in mouse [68]. However, other $\mu$ can also be used.

Since $\max(N) = 1/\mu_N$, $\max(H) = 1/\mu_H$, $\max(D) = 1/\mu_D$, we are using thresholds such that they are $0.2\times$ the maximum activity level of each variable. This ensures the threshold is in a sensible range, without relying on large Hill coefficients to enable switching. Similar values have been used in other studies [48, 69, 70].

For both $n = 2$ and $n = 3$, we will use the parameter $n_s$ to control $\chi$, which governs the feedback strength in the signalling pathway, and in turn, the system's stability.

$\chi$ is defined as the product of the gradients of the regulatory functions evaluated at the HSS, so, if $n = 2$ for example, then

$$\begin{aligned}
&f_s(D) = \frac{D^{n_s}}{\theta_s^{n_s} + D^{n_s}}, \\
&\implies \phi_s = f_s'(D*) = \frac{(\theta_s^{n_s} + D^{n_s}) n_s D*^{n_s-1} - D*^{n_s} n_s D*^{n_s-1}}{(\theta_s^{n_s} + D*^{n_s})^2} \\
&\qquad\qquad = \frac{n_s \theta_s^{n_s} D*^{n_s-1}}{(\theta_s^{n_s} + D*^{n_s})^2}
\end{aligned} \tag{3.1.8}$$

Similarly,

$$\begin{aligned}
&g(N) = \frac{1}{1 + \left(\frac{N}{\theta_g}\right)^{n_g}} \\
&\implies \gamma = -g'(N*) = \frac{n_g N*^{n_g-1} (\frac{1}{\theta_g})^{n_g}}{\left(1 + \left(\frac{N}{\theta_g}\right)^{n_g}\right)^2} = \frac{n_g \theta_g^{n_g} N*^{n_g-1}}{(\theta_g^{n_g} + N*^{n_g})^2}
\end{aligned} \tag{3.1.9}$$

and so,

$$\begin{aligned}\chi &= \phi_s \gamma \\ &= \frac{\left(n_s \theta_s^{n_s} D*^{n_s-1}\right)\left(n_g \theta_g^{n_g} N*^{n_g-1}\right)}{\left(\theta_s^{n_s} + D*^{n_s}\right)^2 \left(\theta_g^{n_g} + N*^{n_g}\right)^2}\end{aligned} \tag{3.1.10}$$

is a function of the Hill coefficient $n_s$.

Evidently, we can use any of the Hill coefficients or thresholds to control $\chi$, but for consistency we will use $n_s$ throughout.

$\chi$ as a function of $n_s$ is shown in Figure 3.4 for $n = 2$ and $n = 3$ to illustrate how $\chi$ varies with $n_s$.

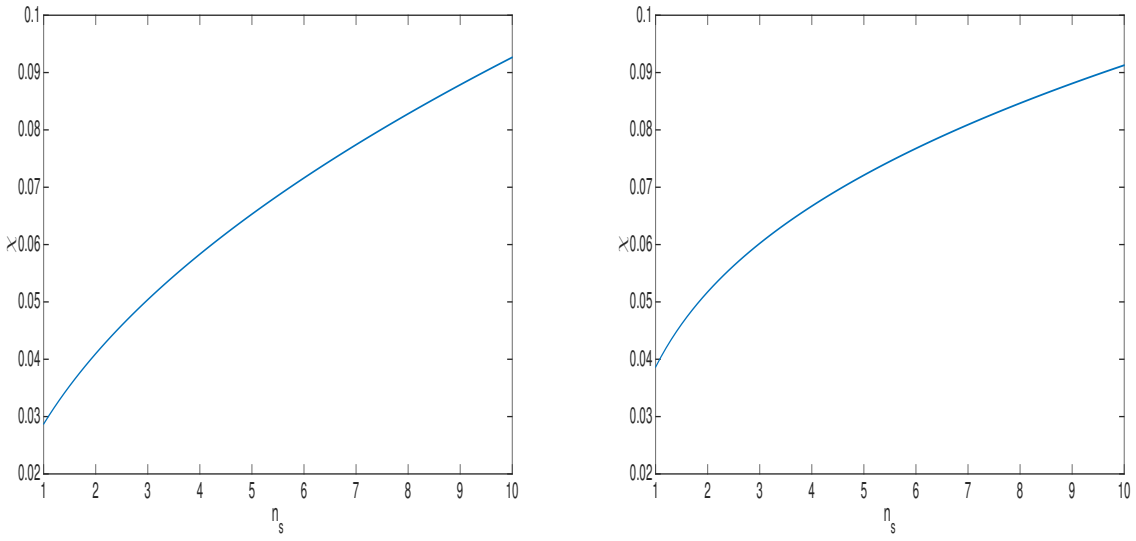


(a) (b)

Figure 3.4: $\chi$ as a function of the Hill coefficient $n_s$, in the cases (a) Two variables per cell, using default parameters (3.1.6); (b) Three variables per cell, using default parameters (3.1.7).

The following simulations have been solved using a variable step Runge-Kutta method, implemented by ode45 in Matlab. The tolerances used are the default values, unless stated otherwise.

### 3.1.1 Surface of Equivalence Dynamics

We first want to show the dynamics in the SoE, in which both cells have identical states. We therefore choose initial conditions, such that $N_1(0) = N_2(0)$, $D_1(0) = D_2(0)$ for $n = 2$, and $N_1(0) = N_2(0)$ , $H_1(0) = H_2(0)$, $D_1(0) = D_2(0)$ for $n = 3$. This ensures that the corresponding variables in each cell remain the same for all $t > 0$.

$\underline{n = 2}$

From the linear stability analysis in Chapter 2, we know that the HSS will remain stable in the SoE for all parameter choices and $\mu$ values, but the nature of this stable fixed point can change.

- If $\mu_N - \mu_D < 2\chi$, the HSS is a stable spiral;
- If $\mu_N - \mu_D \geq 2\chi$, the HSS is a stabe node.

The SoE dynamics for $\mu_N = \mu_D$ are shown in Figure 3.3, for different values of $\chi$. The initial conditions are randomly chosen points in the SoE, such that

$$N_1(0), N_2(0), D_1(0), D_2(0) \in (0, 30)\,,$$

where $N_1(0) = N_2(0)$, $D_1(0) = D_2(0)$.

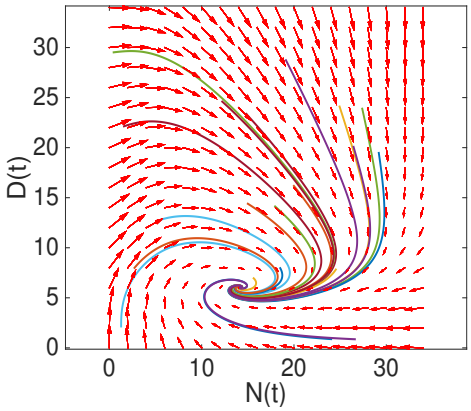


(a)

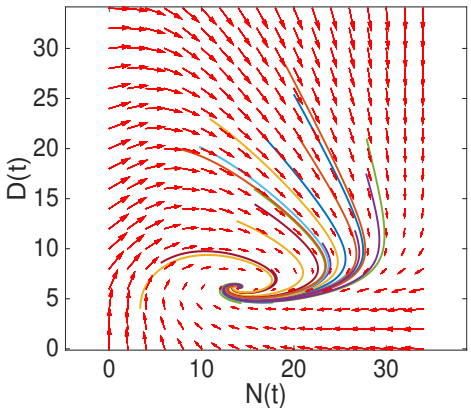


(b)

Figure 3.5: Solution trajectories of the system (3.1.1) using default parameters (3.1.6) and initial conditions such that $N_1(0), N_2(0), D_1(0), D_2(0) \in (0, 30)$, and $N_1(0) = N_2(0)$, $D_1(0) = D_2(0)$, when (a) $n_s = 2$; (b) $n_s = 3$. Both show the HSS as a stable spiral, and as $n_s$ increases, the rate at which solution trajectories approach the HSS also increase.

As $\chi$ is increased we find the infall rate - the rate at which solution trajectories approach the HSS - increases with $\chi$, which reduces the time taken to reach the HSS. This is further illustrated in Figure 3.6, showing the Notch values over time for various $n_s$ values.

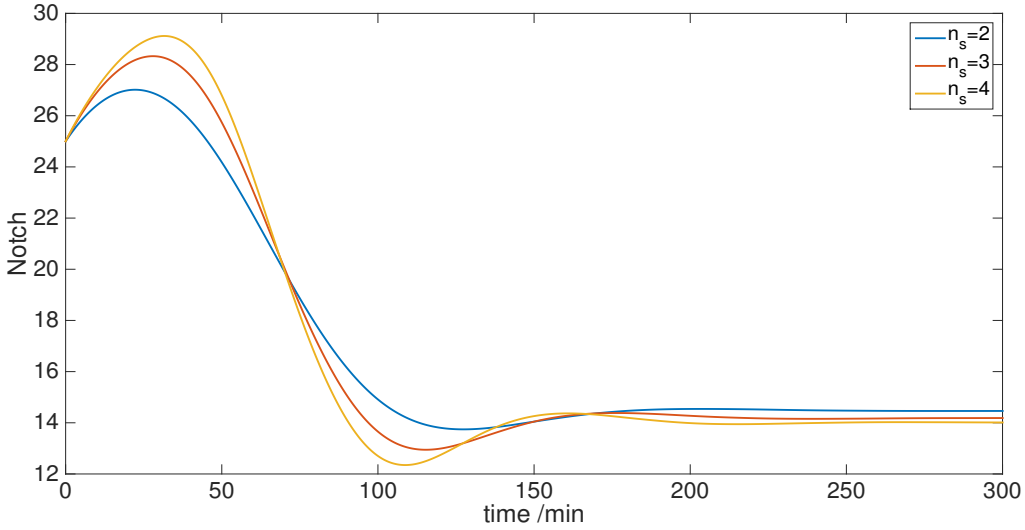


Figure 3.6: Notch dynamics for both cells when using default parameters (3.1.6) and initial conditions such that $N_1(0) = N_2(0)$, $D_1(0) = D_2(0)$, with $n_s = 2,\ 3,\ 4$ ( $\chi = 0.041,\ 0.0504,\ 0.0583$, respectively). As $n_s$ increases, so does the rate of approach to the HSS.

The SoE dynamics for $\mu_N \neq \mu_D$, where $\mu_N = 0.1\ \text{min}^{-1}$ and $\mu_D = 0.03\ \text{min}^{-1}$ are illustrated in Figure 3.7. If $n_s = 2$, then $\chi = 0.0165$, and as expected from the linear stability analysis, the HSS is a stable node.

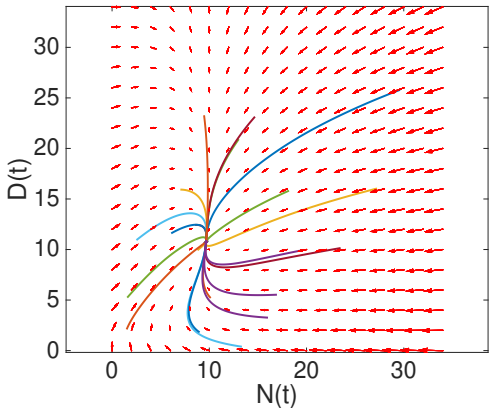


Figure 3.7: Solution trajectories of the system (3.1.1) using default parameters (3.1.6), except $\mu_N = 0.1\ \text{min}^{-1}$. Here, $n_s = 2$, such that $\chi = 0.0165$. Since $\mu_N - \mu_D \geq 2\chi$, the HSS is a stable node.

$\underline{n = 3}$

For $n \geq 3$ it is possible for the HSS to become unstable in the SoE, due to a Hopf bifurcation. Therefore, we want to show the SoE dynamics about this bifurcation point.

Assuming that $\mu_N = \mu_H = \mu_D = \mu$, then linear stability analysis tells us that a Hopf bifurcation exists when

$$\chi = \frac{\mu}{\cos\left(\frac{\pi}{n}\right)} = 2\mu.$$

For our default parameters, a Hopf bifurcation exists when $n_s = 3$, which has a corresponding $\chi = 0.0601$. By running simulations with $n_s = 2, 3, 4$, ($\chi = 0.0518,\ 0.0601,\ 0.0667$, respectively), we can observe what happens to the dynamics as $\chi$ increases, shown in Figure 3.8.

We have again used initial conditions such that they are randomly chosen points on the SoE;

$$N_1(0), N_2(0), H_1(0), H_2(0), D_1(0), D_2(0) \in (0, 30)\,,$$

where $N_1(0) = N_2(0),\ H_1(0) = H_2(0),\ D_1(0) = D_2(0)$.

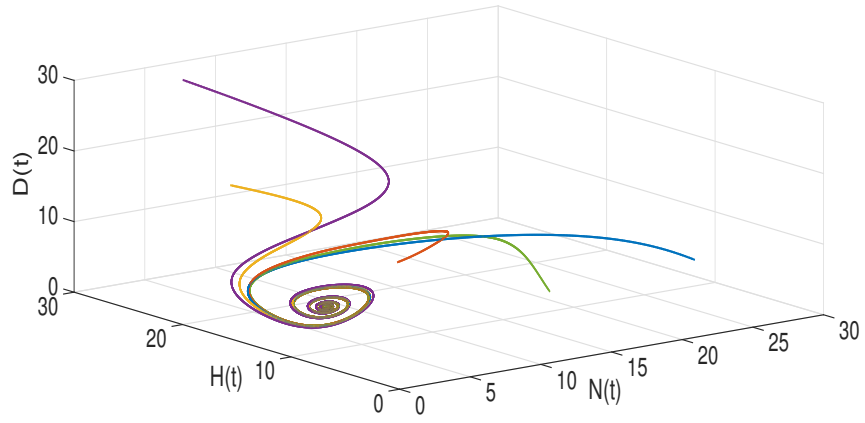


(a)

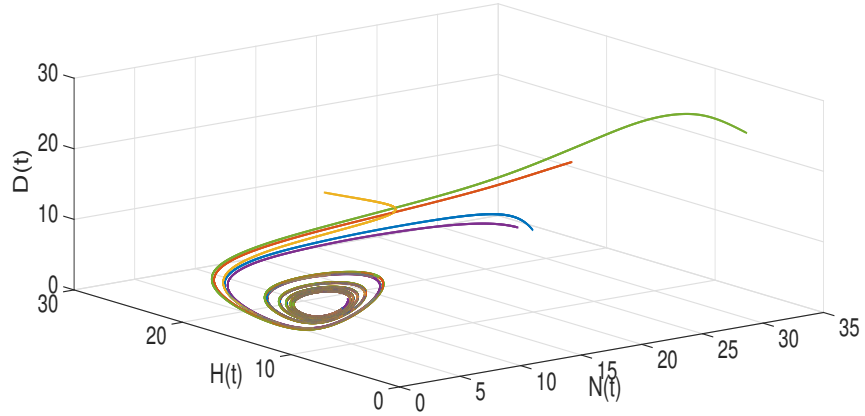


(b)

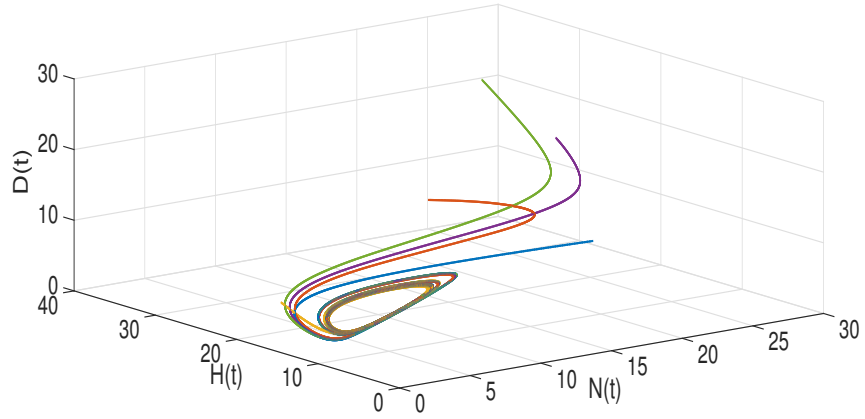


(c)

Figure 3.8: Solution trajectories of the system (3.1.2) using default parameters (3.1.7) and initial conditions such that $N_1(0), N_2(0), H_1(0), H_2(0), D_1(0), D_2(0) \in (0, 30)$, where $N_1(0) = N_2(0)$, $H_1(0) = H_2(0)$, $D_1(0) = D_2(0)$.
(a) $n_s = 2$ and the HSS is a stable spiral; (b) $n_s = 3$ and the HSS becomes an unstable spiral surrounded by a stable periodic orbit; (c) $n_s = 4$, and the periodic orbit surrounding the HSS becomes larger in amplitude and period.

Confirming the linear stability analysis results;

- When $\chi < \frac{\mu}{\cos(\frac{\pi}{n})}$, the HSS is a stable spiral-node;
- When $\chi \geq \frac{\mu}{\cos(\frac{\pi}{n})}$, the HSS is an unstable spiral-saddle, surrounded by a stable periodic orbit.

Additionally, we estimated a period of oscillation at the Hopf bifurcation of

$$T = \frac{2\pi}{\sqrt{3}\,\mu}\text{min},$$

which corresponds to a period $T = 120.9$ min when $\mu = 0.03$ min$^{-1}$. This is confirmed numerically, with simulations showing oscillations in the levels of N, H and D activity with a period of 121.1 min.

There is a stable periodic orbit for all values of $\chi \geq 2\mu$, with both the amplitude and period of oscillation increasing functions of $\chi$.

### 3.1.2 Dynamics of the Full System

Now that we have explored the dynamics when the systems are restricted to the SoE subspace, we want to investigate the behaviour when using initial conditions out of the SoE.

However, we will first give two definitions which will be referred to regularly.

**Definition 3.1.2.** The total difference between cells 1 and 2 is defined as the magnitude of the difference variables:

$$\Delta X(t) \equiv \sqrt{\Delta_N(t)^2 + \Delta_D(t)^2}, \qquad \text{when } n = 2, \tag{3.1.11}$$

$$\Delta X(t) \equiv \sqrt{\Delta_N(t)^2 + \Delta_H(t)^2 + \Delta_D(t)^2}, \qquad \text{when } n = 3. \tag{3.1.12}$$

**Definition 3.1.3.** Time to Switch [TtS] is defined as the time at which the total difference between the cells reaches 80% of the maximum total difference;

$$\Delta X(TtS) \equiv 0.8 \times \max(\Delta X(t)). \tag{3.1.13}$$

**Initial Conditions**

The following results for $n = 2$ and $n = 3$ have used initial conditions of the following form:

$$\underline{X}(0) = \text{SoEP} + \zeta \underline{P}, \tag{3.1.14}$$

where SoEP refers to a position on the Surface of Equivalence, and $\zeta \underline{P}$ is the perturbation out of the SoE from that point. This allows us to think of the initial conditions in the

full system as perturbations from the SoE, which will be useful when determining if the SoE dynamics affect the dynamics of the full system.

We have chosen two sets of initial conditions, A and B, such that they are perturbations from different positions on the SoE. Initial Conditions A have an SoEP at the HSS, and Initial Conditions B have an SoEP at $\underline{0.5}$, such that each variable has a value of 0.5. In this way we are able to confirm the linear stability analysis using initial conditions A, and establish the effects of the SoE dynamics on the full system when using initial conditions B.

0.5 has been chosen for ICB simply because it is not near the HSS, and similar results are obtained if we use a different SoEP, provided it is not in the vicinity of the HSS.

The initial conditions can therefore be defined by

$$\begin{aligned} \text{A} &\equiv \text{HSS} + \zeta \underline{P}, \\ \text{B} &\equiv \underline{0.5} + \zeta \underline{P}. \end{aligned} \tag{3.1.15}$$

The magnitude of perturbation $\zeta \in [10^{-6}, 10^{-1}]$. This ensures the states of each cell start close to the SoE, and by varying $\zeta$ this can show whether the initial distance from the SoE can affect the systems' dynamics.

Unless stated otherwise, the direction of perturbation will be

$$\underline{P} = \begin{pmatrix} 1 \\ -1 \\ -1 \\ 1 \end{pmatrix}, \quad \text{for n=2,} \qquad \underline{P} = \begin{pmatrix} 1 \\ -1 \\ 1 \\ -1 \\ -1 \\ 1 \end{pmatrix}, \quad \text{for n=3.} \tag{3.1.16}$$

We have used this direction such that the perturbation causes the variable levels to differ equally around the HSS, or any other SoE position we are perturbing from. It may be that if we were only looking at perturbations from the HSS we would want to use a perturbation relative to the final possible steady states, but since we are looking at different locations on the SoE, this allows for a more objective comparison between the different initial conditions.

## 3.2 Results for $n = 2$

- **When $\chi < \mu$, the HSS is stable, and is the only steady state of the system.**

To illustrate this point we have used $n_s = 1$, which gives $\chi = 0.0287$ ($< \mu$). Initial conditions are not of the form A or B, and we instead let $N_1(0), N_2(0), D_1(0), D_2(0) \in (0, 34)$, such that the system starts anywhere in the full 4-dimensional space.

The time-courses for the Notch and Delta levels in each cell, for 5 different simulations each with different random initial conditions, are shown in Figure 3.9.

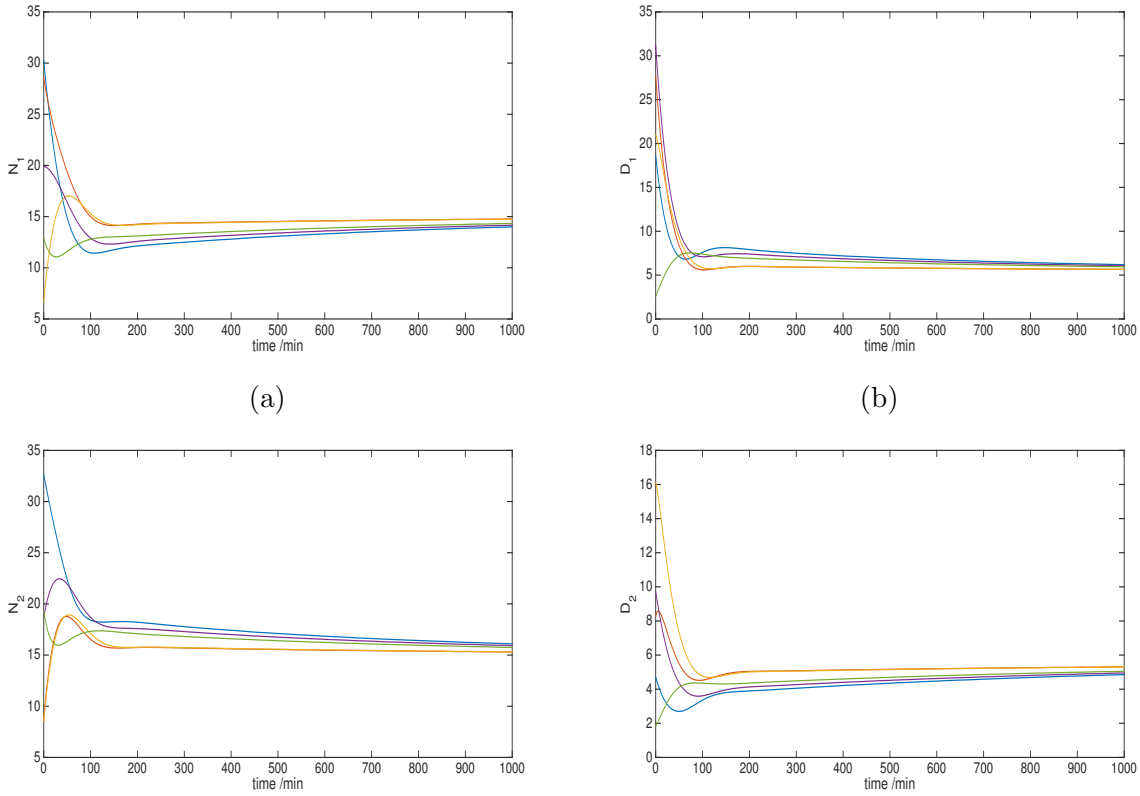


Figure 3.9: The levels of Notch and Delta activity for the system described by (3.1.2), using default parameters (3.1.7) with $n_s = 1$ ($\chi = 0.0287$), and initial conditions such that $N_1(0), N_2(0), D_1(0), D_2(0) \in (0, 34)$. Evidently, the system only has one steady state.

This result does hold; the HSS is stable and the only steady state of the system. For any initial conditions, the system will always finish at the HSS, with the states of the cells equal to one another.

- **The system has a bifurcation which allows for switching when $\chi = \mu$, and for $\chi > \mu$ there exist 3 steady states. The HSS becomes a saddle-type, unstable to perturbations out of the SoE, and the system is now bistable.**

**Switching Times and their dependence on $\chi$ and initial conditions**

i For a given set of initial conditions, TtS reduces as a function of $\chi$;

ii For a given value of $\chi$, TtS reduces as a function of $\zeta$, for either set of initial conditions;

iii Increasing $\zeta$ by an order of magnitude will give a fixed decrease in the TtS, for either set of initial conditions;

iv There is little change in TtS between initial conditions A and B, for a given value of $\chi$ and $\zeta$.

**i** To show that the switching times are a decreasing function of $\chi$ for a given initial condition, Figure 3.10 shows the corresponding Notch and Delta time-courses for both cells, and how their dynamics change with $\chi$, whilst Figure 3.11 illustrates TtS as a function of $\chi$:

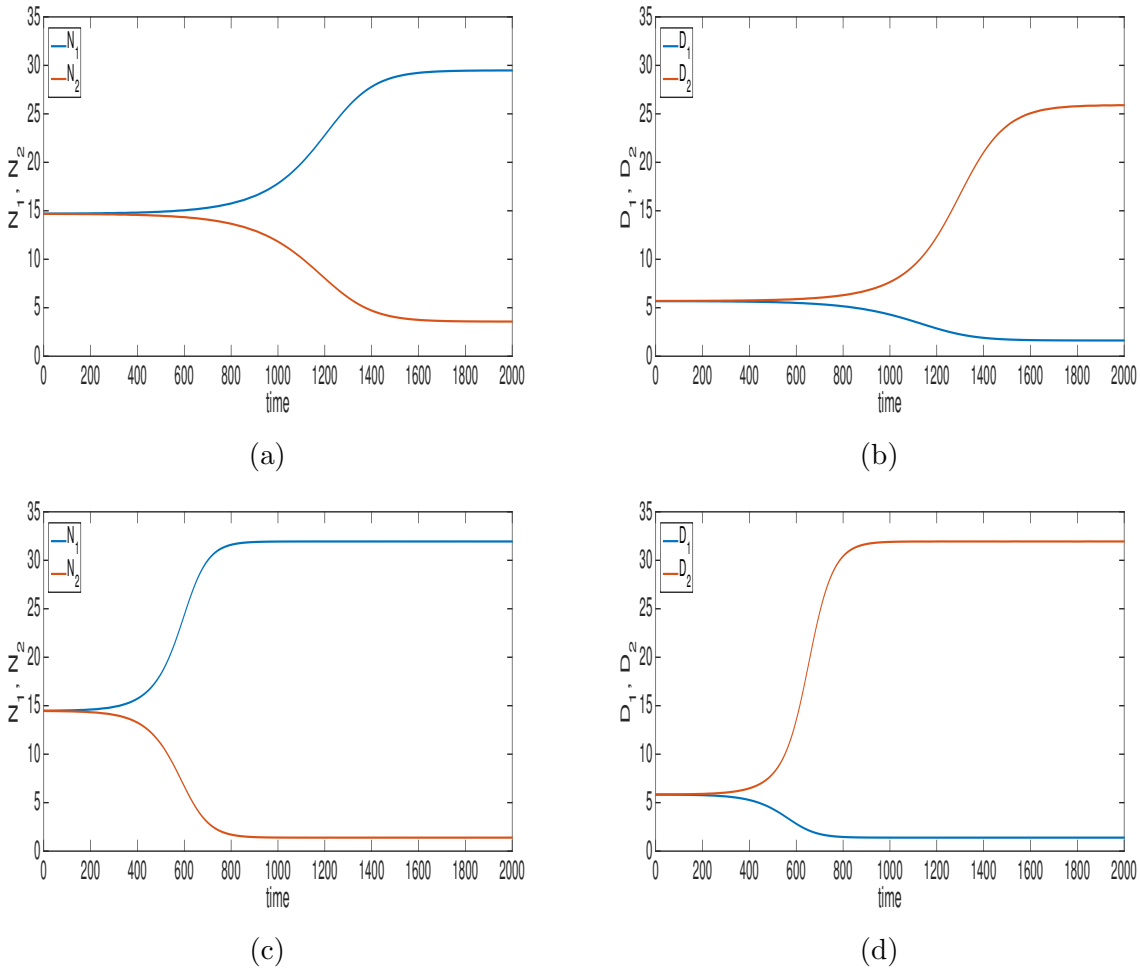


Figure 3.10: The levels of Notch and Delta activity in each cell for the system described by (3.1.1), using default parameters (3.1.6) and initial conditions A with $\zeta = 10^{-2}$.
(a) $N_1(t)$, $N_2(t)$ when $n_s = 1$ ($\chi = 0.0350$); (b) $D_1(t)$, $D_2(t)$ when $n_s = 1$ ($\chi = 0.0350$); (c) $N_1(t)$, $N_2(t)$ when $n_s = 2$ ($\chi = 0.041$); (d) $D_1(t)$, $D_2(t)$ when $n_s = 2$ ($\chi = 0.041$). As $n_s$ is increased, the states of the cells diverge from homogeneity both sooner and at a faster rate.

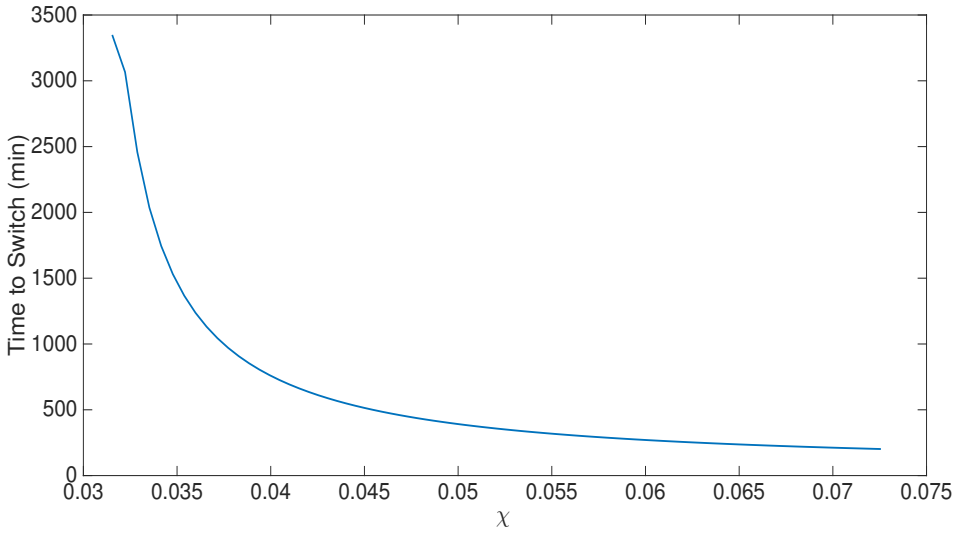


Figure 3.11: Time to Switch as a function of $\chi$ for the system (3.1.1), using default parameters (3.1.6) and initial conditions A with $\zeta = 10^{-2}$. Time to Switch is a continuously decreasing function of $\chi$.

**ii** By plotting TtS($\chi$) when varying $\zeta$ in the initial conditions, this shows that TtS is a decreasing function of $\zeta$ for a given value of $\chi$, and holds for both sets of initial conditions. It is evident that for a given $\zeta$, using either set of initial conditions gives a very similar relationship between TtS and $\chi$, but we will show this explicitly momentarily.

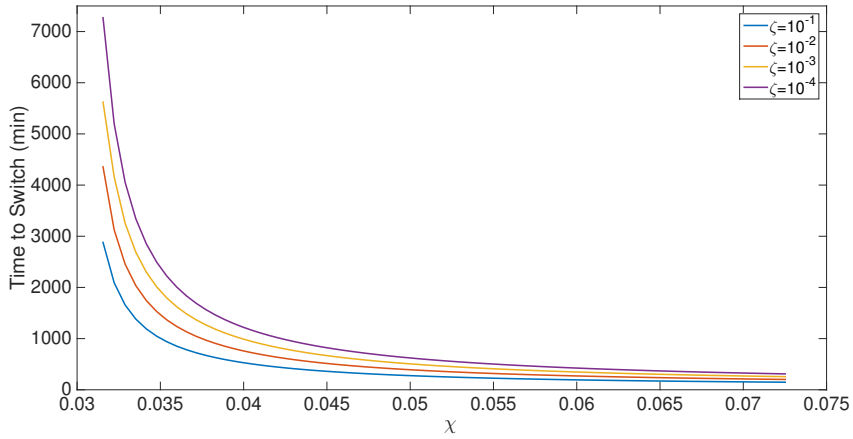


(a)

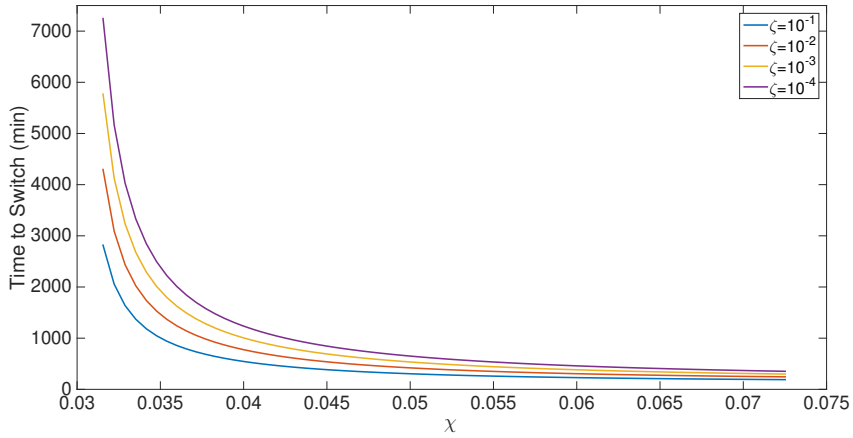


(b)

Figure 3.12: Time to Switch as a function of $\chi$ for the system (3.1.1), using default parameters (3.1.6), with (a) initial conditions A with $\zeta = 10^{-2}$; (b) initial conditions B with $\zeta = 10^{-2}$. For both sets of initial conditions, TtS is a decreasing function of $\chi$, with very little difference between the switching times for each set of initial conditions.

**iii** If TtS = $T^*$ when using initial conditions with $\zeta = 10^{-n}$, then TtS = $T^* + k$ when $\zeta = 10^{-n+1}$, and TtS = $T^* + 2k$ when $\zeta = 10^{-n+2}$, for $k \in \mathbb{R}$, where $k$ is a decreasing function of $\chi$.

This is already shown in Figure 3.12 for both sets of initial conditions, but the result is illustrated well when we plot the Notch and Delta time-courses for increasing values of $\zeta$:

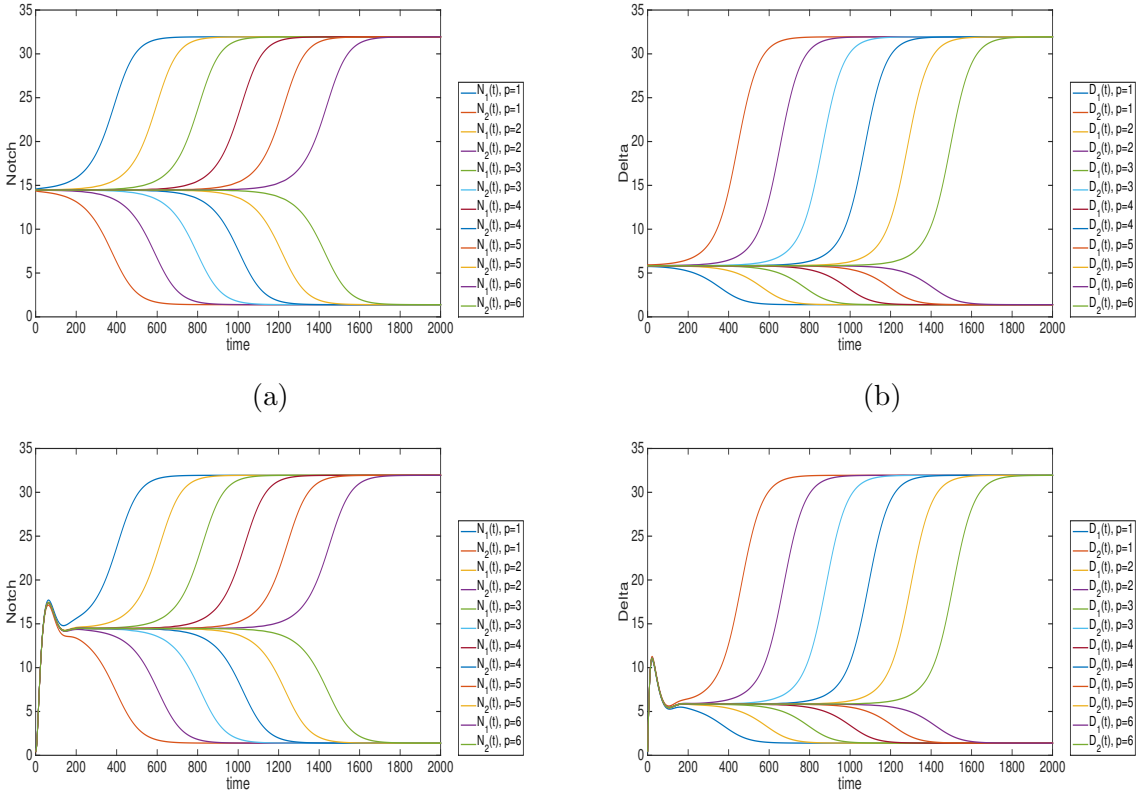


Figure 3.13: Levels of Notch and Delta activity in both cells for the system (3.1.1) using default parameters (3.1.6) with $n_s = 2$. For each set of initial conditions, $\zeta$ is varied, such that $\zeta = 10^{-p}$, for $p = 1, 2, \ldots, 6$. (a) N(t), initial conditions A; (b) D(t), initial conditions A; (c) N(t), initial conditions B; (d) D(t), initial conditions B.

**iv** It is evident from Figure 3.12 that there is little change in TtS for each set of initial conditions for a specific value of $\zeta$, but to show the result explicitly, Figure 3.14 is TtS as a function of $\chi$ for each set of initial conditions, both with $\zeta = 10^{-2}$.

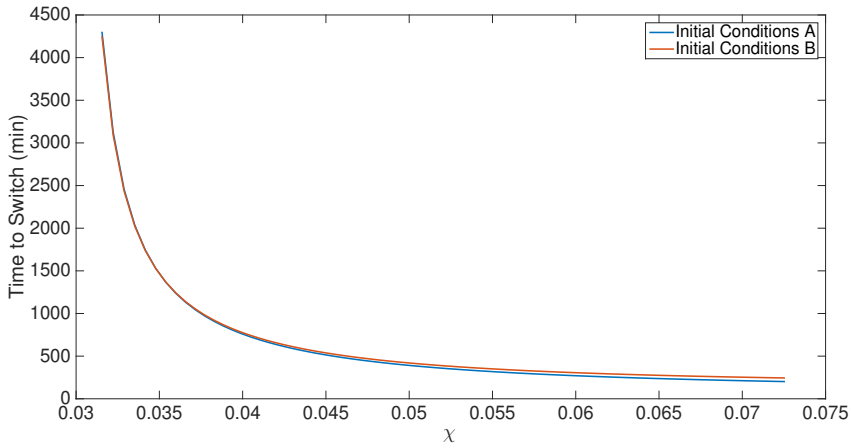


Figure 3.14: Time to Switch as a function of $\chi$ for the system (3.1.1) for both sets of initial conditions A and B with $\zeta = 10^{-2}$, using default parameters (3.1.6).

The fact that TtS decreases linearly when increasing the order of magnitude of $\zeta$ allows us to make the following proposition:

**Proposition 3.2.1.** *The total difference between the two cells behaves like*

$$\Delta X(t) = \Delta X(0)\mathrm{e}^{Mt}, \quad M \in \mathbb{R}. \tag{3.2.1}$$

If this proposition is true, and TtS $= T^*$, then

$$\Delta X(T^*) = \Delta X(0)\mathrm{e}^{MT^*},$$

$$\implies M = \frac{1}{T^*}\ln\left(\frac{\Delta X(T^*)}{\Delta X(0)}\right). \tag{3.2.2}$$

Therefore, for each value of $\chi$ and $\zeta$, we can use the results of the numerical simulations to calculate $M$.

From this proposition, we expect $\ln(\Delta X(t)) = \ln(\Delta X(0)) + Mt$.

By plotting $\ln(\Delta X(t))$ for a given value of $\chi$ and various values of $\zeta$, we find that $M$ is a constant until the vicinity of the switched steady state, independent of $\zeta$, shown in Figure 3.15.

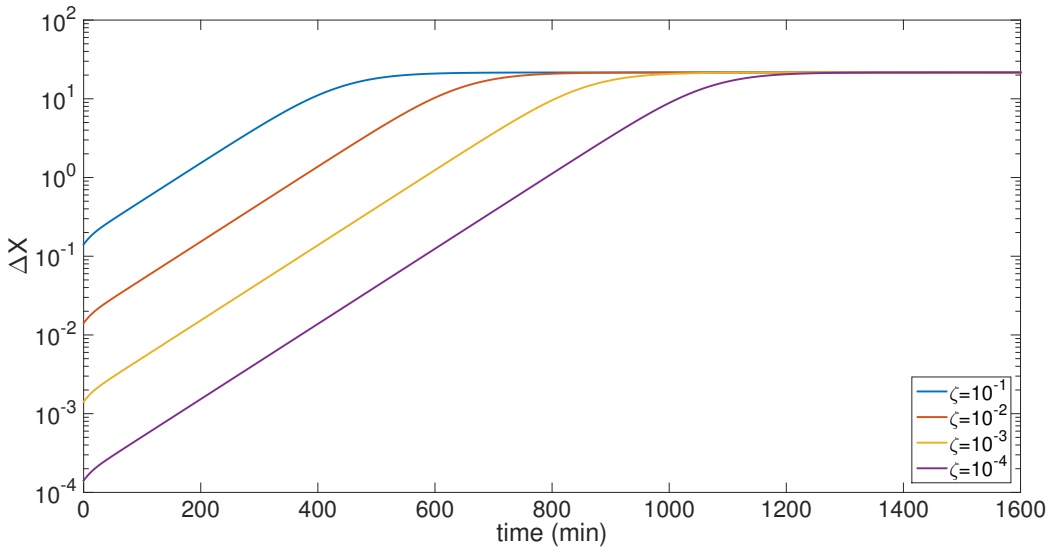


(a)

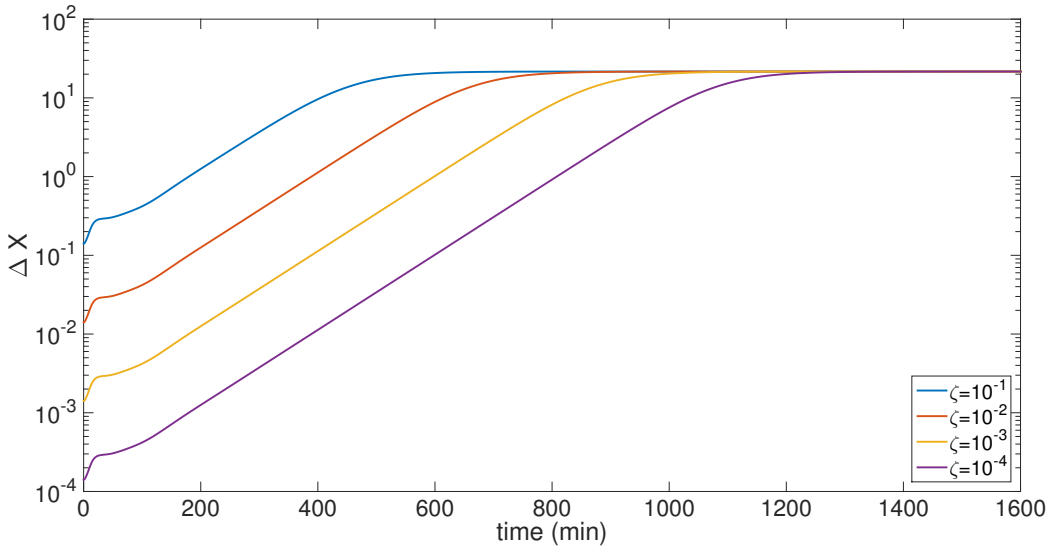


(b)

Figure 3.15: $\ln(\Delta X(t))$ for the system (3.1.1) using default parameters (3.1.6) with $n_s = 2$ ($\chi = 0.041$).
(a) Initial conditions A with various $\zeta$; (b) Initial conditions B with various $\zeta$. In both cases, $M$, the gradient of $\ln(\Delta X(t))$, is nearly constant until the vicinity of the switched steady state, independent of $\zeta$.

By plotting $\ln(\Delta X(t))$ for a fixed $\zeta$ and increasing values of $\chi$, we also find that $M$ is an increasing function of $\chi$, shown in Figure 3.16.

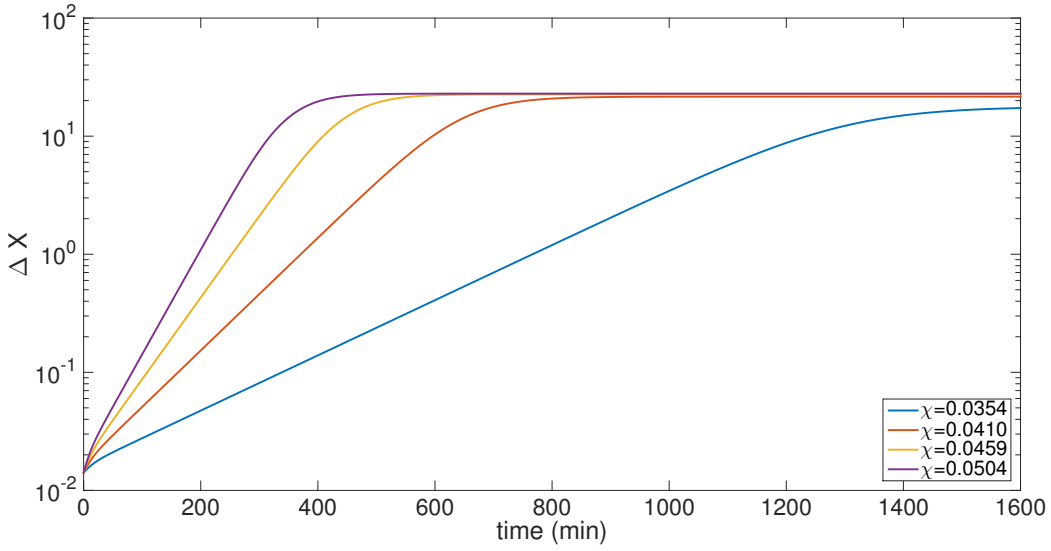


(a)

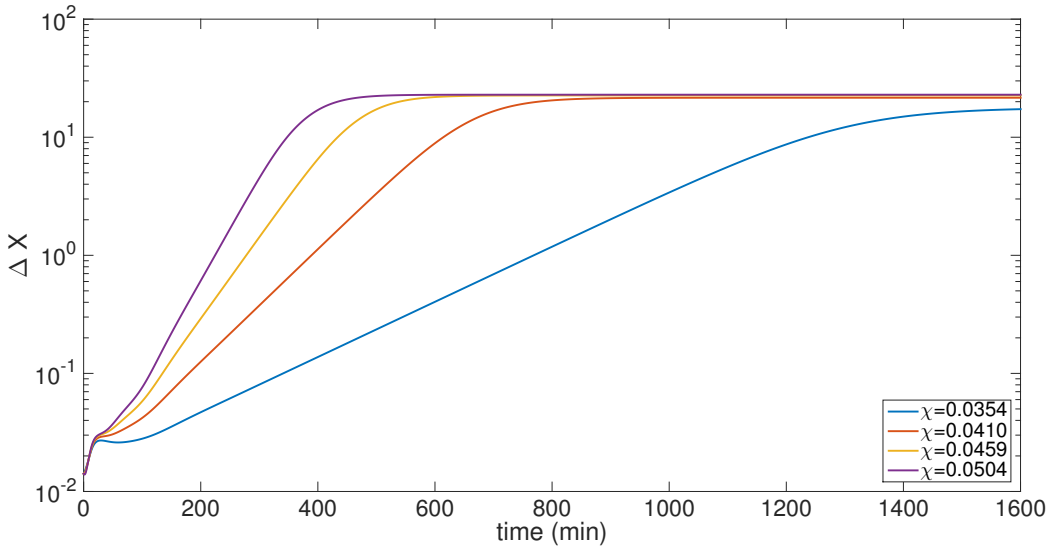


(b)

Figure 3.16: $\ln(\Delta X(t))$ for the system (3.1.1) using default parameters (3.1.6) with $n_s$ = 1.5, 2, 2.5, 3 ($\chi$ = 0.0354, 0.041, 0.0459, 0.0504, respectively).
(a) Initial conditions A with $\zeta = 10^{-2}$; (b) Initial conditions B with $\zeta = 10^{-2}$. In both cases, we see that $M$, the gradient of $\ln(\Delta X(t))$, is an increasing function of $\chi$.

**Proposition 3.2.2.** *As simulations show that* $\Delta X(t) = \Delta X(0)\mathrm{e}^{Mt}$ *nearly all the way to the switched steady state, and linear stability analysis shows that* $\Delta X(t) = \Delta X(0)\mathrm{e}^{\lambda_D t}$ *close to the HSS, we propose*

$$M = \lambda_D = \chi - \mu. \tag{3.2.3}$$

Using the expression in Proposition 3.2.1 to numerically calculate $M$ for each value of

$\chi$, we can plot $M(\chi)$ and $\lambda_D(\chi)$ to test this proposition. The result is shown in Figure 3.17 for both sets of initial conditions.

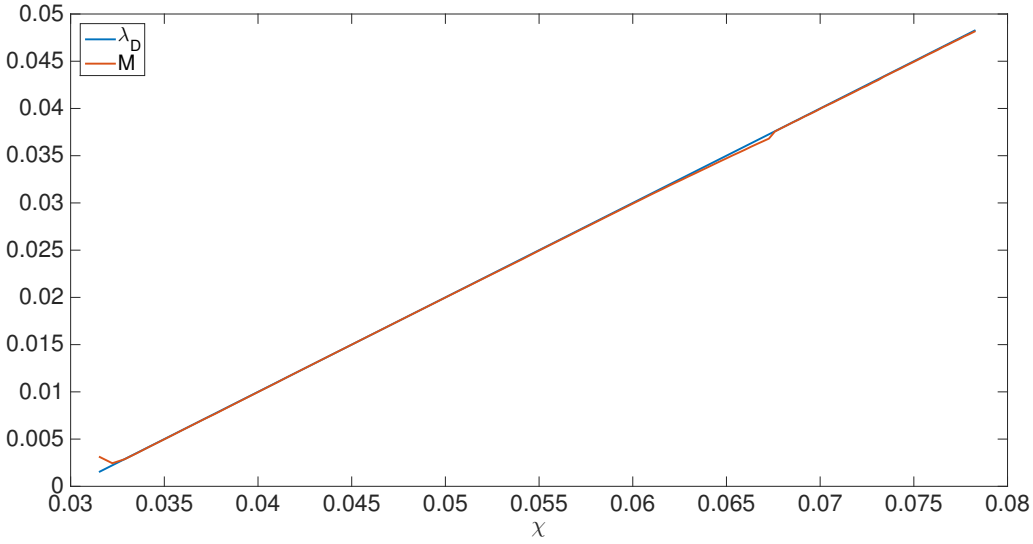


(a)

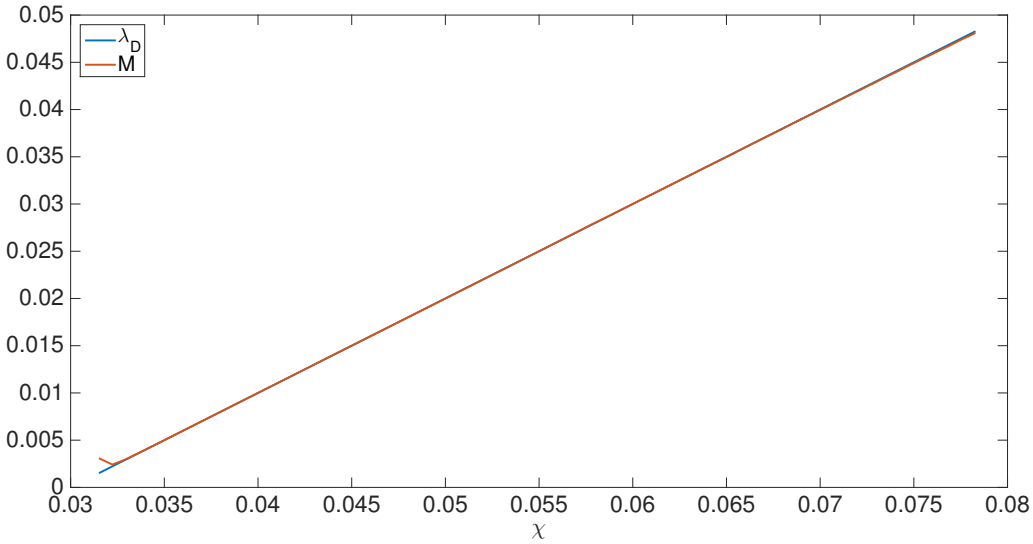


(b)

Figure 3.17: Comparison of $\lambda_D = \chi - \mu$ and calculated $M$ as functions of $\chi$ for the system (3.1.1). (a) Initial conditions A; (b) Initial conditions B. In both cases, $\lambda_D$ is highly accurate in predicting the growth rate of the difference between the two cells.

Evidently, Proposition 3.2.2 holds, and $M = \lambda_D \ \forall \chi > \mu$.

Therefore, not only does the linear stability analysis from the previous chapter hold, but $\lambda_D$ is highly accurate in predicting the growth of the difference between the cells all the way to the vicinity of the switched steady state.

## Results when $n = 3$

We will first show the results which closely follow those for $n = 2$, followed by results which are unique to $n = 3$.

**i** When $\chi < \mu$, the HSS is stable, and the only steady state of the system.

As we saw in Figure 3.9 for $n = 2$, the state of the system will always be attracted to the HSS for any initial conditions (Data not shown).

**ii** There exists a bifurcation when $\chi = \mu$, such that switching is possible when $\chi > \mu$.

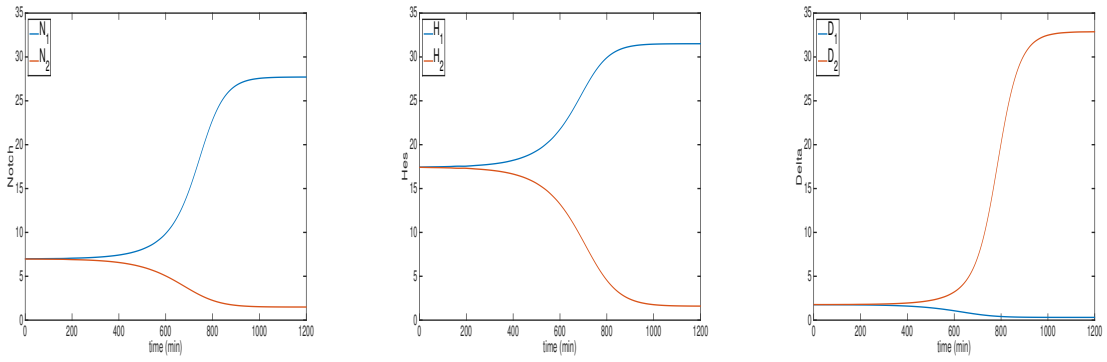


(a) (b) (c)

Figure 3.18: Solution for (3.1.2) using default parameters (3.1.7) with $n_s = 3$ ($\chi = 0.0601$), and initial conditions A with $\zeta = 10^{-2}$. Since $\chi > \mu$, the system is able to diverge from homogeneity to one of the switched steady states.

**iii** For initial conditions A, all TtS results hold regarding $\chi$, $\zeta$ relationships:

When we use initial conditions A, the temporal dynamics behave the same as the $n = 2$ case, regardless of the dynamics in the SoE. We find that:

- Time to Switch is a decreasing function of $\chi$;
- For a given $\chi$, TtS reduces as a function of $\zeta$;
- Increasing $\zeta$ by an order of magnitude gives a fixed decrease in the TtS;

The results are illustrated in Figures 3.19 to 3.21, accordingly.

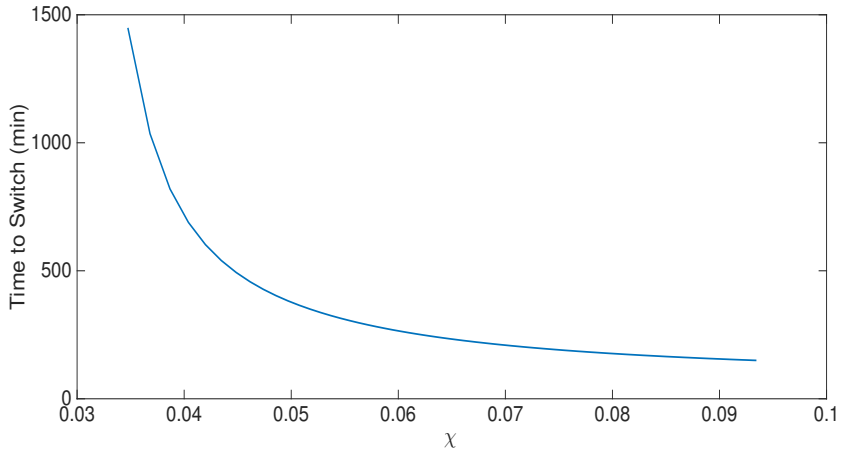


Figure 3.19: TtS as a function of $\chi$ for the system (3.1.2), using default parameters (3.1.7) and initial conditions A with $\zeta = 10^{-2}$. For this set of initial conditions, TtS is a continuously decreasing function of $\chi$.

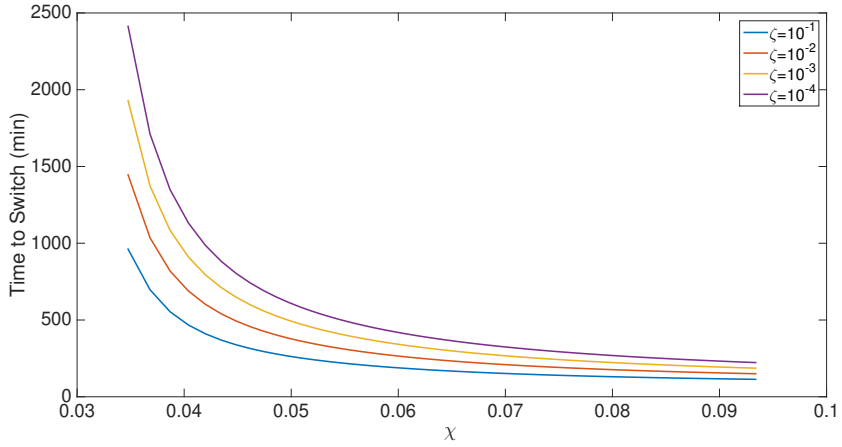


Figure 3.20: TtS as a function of $\chi$ for the system (3.1.2), using default parameters (3.1.7) and initial conditions A with various $\zeta$. TtS is a continuously decreasing function of $\chi$, and for a given value of $\chi$, TtS is a decreasing function of $\zeta$.

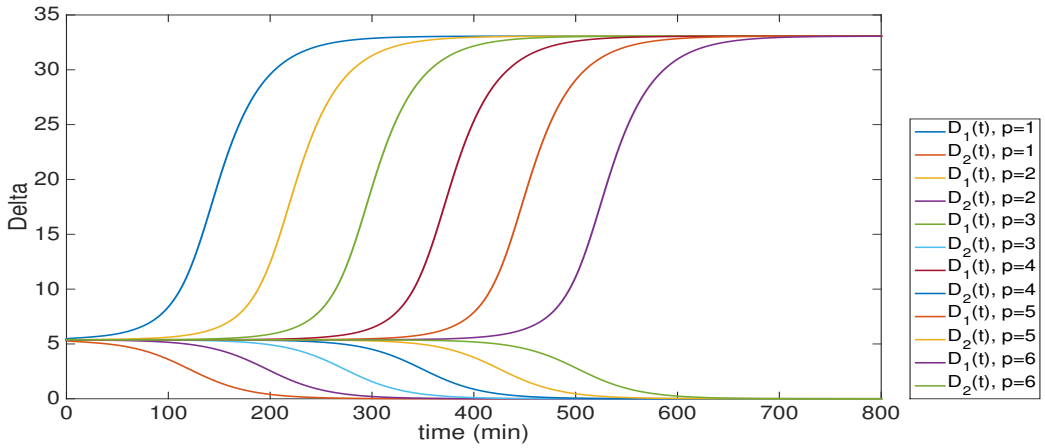


Figure 3.21: The levels of Delta activity in both cells for system (3.1.2), using default parameters (3.1.7) with $n_s = 3$ ($\chi = 0.0601$), and initial conditions A with $\zeta = 10^{-p}$, $p = 1, 2, \ldots 6$.

Since the dynamics do match so closely to the $n = 2$ model, we can assume that Proposition 3.2.1 holds for initial conditions A. To clarify:

**Proposition 3.2.3.** *For initial conditions in the vicinity of the HSS, the total difference between the cells behaves like*

$$\Delta X(t) = \Delta X(0) e^{Mt}, \quad M \in \mathbb{R}. \tag{3.2.4}$$

By plotting $\ln(\Delta X(t))$ for a given value of $\chi$ and various values of $\zeta$, we find that $M$ is a constant until the vicinity of the switched steady state, independent of $\zeta$, shown in Figure 3.22.

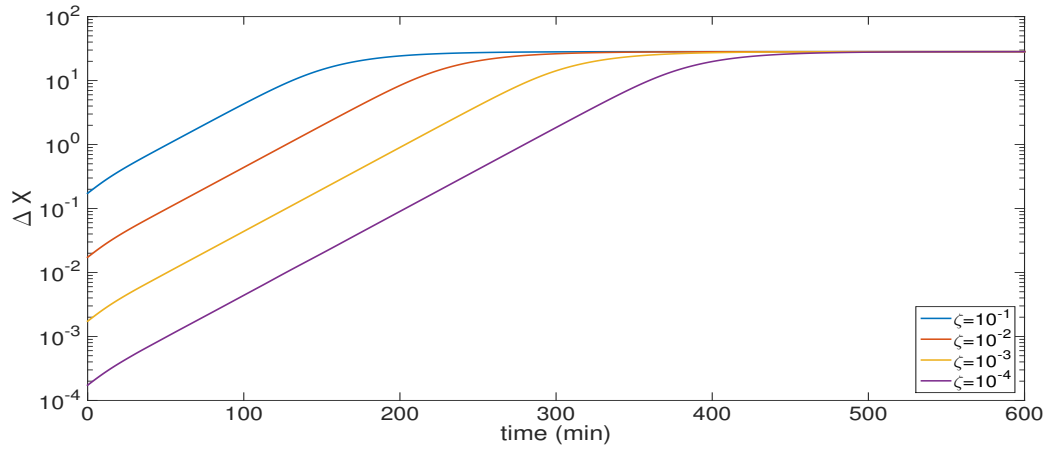


Figure 3.22: $\ln(\Delta X(t))$ for the system (3.1.2), using default parameters (3.1.7) with $n_s = 3$ ($\chi = 0.0601$), and initial conditions A with various $\zeta$. We see that $M$, the gradient of $\ln(\Delta X(t))$, is nearly constant until the switched steady state, independent of $\zeta$.

By plotting $\ln(\Delta X(t))$ for a fixed $\zeta$ and increasing values of $\chi$, we also find that $M$ is an increasing function of $\chi$, shown in Figure 3.23.

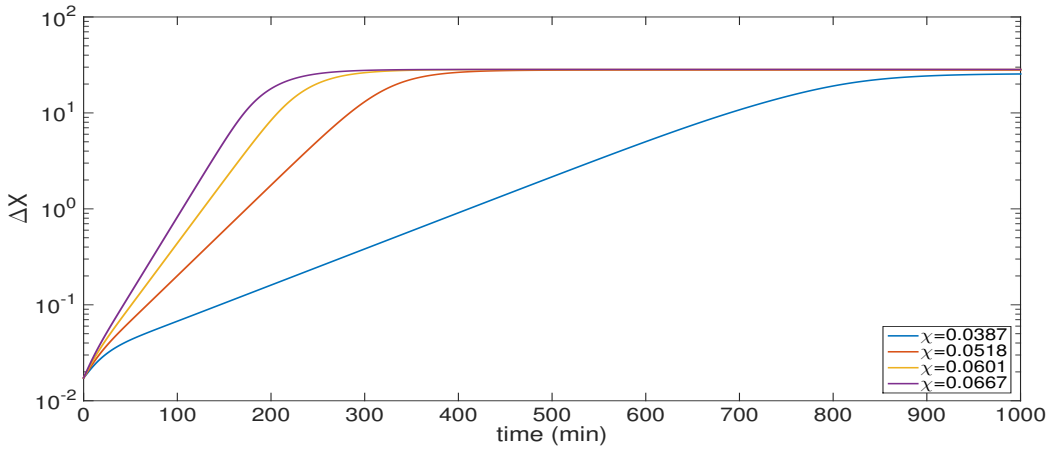


Figure 3.23: $\ln(\Delta X(t))$ for the system (3.1.2) using default parameters (3.1.7) with $n_s$ = 1.5, 2, 3, 4 ($\chi$ = 0.0387, 0.0518, 0.0601, 0.0667, respectively), and initial conditions A with $\zeta = 10^{-2}$. We see that $M$, the gradient of $\ln(\Delta X(t))$, is an increasing function of $\chi$.

**Proposition 3.2.4.** *As simulations show that* $\Delta X(t) = \Delta X(0)e^{Mt}$ *for initial conditions A, and linear stability analysis shows that* $\Delta X(t) = \Delta X(0)e^{\lambda_D t}$ *close to the HSS, we propose*

$$M = \lambda_D = \chi - \mu. \tag{3.2.5}$$

By numerically calculating $M$ for each value of $\chi$, we can plot $M(\chi)$ and $\lambda_D(\chi)$. The result is shown in Figure 3.24.

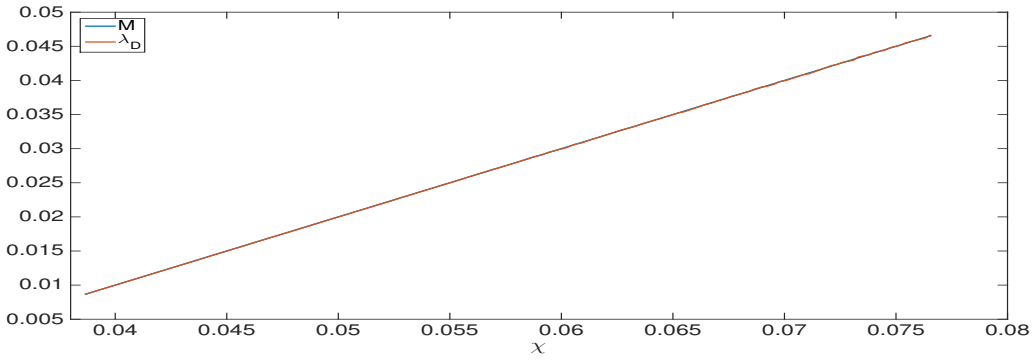


Figure 3.24: Comparison of $\lambda_D = \chi - \mu$ and calculated M as functions of $\chi$ for the system (3.1.2) using initial conditions A. Evidently, $\lambda_D$ is highly accurate in predicting the growth rate of the difference between the two cells.

So, again, we find that Proposition 3.2.4 holds, and $M = \lambda_D \ \forall \chi > \mu$.

Therefore, when we use initial conditions A such that the state of the system starts in the vicinity of the HSS, not only does the linear stability analysis from the previous chapter hold, but $\lambda_D$ is very accurate in predicting the growth of the difference between the cells. This holds not just about the HSS, but continues to hold all the way until near the switched steady state.

**New Results**

As we saw in the section on SoE dynamics, the $n = 3$ system can have a Hopf bifurcation, which is not possible for $n = 2$. A Hopf bifurcation exists when $\chi = 2\mu$, and for $\chi \geq 2\mu$, the HSS is an unstable spiral-saddle (since there is still an eigenvalue with $\mathrm{Re}(\lambda_M) < 0$) surrounded by a stable periodic orbit.

We find that, for initial conditions close to to the SoE and out of the vicinity of the HSS (initial conditions B), the dynamics of the system are affected when $\chi \geq 2\mu$.

For initial conditions B, when $\chi \geq 2\mu$, the following results hold:

1 **There exists stable, in-phase oscillations when $\chi \geq 2\mu$ in the levels of activity for $N$, $H$ and $D$ in both cells as the state of the system moves away from homogeneity to one of the switched steady states.**

This can be observed in Figure 3.25 , which shows $N(t)$, $H(t)$ and $D(t)$ for $\chi \geq 2\mu$. As $\chi$ increases the oscillations grow in amplitude and period, and the switching time increases.

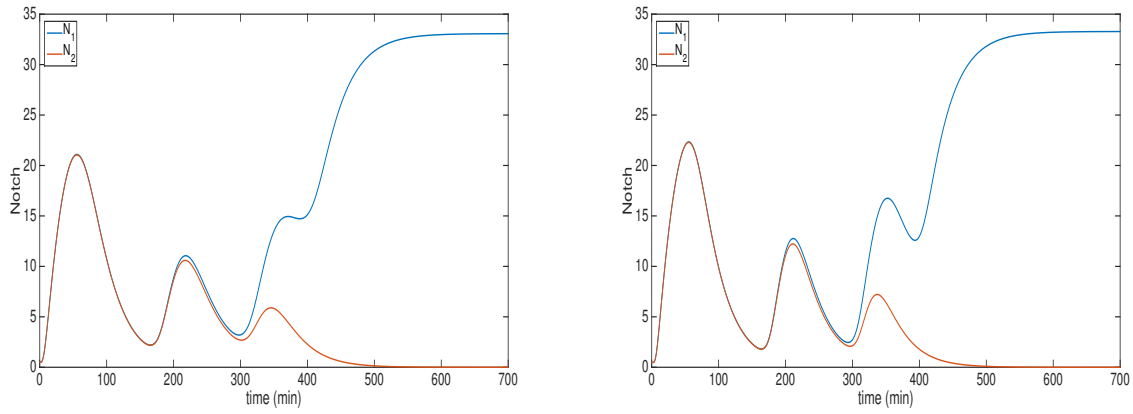


(a)




(b)

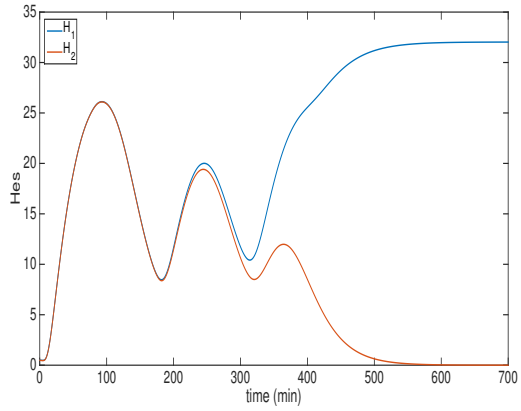


(c)

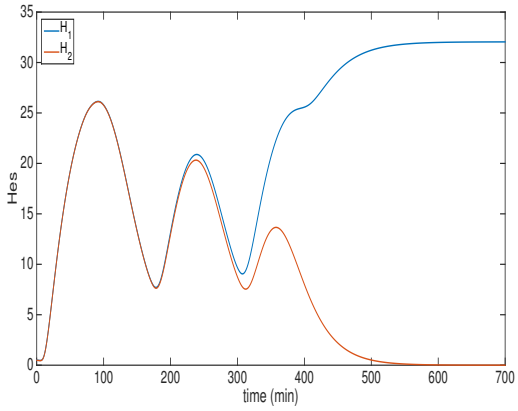


(d)

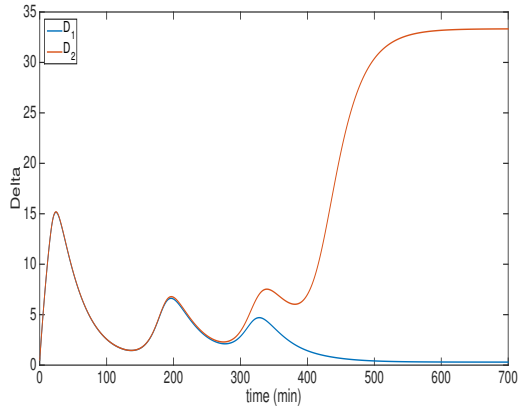


(e)

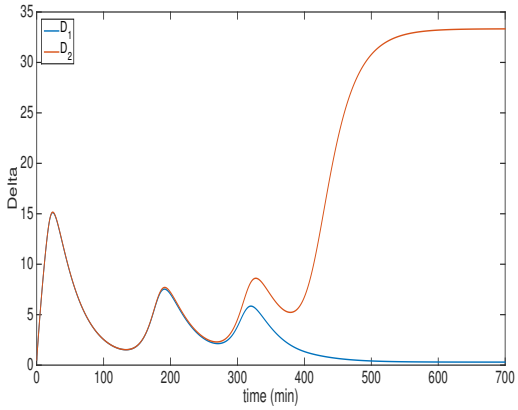


(f)

Figure 3.25: Solution of (3.1.2) using default parameters (3.1.7) and initial conditions B with $\zeta = 10^{-2}$.
(a) N(t), $n_s = 3$ ($\chi = 0.0601$); (b) N(t), $n_s = 4$ ($\chi = 0.0721$); (c) H(t), $n_s = 3$ ($\chi = 0.0601$); (d) H(t), $n_s = 4$ ($\chi = 0.0721$); (e) D(t), $n_s = 3$ ($\chi = 0.0601$); (f) D(t), $n_s = 4$ ($\chi = 0.0721$). As $\chi$ increases, the observed oscillations grow in both amplitude and period, with TtS no longer a continuously decreasing function of $\chi$.

Furthermore, the closer the state of the system starts to the SoE, the longer the oscillatory dynamics last, with the overall TtS increasing. This is easily demonstrated when using a smaller value of $\zeta$ in the initial conditions.

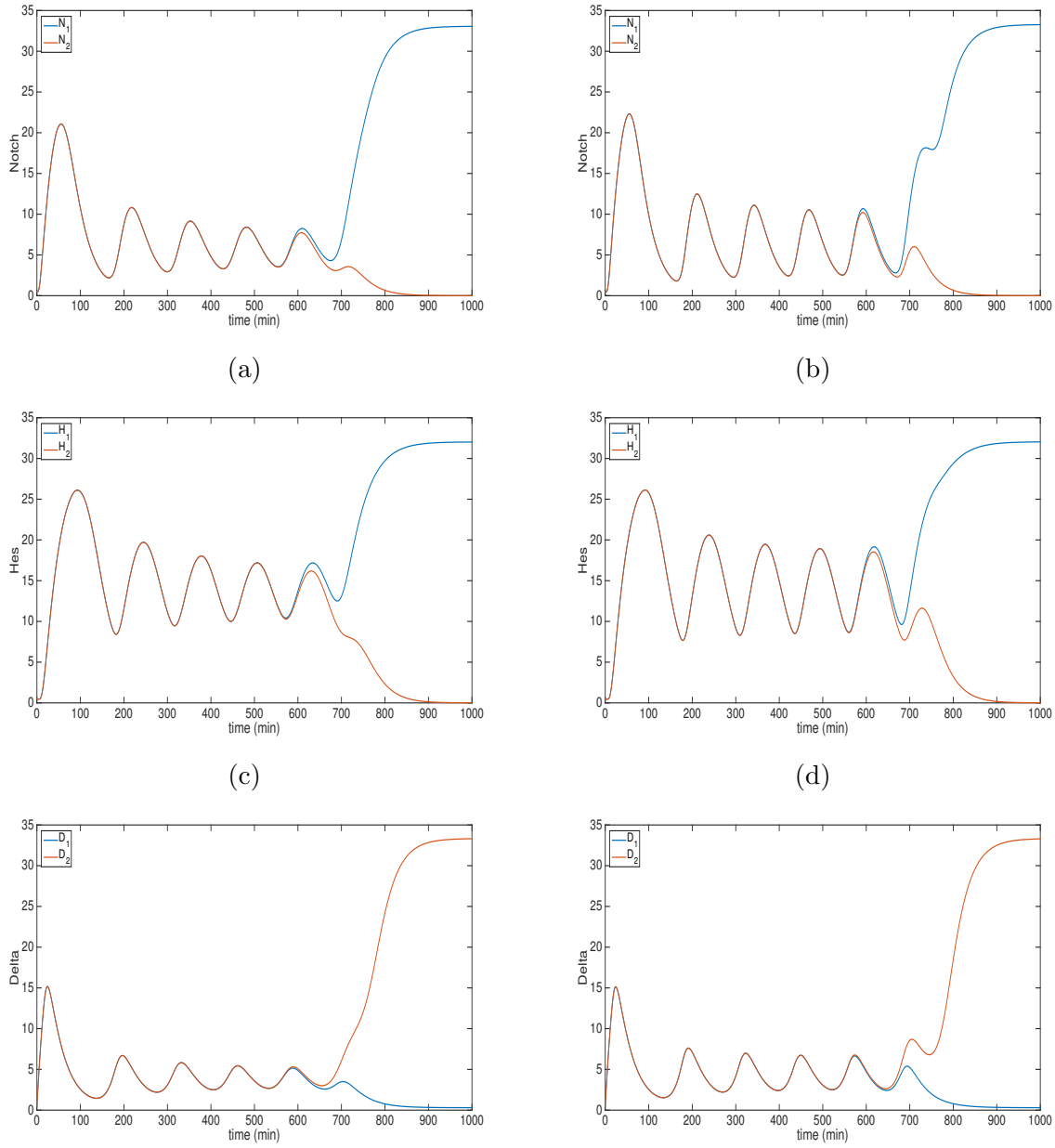


Figure 3.26: Solution of (3.1.2) using default parameters (3.1.7) and initial conditions B with $\zeta = 10^{-6}$.
(a) N(t), $n_s = 3$ ($\chi = 0.0601$); (b) N(t), $n_s = 4$ ($\chi = 0.0721$); (c) H(t), $n_s = 3$ ($\chi = 0.0601$); (d) H(t), $n_s = 4$ ($\chi = 0.0721$); (e) D(t), $n_s = 3$ ($\chi = 0.0601$); (f) D(t), $n_s = 4$ ($\chi = 0.0721$). When using a smaller $\zeta$ in the initial conditions, oscillatory dynamics are present for longer, causing a distinct increase in the Time to Switch.

2 **Time to Switch is no longer a decreasing function of $\chi$, and now reaches a minimum at $2\mu$ when there exists a Hopf bifurcation point. For $\chi \geq 2\mu$, TtS is an increasing function of $\chi$, with $\frac{dTtS}{d\chi}$ changing with $\zeta$.**

When there exists a Hopf bifurcation, the dynamics change in the SoE, and there exists a stable periodic orbit. For $\chi \geq 2\mu$, this periodic orbit introduces oscillatory behaviour in the states of the cells, which causes the TtS to no longer continue decreasing as a function of $\chi$.

TtS as a function of $\chi$ is plotted in Figure 3.27, where we have used $\zeta = 10^{-4}$ in the initial conditions.

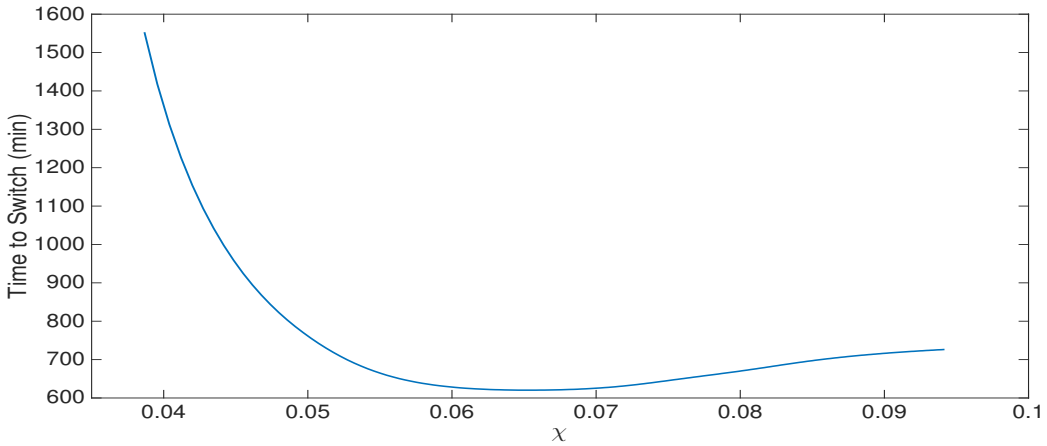


Figure 3.27: Time to Switch as a function of $\chi$ for the system (3.1.2) using default parameters (3.1.7) and initial conditions B with $\zeta = 10^{-4}$. Time to Switch is a decreasing function of $\chi$ until $\chi = 2\mu$, at which point it becomes an increasing function of $\chi$.

As the periodic orbit increases in amplitude with $\chi$, the oscillatory dynamics become more prominent in the cells' variables. TtS now increases with $\chi$, and the rate of increase now depends on $\zeta$.

TtS as a function of $\chi$, $\chi \geq 2\mu$ is plotted in Figure 3.28, for various $\zeta$ in the initial conditions.

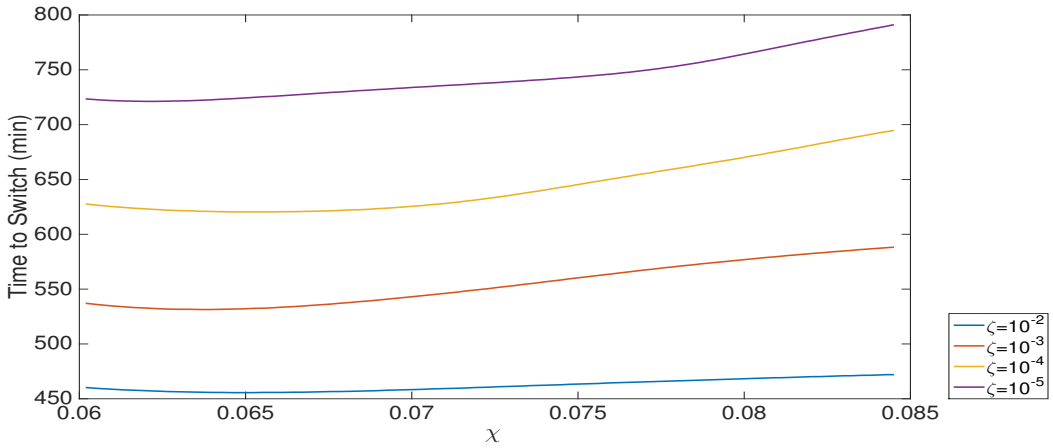


Figure 3.28: Time to Switch as a function of $\chi$ ($\chi \geq 2\mu$) for the system (3.1.2) using default parameters (3.1.7) and initial conditions B with various $\zeta$. For $\chi \geq 2\mu$, TtS is an increasing function of $\chi$, but the rate of increase is dependent on $\zeta$.

3. $\Delta X(t) \neq \Delta X(0)\mathrm{e}^{Mt}$**, but now appears to behave like**

$$\Delta X(t) = \Delta X(0)\mathrm{e}^{Mt}P(t), \tag{3.2.6}$$

**for some periodic function** $P(t)$**.**

This type of solution is typical of those found by Floquet theory, which is used when solving dynamical systems which display periodic dynamics. The theory is summarised well in [71,73], but its application is difficult when not knowing the exact form of the periodic functions in the governing equations. However, we can use this method numerically for analysing the local stability around the periodic orbit, as opposed to the HSS, which can give us an approximation for the growth rate between the cells.

As we start to see oscillations in the levels of Notch, Hes and Delta, we find that the difference between the cells is no longer just an exponential function, but there is now an additional periodic function in the expression.

These new dynamics can be seen when plotting $\ln(\Delta X(t))$ for $\chi \geq 2\mu$, shown in Figure 3.29.

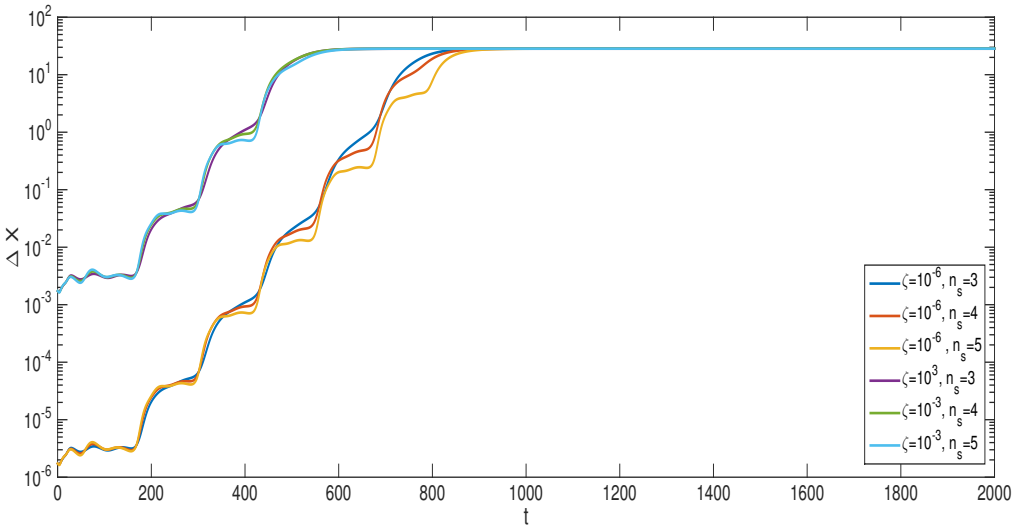


Figure 3.29: $\ln(\Delta X(t))$ for the system (3.1.2) using default parameters (3.1.7) with various $n_s$, and initial conditions B with $\zeta = 10^{-6}$ and $\zeta = 10^{-3}$. As $n_s$ is increased, there is less growth in $\Delta X$ each period. The same oscillatory behaviour is present for either $\zeta$ value, but the behaviour is more prominent when the system starts closer to the SoE.

We find that as $\chi$ is increased, there is less growth in $\Delta X$ each period. The same oscillatory behaviour is present when we use different $\zeta$, but the behaviour is more prominent when starting closer to the SoE.

**Proposition 3.2.5.** *When starting close to the SoE, the dynamics observed on the SoE cause oscillatory behaviour in the full 6-dimensional system.*

The three previous results all support this statement well. When there exists a periodic orbit in the SoE, and the state of the system starts near the SoE, the effects are visible in the states of the cells.

When using the Mean and Difference variables, we find that the Mean variables display similar dynamics as those observed on the SoE. In turn, these affect the Difference variables, evident by the periodic behaviour observed in $\ln(\Delta X(t))$.

To see this behaviour clearer, Figure 3.30 shows plots of $(\ln(M_N(t)),\ \ln(M_D(t)),\ \ln(\Delta X(t)))$, for various $\chi$ and $\zeta$.

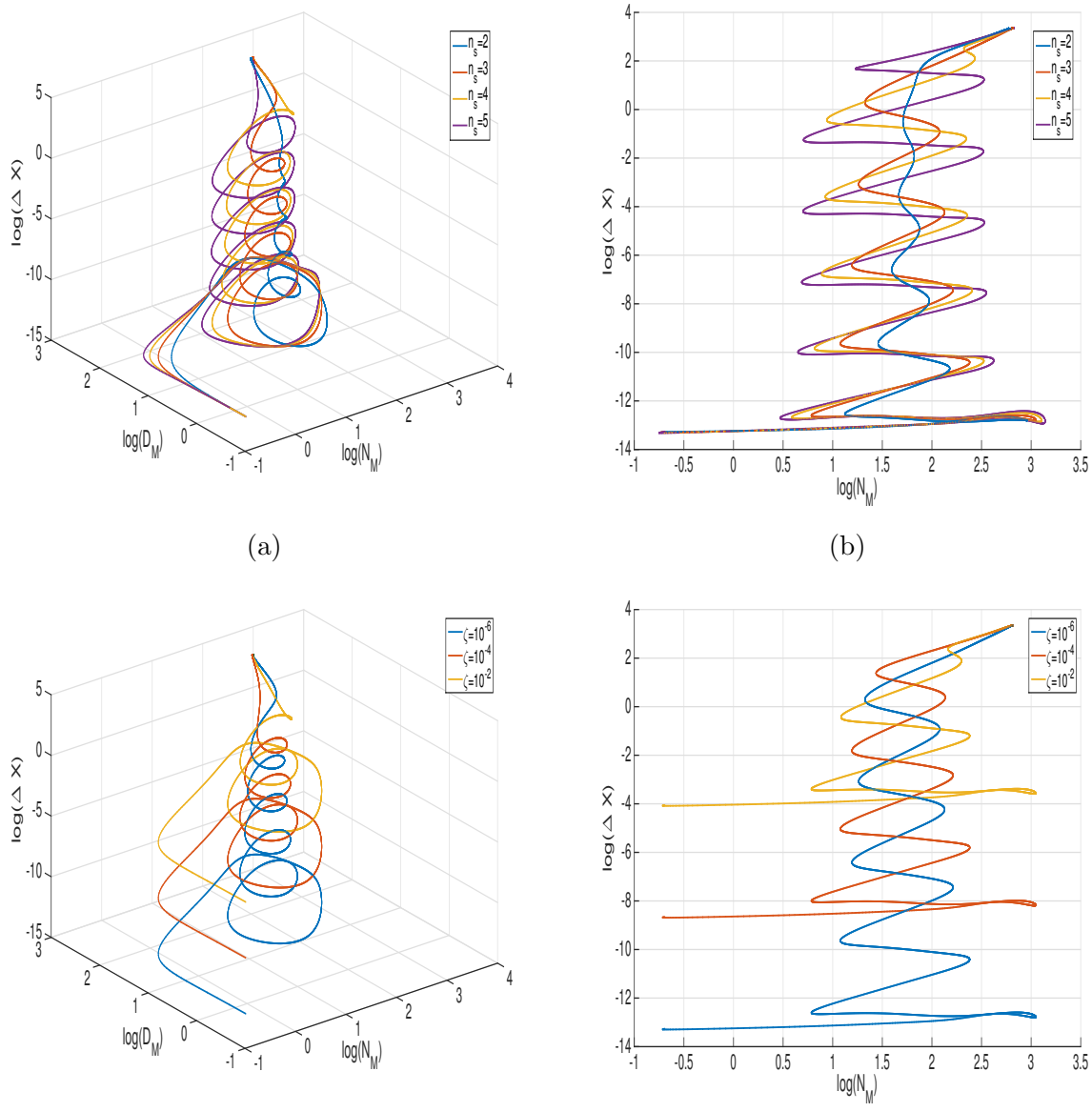


Figure 3.30: Plots of $\ln(M_N(t))$, $\ln(M_D(t))$, $\ln(\Delta X(t))$ for the system (3.1.2), using default parameters (3.1.7) with various $n_s$, and initial conditions B with various $\zeta$.
(a), (b): $\zeta = 10^{-6}$, $n_s = 2,\ 3,\ 4,\ 5$ ($\chi = 0.0518,\ 0.0602,\ 0.0667,\ 0.0721$, respectively). When $\mu < \chi < 2\mu$, there is a stable spiral in the Mean variables, which decreases in amplitude as $\Delta X$ increases. When $\chi \geq 2\mu$, the states of the Mean variables are almost periodic until the vicinity of the switched steady state.
(c), (d): $n_s = 4$ ($\chi = 0.0664$), $\zeta = 10^{-2},\ 10^{-4},\ 10^{-6}$. The same qualitative behaviour is observed independent of $\zeta$, but the closer the system starts to the SoE, the greater the number of oscillations observed in the states of the Mean variables, and the greater the Time to Switch of the system.

From Figure 3.30 we can make the following statements:

- When $\mu < \chi < 2\mu$, we can see there is a stable spiral in the Mean variables, which decays in amplitude as $\Delta X$ increases.
- For $\chi \geq 2\mu$, the Mean variables are almost periodic until the vicinity of the switched steady state, clearly seen in Figure 3.30(b). This introduces a periodic expression in $\Delta X$.
- The amplitude and period are both increasing functions of $\chi$, whilst the growth per period in $\Delta X(t)$ appears to decrease.
- The SoE dynamics (Mean dynamics) propagate from the SoE up to the switched steady state, with a near-constant periodicity until reaching the steady state.
- The closer the system starts to the SoE, the greater the effect the SoE dynamics have on the full system. The Mean variables display a greater number of oscillations, evident in Figures 3.30(c), (d), where the different initial conditions start on the 'coil', in addition to the increased switching times we saw previously.

**An approach for calculating the growth rate of $\Delta X(t)$**

Based on the Mean variables displaying almost purely oscillatory dynamics until reaching the steady state, we can assume it is the periodic orbit in the SoE which causes $\Delta X(t) \neq \Delta X(0)\mathrm{e}^{Mt}$.

Therefore, $\lambda_D = \chi - \mu$ from the linear stability analysis of the HSS no longer holds as an estimation for $M$ primarily because the solution trajectory of the system can no longer reach the vicinity of the HSS, due to the stable periodic orbit.

**Proposition 3.2.6.** *$M(\chi)$ reaches a maximum when $\chi = 2\mu$, and the presence of the periodic orbit in the SoE, which increases in stability with $\chi$, causes $M(\chi)$ to decrease for $\chi \geq 2\mu$.*

Numerically we have seen that the Mean variables are ~ periodic, very close to the dynamics observed in the SoE. So, instead of forming the linearised equations to determine behaviour close to the HSS, it makes more sense to form linearised equations to determine the behaviour close to the periodic orbit. As stated above, this method is typical of Floquet analysis.

Referring back to Section 2.2, rather than using $N(t) = N^* + n(t)$, etc. we can use

$$N(t) = N_{PO}(t) + n(t), \tag{3.2.7}$$

where $N_{PO}(t)$ is the corresponding level of Notch on the periodic orbit, such that it is a periodic function with period $T$. $n(t)$ is the associated perturbation from the periodic orbit at time $t$.

This then introduces oscillatory terms into the linearised Difference equations, now determined by

$$\dot{\underline{\Delta}} = J_\Delta(t)\,\underline{\Delta}, \tag{3.2.8}$$

where

$$J_\Delta(t) = \begin{bmatrix} -\mu & 0 & -\Phi_s(t) \\ \Phi_2(t) & -\mu & 0 \\ 0 & -\Gamma(t) & -\mu \end{bmatrix}, \tag{3.2.9}$$

such that

$$\Phi_s(t) \equiv \frac{\partial f_s}{\partial D}\Big|_{D_{PO}(t)} > 0, \quad \Phi_2(t) \equiv \frac{\partial f_2}{\partial N}\Big|_{N_{PO}(t)} > 0, \quad \Gamma(t) \equiv -\frac{\partial g}{\partial H}\Big|_{H_{PO}(t)} > 0.$$

In turn, this means that the eigenvalues of $J_\Delta(t)$ also have periodicity.

Therefore, we now want to numerically calculate $\lambda_\Delta$ at each point on the periodic orbit over a period, so we can define

$$\lambda_{PO}(t) \equiv \max(\mathrm{Re}(\lambda_\Delta(t)), \tag{3.2.10}$$

as the eigenvalue with the largest real part at time $t$.

This allows us to then calculate the mean of $\lambda_{PO}(t)$ for a period, such that

$$\Lambda = \frac{1}{T}\int_t^{t+T} \lambda_{PO} dt. \tag{3.2.11}$$

If we then use this as our estimation for the growth rate, we expect

$$\Delta X(t) = \Delta X(0) \mathrm{e}^{\Lambda t} P(t). \tag{3.2.12}$$

Now, if we plot $\ln(\Delta X(t))$ and $\ln(\Delta X(0)) + \Lambda t$, we find that this does indeed give a good estimate for the growth rate of $\Delta X(t)$. This is shown below in Figure 3.31.

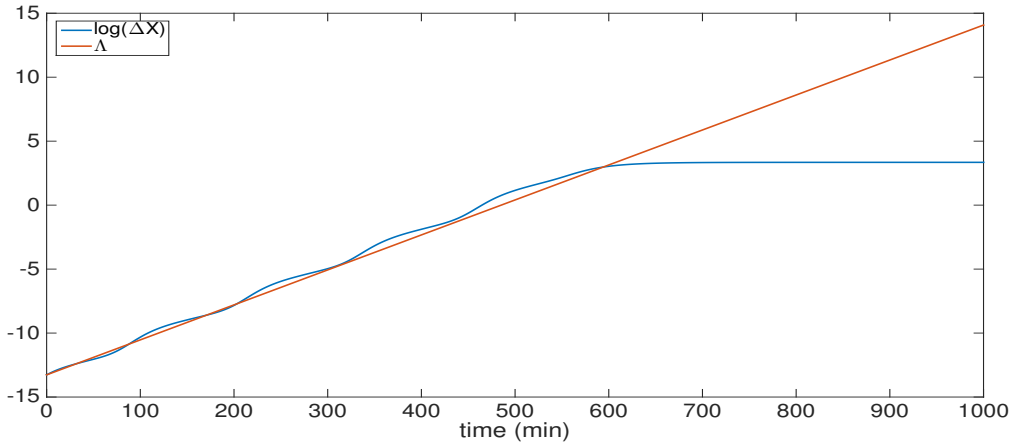


Figure 3.31: $\ln(\Delta X(t))$ and $\Lambda$ for the system (3.1.2) using default parameters (3.1.7) with $n_s = 3$ ($\chi = 0.0601$), where $\Lambda$ is our estimation for the growth rate of the difference between the two cells. Indeed, $\Lambda$ accurately predictes the rate at which $\Delta X$ grows until the vicinity of the switched steady state.

It appears that the accuracy decreases as the state of the system approaches the steady state, but this is to be expected from a linear prediction.

Accuracy does decrease for greater values of $\chi$, as shown in Figure 3.32, but nevertheless, this method captures the qualitative behaviour of the growth rate of $\Delta X(t)$.

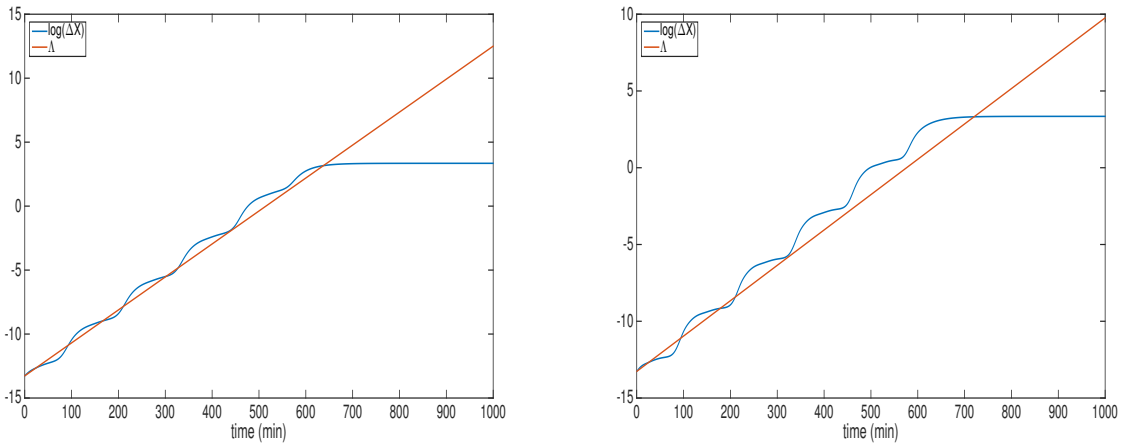


(a) (b)

Figure 3.32: $\ln(\Delta X(t))$ and $\Lambda$ for the system (3.1.2) using default parameters (3.1.7), where (a) $n_s = 4$ ($\chi = 0.0667$); (b) $n_s = 5$ ($\chi = 0.0721$). As $n_s$ is increased, $\Lambda$ predicts the growth rate of $\Delta X$ with less accuracy, underestimating the actual growth rate of $\Delta X$.

The full relationship between $\chi$ and $\Lambda$ is shown in Figure 3.33.

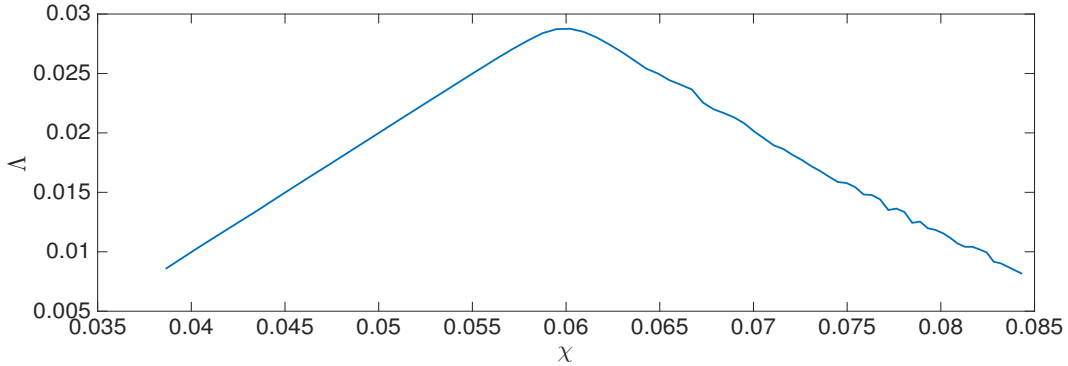


Figure 3.33: $\Lambda$, the estimated growth rate of $\Delta X(t)$, as a function of $\chi$, for the system (3.1.2) using default parameters (3.1.7) and initial conditions B. $\Lambda \sim \chi - \mu$ until $\chi = 2\mu$, at which point it becomes a decreasing function of $\chi$.

An additional characteristic that we have observed when calculating $\Lambda$ is that there is a duration of each period where there is very little growth in $\Delta X(t)$, which increases with $\chi$. From plotting $\lambda_{PO}(t)$ for a period of oscillation (Figure 3.34), we see the reason behind this.

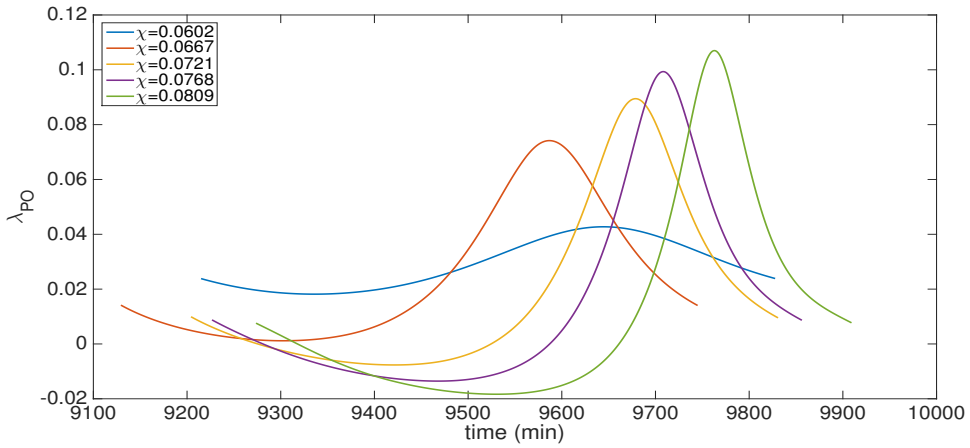


Figure 3.34: $\lambda_{PO}$ evaluated for one period of the periodic orbit in the SoE, for the system (3.1.2) using default parameters (3.1.7) with various $n_s$, and initial conditions such that the system begins on the periodic orbit in the SoE.

As $\chi$ increases, the $\max(\lambda_{PO})$ does increase, but we also find that for an increasing proportion of the orbit, $\lambda_{PO} < 0$. This means that parts of the periodic orbit are stable to perturbations, causing $\Delta X(t)$ to have a smaller growth rate, and even decrease for large enough $\chi$.

### 3.2.1 Summary of Results

These results for $n = 2$ and $n = 3$ have shown that a Hopf bifurcation has the potential to change the dynamics of the system. By analysing the behaviour when the system is in the SoE, we show that where the HSS is always stable for $n = 2$, it can become unstable when $n = 3$, creating a stable periodic orbit in the SoE.

We confirm the result of the linear stability analysis that for any $n$, the growth rate of the difference between the cells when starting near the HSS behaves like $\Delta X(t) = \Delta X(0)e^{\lambda t}$, and accurately predicts the growth rate all the way to the switched steady state.

Finally, we show that, for $n = 3$, when there exists a periodic orbit in the SoE, and the state of the system starts near the SoE but away from the HSS, the states of each variable now display oscillatory dynamics prior to the states of the cells reaching one of the steady states. Although we have only shown this behaviour in the case of $n = 3$, the same is true for all $n > 2$ (Data not shown).

This directly answers our first proposed question; oscillatory dynamics are possible in a lateral inhibition model without the presence of delays, and can be achieved provided there are at least 3 components in each cell.

This is also a nice example of a system driven by an overall positive feedback loop which promotes bistability, with the existence of a 3-component negative feedback loop in a subspace of the system. This introduces an interaction of different feedbacks, resulting in a combination of characteristics from both, allowing the system to do bistable switching,

whilst also displaying oscillatory dynamics.

When there does exist a periodic orbit in the SoE, and the state of the system is affected by it, linear stability analysis can no longer provide a prediction for the growth rate of the differences between the cells. However, by using a numerical approach based on Floquet analysis [71], we have been able to intuitively explain why the growth rate of differences behaves as it does. It may not be able to provide an exact analytic expression for the growth, but it holds reasonably well.

## 3.3 Two cells governed by Delay Differential Equations

Following the same structure as the previous section, we are looking at two models of 2-cell systems, in which one has a single component per cell and the other has two components per cell.

From Section 2.2.5, we know there always exists a homogeneous steady state [HSS] in the Surface of Equivalence [SoE], and depending on the model parameters, the HSS is either stable or unstable.

The results obtained for the bifurcation conditions do not need to be verified so vigorously in this case, as similar systems have been studied previously by [50]. Instead, we will state the results, with supporting figures where necessary. We do want to confirm the analytic results regarding the comparison between the ODE and DDE models, to illustrate how all behaviours are qualitatively equivalent, and that results previously only seen for systems with an included delay can be achieved in a finite-dimensional system.

We will first look at results in which the systems are on the SoE before exploring the full behaviour of each system, but first, we will introduce any changes to notation from the previous Chapter, and the model parameters.

### Notation and Parameters

Again, we can use these systems to model the Delta-Notch pathway, but in the case of $m = 1$, each component in the cells does not have to be explicitly defined. Instead, a single variable can represent the levels of both Delta and Notch.

From the notation in Chapter 2, in which the single variable of each cell was denoted $y_1$ and $y_2$, for consistency we will now refer to these as $D_1$ and $D_2$, respectively.

The $m = 1$ system is now represented by the DDEs:

$$\dot{D}_1 = -\mu D_1 + g\left(D_2(t-\tau)\right), \qquad \dot{D}_2 = -\mu D_2 + g\left(D_1(t-\tau)\right). \tag{3.3.1}$$

In the case of $m = 2$, we have 4 variables in total, $y_{1,1}$, $y_{2,1}$, $y_{1,2}$ and $y_{2,2}$. We will now refer to $y_{1,1}$, $y_{1,2}$ as $N_1$ and $N_2$, and we will refer to $y_{2,1}$, $y_{2,2}$ as $D_1$ and $D_2$.

The $m = 2$ system is now represented by the DDEs:

$$\begin{aligned} \dot{N}_1 &= -\mu_N N_1 + f_s(D_2(t-\tau_s)), & \dot{N}_2 &= -\mu_N N_2 + f_s(D_1(t-\tau_s)), \\ \dot{D}_1 &= -\mu_D D_1 + g(N_1(t-\tau_1)), & \dot{D}_2 &= -\mu_D D_2 + g(N_2(t-\tau_1)). \end{aligned} \tag{3.3.2}$$

**Definition 3.3.1.** We can make a change of variables to Mean and Difference variables $M$ and $\Delta$, where, for $m = 1$,

$$M \equiv \frac{D_1 + D_2}{2}, \qquad \Delta = \frac{D_1 - D_2}{2}, \tag{3.3.3}$$

and for $m = 2$,

$$M_N \equiv \frac{N_1 + N_2}{2}, \qquad M_D \equiv \frac{D_1 + D_2}{2} \tag{3.3.4}$$

and

$$\Delta_N \equiv \frac{N_1 - N_2}{2}, \qquad \Delta_D \equiv \frac{D_1 - D_2}{2}. \tag{3.3.5}$$

The regulation functions $f_s$ and $g$ are the same as those defined by (3.15);

$$f_s(x) = \frac{x^{n_s}}{\theta_s^{n_s} + x^{n_s}}, \qquad g(x) = \frac{1}{1 + (x/\theta_g)^{n_g}}. \tag{3.3.6}$$

**Simulation Parameters**

The results for this section were obtained using

$$\begin{aligned} &\mu = 0.03 \text{ min}^{-1}, \\ &\theta_g = \frac{0.2}{\mu} \text{ min}, \\ &\tau = 40.31 \text{ min}, \end{aligned} \tag{3.3.7}$$

for $m = 1$, and

$$\begin{aligned} &\mu_N = \mu_D = \mu = 0.03 \text{ min}^{-1}, \\ &\theta_s = \theta_g = \frac{0.2}{\mu} \text{ min}, \\ &n_g = 2, \\ &\tau_s = 4 \text{ min}, \ \tau_1 = 16.15 \text{ min}, \implies \tau = 20.15 \text{ min}, \end{aligned} \tag{3.3.8}$$

for $m = 2$, unless stated otherwise.

The parameter choices for $\mu$ and $\theta$ follow the same justification as in the ODE models, and the delays have been chosen such that each system will have a Hopf bifurcation for the same value of $\chi$ as the ODE $n = 3$ model (when $\chi = 2\mu$).

For $m = 1$ we use the parameter $n_g$ to control $\chi$ (previously denoted as $\gamma$ in the single-variable case, but we will now use $\chi$ for consistency), and for $m = 2$ we will use the parameter $n_s$ to control $\chi$.

The following simulations were solved using a variable step Runge-Kutta method, implemented by dde23 in Matlab. The tolerances used are default, unless stated otherwise.

### 3.3.1 Surface of Equivalence Dynamics

We will first show the dynamics of the SoE, in which both cells have identical states. We choose initial conditions such that $D_1(0) = D_2(0)$ for $m = 1$, and $N_1(0) = N_2(0)$, $D_1(0) = D_2(0)$ for $m = 2$. As discussed in Section 1.6, the initial conditions for delay differential equations must take the system's history into account. Therefore, we have used initial conditions such that for the system's history, the initial conditions are a constant.

From the linear stability analysis in Chapter 2, we know that the HSS can become unstable in the SoE in both cases, due to a Hopf bifurcation. The stability analysis tells us that a Hopf bifurcation exists when

$$\chi > \mu, \qquad \tau = \frac{\pi - m\tan^{-1}(\frac{\omega}{\mu})}{\omega}.$$

In Chapter 2, we state that it is possible for an $m = 1$ and $m = 2$ system with time delays to have a Hopf bifurcation for the same value of $\chi$ as an $n = 3$ system without a time delay.

Now, there exists a Hopf bifurcation in the $n = 3$ case when $\chi = 2\mu$, and since $\omega = \sqrt{\chi^2 - \mu^2}$ when there exists a Hopf bifurcation point, then $\omega = \sqrt{3}\,\mu$. Therefore, for $m = 1$ and $m = 2$, there corresponding delays necessary for a Hopf bifurcation when $\chi = 2\mu$ are

$$\tau = \frac{\pi - \tan^{-1}(\sqrt{3})}{\sqrt{3}\,\mu} = 40.31 \text{ min}, \tag{3.3.9}$$

for $m = 1$, and

$$\tau = \frac{\pi - 2\tan^{-1}(\sqrt{3})}{\sqrt{3}\,\mu} = 20.15 \text{ min}, \tag{3.3.10}$$

for $m = 2$.

#### $m = 1$

When $n_g = 2.79$, $\chi = 0.0601$, and when $\tau = 40.31$ min, there exists a Hopf bifurcation. This corresponds to the existence of a stable periodic orbit in the SoE, and its existence is made evident by the stable oscillations in the level of Delta activity in each cell, as shown in Figure 3.35.

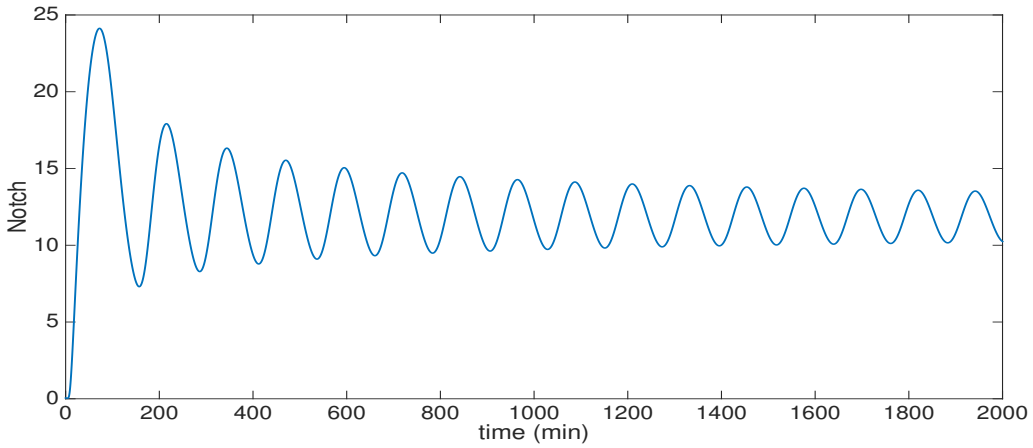


Figure 3.35: Solution to the system (3.3.1) using default parameters (3.3.7) with $n_g = 2.79$ and initial conditions $D_1(0) = D_2(0) = 0.5$. We observe stable oscillations in the levels of Delta activity, corresponding to the solution trajectory being attracted on to the stable periodic orbit in the SoE.

## $\underline{m = 2}$

When $n_s = 2.45$, $\chi = 0.0601$, and when $\tau = 20.15$min, there exists a Hopf bifurcation. This is made evident by the stable oscillations in the levels of Notch and Delta activity in each cell, and from the stable periodic orbit in the SoE. These are shown in Figures 3.36 and 3.37.

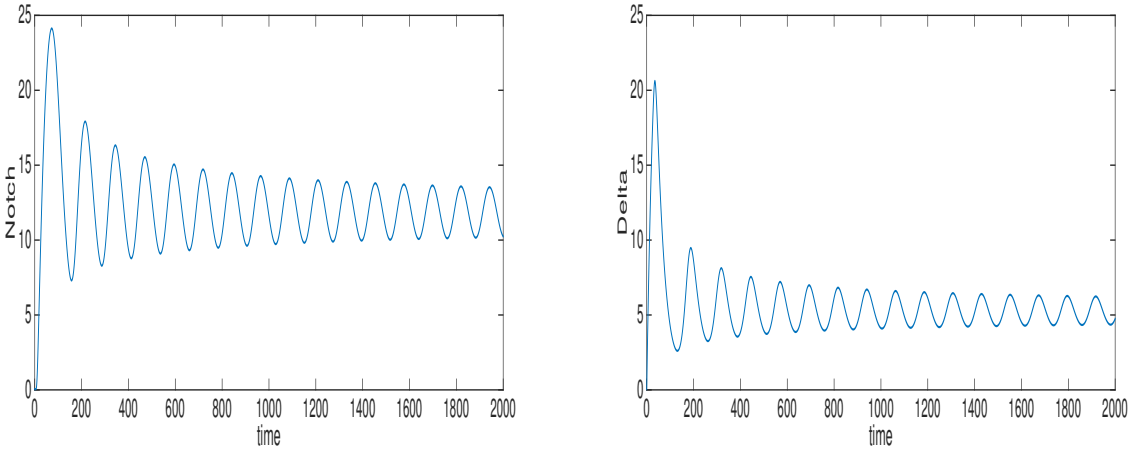


(a) (b)

Figure 3.36: Solution to the system (3.3.2) using default parameters (3.3.8) with $n_s = 2.45$ and initial conditions $N_1(0) = N_2(0) = D_1(0) = D_2(0) = 0.5$. We observe stable oscillations in the levels of Notch and Delta activity, corresponding to the solution trajectory being attracted on to the stable periodic orbit in the SoE.

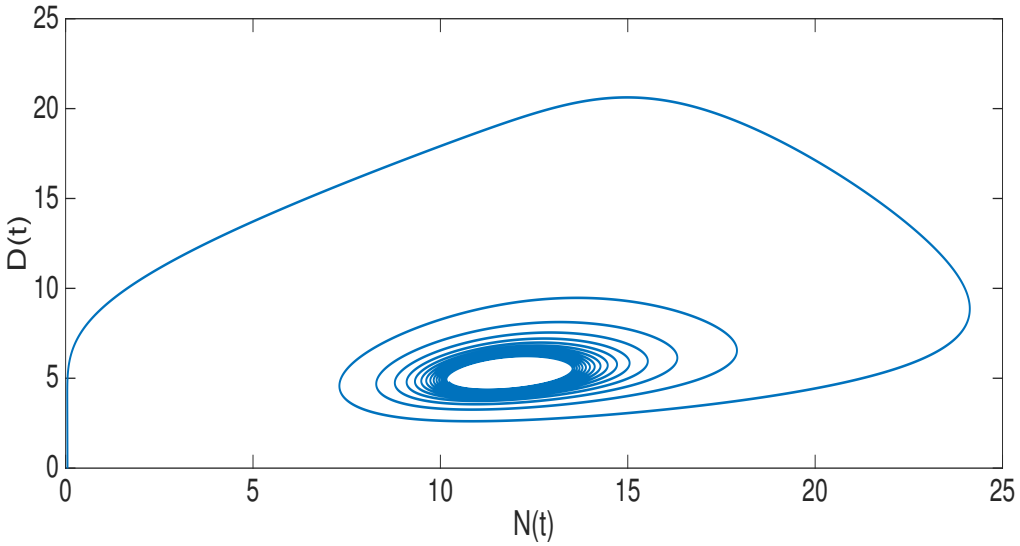


Figure 3.37: Solution trajectory of the system (3.3.2) using default parameters (3.3.8) with $n_s = 2.45$ and initial conditions $N_1(0) = N_2(0) = D_1(0) = D_2(0) = 0.5$. We observe a stable periodic orbit surrounding the HSS in the SoE.

Therefore, both of these systems have a Hopf bifurcation for the same $\chi$ as the $n = 3$ model (and each other) when they have the delays stated above.

Hence, an $n$-component ODE system and $m$-component DDE system (where $n > m$) will have a Hopf bifurcation for the same value of $\chi$, provided there is a delay of

$$\tau = \frac{(n-m)\pi}{n\omega}, \tag{3.3.11}$$

and an $m$-component DDE system and a $k$-component DDE system (where $k > m$) will both have a Hopf bifurcation for the same value of $\chi$, provided the delays satisfy

$$\tau_k = \left(\frac{k}{m}\right)\tau_m - \frac{(k-m)\pi}{m\omega}, \tag{3.3.12}$$

as stated in the discussion of Section (2.2).

### 3.3.2 Dynamics of the Full System

Now we have explored the dynamics on the SoE subspace and shown that the relationship for 'equivalent' Hopf bifurcations between the ODE models and DDE models hold, we can now look at the behaviours of each system when using initial conditions not in the SoE.

Since these systems have been studied extensively, we will be highlighting the main dynamics and comparing the behaviours with what we saw when modelling the $n = 3$ ODE system.

We will be using equivalent definitions for the total difference between the cells and the Time to Switch, but for clarify, we will redefine them here.

**Definition 3.3.2.**

$$\Delta X(t) \equiv \sqrt{\Delta(t)^2}, \qquad \text{when } m = 1, \tag{3.3.13}$$

$$\Delta X(t) \equiv \sqrt{\Delta_N(t)^2 + \Delta_D(t)^2}, \qquad \text{when } m = 2. \tag{3.3.14}$$

**Definition 3.3.3.** Time to Switch [TtS] is defined as when the total difference between the cells reaches 80% of the maximum total difference;

$$\text{TtS} \equiv 0.8 \times \max(\Delta X(t)). \tag{3.3.15}$$

**Initial Conditions**

The following results for $m = 1$ and $m = 2$ have used initial conditions of the same form as the previous section;

$$\underline{X}(0) = \text{SoEP} + \zeta \underline{P}, \tag{3.3.16}$$

where SoEP refers to a position on the Surface of Equivalence, and $\zeta \underline{P}$ is the perturbation out of the SoE from that point.

We have chosen the same two sets of initial conditions, A and B, such that they are perturbations from different positions on the SoE. Initial Conditions A have an SoEP at the HSS, and Initial Conditions B have an SoEP at $\underline{0.5}$, such that each variable has a value of 0.5.

The initial conditions can therefore be defined by

$$\begin{aligned} \text{A} &\equiv \text{HSS} + \zeta \underline{P}, \\ \text{B} &\equiv \underline{0.5} + \zeta \underline{P}. \end{aligned} \tag{3.3.17}$$

The magnitude of perturbation $\zeta \in [10^{-6}, 10^{-1}]$. This ensures the states of each cell start close to the SoE, and by varying $\zeta$ this can show whether the initial distance from the SoE can affect the systems' dynamics.

As we have stated above in the section on the Surface of Equivalence, these initial conditions are not just at $\underline{X}(0)$, but are the initial conditions for $\underline{X}(t)$ for $t \in [-\tau, 0]$.

Unless stated otherwise, the direction of perturbation will be

$$\underline{P} = \begin{pmatrix} 1 \\ -1 \end{pmatrix}, \quad \text{for m=1,} \qquad \underline{P} = \begin{pmatrix} 1 \\ -1 \\ -1 \\ 1 \end{pmatrix}, \quad \text{for m=2.} \tag{3.3.18}$$

We have used this direction such that the perturbation causes the variable levels to differ equally around the HSS, or any other SoE position we are perturbing from. It may be that if we were only looking at perturbations from the HSS we would want to use a perturbation relative to the final possible steady states, but since we are looking at different locations on the SoE, this allows for a more accurate comparison between the different initial conditions.

## 3.4 Results for $m = 1$ and $m = 2$

### 3.4.1 Results when using Initial Conditions A

When we use initial conditions A in each of the systems, the dynamics observed are equivalent to the $n = 3$ case, and the following results all hold.

- The HSS is stable when $\chi < \mu$, and is the only steady state of the system.

This result is true for all models of this form, with the result explicitly shown for $m = 1$ in Figure 3.38.

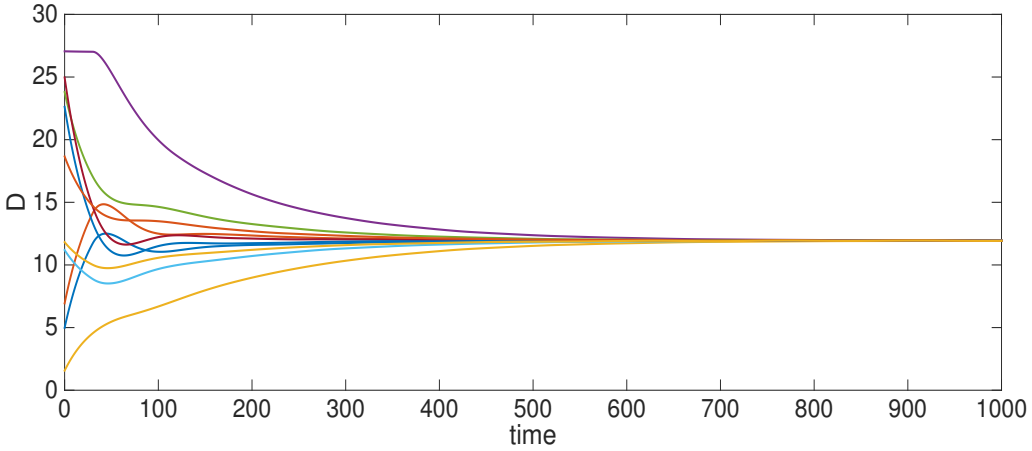


Figure 3.38: Solutions to (3.3.1) using default parameters (3.3.7) with $n_g = 1$ ($\chi = 0.02$), and initial conditions $D_1(0)$, $D_2(0) \in [0, 30]$. Since $\chi < \mu$, the HSS is the only steady state of the system.

The same holds for $m = 2$, but the data is not shown here.

- There exists a bifurcation when $\chi = \mu$, such that switching is possible when $\chi > \mu$.

This can be seen in the following Figures 3.39 and 3.40, illustrating the time-courses of each variable in the cells, for $m = 1$ and $m = 2$ respectively.

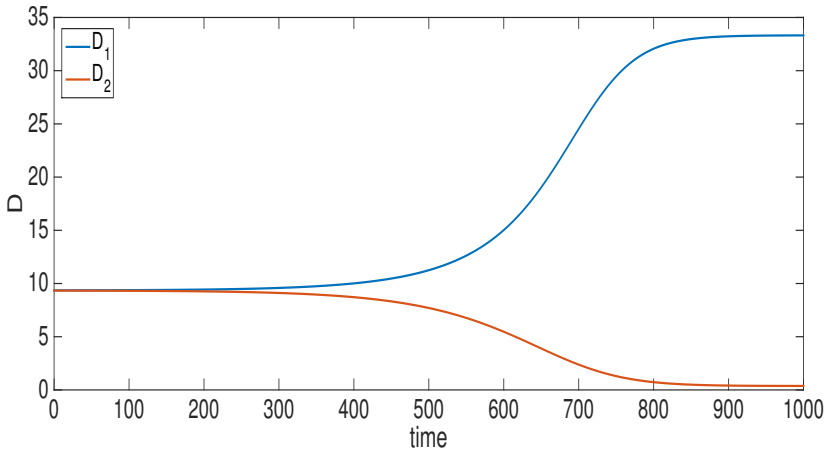


Figure 3.39: Solution of (3.3.1) using default parameters (3.3.7) with $n_g = 2.79$ ($\chi = 0.0601$) and initial conditions A with $\zeta = 10^{-2}$.

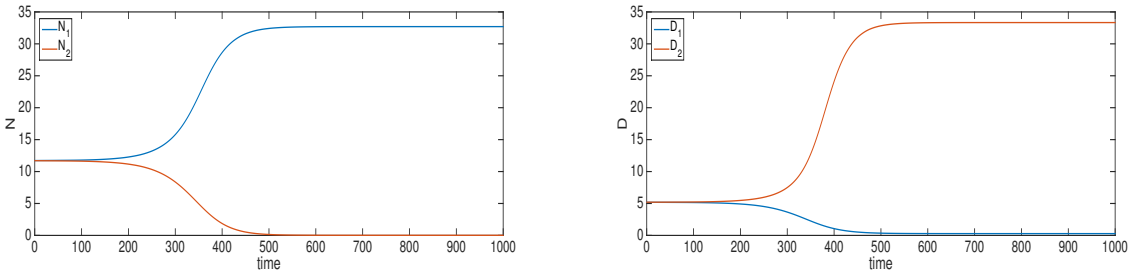


(a) (b)

Figure 3.40: Solution of (3.3.2) using default parameters (3.3.8) with $n_s = 2.45$ ($\chi = 0.0601$) and initial conditions A with $\zeta = 10^{-2}$.

- Time to Switch is a decreasing function of $\chi$.

This result holds for all systems when the initial conditions are close to the HSS. TtS is a continuously decreasing function of $\chi$, and is independent of $\zeta$. This is shown for $m = 1$ in Figure 3.41 and for $m = 2$ in Figure 3.42.

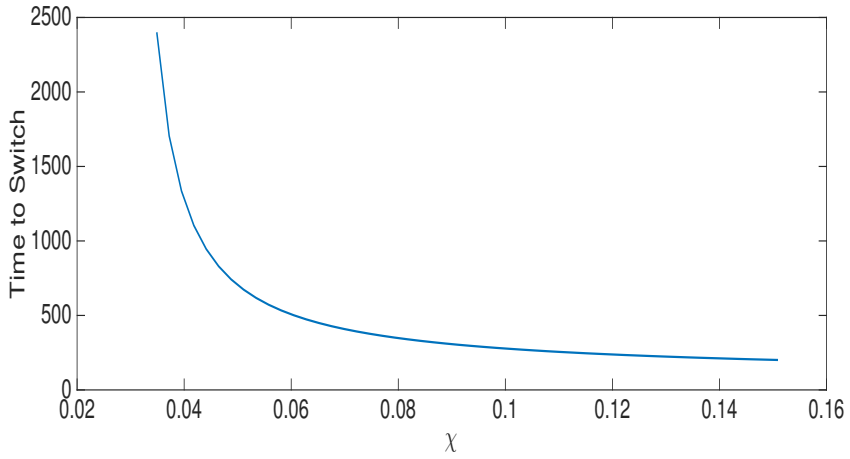


Figure 3.41: Time to Switch as a function of $\chi$ for the system (3.3.1) using default parameters (3.3.7) and initial conditions A with $\zeta = 10^{-1}$. Time to Switch is a continuously decreasing function of $\chi$.

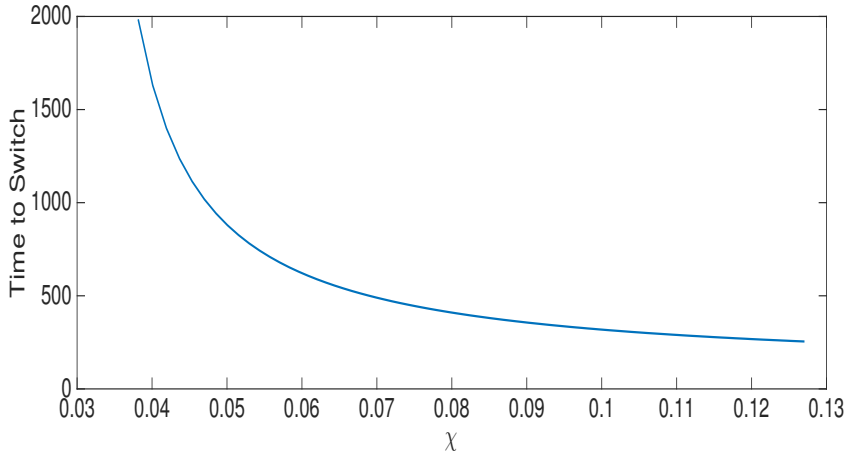


Figure 3.42: Time to Switch as a function of $\chi$ for the system (3.3.2) using default parameters (3.3.8) and initial conditions A with $\zeta = 10^{-4}$. Time to Switch is a continuously decreasing function of $\chi$.

- For a given value of $\chi$, TtS is a decreasing function of $\zeta$.

This can be seen in in Figures 3.43 and 3.44 for $m = 1$ and $m = 2$ respectively.

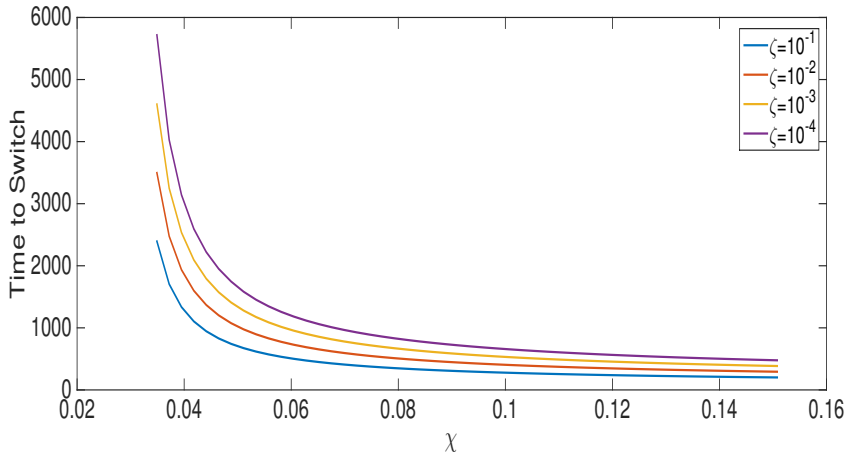


Figure 3.43: Time to Switch as a function of $\chi$ for the system (3.3.1) using default parameters (3.3.7) and initial conditions A with various $\zeta$. Time to Switch is a continuously decreasing function of $\chi$, independent of $\zeta$, and for any given value of $\chi$, Time to Switch is a decreasing function of $\zeta$.

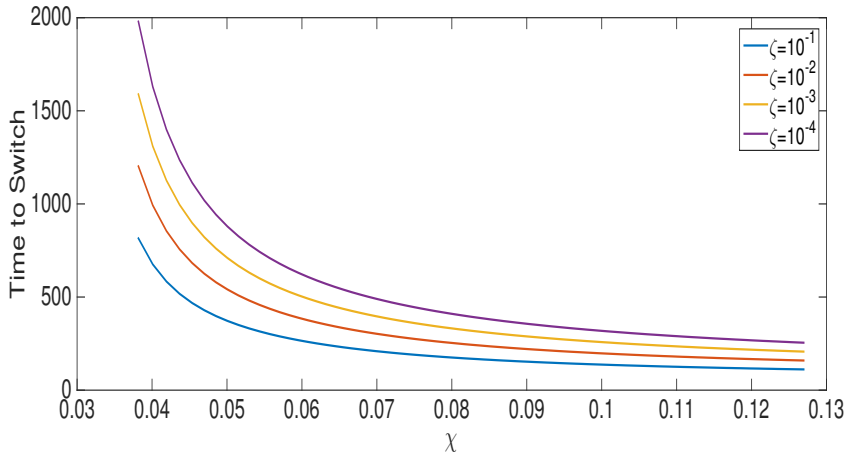


Figure 3.44: Time to Switch as a function of $\chi$ for the system (3.3.2) using default parameters (3.3.8) and initial conditions A with various $\zeta$. Time to Switch is a continuously decreasing function of $\chi$, independent of $\zeta$, and for any given value of $\chi$, Time to Switch is a decreasing function of $\zeta$.

- For a given $\chi$, increasing $\zeta$ by an order of magnitude will give a fixed decrease in the Time to Switch.

This result is clearly captured when we plot the Delta time-course for $m = 1$ with various $\zeta$ in the initial conditions:

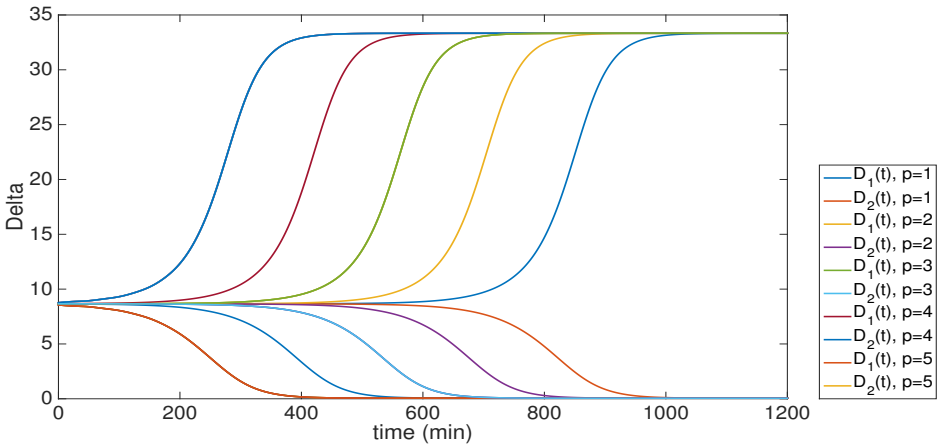


Figure 3.45: The levels of Delta activity in both cells for system (3.3.1), using default parameters (3.3.7) with $n_g = 2.79$ ($\chi = 0.0601$), and initial conditions A with $\zeta = 10^{-p}$, $p = 1, 2, \ldots 5$.

and similarly, when we plot the Notch and Delta time-courses for $m = 2$:

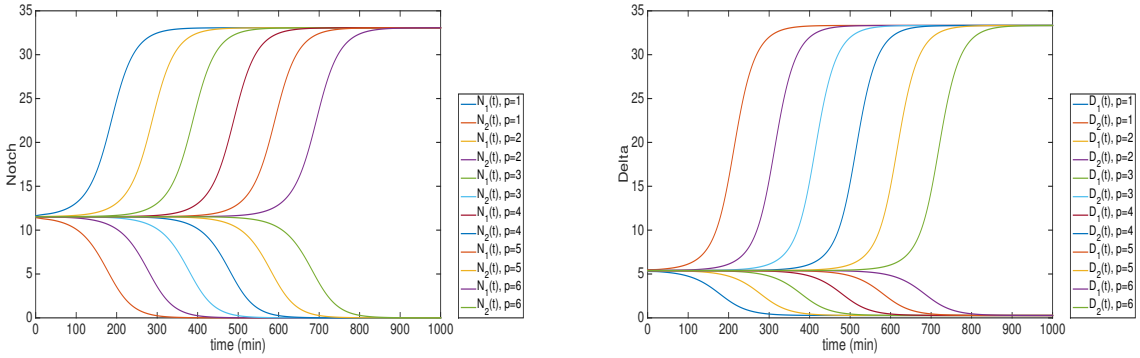


(a) (b)

Figure 3.46: The levels of Notch and Delta activity in both cells for system (3.3.2), using default parameters (3.3.8) with $n_s = 2.45$ ($\chi = 0.0601$), and initial conditions A with $\zeta = 10^{-p}$, $p = 1, 2, \ldots 6$.

It is evident that, regardless of the number of components there are in the two cells, or whether we use equations with time-delays or not, that when using initial conditions close to the HSS, the dynamics of the system are qualitatively equivalent.

This suggests that the growth of the differences between the cells will behave the same as the ODE systems. Therefore, we can propose the following:

**Proposition 3.4.1.** *The total difference between the two cells behaves like*

$$\Delta X(t) = \Delta X(0) e^{Mt}, \quad M \in \mathbb{R}. \tag{3.4.1}$$

When we plot $\ln(\Delta X(t))$ for a given $\chi$ and various values of $\zeta$, shown in Figure 3.47, $M$ is constant until the vicinity of the switched steady state, and holds well for both $m = 1$ and $m = 2$.

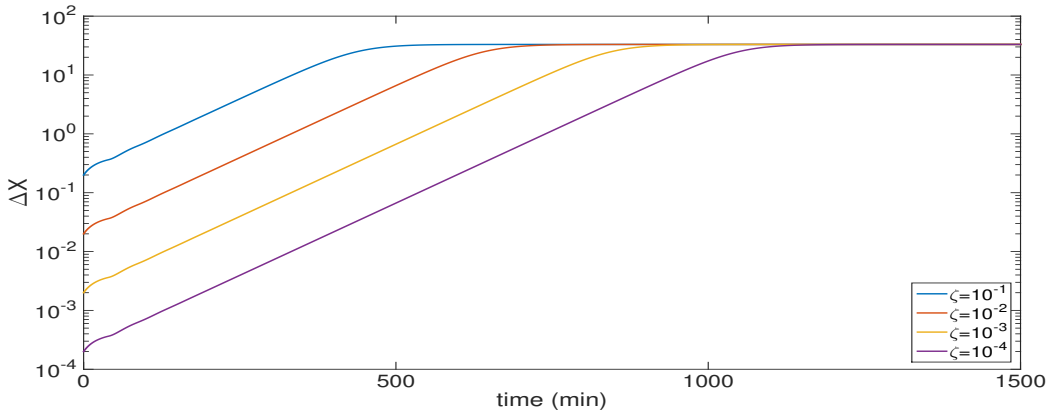


(a)

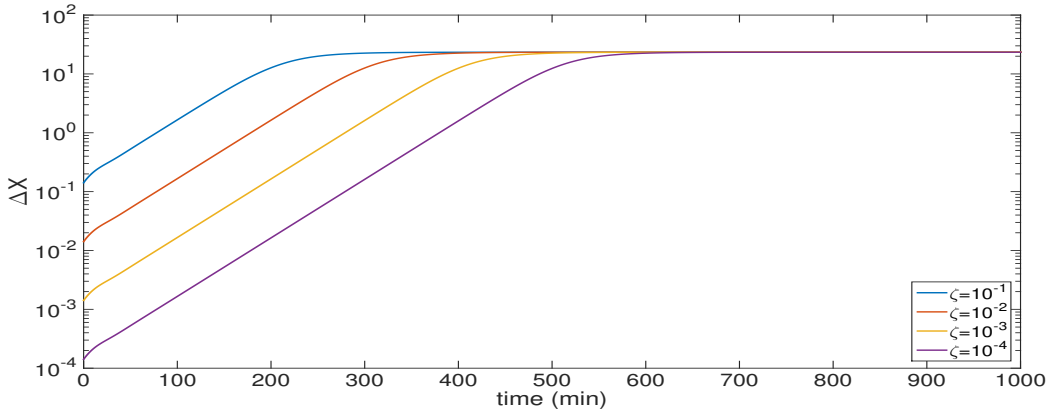


(b)

Figure 3.47: (a): $\ln(\Delta X(t))$ for (3.3.1) using default parameters (3.3.7) with $n_g = 2$ ($\chi = 0.0418$) and initial conditions A with various $\zeta$; (b): $\ln(\Delta X(t))$ for (3.3.2) using default parameters (3.3.8) with $n_s = 1.2$ ($\chi = 0.0418$) and initial conditions A with various $\zeta$.
For both systems, $M$, the gradient of $\ln(\Delta X(t))$, is constant until the state of the system reaches the switched steady state, independent of $\zeta$.

Similarly, when we plot $\ln(\Delta X(t))$ for a given $\zeta$ and increasing values of $\chi$, it is also true that $M$ is an increasing function of $\chi$. This hold for both $m = 1$ and $m = 2$ also, illustrated below in Figure 3.48.

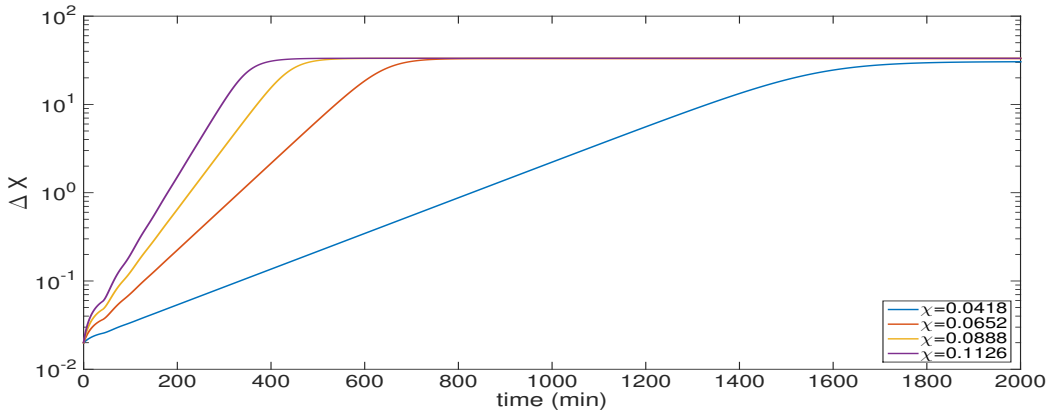


(a)

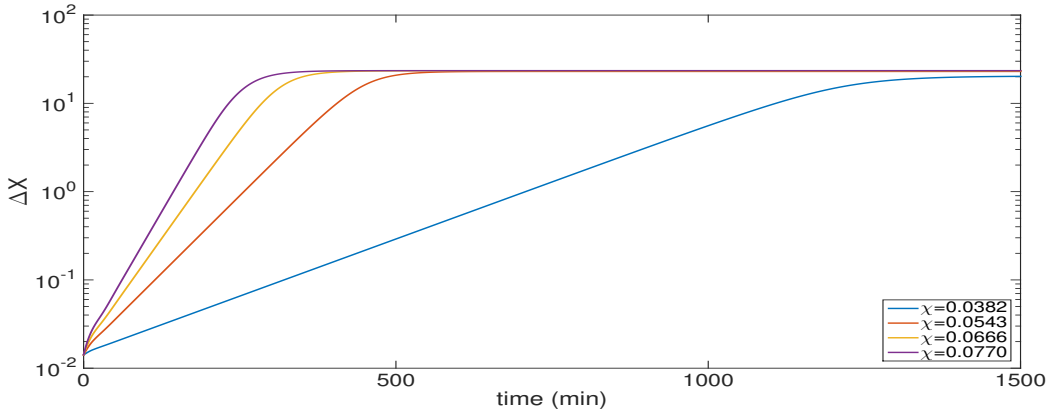


(b)

Figure 3.48: (a): $\ln(\Delta X(t))$ for (3.3.1) using default parameters (3.3.7) with various $n_g$ and initial conditions A with $\zeta = 10^{-2}$; (b): $\ln(\Delta X(t))$ for (3.3.2) using default parameters (3.3.8) with various $n_s$ and initial conditions A with $\zeta = 10^{-2}$.
For both systems, $M$, the gradient of $\ln(\Delta X(t))$, is an increasing function of $\chi$.

As these results further support what we have observed previously, this leads to the following proposition.

**Proposition 3.4.2.** *Simulations show that* $\Delta X(t) = \Delta X(0)\mathrm{e}^{Mt}$ *for initial conditions A, and linear stability analysis shows that* $\Delta X(t) = \Delta X(0)\mathrm{e}^{\lambda_D t}$ *close to the HSS. Therefore, we propose, for* $m = 1$ *and* $m = 2$*,*

$$M = \lambda_D = -\mu + \chi \mathrm{e}^{-\lambda_D \tau/m}. \tag{3.4.2}$$

By numerically calculating $M$ for each value of $\chi$, we can plot $M(\chi)$ and $\lambda_D(\chi)$, for each $m = 1$ and $m = 2$. The results are shown in Figure 3.49.

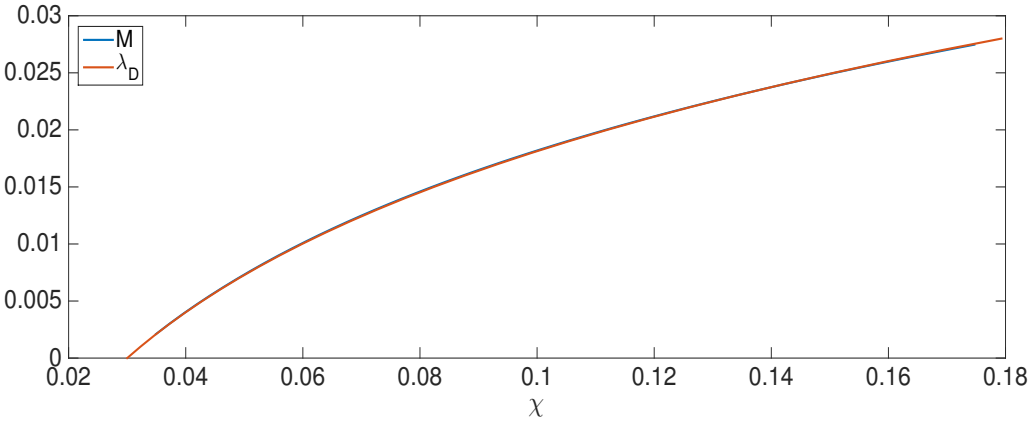


(a)

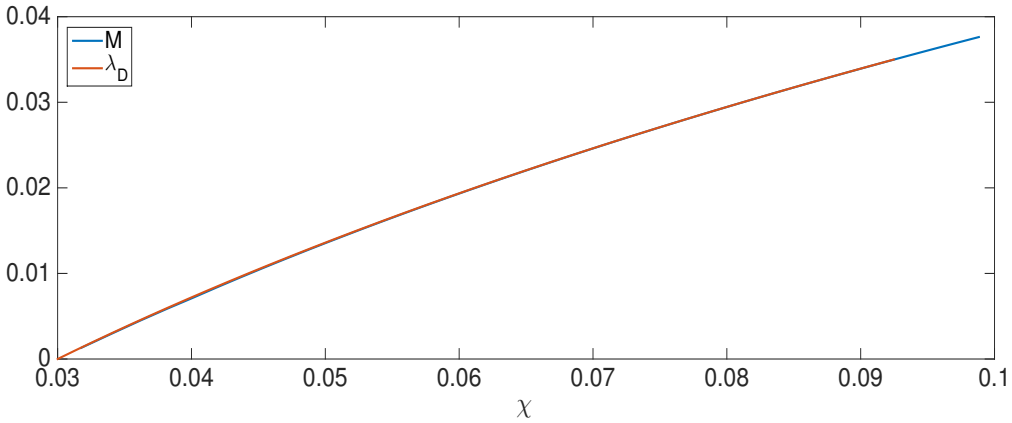


(b)

Figure 3.49: (a): Comparison of $\lambda_D = -\mu + \chi e^{-\lambda_D \tau}$ and calculated M as functions of $\chi$ for the system (3.3.1) using initial conditions A; (b): Comparison of $\lambda_D = -\mu + \chi e^{-\lambda_D \tau/2}$ and calculated M as functions of $\chi$ for the system (3.3.2) using initial conditions A.
Evidently, $\lambda_D$ is highly accurate in predicting the growth rate of the difference between the two cells for both systems.

Hence, Proposition 3.4.2 holds for both $m = 1$ and $m = 2$. Unlike the ODE systems, the growth rate of the total difference between the cells no longer increases linearly with $\chi$, with the gradient decreasing with $\chi$. In the ODE models, $\lambda_D = \chi - \mu$ for all values of $n$, but now, due to the additional exponential term in the expression for $\Delta X(t)$, the growth rate changes for different $m$, and the fewer components there are per cell, the smaller the growth rate of $\Delta X(t)$.

For comparison, the associated growth rates for the ODE $n = 3$ system, and the $m = 1$, $m = 2$ DDE systems are shown in Figure 3.48.

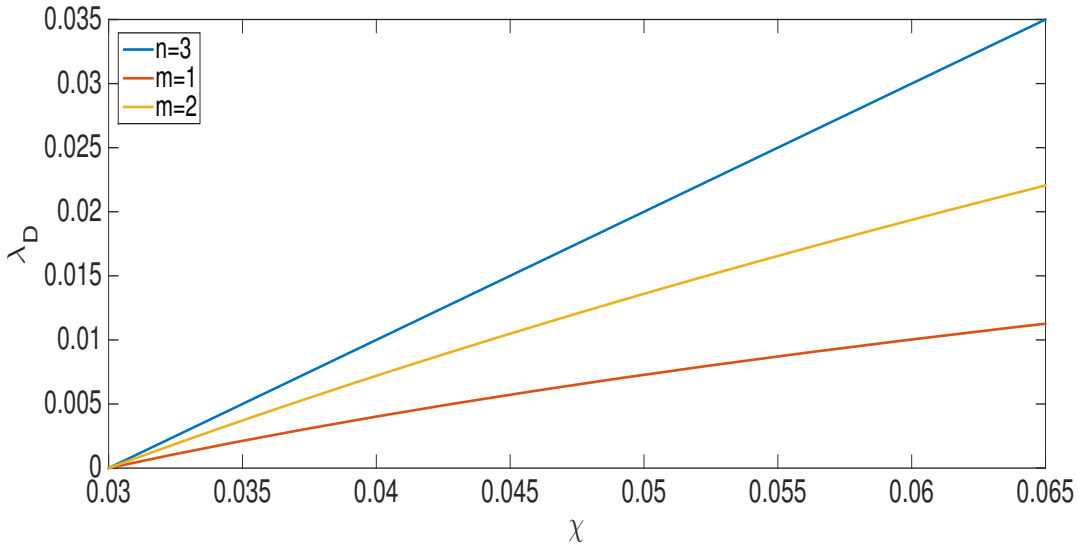


Figure 3.50: Comparison of $\lambda_D$ expressions for the systems (3.1.2), (3.3.1) and (3.3.2) as functions of $\chi$. We see a linear relationship for the $n = 3$ case, but in the cases of $m = 1$ and $m = 2$, the rate at which $\lambda_D$ increases is a decreasing function of $\chi$.

### 3.4.2 Results when using Initial Conditions B

When modelling the $n = 3$ ODE system we found that the behavioural dynamics of the system differed when using either initial conditions A or B, due to the nature of the HSS in the SoE.

By then showing how the $m = 1$ and $m = 2$ DDE systems can both display equivalent SoE dynamics to the $n = 3$ model, we expect to see similar behaviours when using initial conditions B in the full system.

**Note.** The following results have used values of $\tau$ which correspond to the systems having a Hopf bifurcation when $\chi = 2\mu$, to be able to give a more direct comparison between these models and the $n = 3$ ODE model. However, the following results will also hold for a different $\chi$, $\tau$ combination, provided the necessary Hopf bifurcation conditions are met.

When we use initial conditions B in the $m = 1$ and $m = 2$ DDE systems with respective delays of 40.31 min and 20.15 min, the following results hold:

1 **When $\chi \geq 2\mu$, there exist stable, in-phase oscillations in the levels of activity of the cells' variables as the state of the system moves from homogeneity to one of the switched steady states.**

To show this behaviour, Figure 3.51 shows $D(t)$ for $m = 1$ and Figure 3.52 shows $N(t)$ and $D(t)$ for $m = 2$ as $\chi$ is increased from less than $2\mu$ to greater than $2\mu$.

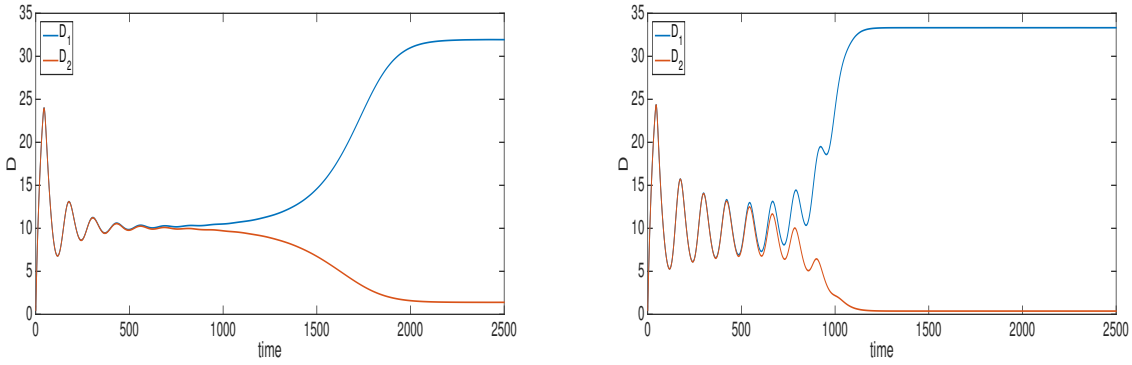


(a) (b)

Figure 3.51: Solution of (3.3.1) using default parameters (3.3.7) and initial conditions B with $\zeta = 10^{-2}$. (a) $n_g = 2.4$ ($\chi < 2\mu$), decaying transient oscillations are present prior to divergence from homogeneity; (b) $n_g = 3$ ($\chi > 2\mu$), stable transient oscillations are present as the states of the cells diverge from homogeneity.

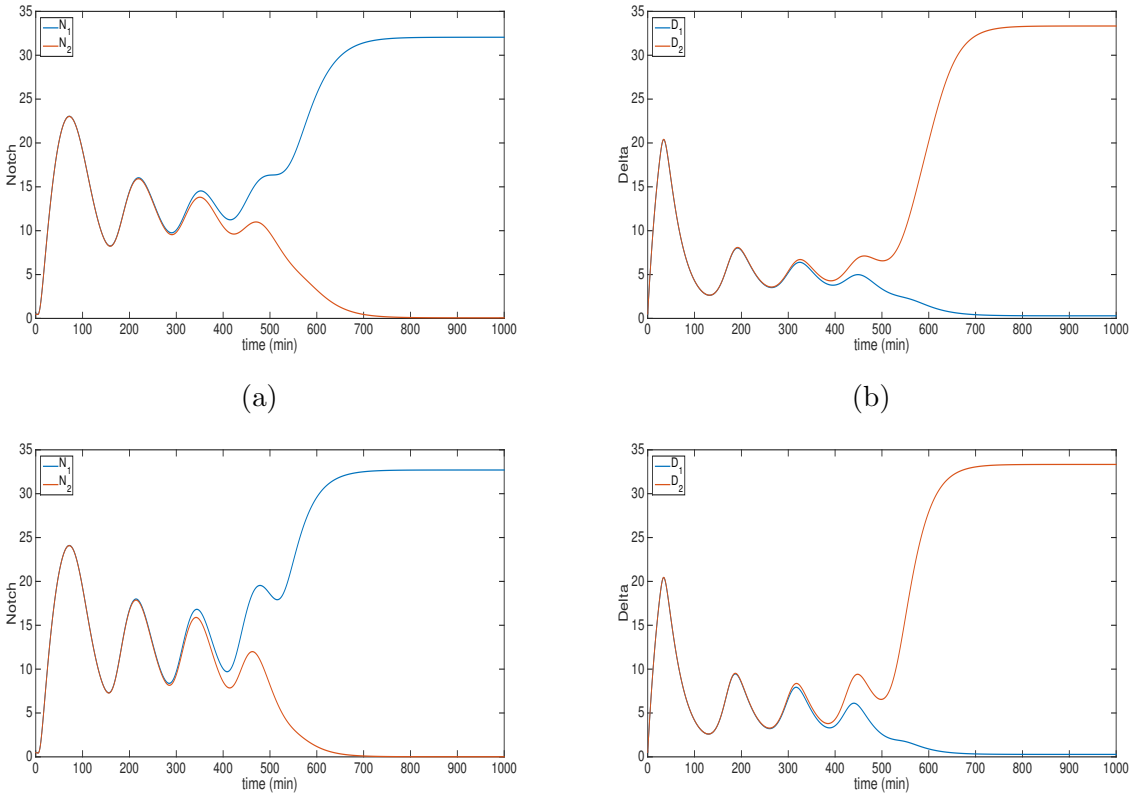


(a) (b)

(c) (d)

Figure 3.52: Solution of (3.3.2) using default parameters (3.3.8) and initial conditions B with $\zeta = 10^{-2}$. (a) $N(t)$, $n_s = 2.4$ ($\chi < 2\mu$); (b) $D(t)$, $n_s = 2.4$ ($\chi < 2\mu$). Decaying transient oscillations are present prior to divergence from homogeneity.
(c) $N(t)$, $n_s = 2.5$ ($\chi > 2\mu$); (b) $D(t)$, $n_s = 2.5$ ($\chi > 2\mu$). Stable transient oscillations are present as the states of the cells diverge from homogeneity.

Furthermore, the closer the states of the systems start to the SoE, the longer the oscillatory dynamics last, causing the TtS to increase. This is demonstrated when using a smaller value of $\zeta$ in the initial conditions, shown in Figures 3.53 and 3.54 when $\chi = 2\mu$.

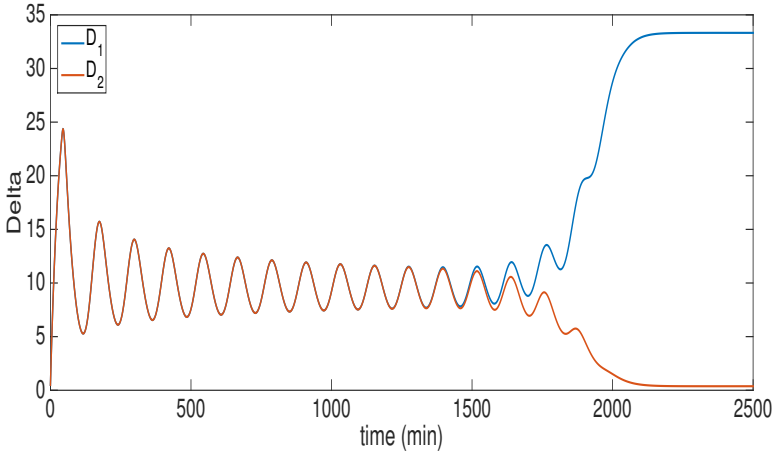


Figure 3.53: Solution of (3.3.1) using default parameters (3.3.7) with $n_g = 2.79$ ($\chi = 0.0601$) and initial conditions B with $\zeta = 10^{-6}$. When a smaller $\zeta$ used in the initial conditions, oscillatory dynamics are present for longer, and the Time to Switch for the system increases.

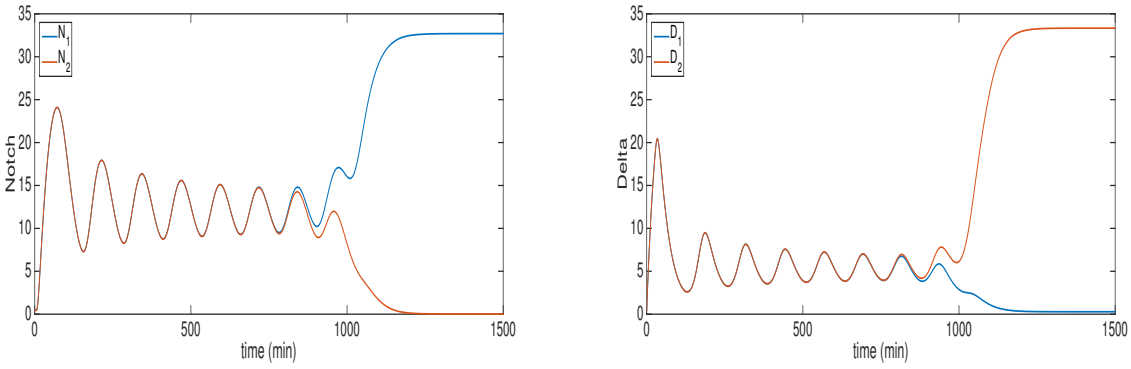


(a) (b)

Figure 3.54: Solution of (3.3.2) using default parameters (3.3.8) with $n_s = 2.45$ ($\chi = 0.0601$) and initial conditions B with $\zeta = 10^{-6}$. When a smaller $\zeta$ used in the initial conditions, oscillatory dynamics are present for longer, and the Time to Switch for the system increases.

2 **Time to Switch is only a decreasing function of $\chi$ when $\mu < \chi < 2\mu$. For $\chi \geq 2\mu$, TtS is now an increasing function of $\chi$, with $\frac{dTtS}{d\chi}$ a decreasing function of $\zeta$.**

When there exists a Hopf bifurcation, the dynamics in the SoE change and there now exists a stable periodic orbit, or a stable oscillation along the SoE for $m = 1$. For $\chi \geq 2\mu$,

this periodic orbit introduces oscillatory behaviour in the states of the cells, and TtS stops decreasing as a function of $\chi$.

TtS as a function of $\chi$ in plotted in Figure 3.55 for $m = 1$, and in Figure 3.56 for $m = 2$. In both cases, we have used $\zeta = 10^{-2}$ in the initial conditions.

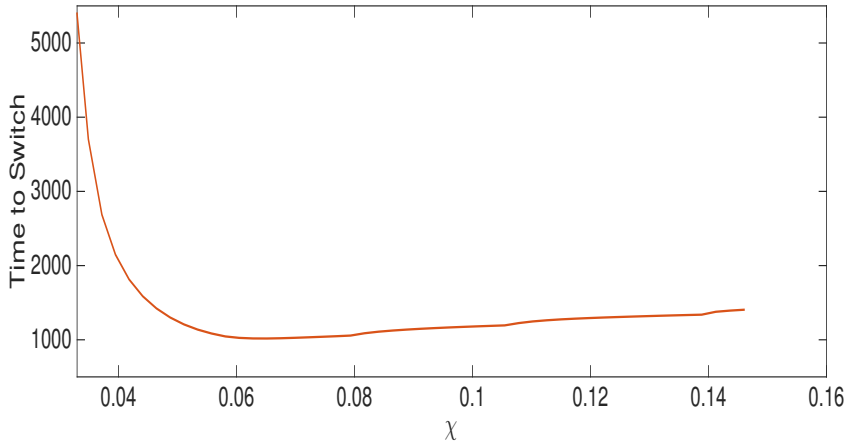


Figure 3.55: Time to Switch as a function of $\chi$ for the system (3.3.1) using default parameters (3.3.7) and initial conditions B with $\zeta = 10^{-2}$. Time to Switch is a decreasing function of $\chi$ until $\chi = 2\mu$, at which point it becomes an increasing function of $\chi$.

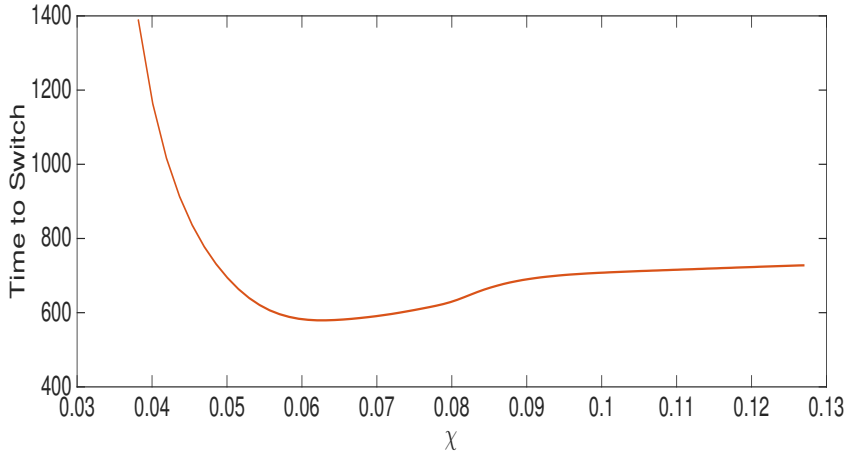


Figure 3.56: Time to Switch as a function of $\chi$ for the system (3.3.2) using default parameters (3.3.8) and initial conditions B with $\zeta = 10^{-2}$. Time to Switch is a decreasing function of $\chi$ until $\chi = 2\mu$, at which point it becomes an increasing function of $\chi$.

With the amplitude and period of the periodic orbit increasing with $\chi$, the oscillatory dynamics in the cells' variables gain prominence.

So, for $\chi \geq 2\mu$, TtS is an increasing function of $\chi$, with the rate of increase dependent on the magnitude of $\zeta$. TtS as a function of $\chi$ for $\chi \geq 2\mu$ with various $\zeta$ is shown in Figures 3.57 and 3.58, for $m = 1$ and $m = 2$, respectively.

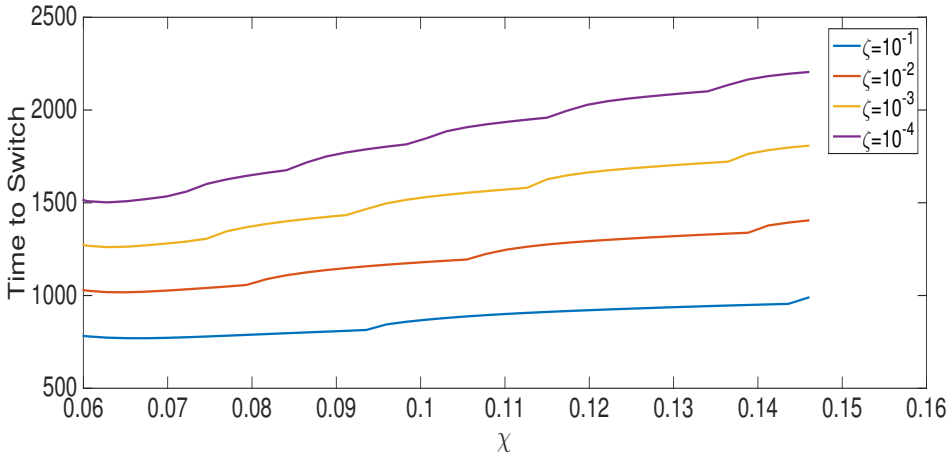


Figure 3.57: Time to Switch as a function of $\chi$ ($\chi \geq 2\mu$) for the system (3.3.1) using default parameters (3.3.7) and initial conditions B with various $\zeta$. For $\chi \geq 2\mu$, Time to Switch is an increasing function of $\chi$, with the rate of increase an increasing function of $\zeta$.

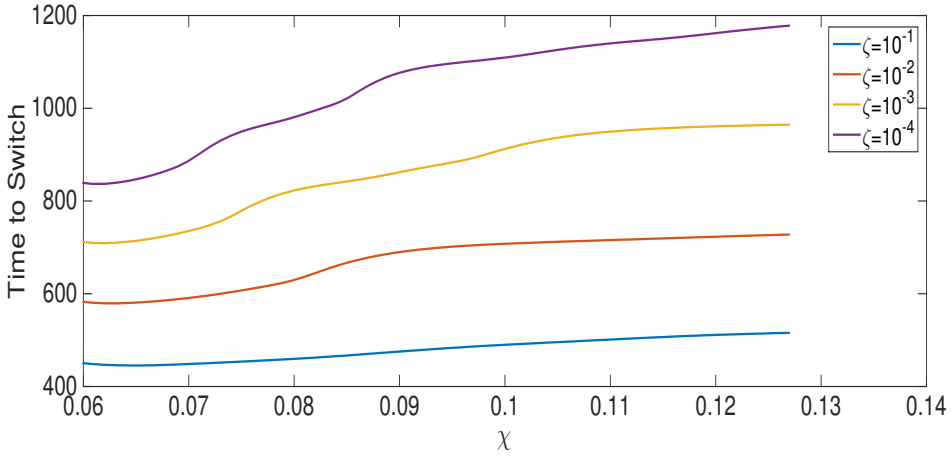


Figure 3.58: Time to Switch as a function of $\chi$ ($\chi \geq 2\mu$) for the system (3.3.1) using default parameters (3.3.7) and initial conditions B with various $\zeta$. For $\chi \geq 2\mu$, Time to Switch is an increasing function of $\chi$, with the rate of increase dependent on $\zeta$.

3 $\Delta X(t) \neq \Delta X(0)\mathrm{e}^{Mt}$**, but now appears to behave like**

$$\Delta X(t) = \Delta X(0)\mathrm{e}^{Mt}P(t), \tag{3.4.3}$$

**for some periodic function** $P(t)$**.**

If we plot $\ln(\Delta X(t))$ for a given $\chi \geq 2\mu$, we find that there is no longer a linear increase to the switched steady state, but there is now an additional periodicity observed. This can be seen in Figure 3.59 for both $m = 1$ and $m = 2$.

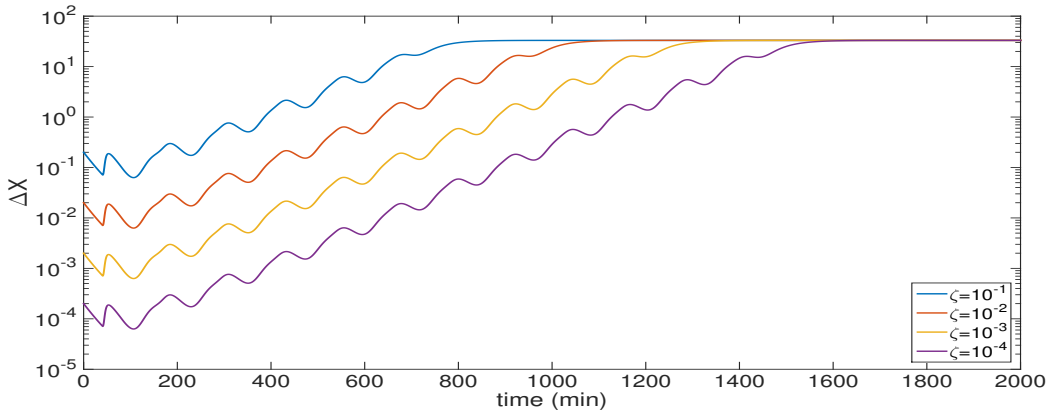


(a)

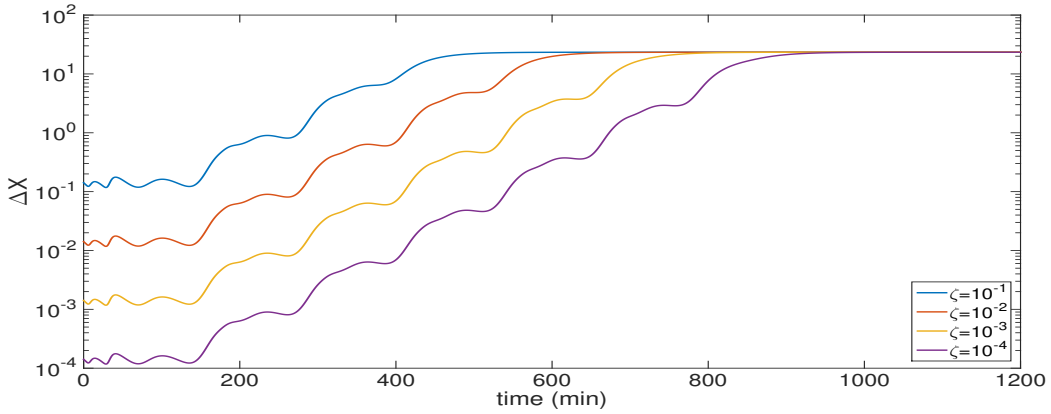


(b)

Figure 3.59: (a): $\ln(\Delta X(t))$ for the system (3.3.1) using default parameters (3.3.7) with $n_g = 2.79$ ($\chi = 0.0601$) and initial conditions B with various $\zeta$; (b): $\ln(\Delta X(t))$ for the system (3.3.2) using default parameters (3.3.8) with $n_s = 2.45$ ($\chi = 0.0601$) and initial conditions B with various $\zeta$.
In both cases, we observe a periodic growth in $\Delta X$ over time, and the closer the systems start to the SoE.

Additionally, if we plot $\ln(\Delta X(t))$ for increasing $\chi$, we find that the gradient of the difference, ignoring the periodic function, is a decreasing function of $\chi$. This can be seen in Figure 3.60 for both $m = 1$ and $m = 2$.

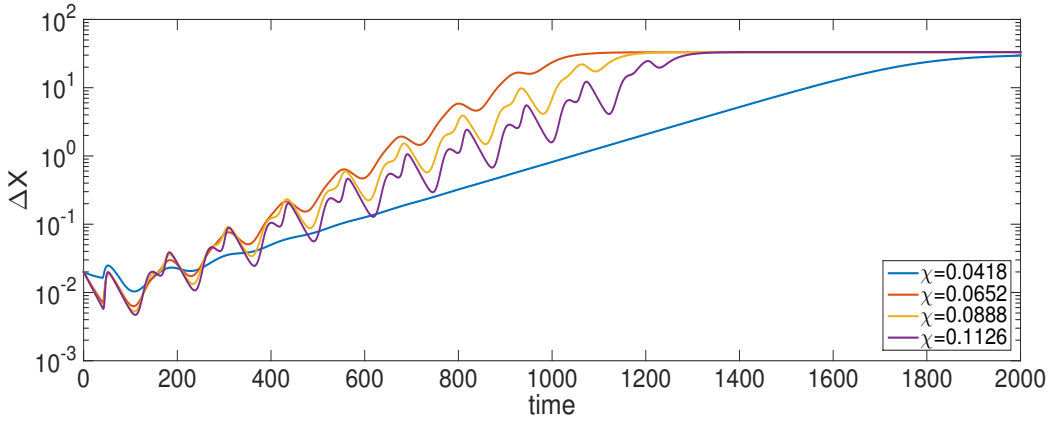


(a)

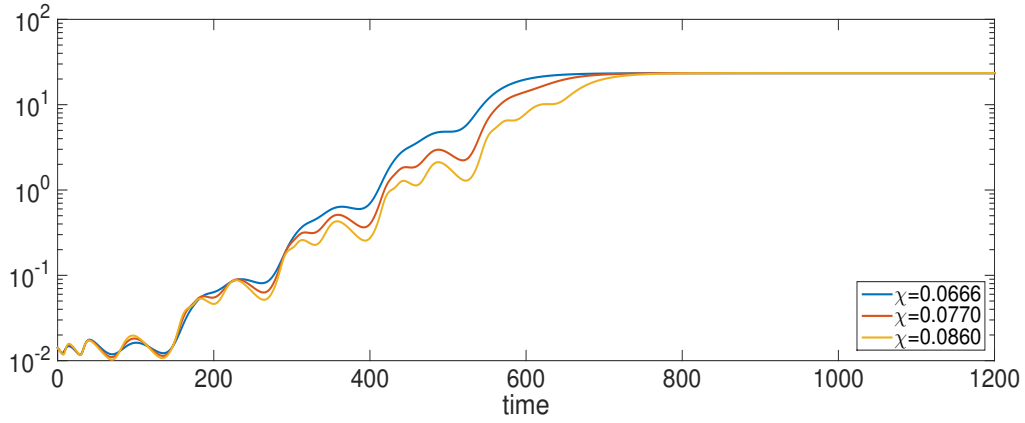


(b)

Figure 3.60: (a): $\ln(\Delta X(t))$ for the system (3.3.1) using default parameters (3.3.7) with various $n_g$ and initial conditions B with $\zeta = 10^{-2}$; (b): $\ln(\Delta X(t))$ for the system (3.3.2) using default parameters (3.3.8) with various $n_s$ and initial conditions B with $\zeta = 10^{-2}$. As $\chi$ is increased (above $\chi = 2\mu$), the prominence of the periodicity in the growth rate of $\Delta X$ increases, causing the time taken for the state of the system to reach the switched steady state to increase.

**Proposition 3.4.3.** *When the state of the system starts close to the SoE, away from the HSS, the dynamics observed in the SoE cause oscillatory behaviour in the full system.*

The three previous results and the similarities to the $n = 3$ ODE model we have observed, all support this proposition well. When there is a periodic orbit in the SoE and the system's initial conditions are close to the SoE, the effects are visible in the states of the cells.

When using the Mean and Difference variables, the Mean variables display similar dynamics to those observed in the SoE, which, in turn, affect the Difference variables, as we have already seen.

To observe this more clearly, Figure 3.61 shows plots of $(\ln(M_D(t)), \ln(\Delta X(t)))$ using various $\chi$ and $\zeta$ for $m = 1$, and Figure 3.62 shows $(\ln(M_N(t)), \ln(M_D(t)), \ln(\Delta X(t)))$ for

$m = 2$.

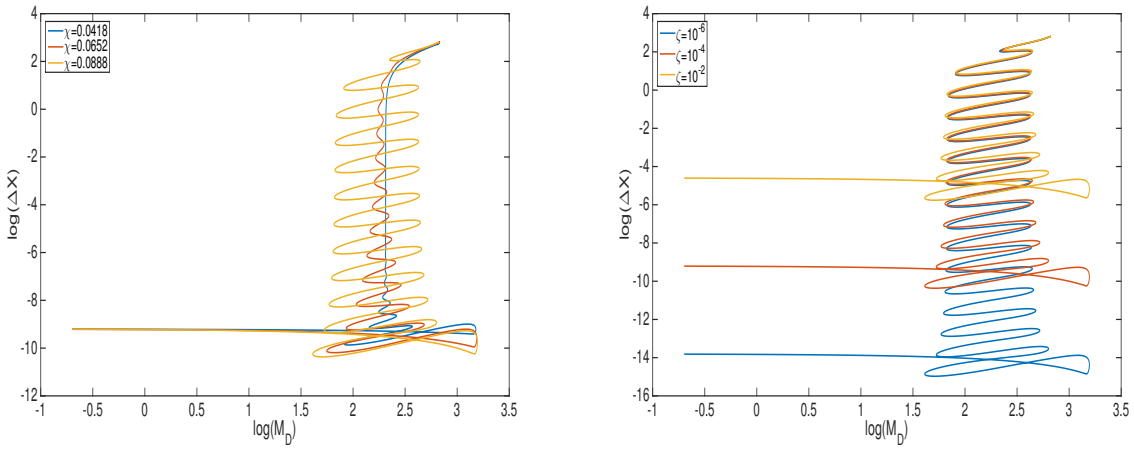


(a) (b)

Figure 3.61: $\ln(M_D(t))$, $\ln(\Delta X(t))$ for the system (3.3.1) using default parameters (3.3.7) with various $n_g$ and initial conditions B with various $\zeta$.
(a): $\zeta = 10^{-2}$, $n_g = 2,\ 3,\ 4$ ($\chi = 0.0418,\ 0.0652,\ 0.0888$, respectively). When $\mu < \chi < 2\mu$ there is a stable spiral in the Mean variable, which decreases in amplitude as $\Delta X$ increases. When $\chi \geq 2\mu$, the state of the Mean variable is almost periodic until the switched steady state.
(b): $n_g = 4$ ($\chi = 0.0888$), $\zeta = 10^{-2},\ 10^{-4},\ 10^{-6}$. The same qualitative behaviour is observed independent of $\zeta$, but the closer the system starts to the SoE, the greater the number of oscillations observed in the state of the Mean variable, and the greater the Time to Switch for the system.

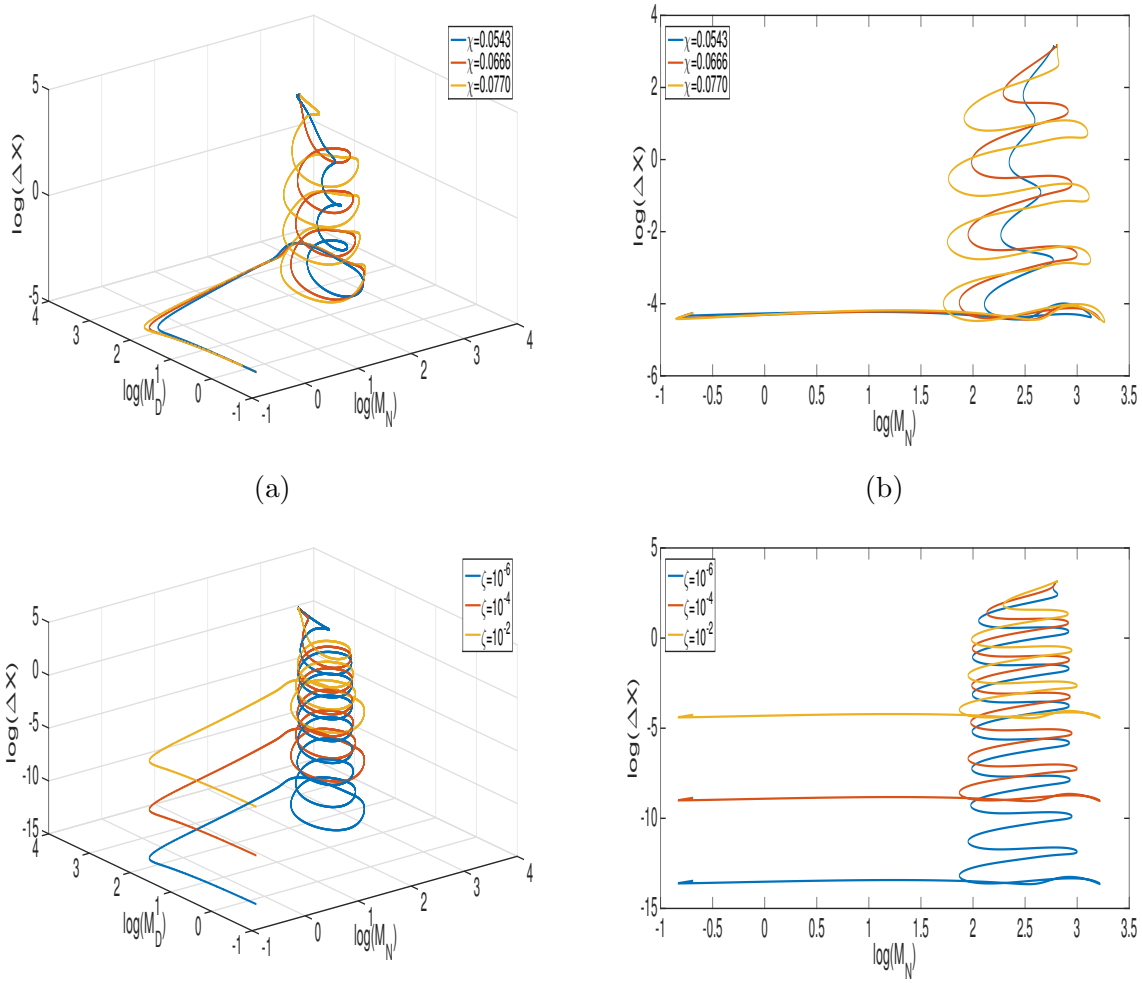


Figure 3.62: $\ln(M_N(t))$, $\ln(M_D(t))$, $\ln(\Delta X(t))$ for the system (3.3.2) using default parameters (3.3.8) with various $n_s$ and initial conditions B with various $\zeta$.
(a), (b): $\zeta = 10^{-2}$, $n_g = 2,\ 3,\ 4$ ($\chi = 0.0543,\ 0.0666,\ 0.070$, respectively). When $\mu < \chi < 2\mu$ there is a stable spiral in the Mean variables, which decreases in amplitude as $\Delta X$ increases. When $\chi \geq 2\mu$, the states of the Mean variables are almost periodic until the switched steady state.
(c), (d): $n_g = 3$ ($\chi = 0.0666$), $\zeta = 10^{-2},\ 10^{-4},\ 10^{-6}$. The same qualitative behaviour is observed independent of $\zeta$, but the closer the system starts to the SoE, the greater the number of oscillations observed in the states of the Mean variables, and the greater the Time to Switch for the system.

From Figures 3.61 and 3.62, we are able to provide the following statements:

- When $\mu < \chi < 2\mu$, we can see there is a stable spiral in the Mean variables, which decays in amplitude as $\Delta X$ increases. This is seen in Figure 3.61(a) for $\chi = 0.0418$, and Figure 3.62(b) for $\chi = 0.0543$.

- For $\chi \geq 2\mu$, the Mean variables are almost periodic until the vicinity of the switched

steady state, clearly seen in Figure 3.61 (a) and 3.62 (b). This introduces a periodic expression in $\Delta X(t)$.

- The amplitude and period are both increasing functions of $\chi$, whilst the growth per period in $\Delta X(t)$ appears to decrease.
- The SoE dynamics (Mean dynamics) propagate from the SoE up to the switched steady state, with a near-constant periodicity until reaching the steady state. This is shown clearest in Figure 3.61 (b) and 3.62(d).
- The closer the system starts to the SoE, the greater the effect the SoE dynamics have on the full system. The Mean variables display a greater number of oscillations, evident in Figures 3.61(b) and 3.62 (c), (d), from where the different initial conditions start on the 'coil', in addition to the increased switching times we saw previously.

Despite the behaviour being so similar to the $n = 3$ ODE model, trying to use the same approach for calculating the growth rate no longer works for these models. However, from the $\ln(\Delta X(t))$ figures with increasing values of $\chi$, it is clear that the growth rate does reach a maximum when $\chi = 2\mu$.

Additionally, we were able to successfully use a line of best fit approach to calculate the gradient of $\ln(\Delta X(t))$ for $m = 2$, with the result clearly demonstrating this behaviour.This is shown in Figure 3.63

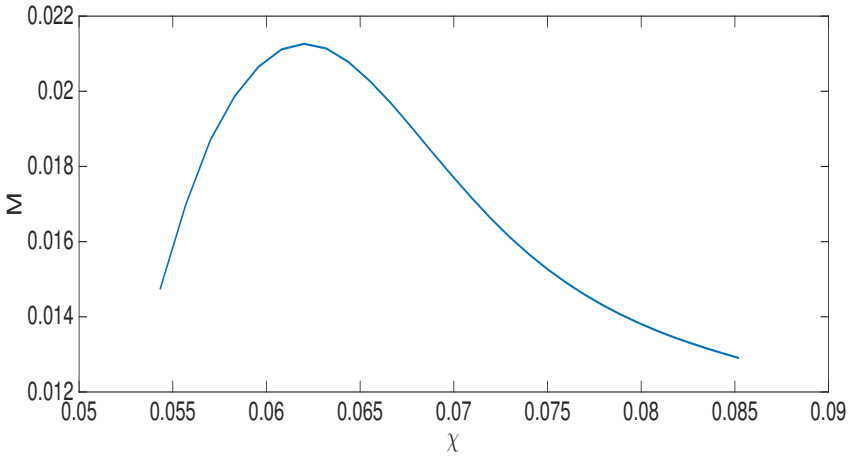


Figure 3.63: $M$, the numerical estimate for the growth rate of $\Delta X(t)$, as a function of $\chi$ for the system (3.3.2) using default parameters (3.3.8) and initial conditions B. It is evident that the growth rate of $\Delta X$ reaches a maximum when $\chi = 2\mu$, from which point it becomes a decreasing function of $\chi$.

Therefore, it is still possible to make the same proposition for these systems with conviction.

**Proposition 3.4.4.** *$M(\chi)$ reaches a maximum when $\chi = 2\mu$, and the presence of the periodic orbit in the SoE causes $M(\chi)$ to decrease for $\chi \geq 2\mu$.*

## Summary of Results

These simulations confirm:

- The nature of the homogeneous steady state, and its stability as a function of $\chi$ and $\tau$. The HSS becomes unstable to perturbations when $\chi > \mu$, and there exists a Hopf bifurcation when

$$\chi > \mu, \quad \tau = \frac{\pi - m\tan^{-1}\left(\frac{\omega}{\mu}\right)}{\omega};$$

- The growth rate of perturbations from the HSS when unstable is determined by

$$\Delta X(t) = \Delta X(0)e^{\lambda_D t}$$

where $\lambda_D = -\mu + \gamma e^{-\lambda_D \tau/m}$. This is illustrated for both $m = 1$ and $m = 2$ systems in Figure 3.49, and holds accurately not just at the HSS, but all the way to the systems' final states.

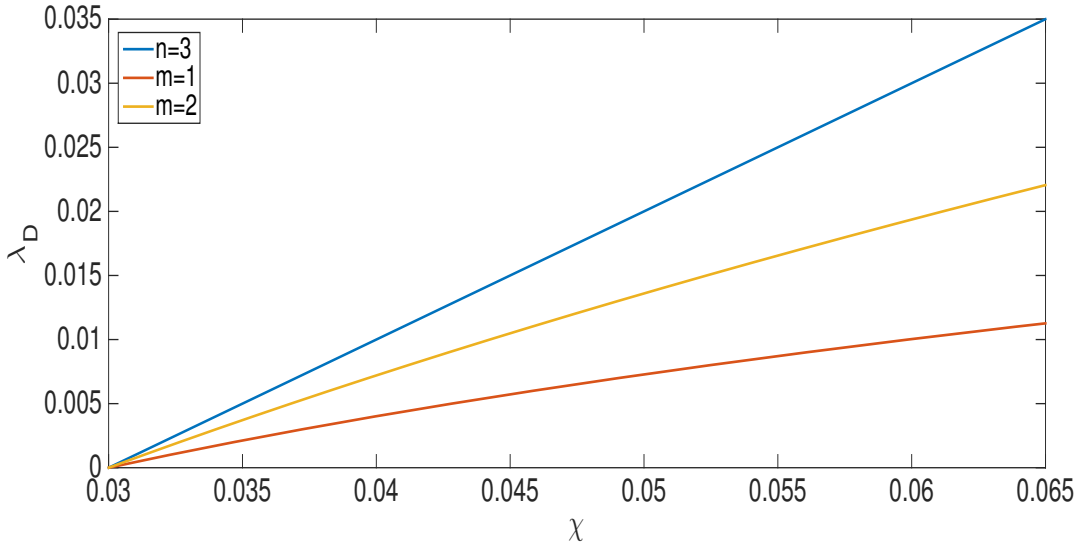


Figure 3.64: Comparison of $\lambda_D$ expressions for the systems (3.1.2), (3.3.1) and (3.3.2) as functions of $\chi$. We see a linear relationship for the $n = 3$ case, but in the cases of $m = 1$ and $m = 2$, the rate at which $\lambda_D$ increases is a decreasing function of $\chi$.

- A system governed by $m$ DDEs per cell is capable of displaying qualitatively equivalent dynamics to a system governed by $n$ ODEs per cell (where $n > m$), and can go through a Hopf bifurcation for the same value of $\chi$, provided there is a delay

$$\tau = \frac{(n-m)\pi}{n\omega}.$$

Comparing Figures 3.25, 3.26 with Figures 3.53, 3.54, we observe the $n = 3$, $m = 1$ and $m = 2$ systems all displaying oscillations during switching, for which all have equal values of $\chi$;

- A system governed by $m$ DDEs per cell is capable of displaying qualitatively equivalent dynamics to a system governed by $k$ DDEs per cell (where $k > m$), and can go through a Hopf bifurcation for the same value of $\chi$, provided the delays are related by

$$\tau_k = \frac{k}{m}\,\tau_m - \frac{(k-m)\pi}{m\omega};$$

This is illustrated nicely in Figures 3.53 and 3.54, which show both systems displaying oscillations during switching for an equal value of $\chi$;

- The total delay per cell is used to determine conditions for a Hopf bifurcation, and how this delay is distributed throughout the pathway dictates the phase difference between the cell's variables;

- Provided $\chi > \mu$, there always exists a delay which can ensure the system undergoes a Hopf bifurcation, illustrated below in Figure 3.65;

- For a given value of $\chi > \mu$, the greater the number of components per cell, the smaller the delay necessary to ensure a Hopf bifurcation.

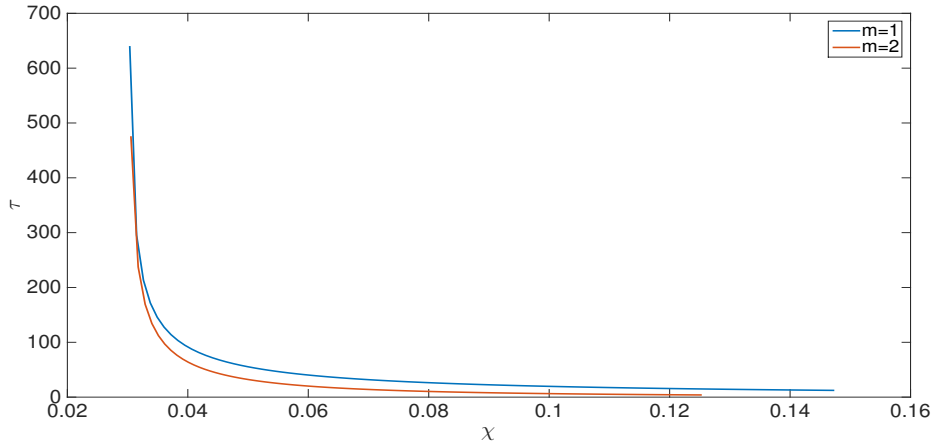


Figure 3.65: Relationship between $\chi$ and $\tau$ for the existence of a Hopf bifurcation, as described by equation (2.2.95), for both $m = 1$ and $m = 2$. For a given value of $\chi$, the greater the number of components per cell, the smaller the time delay necessary for a Hopf bifurcation.

## 3.5 Multicellular Populations

As discussed in the beginning of Section 2.3, if we want to investigate the dynamics of a larger population of cells on a hexagonal lattice, it is simplest to gradually increase the population from two cells, and then change the geometry of the population. We will first look at multicellular systems which also have a period-2 pattern of cell-types, such as a ring of cells, or cells on a square lattice, and then change the geometry to a hexagonal lattice.

As we showed in the linear stability analysis for systems which display a period-2 pattern, bifurcation conditions hold for the same parameter values as the 2-cell system, and if initial conditions are chosen such that the system forms a perfect pattern of alternating cell-types, there will be little temporal variability between the models.

However, using the approach of analysing the cell-type dynamics rather than individual cell dynamics does not tell us what happens when the initial conditions of the system lead to an imperfect pattern of cell-types.

If the initial state of each cell is of a similar form as the those defined in the previous Section, such that

$$X_k(0) = SoEP + \zeta \underline{R}, \tag{3.5.1}$$

where $X_k$ is the state of the cell $k$, $SoEP$ is a position on the SoE, $\zeta$ is the magnitude, and $\underline{R}$ is a vector of random numbers in [0,1] of length $n$ (number of components in each cell), the pattern of cell-types would be more likely to have imperfections.

Initial conditions of this type are more likely to reduce the coherency of the signal each cell receives from its multiple neighbours regarding which state to adopt, affecting the ratio of different cell-types and introducing temporal variability in the cell-fate decision process. These are two aspects which cannot be addressed from a 2-cell system, or linear stability analysis.

Therefore, for different multicellular systems, we can address the following questions:

1. For a 2-cell system, how is Time to Switch affected when using initial conditions with a random perturbation from homogeneity?

2. Does a more complex arrangement of the population (each cell has an increased number of neighbours) affect the cells' switching times, and increase the range of switching times?

3. For a given arrangement of cells, does the population size affect the ratio of cell types and temporal variability in the system forming a pattern of different cell-types?

To answer these questions we will evaluate the temporal dynamics of different multicellular populations, arranged on different geometric arrays, but all using the same form of signalling, with equal model parameters and initial conditions.

We will investigate systems arranged as:

i A ring of cells;

ii Cells on a square lattice;

iii Cells on a hexagonal lattice.

Since the number of neighbours each cell has increases through the different arrangements, we can think of these as increasing in geometric complexity.

In addition to this comparison of different cell arrangements, we have also simulated the system of cells on a hexagonal lattice further, to verify the results obtained from the linear stability analysis from Section 2.3.1

### 3.5.1 Arrangements, model parameters and initial conditions

All of the following results have been for cells with three variables each (Notch, Hes and Delta for consistency), such that each pair of neighbouring cells is connected via an equivalent pathway as those seen in the 2-cell systems.

**Ring of Cells**

If we have a ring of $n$ cells, then the dynamics of each cell $\underline{X}_j$ can be described by

$$\begin{aligned}\dot{N}_j &= -\mu_N N_j + f_s\left(\frac{D_{j-1}+D_{j+1}}{2}\right),\\ \dot{H}_j &= -\mu_H H_j + f_2(N_j),\\ \dot{D}_j &= -\mu_D D_j + g(H_j),\end{aligned} \tag{3.5.2}$$

where $j = 1, 2, \ldots, n$.

**Cells on a square lattice**

If we denote each cell in the array by $\underline{X}_{p,q}$, where $p$ denotes the cell's column and $q$ denotes the cell's row in the array, then the dynamics of each cell can be described by the equations

$$\begin{aligned}\dot{N}_{p,q} &= -\mu_N N_{p,q} + f_s\left(\frac{D_{p-1,q}+D_{p+1,q}+D_{p,q-1}+D_{p,q+1}}{4}\right),\\ \dot{H}_{p,q} &= -\mu_H H_{p,q} + f_2(N_{p,q}),\\ \dot{D}_{p,q} &= -\mu_D D_{p,q} + g(H_{p,q}),\end{aligned} \tag{3.5.3}$$

The labelling scheme for this system is illustrated in Figure 3.66.

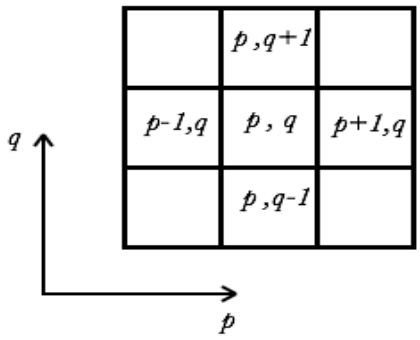


Figure 3.66: Labelling scheme used for cells arranged on a square lattice.

**Cells on a hexagonal lattice**

If we again denote each cell in the array by $\underline{X}_{p,q}$, then the dynamics of each cell can be described by the equations

$$\begin{aligned}
\dot{N}_{p,q} &= -\mu_N N_{p,q} + f_s\left(\frac{D_{p-1,q} + D_{p-1,q+1} + D_{p,q+1} + D_{p+1,q} + D_{p+1,q-1} + D_{p,q-1}}{6}\right), \\
\dot{H}_{p,q} &= -\mu_H H_{p,q} + f_2(N_{p,q}), \\
\dot{D}_{p,q} &= -\mu_D D_{p,q} + g(H_{p,q}).
\end{aligned} \tag{3.5.4}$$

The labelling scheme for this system is illustrated in Figure 3.67.

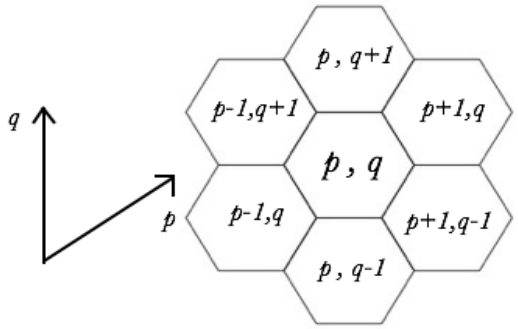


Figure 3.67: Labelling scheme used for cells arranged on a hexagonal lattice.

In all cases, we have used periodic boundary conditions, such that every cell has the same number of distinct neighbours.

**Model Parameters**

In all cases, we have used the parameters

$$\begin{aligned} &\mu_N = \mu_H = \mu_D = \mu = 0.03\text{min}^{-1}, \\ &\theta_s = \theta_2 = \theta_g = \frac{0.2}{\mu}\text{min}, \\ &n_s = 3,\ n_2 = 2,\ n_g = 3. \end{aligned} \tag{3.5.5}$$

These correspond to each system having a Hopf bifurcation, such that there exists a periodic orbit in the SoE.

**Initial Conditions**

We want to use initial conditions of a similar form as those used in the 2-cell systems, such that

$$A \equiv HSS + \zeta \underline{R}, \qquad B \equiv \underline{0.5} + \zeta \underline{R}, \tag{3.5.6}$$

where $\zeta = 10^{-2}$ or $\zeta = 10^{-6}$, and $\underline{R}$ is a vector of length $3n$ containing random values drawn from a standard normal distribution.

**Definitions**

Now that there are multiple cells in the system, we can no longer define Time to Switch as the time taken for the system to switch. Since cells will now commit to their final states at different times, we want to have a definition for TtS on an individual level.

As discussed in Chapter 1, Primary Fate [PF] cells are those which take the steady state corresponding to a high level of Delta and low level of Notch, whilst Secondary Fate cells are those which take the other steady state, corresponding to high levels of Notch and low levels of Delta.

For the remainder of this chapter, we will only be concerned with the switching times of Primary Fate cells, so we therefore want the following definitions:

**Definition 3.5.1.** A cell $j$ becomes a Primary Fate [PF] cell when

$$D_j = 0.8 \times \max(D), \tag{3.5.7}$$

where $\max(D) = 1/\mu_D$.

**Definition 3.5.2.** Time to Switch [TtS] is now defined as the time at which a cell becomes a Primary Fate cell;

$$D_j(TtS) \equiv 0.8 \times \max(D(t)). \tag{3.5.8}$$

### 3.5.2 Results

For each model and choice of initial conditions, we have carried out 100 simulations. The results presented are the mean results from each 100 simulations.

**1** To answer the first question, we want to compare the switching times of a 2-cell system when the system's initial conditions either use a perturbation $\underline{P}$, or $\underline{R}$, where

$$\underline{P} = \begin{pmatrix} 1 \\ -1 \\ 1 \\ -1 \\ -1 \\ 1 \end{pmatrix}.$$

The switching times for two-cell systems using different initial conditions are presented in Tables 3.1 and 3.2.

| 2 Cells | |
|---|---|
| Initial Conditions | TtS |
| A, $\zeta = 10^{-2}$, $\underline{P}$ | 273.6 |
| A, $\zeta = 10^{-6}$, $\underline{P}$ | 578.4 |
| B, $\zeta = 10^{-2}$, $\underline{P}$ | 472.8 |
| B, $\zeta = 10^{-6}$, $\underline{P}$ | 813.7 |

Table 3.1: Time to Switch for a system of two cells when using using initial conditions A and B with $\zeta = 10^{-2}$ or $10^{-6}$ and a perturbation $\underline{P}$ from the SoE, and parameters given by (3.5.5).
For each initial condition A or B, Time to Switch is a decreasing function of $\zeta$, such that it takes longer for the system to switch when starting closer to the SoE. Additionally, for a given $\zeta$, Time to Switch is always greater for initial conditions B than initial conditions A.

| 2 Cells | | | |
|---|---|---|---|
| Initial Conditions | Mean TtS | TtS Range | Standard Deviation |
| A, $\zeta = 10^{-2}$, $\underline{R}$ | 310.54 | 250.4-452 | 36.010 |
| A, $\zeta = 10^{-6}$, $\underline{R}$ | 615.79 | 565.8-744.8 | 36.112 |
| B, $\zeta = 10^{-2}$, $\underline{R}$ | 505.78 | 459.4-673.2 | 41.664 |
| B, $\zeta = 10^{-6}$, $\underline{R}$ | 857.88 | 799-982.6 | 27.309 |

Table 3.2: Mean Time to Switch and mean range of switching times for a system of two ells when using using parameters (3.5.5) and initial conditions (3.5.6). For each choice of initial conditions, we have run 100 simulations, such that each run uses a different perturbation vector $\underline{R}$.

As we have already seen, when there is a periodic orbit in the SoE, there is a noticeable difference in TtS between initial conditions A and B with equal $\zeta$, where this difference is a decreasing function of $\zeta$. This still holds true when using a random perturbation $\underline{R}$, with the differences between the initial conditions only differing slightly.

So, on average, TtS increases when using a random perturbation $\underline{R}$ rather than $\underline{P}$ in the initial conditions. But, the lower range of TtS for some $\underline{R}$ is less than TtS when using $\underline{P}$.

Hence, TtS will generally increase if we use a random perturbation, but occasionally, a random perturbation will be closer to the direction of the switched steady state than $\underline{P}$, causing a lower switching time. This is true for all sets of initial conditions.

To see the effect of geometric complexity, we want to compare the switching times of systems with different cellular arrangements.

Firstly we will compare different systems which can form a period-2 pattern, and then compare these to a system on a hexagonal array.

By looking at different population sizes for each geometry, we can also address the third question.

The results are presented in Tables 3.3, 3.4 and 3.5.

| Ring of Cells | | | | | |
|---|---|---|---|---|---|
| Initial Conditions | Population Size | Primary Fate Proportion | Mean TtS | Mean TtS Range | Standard Deviation |
| A, $\zeta = 10^{-2}$, $\underline{R}$ | 10 | 0.462 | 270.00 | 244.04-303.15 | 36.069 |
| | 50 | 0.453 | 272.42 | 227.42-363.27 | 36.296 |
| | 100 | 0.455 | 272.32 | 222.35-386.25 | 36.688 |
| A, $\zeta = 10^{-6}$, $\underline{R}$ | 10 | 0.491 | 580.82 | 568.33-595.39 | 35.542 |
| | 50 | 0.470 | 582.22 | 544.62-668.51 | 34.438 |
| | 100 | 0.470 | 584.40 | 539.64-697.68 | 35.834 |
| B, $\zeta = 10^{-2}$, $\underline{R}$ | 10 | 0.487 | 558.82 | 537.78-582.68 | 35.532 |
| | 50 | 0.465 | 566.93 | 508.06-670.43 | 44.887 |
| | 100 | 0.464 | 564.95 | 500.63-692.22 | 43.852 |
| B, $\zeta = 10^{-6}$, $\underline{R}$ | 10 | 0.499 | 896.47 | 889.72-903.43 | 35.532 |
| | 50 | 0.471 | 909.57 | 868.0-1008.6 | 42.599 |
| | 100 | 0.472 | 907.93 | 861.8-1032.2 | 41.940 |

Table 3.3: Time to Switch, range of switching times and proportion of Primary Fate cells for cells arranged on a ring, as described by (3.5.2), using parameters (3.5.5) and initial conditions (3.5.6). For each choice of initial conditions and population size, we have run 100 simulations, such that each run uses a different perturbation vector $\underline{R}$.

| Square Array of Cells | | | | | |
|---|---|---|---|---|---|
| Initial Conditions | Population Size | Primary Fate Proportion | Mean TtS | MeanTtS Range | Standard Deviation |
| A, $\zeta = 10^{-2}$, $\underline{R}$ | 36 | 0.467 | 399.38 | 343.98-591.59 | 35.755 |
| | 144 | 0.425 | 397.44 | 340.55-620.51 | 34.851 |
| | 324 | 0.424 | 398.64 | 337.11-651.36 | 35.270 |
| A, $\zeta = 10^{-6}$, $\underline{R}$ | 36 | 0.495 | 707.69 | 658.34-894.3 | 37.879 |
| | 144 | 0.445 | 718.61 | 661.82-939.77 | 34.616 |
| | 324 | 0.443 | 715.71 | 654.89-935.55 | 34.249 |
| B, $\zeta = 10^{-2}$, $\underline{R}$ | 36 | 0.484 | 616.34 | 549.42-776.09 | 37.29 |
| | 144 | 0.429 | 616.97 | 548.22-913.36 | 36.054 |
| | 324 | 0.432 | 615.93 | 531.03-873.31 | 36.325 |
| B, $\zeta = 10^{-6}$, $\underline{R}$ | 36 | 0.497 | 957.71 | 886.3-1180.6 | 38.560 |
| | 144 | 0.455 | 966.79 | 897.5-1205.9 | 33.159 |
| | 324 | 0.444 | 968.28 | 892.9-1260.1 | 34.569 |

Table 3.4: Time to Switch, range of switching times and proportion of Primary Fate cells for cells arranged on a square lattice, as described by (3.5.3), using parameters (3.5.5) and initial conditions (3.5.6). For each choice of initial conditions and population size, we have run 100 simulations, such that each run uses a different perturbation vector $\underline{R}$.

| Hexagonal Array of Cells | | | | | |
|---|---|---|---|---|---|
| Initial Conditions | Population Size | Primary Fate Proportion | Mean TtS | Mean TtS Range | Standard Deviation |
| A, $\zeta = 10^{-2}$, $\underline{R}$ | 36 | 0.314 | 520.18 | 439.52-799.37 | 51.247 |
| | 144 | 0.276 | 530.64 | 443.36-838.67 | 44.698 |
| | 324 | 0.277 | 529.09 | 428.76-851.02 | 46.835 |
| A, $\zeta = 10^{-6}$, $\underline{R}$ | 36 | 0.333 | 1047.1 | 958.7-1249.3 | 50.776 |
| | 144 | 0.302 | 1064.8 | 982.2-1343.3 | 44.982 |
| | 324 | 0.289 | 1069.6 | 975.0-1365.5 | 45.202 |
| B, $\zeta = 10^{-2}$, $\underline{R}$ | 36 | 0.322 | 818.05 | 725.0-1044.1 | 52.767 |
| | 144 | 0.284 | 833.68 | 730.3-1117.3 | 52.3222 |
| | 324 | 0.284 | 829.3 | 727.4-1119.5 | 49.933 |
| B, $\zeta = 10^{-6}$, $\underline{R}$ | 36 | 0.332 | 1379.5 | 1301.6-1589.7 | 52.824 |
| | 144 | 0.308 | 1409.1 | 1332.5-1670.5 | 48.579 |
| | 324 | 0.295 | 1414.5 | 1331.5-1699.2 | 47.240 |

Table 3.5: Time to Switch, range of switching times and proportion of Primary Fate cells for cells arranged on a hexagonal lattice, as described by (3.5.4), using parameters (3.5.5) and initial conditions (3.5.6). For each choice of initial conditions and population size, we have run 100 simulations, such that each run uses a different perturbation vector $\underline{R}$.

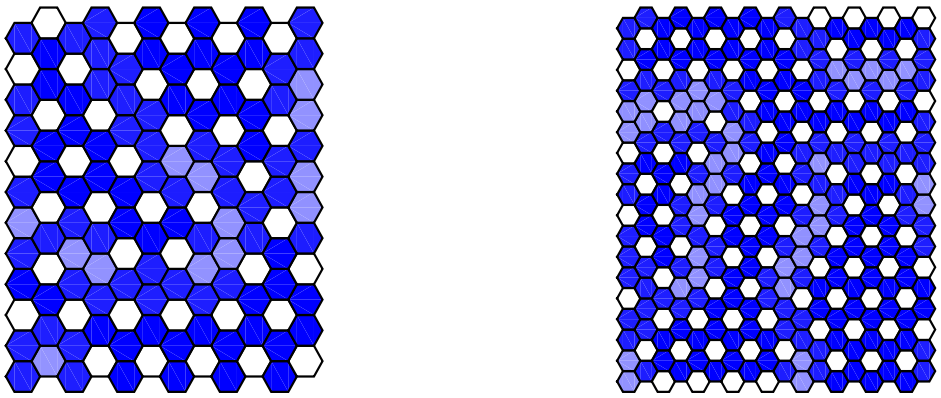

(a) (b)

Figure 3.68: Examples of the final patterns cell-states on a $12 \times 12$ and $18 \times 18$ hexagonal lattice. Each hexagon displays the final level of the cell's Delta activity, where white signifies a high Delta level - and Primary Fate cell - and dark blue signifies a low Delta level. In each case, the proportion of Primary Fate cells is just under 1/3.

**2** In nearly all cases, increasing the complexity of cell arrangement increases the mean Time to Switch for comparable initial conditions. Comparing systems with more than 2 cells, we find that the mean TtS range increases with complexity, and this range is always greater for initial conditions with $\zeta = 10^{-2}$.

The only exception to this is the mean TtS for 2 cells and a ring of cells, when using initial conditions A with either value of $\zeta$.

In a ring of cells, each cell has 2 neighbours, and the greater the coherency of the signal received from these neighbours, the faster this cell determines its fate. So, if we have a ring of $n$ cells all starting near the HSS, the likelihood of any cell receiving a coherent signal from its neighbours and a low switching time increases with $n$. If we then repeat the simulation 100 times, and the majority of simulations have at least one cell which quickly determines its fate, this will have a significant effect on the mean time to switch.

Additionally, when patterning begins this sends a travelling wave through the ring, which can result in a whole section of the population patterning faster than the average 2-cell simulation.

Other than this exception, for a given set of initial conditions, the mean TtS increases with the geometric complexity of the system.

There is also a significant increase in the range of switching times between the ring of cells and cells on a square array for each set of initial conditions (We have not included the 2-cell system here, as the range in that case is the range of switching times between each run of the simulation, as opposed to the range of switching times throughout the population for a single simulation).

This increase in range is expected. If we are increasing the number of neighbours each cell has from 2 to 4, this increases the likelihood of less coherent signalling, and the less coherent the signals being received are, the longer the switching time.

Another factor of increasing the complexity is a general reduction in the proportion of PF cells produced in the system. For a ring of cells, the mean proportion of PF cells is 0.472, whilst for a square array of cells it is 0.453. Since the pattern on a square array is 2-dimensional, the pattern can now propagate in multiple directions. This increases the likelihood of 2 emerging patterns within the same array having more defects (imperfections in the periodicity of the pattern) than a ring of cells.

We have also looked at cells on a hexagonal array, and we find that there is a significant increase in the mean TtS, a broader range of switching times, and a lower proportion of PF cells for each set of initial conditions. However, this is not a system which can produce a period-2 pattern, and as we have seen from the linear stability analysis for a system producing a period-3 pattern, we expect the difference between the cells to grow at a slower rate, and therefore have a later switching time.

**3** The size of the population does affect both the ratio of cell-types and the temporal variability with the systems.

For any of the cell arrangements, there is always a decrease in the proportion of PF cells between the smallest population size and the larger two. In some cases, such as using initial conditions B with a $\zeta = 10^{-6}$ in a square array of cells, there is a continual decrease in PF proportion when increasing the population, but it is more likely that the proportion of PF cells is approximately even for the two largest population sizes for each initial condition.

Similarly, there is generally an increase in the mean TtS between the smallest population size and the larger two, which is always more distinct when using initial conditions B. In some cases, such as initial conditions A with $\zeta = 10^{-2}$ in a square array of cells, there is negligible difference between the mean switching times, but it is more likely that the mean TtS increases with the population size.

However, the range of switching times always increases with population size, for any cell arrangement and for any set of initial conditions. Again, we would expect this to be the case, since the more cells there are in the system, the greater the number of cells which will adopt PF, resulting in a broader range of switching times.

### 3.5.3 Numerical Results for cells on a Hexagonal Array

The following results are for cells on a $6 \times 6$ hexagonal array with periodic boundary conditions, such that every cell has 6 neighbours, as described by equation (3.5.4). Each cell consists of three variables Notch, Hes and Delta, and the parameters used are the same as those stated in equation (3.5.5), except we are varying $n_s$. Additionally, we have chosen a perturbation which produces a perfect pattern of cell types, illustrated in Figure 3.69.

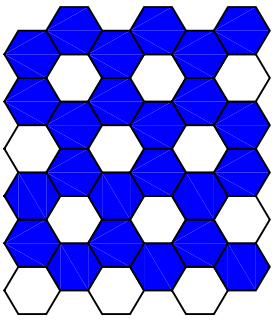

Figure 3.69: Example of a final pattern of cell-states on a $6 \times 6$ hexagonal lattice, described by (3.5.4), where the initial conditions used have produced a perfect pattern, such that exactly 1/3 of the population is a Primary Fate cell. White signifies a cell with a high Delta level - corresponding to a Primary Fate cell- and dark blue signifies a cell with a low Delta level.

i **A larger $\chi$ is required for the system to be able switch from homogeneity in comparison to a 2-cell system.**

The main difference we found from the linear stability analysis between a 2-cell system and this multicellular system was the value of $\chi$ needed for before switching from homogeneity can occur. When using $n_s = 0.8$, this corresponded to $\chi = 0.0348$, and the linear stability analysis predicts that the system is unable to switch for $\chi < \sqrt[3]{2}\,\mu = 0.0378$. The levels of Notch activity are shown in Figure 3.70, and we can see that the states of each cell are attracted to the homogeneous steady state, which, for this value of $\chi$, is the only steady state of the system.

For the same value of $\chi$ in a 2-cell system, the system would be able to diverge from homogeneity, since the condition for switching is $\chi > \mu = 0.03$. Hence, a larger $\chi$ is required for switching from homogeneity for a system on a hexagonal lattice in comparison to a 2-cell system.

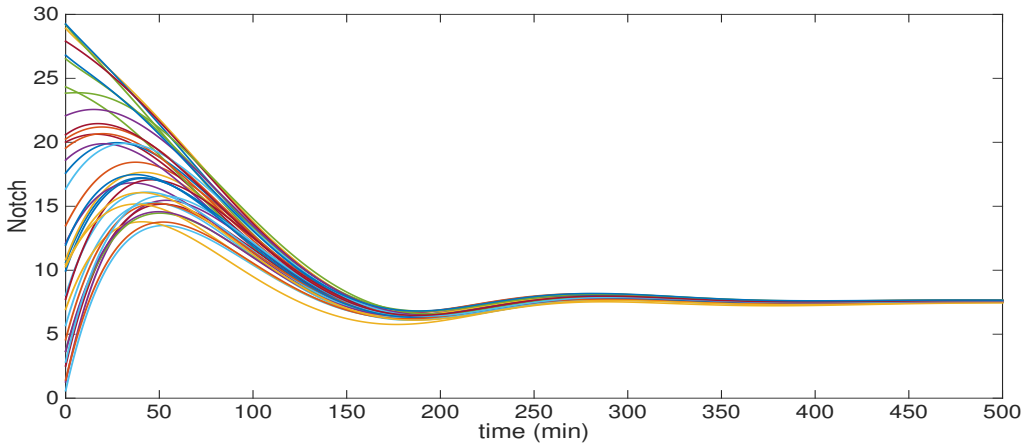


Figure 3.70: The levels of Notch activity in each cell for a population arranged in a $6 \times 6$ hexagonal lattice, as described by (3.5.3), using parameters (3.5.5) with $n_s = 0.8$ ($\chi = 0.0348$), and random initial conditions in $(0, 30)$. Since $\chi < \sqrt[3]{2}\,\mu = 0.0378$, the HSS is the only steady state of the system.

ii **A Hopf bifurcation exists for the same value of $\chi$, in comparison to a 2-cell system.**

When $\chi = 0.06$ there exists a Hopf bifurcation in the system, as we expect. Again, this generates a stable periodic orbit in the SoE, and for initial conditions which start near the SoE, away from the HSS, the states of the cells are affected.

As we saw for the 2-cell system, when the state of the system starts near the HSS, there is no effect from the periodic orbit. However, for the same form of initial conditions, there is a large increase in switching times. This is due to the difference in the $\lambda_D$ expressions which govern the growth of the difference between alternative cell types. For two cells, this

was given by $\lambda_D = \chi - \mu$, but for the hexagonal array of cells, this is given by $\lambda_D = 2^{-1/3}\chi - \mu$. Therefore, we expect the cells to reach their destined fates later.

For initial conditions B, there are stable, in-phase oscillations in every one of the cells. Similarly to initial conditions A, the difference between alternative cell types grows at a slower rate, and due to the periodic orbit in the SoE, this effect is even more obvious. In comparison to the 2-cell model, not only are we seeing a much later TtS, but oscillations in the state of the system persist for a greater duration.

The associated 2-cell dynamics are illustrated in Figures 3.25 and 3.26, and the dynamics for cells on a hexagonal lattice are shown below in Figure 3.71. Evidently, for equivalent initial conditions, oscillatory dynamics are prevalent for considerably longer for cells on a hexagonal lattice, and the associated switching times are later.

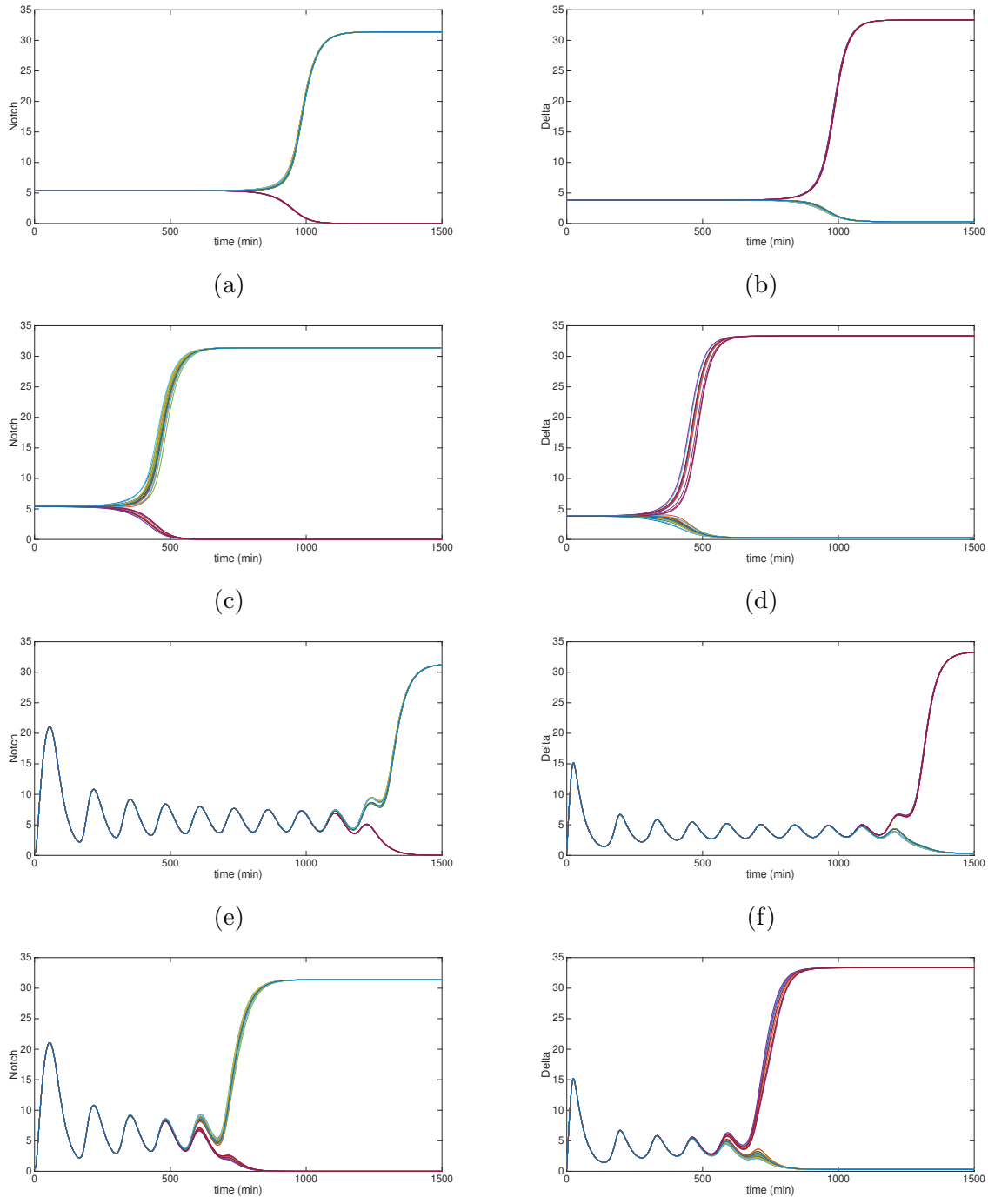


Figure 3.71: Levels of Notch and Delta activity in every cell for a population arranged on a $6 \times 6$ hexagonal lattice, as described by (3.5.3), using parameters (3.5.5) and initial conditions given by (3.5.6).
(a) $N(t)$, initial conditions A with $\zeta = 10^{-6}$; (b) $D(t)$, initial conditions A with $\zeta = 10^{-6}$; (c) $N(t)$, initial conditions A with $\zeta = 10^{-2}$; (d) $D(t)$, initial conditions A with $\zeta = 10^{-2}$; (e) $N(t)$, initial conditions B with $\zeta = 10^{-6}$; (f) $D(t)$, initial conditions B with $\zeta = 10^{-6}$; (g) $N(t)$, initial conditions B with $\zeta = 10^{-2}$; (h) $D(t)$, initial conditions B with $\zeta = 10^{-2}$.

iii **Time to Switch is a decreasing function of $\chi$ when using initial conditions A, but when using initial conditions B, Time to Switch reaches a minimum when there exists a Hopf bifurcation, and then increases for $\chi \geq 2\mu = 0.06$.**

Time to Switch for all PF cells is illustrated in Figure 3.72 for both sets of initial conditions, using both $\zeta = 10^{-2}$ and $\zeta = 10^{-6}$. As we have already established in the previous comparison of different geometries, cells on a hexagonal array will always have a greater switching time than those in a 2-cell system, as a direct result of the system's geometry.

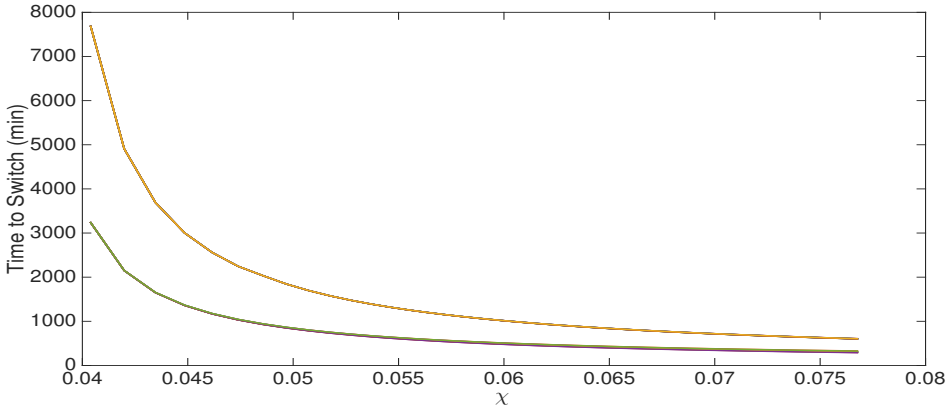


(a)

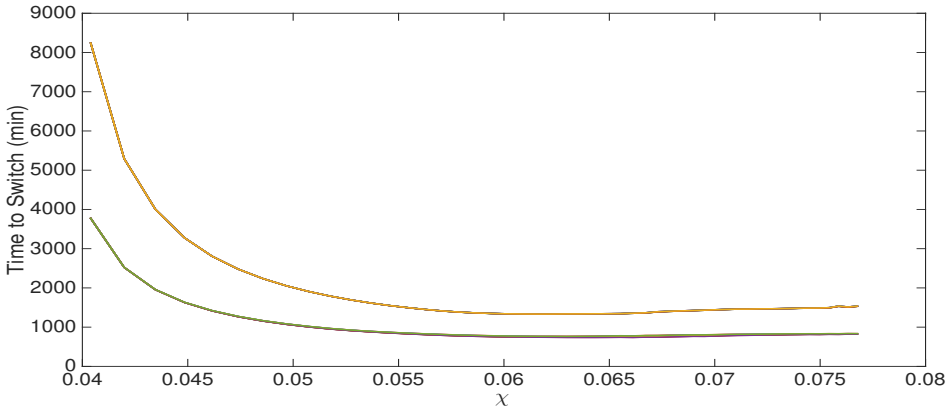


(b)

Figure 3.72: Time to Switch as a function of $\chi$ for Primary Fate cells in a population arranged on a $6 \times 6$ hexagonal lattice, described by (3.5.3) using parameters (3.5.5) with varying $n_s$. (a) Initial conditions A with $\zeta = 10^{-6}$ and $\zeta = 10^{-2}$. Time to Switch is a continuously decreasing function of $\chi$, and for a given $\chi$, a decreasing function of $\zeta$.
(b) Initial conditions B with $\zeta = 10^{-6}$ and $\zeta = 10^{-2}$. Time to Switch is a decreasing function of $\chi$ until $\chi = 2\mu$, where it begins to increase.
We observe very little variability between the switching times of the PF cells, but this does increase for larger $\chi$, and when using a larger $\zeta$ in the initial conditions.

iv **For a population of cells on a hexagonal lattice, it is possible for the states of the cells in the system to demonstrate stable, in-phase oscillations stable to all perturbations.**

As we discussed in the results of the linear stability analysis for a hexagonal array in the previous chapter, cells on a hexagonal array do not just show less coherency and a slower growth rate than period-2 systems, but provided there are enough components per cell, or there is a large enough delay in the signal between cells, the system will have a Hopf bifurcation before switching can occur, with respect to $\chi$. If this is true in the full system, then this would allow for oscillatory behaviour in the state of the system, stable to all perturbations.

To verify if this result holds and is not a result only of the linear stability analysis, we will look at single-component cells on a hexagonal array, connected via the delay differential equations

$$\dot{D}_{p,q} = -\mu D_{p,q} + g\left(\bar{D}_{p,q}(t-\tau)\right), \tag{3.5.9}$$

where

$$\bar{D}_{p,q} = \frac{D_{p-1,q} + D_{p-1,q+1} + D_{p,q+1} + D_{p+1,q} + D_{p+1,q-1} + D_{p,q-1}}{6}.$$

From equation (2.3.53), we know that if each cell only has one component and $\chi = \sqrt[4]{2}\,\mu$, a delay of $\tau = 133.1$ min is required for a Hopf bifurcation.

Using parameters

$$\mu = 0.03\ \text{min}^{-1}, \quad \theta_s = 0.2/\mu\ \text{min}, \quad n_s = 1.74\ (\chi = 0.0357), \quad \tau = 133.1\ \text{min}, \tag{3.5.10}$$

and initial conditions

$$X_j(0) \in (0, 30),$$

for cell $j$, we find that this result holds well. The states of each cell are attracted to the stable periodic orbit in the SoE, resulting in the states of the cells displaying stable in-phase oscillations.

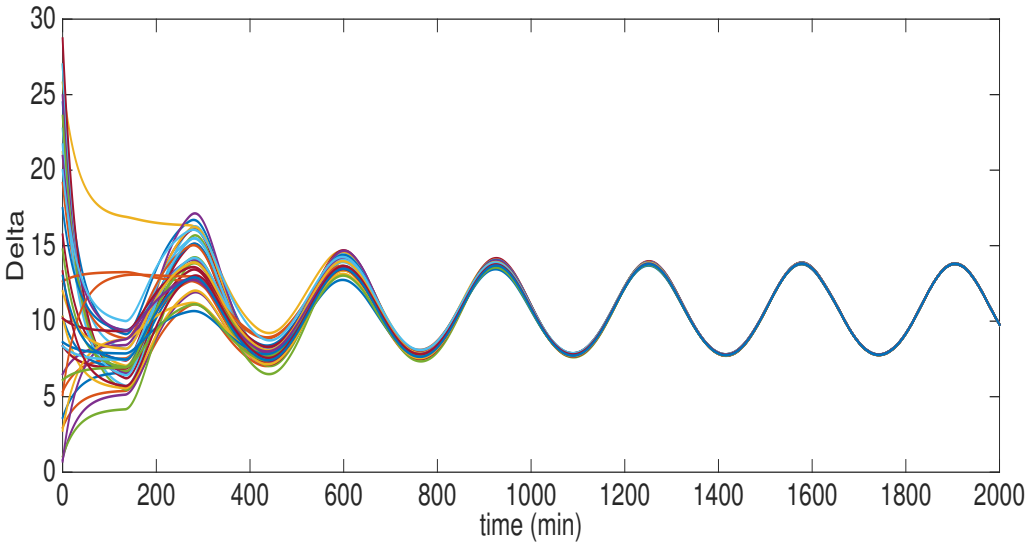


Figure 3.73: Levels of Delta activity in each cell on a $6 \times 6$ hexagonal lattice described by (3.5.9) using parameters (3.5.10) and initial conditions $X_j(0) \in (0, 30)$ for cell $j$.
This position in parameter space allows for stable, in-phase oscillations in the states of each cell, such that the system cannot diverge from homogeneity.

## 3.6 Discussion

### 3.6.1 Summary of Results

**Two Cells**

For systems of two cells governed by ODEs, there is a distinct difference in the dynamics between cells with $\leq 2$ components and those with $> 2$ components.

If there are either one or two components per cell, the system will be able to switch when $\chi > \mu$, but cannot have a Hopf bifurcation, due to the conditions given by Equation 2.1.35. So for initial conditions of the form (3.1.15), Time to Switch is a continuously decreasing function of $\chi$. We also find that, for a given initial condition, if we vary the magnitude of $\zeta$, Time to Switch is a decreasing function of $\zeta$. Furthermore, the predicted growth rate of the difference between cells from the linear stability analysis in Chapter 2 holds excellently, not just for initial conditions in the vicinity of the HSS, but anywhere in the vicinity of the SoE. This is illustrated in Figures 3.12, 3.15 and 3.16.

If there are three components per cell, the system will be able to switch when $\chi > \mu$, and a Hopf bifurcation when $\chi = 2\mu$. For initial conditions of the form (3.1.15), we see different behaviours depending on which initial conditions we choose. If the system starts in the vicinity of the HSS, the same results as those stated above all hold. Even though the system has a Hopf bifurcation at $\chi = 2\mu$ which changes the stability of the HSS in the SoE, if starting close to the HSS, the Hopf bifurcation has no effect on the solution trajectory. The predicted growth rate also still holds accurately.

If the system starts near the SoE, but not in the vicinity of the HSS, oscillatory dynamics are observed in the states of the cells when $\chi \geq 2\mu$, which causes Time to Switch to no longer behave as a continuously decreasing function of $\chi$.

With respect to $\chi$, Time to Switch decreases in a similar fashion to the $n = 2$ model until $\chi = 2\mu$. From there on, Time to Switch increases with $\chi$, albeit very gradually. This is shown in Figure 3.27. In terms of the difference between the cells, the prediction from linear stability analysis no longer holds, due to the periodic orbit surrounding the HSS in the SoE. We find that when using an approach from Floquet theory to predict the growth rate, this does give a relatively good estimate from what we observe in numerical simulations. However, this approximation loses accuracy as $\chi$ increases, underestimating the growth we observe in simulations.

For systems governed by DDEs with either one or two components per cell, we find that the behaviours exhibited are qualitatively equivalent to those of the $n = 3$ ODE system. The systems are able to switch when $\chi > \mu$, and from linear stability analysis, a Hopf bifurcation exists when the conditions given by (2.2.95) are met.

Again, for initial conditions in the vicinity of the HSS, Time to Switch is a continuously decreasing function of $\chi$, shown in Figure 3.41. For a fixed value of $\chi$, Time to Switch decreases as a function of $\zeta$, the magnitude of perturbation from the HSS. The growth rate of the difference between the cells holds excellently, not just in the vicinity of the HSS, but all the way until the switched steady state.

Similarly, for initial conditions in the vicinity of the SoE but away from the HSS, oscillatory dynamics are observed when the conditions given by (2.2.96) are met. This causes Time to Switch to no longer act as a continuously decreasing function of $\chi$, and once the conditions for the Hopf bifurcation are met, Time to Switch increases with $\chi$. This is true for both $m = 1$ and $m = 2$ models, illustrated by Figures 3.55 and 3.56.

Temporal Comparison

In subsection 2.2.7, we give an analytic comparison between ODE models and DDE models to demonstrate they are capable of having a Hopf bifurcation for the same value of $\chi$, provided an appropriate time delay is used. Since an $n = 3$ ODE model has a Hopf bifurcation when $\chi = 2\mu$, we used delays in the DDE model such that $\chi = 2\mu$ would also be needed for a Hopf bifurcation. As we have demonstrated, this holds well, with clear oscillatory dynamics observed for both $m = 1$ and $m = 2$ when $\chi \geq 2\mu$.

However, despite the qualitatively equivalent dynamics for each model, due to the difference in the eigenvalue expressions which determine the growth rate of the total difference between the cells, there is a distinct temporal difference between each model. Since we have fixed the delays such that a Hopf bifurcation occurs at $\chi = 2\mu$, this causes the growth rate to be less when a larger delay is used. This is illustrated clearly in Figure 3.64. Hence, for a given value of $\chi$, we will have a different growth rate in each

model, resulting in various switching times between the systems. This supports findings in [50], who show that the inclusion of a time delay reduces the growth rate of the pattern.

**Larger Populations**

For larger populations of cells, we used the same parameters throughout, given by (3.5.5). This allowed us to focus on the relationship between switching times and the geometric structure and arrangement of the population.

We found that, for all systems capable of producing a period-2 pattern, increasing the number of neighbours each cell had caused an increase in the mean Time to Switch, especially for initial conditions that were nearly homogeneous, but not in the vicinity of the HSS. When using a random perturbation from the SoE for the initial conditions of each cell, this introduced less coherency in the signal each cell received from its neighbours.

For systems of more than two cells capable of producing a period-2 pattern, the mean Time to Switch and range of switching times is always greater for a population on a square lattice in comparison to on a ring. By increasing the number of neighbours each cell has, this increases the likelihood of less coherent signalling. The less coherent the signals being received, the longer it will take for the system to pattern.

Additionally, increasing the overall population has negligible effect on the mean Time to Switch, but is does always increase the range of switching times throughout the population. Again, due to the stochasticity of the initial conditions, this is an expected result.

Increasing the population also increasing the likelihood of a pattern emerging from more than one location in the lattice, and we have found this causes a slight decrease in the proportion of PF cells in the final spatial pattern.

**Cells on a Hexagonal Lattice**

For a population of cells arranged on a hexagonal lattice, we have found that the system will form a period-3 pattern of alternate cell types for homogeneous initial conditions with a stochastic perturbation, such that there is no predetermined pattern.

Due to the smaller ratio of PF cells, a larger $\chi$ is necessary for switching, as predicted by the linear stability analysis for this system. In comparison to a period-2 patterned system, a slower rate of patterning occurs for a population on a hexagonal lattice. Results from the numerical simulations support this well, with significantly later commitment times than any of the period-2 systems. This supports previous work in [48,91], who state that for cells on a hexagonal lattice, a greater feedback strength is required for switching from homogeneity, and a slower rate of patterning occurs.

Since the linear stability analysis predictions for this system were made under the assumption of a perfectly formed pattern, we find that the prediction for the growth rate

of differences between neighbouring cells is the upper bound for cell fate commitment, with most cells switching slightly slower than this. Again, this is due to the stochasticity in the initial conditions, which prevents a predetermined pattern. This also introduces a much larger range of switching times, and a decrease in the proportion of PF cells, both of which are robust to population size.

In terms of a Hopf bifurcation, linear stability analysis predicts this accurately, and when $\chi \geq 2\mu$, for nearly homogeneous initial conditions away from the HSS, we observe global in-phase oscillations in the state of each cell prior to switching. Since we use a random perturbation from homogeneity in the initial conditions, we find that the states of the cells become more homogeneous before diverging to one of the two final states, and the observed oscillatory dynamics cause a slower rate of patterning.

This supports results in [48], who propose cells will first become more similar before diverging, and further supports our previous finding that if there exist oscillatory dynamics in the states of the cells, linear stability analysis can no longer predict the rate of patterning. In [50,51], both state that the outcome of linear stability analysis is not applicable to transient system behaviour, and therefore, the change of variables to Mean and Difference makes linear stability analysis highly valuable in this study, making it possible to predict whether or not transient oscillations leading to differentiation will occur.

Therefore, despite the assumptions made about the final spatial pattern of the system, using the method of reduction proposed in Section 2.3 to analyse cell-type dynamics proves a useful technique for finding bifurcation conditions and predicting the upper bound in patterning rates, without oversimplification of the system.

With respect to Time to Switch throughout the population, although the range of switching times increases, the relationships we observe between Time to Switch and $\chi$ in the 2-cell models hold well for this system. When the system has initial conditions such that the states of the cells are in the vicinity of the HSS, Time to Switch is a continuously decreasing function of $\chi$ for every cell in the system. When the system has initial conditions in the vicinity of the SoE but away from the HSS, Time to Switch is a decreasing function of $\chi$ until $\chi = 2\mu$, at which point it becomes an increasing function. This increase is more prominent when a smaller $\zeta$ is used in the initial conditions, illustrated in Figure 3.72(b). From the 2-cell analysis, this is expected, since the closer the system starts to the SoE, the greater the effect of the stable periodic orbit in the SoE has on the system.

As discussed at the end of the previous chapter, the linear stability analysis from the reduced hexagon model, with the assumption of a perfect period-3 pattern, predicts

there is some parameter space in which conditions for a Hopf bifurcation are met before switching from homogeneity can occur.

For a delay system, we have shown that this is indeed a possibility, and for *any* initial conditions, the state of the system will show stable oscillations about the HSS, such that the whole population demonstrates in-phase oscillations.

This behaviour is novel, and has not been proposed, or observed, in any previous studies of Delta-Notch signalling on larger spatial arrays. For ODE models that have been studied on a hexagonal array [48,91], either two or three components per cell were included, and as we have explained, there needs to be at least eight component per cell.

For delay models on a hexagonal array [52], the focus was how sustained oscillations during patterning, aided by *cis*-inhibition, can generate patterns free from defects. Regimes where a final patterned state of alternate cell fates was not possible were not considered in this study.

### 3.6.2 Parameter Sensitivity

For the models we have studied, there have been many factors to take into account when solving each one; parameter values, initial conditions, the arrangement of cells and the size of the population.

The effect of parameter values and initial conditions have been primarily investigated for the case of two cells, although a range of parameters and initial conditions have also been considered for lattices of hexagonal cells. For the larger arrays, different population sizes have also been considered.

#### Two Cells

For 2-cell systems, initial conditions do not usually affect the type of pattern formed, provided they are fairly homogeneous. However, depending on the number of components per cell and the parameter choices, the transient dynamics, and the temporal dynamics, are highly dependent on the initial conditions.

For a system of two cells each with two components, governed by equations (3.1.1), changing parameters has three possible effects on the final pattern formed, and the associated temporal dynamics:

i) Quantitative changes: The values of the steady states change, but no qualitative changes occur. This can be caused by changing $n_s, n_g, \theta_s, \theta_g, \mu_N, \mu_D$, provided $\chi > \sqrt{\mu_N \mu_D}$.

ii) Minor qualitative changes: The nature of the pattern is unaffected, but the fates of individual cells can be interchanged. Various parameters can cause this, but the nature of the perturbation in the initial conditions dictates this.

iii) Major qualitative changes: The nature of the pattern changes. This can be observed by varying $n_s, n_g, \theta_s, \theta_g, \mu_N, \mu_D$, such that $\chi < \sqrt{\mu_N \mu_D}$. This causes the number of fixed points to change from three to one, and the final pattern of alternate cell-fates is replaced by a homogeneous state.

For initial conditions of the form (3.1.15), Time to Switch is a continuously decreasing function of $\chi$, so varying any parameter which affects $\chi$, namely $n_s, n_g, \theta_s, \theta_g$, will directly affect the switching times of the cells. As seen in Figure 3.12, Time to Switch is very sensitive for small $\chi$ ($\chi > \mu$), and becomes less sensitive as $\chi$ increases. The SoEP - Surface of Equivalence Position - in the initial conditions (3.1.15) has negligible effect on the Time to Switch, but $\zeta$, the magnitude of perturbation from the SoE, causes a significant temporal change.

For systems with three components, governed by equations (3.1.2), the same changes hold as for the $n = 2$ case, but there is an additional quantitative change.

If any of $n_s, n_1, n_g, \theta_s, \theta_1, \theta_g$ are altered such that $\chi \geq 2\mu$, transient oscillations are observed in the states of the cells during patterning. This does cause an increase in the time taken for the cells to switch, but it does not affect the final spatial pattern.

The same is true for systems with a time delay, for either $m = 1$ or $m = 2$. If any of the Hill coefficients, thresholds, or the time delays are altered such that

$$\chi > \mu, \quad \tau \geq \frac{\pi - m \tan^{-1}\left(\frac{\omega}{\mu}\right)}{\omega},$$

transient oscillations are observed in the states of the cells during patterning. Again, this causes an increase in the time taken for cells to switch, but the final spatial pattern is unaffected. Due to the slower growth rates for systems with a time delay, the increase in switching times is even more evident.

### 3.6.3 Conclusions

This chapter on the global dynamics of our lateral inhibition systems, in conjunction with the findings from linear stability analysis in the previous chapter, has allowed us to present an extensive, detailed study for systems which communicate in this way.

We have been able to show that transient oscillations are *not* unique to models with a time delay, but are actually a feature of any system governed by a double-negative (positive) feedback loop, with a subspace governed by a negative feedback loop, such that the system can have a Hopf bifurcation.

Furthermore, switching times no longer continuously decrease when increasing the feedback strength between neighbouring cells. For nearly homogeneous initial conditions away from the HSS, Time to Switch as a function of $\chi$ reaches a minimum when there is

a Hopf bifurcation, and then due to the presence of a periodic orbit in the SoE, Time to Switch increases with $\chi$.

For models of more than two cells, mean switching times and the range of switching times increase when the complexity of the arrangement - measured by the number of direct neighbours each cell has - increases. This increase is most prominent when changing the arrangement from a square lattice to a hexagonal lattice. Since the periodicity changes from a period-2 pattern to a period-3 pattern, there is a slower growth rate for cells diverging from homogeneity, as accurately predicted from the previous linear stability analysis.

Finally, we have shown that for systems on a hexagonal lattice, there exists parameter space such that there are stable in-phase oscillations about the HSS, and this periodic orbit is the only attractor of the system. This is a novel finding, and a direct result of the structural geometry of the system.

To validate the finding of these models, it may be possible to build a synthetic model and recreate our findings. We saw this in [94], in which a genetic lateral inhibition circuit was built in Chinese hamster ovary cells, and were able to show that it had the potential to cause a cell-type bifurcation among a genetically homogeneous population.

To create a system which showed oscillations prior to switching, parameters - determined by strength of promotors, stabilities - would have to be engineered such that the system was in the correct region of parameter space, and initial conditions such that the cells start close to the Surface of Equivalence.

When a synthetic oscillator was created [30], the promoters had to be carefully engineered so that the system was in the right part of parameter space for oscillations. Similarly, in experiments to study Hes1 oscillations [68], it was required to serum-shock the cells at the start of the experiment to synchronise Hes1 oscillations between the cells.

So, it may be possible to recreate our model, but it would take some careful engineering and experimentation.

If our system is capable of demonstrating oscillatory dynamics, we could use Time to Switch as means of model validation. From Figure 3.72(b), there are two distinct regimes for Time to Switch as a function of $\chi$. For $\mu < \chi < 2\mu$, Time to Switch is a fast decreasing function, and for $\chi > 2\mu$, it is a slowly increasing function of $\chi$. If we were to introduce a Notch inhibitor into the cells, this would ultimately decrease $\chi$. If this caused Time to Switch to slightly decrease, we would be in the regime to the right of $\chi = 2\mu$, and if it caused Time to Switch to noticeably increase, we would be in the regime to the left of $\chi = 2\mu$.

# Chapter 4

# Multicellular Pattern Formation in an Adaptive Population

In this chapter we want to further investigate the dynamics of a population of cells governed by Delta-Notch mediated lateral inhibition, and assess how the previous results hold in a changing environment.

From the linear stability analysis in Chapter 2 and numerical simulations in Chapter 3, we have been able to determine how the states of two cells starting near homogeneity can diverge from one another to different final states, and how this behaviour changes for different parameter values and initial conditions. We have also been able to show how these behaviours translate to larger populations of cells, and how these can be affected based on the geometric arrangement of the population, and the coherency of cellular signalling.

However, everything so far has been a result of a static population with no temporal restrictions, such that cells do not move or change shape, and there is no time limit in which the system must pattern. Therefore, in this chapter we want a more realistic environment with an adaptive population, such that cells now have a cell-cycle, and are capable of cell division and differentiation. By including these cellular characteristics we can ask the following questions:

1. Are the behavioural dynamics observed in a static population still present in a spatially changing environment, and if so, to what extent?

2. How do the timescales of cell-cell interactions from a static population interact with the timescales of the biological processes we want to include?

These are the main questions we will be addressing throughout this chapter, but as they are both broad questions, we will propose more specific sub questions at the beginning of each section.

Firstly, these simulations have been done using a vertex dynamics model and implemented via Chaste, an open source C++ simulation package for multi-scale modelling of biological and physiological processes. Vertex models are a class of off-lattice models,

in which each cell is approximated geometrically by a polygon that represents the cell's membrane, with vertices and edges shared between adjacent cells. Most vertex models represent either a cross-section of an epithelial sheet, or just the apical surface of an epithelial sheet. Full details for the underlying mechanics of vertex dynamics models are provided in [92].

Again, we are modelling cells on a hexagonal lattice, with either free boundary conditions, or toroidal periodic boundary conditions.

## System Equations, Parameters and Initial Conditions

We are using the same equations as those describing the dynamics of cells on a hexagonal lattice from the previous chapter, such that for each cell $\underline{X}_{p,q}$

$$\begin{aligned}
\dot{N}_{p,q} &= -\mu_N N_{p,q} + f_s\left(\frac{D_{p-1,q} + D_{p-1,q+1} + D_{p,q+1} + D_{p+1,q} + D_{p+1,q-1} + D_{p,q-1}}{6}\right), \\
\dot{H}_{p,q} &= -\mu_H H_{p,q} + f_2(N_{p,q}), \\
\dot{D}_{p,q} &= -\mu_D D_{p,q} + g(H_{p,q}),
\end{aligned} \tag{4.0.1}$$

### Model Parameters

In all cases, we have used the parameters

$$\begin{aligned}
&\mu_N = \mu_H = \mu_D = \mu = 0.03\text{min}^{-1}, \\
&\theta_s = \theta_2 = \theta_g = \frac{0.2}{\mu}\text{min}, \\
&n_2 = 2,\ n_g = 3.
\end{aligned} \tag{4.0.2}$$

We will be using various $n_s$ throughout, so we will specify where necessary.

### Initial Conditions

We want to use initial conditions of the form as those used in Section (3.5), such that

$$A \equiv HSS + \zeta\underline{R}, \qquad B \equiv \underline{0.5} + \zeta\underline{R}, \tag{4.0.3}$$

where $\zeta = 10^{-2}$.

Each entry in $\underline{R}$ is now a random number chosen from a uniform distribution over $[0, 1]$.

To address question 1, we must first verify that a static population model in a vertex model behaves the same as the numerical simulations from Matlab in Chapter 3. Then, we can introduce cell cycles, such that a cell will divide into two daughter cells at the end of its cell cycle, increasing the cell population. By allowing each cell to go through

a given number of cell divisions, we can determine if the dynamics seen in the previous chapters are conserved, or if they are only a feature of a static environment.

We will start with each cell having just one division before introducing multiple cell-cycles, and focus on addressing the following:

1. If each cell undergoes a single division, this causes the population to lose its regular geometry. How does this affect:
   (a) The switching times of Primary Fate cells?
   (b) The ratio of Primary and Secondary Fate cells, once each cell has decided their fate?
2. When a cell divides, this causes a change to the signals between itself and its neighbours. Are the dynamics previously observed, such as oscillatory dynamics in the variables of the cells, still present, or do they disappear when allowing the population to grow?

## 4.1 Model Verification for Simulations Implemented in Chaste

This section is simply to verify that the dynamics observed in Matlab simulations are still present when using Chaste, with both models displaying quantitatively similar behaviours.

Similarly to the Matlab simulations, the system consists of 36 hexagonal cells arranged on a $6 \times 6$ lattice with toroidal periodic boundary conditions. We are using the standard model parameters and looking at both sets of initial conditions A and B with $n_s$ taking the value 2, 3 or 4.

For each parameter combination and choice of initial conditions, 20 simulations have been carried out in both a vertex model via Chaste, and Matlab.

### 4.1.1 Simulation Results

These simulations verify that the two methods of modelling this system are in agreement, with both displaying quantitatively similar dynamics. The window of switching times for PF cells, the mean Time to Switch, and the ratio of different cell-types are all in accordance. Additionally, for initial conditions B with $n_s = 3$ or $n_s = 4$, oscillations are present in the states of the cells, and both models have periods of oscillation of $\sim 121$ min and $\sim 130$ min, respectively, in agreement with what we have seen previously.

Figure 4.1 clarifies these results, showing an example solution for simulations in Chaste and Matlab.

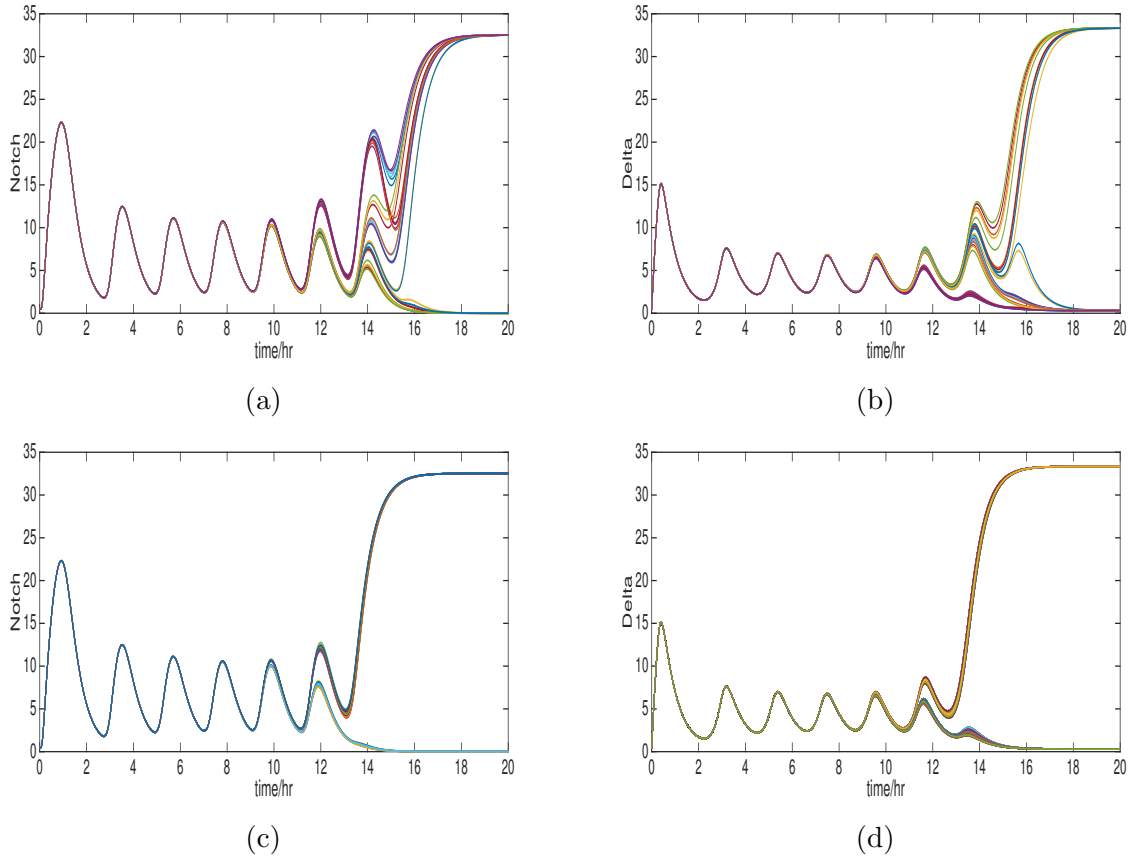


Figure 4.1: Levels of Notch and Delta activity for the system (4.0.1) using parameters (4.0.2) with $n_s = 3$ ($\chi = 0.0601$), and initial conditions B from (4.0.3).
(a), (b): Notch and Delta activity when running the simulation in Matlab;
(c), (d):Notch and Delta activity when running the simulation using a vertex model implemented in Chaste.
The differences between the simulations are due to the choice of $R$ in the initial conditions; if the same perturbation $R$ had been used in each simulation, the plots would be identical.

## 4.2 Introducing Cell Proliferation

We now introduce cell proliferation by allowing each cell to undergo a period of division, followed by a 'non-dynamic' window, in which the population can establish its final pattern. Since we want to understand the interplay between the timescales of cell-cell kinetics and the biological processes, we will be using cell-cycle lengths of ~ 6 hr, ~ 10 hr, and ~ 16 hr. From the previous simulations we know that different parameter values and initial conditions can cause large temporal variability, and these different cycle lengths are within the possible range of switching times.

We are varying the length of the cell cycle because there is sufficient evidence throughout different stages of development that by increasing the length of the cell-cycle, a greater proportion of PF cells can be generated each cycle. This has been shown experimentally by [62,65], and more recently, both experimentally and via a mathematical model in [83].

The cycle lengths for each cell have been determined using a Gamma distribution, with parameters chosen such that the possible cycle lengths have a range of ~ 2 hr, centred around the mean lengths of 6, 10 and 16 hr. The simulations will start such that each cell is in a randomly chosen phase of their cycle, and will undergo division individually, as opposed to collectively. This avoids unrealistic synchronous adjacent divisions, and keeping the system is a quasistatic regime provides a better method for observing the effects on coherence in signalling between cells.

In these simulations, when a cell goes through a division it first undergoes a period of growth (G1) to double in size before dividing. This allows the daughter cells to be approximately the same size as their mother and the neighbouring cells. The cells divide in the direction of the shortest axis through their centroid, which causes the initial regularity of the population to quickly change into an irregular lattice of cells. This is discussed further in the discussion at the end of the chapter.

### 4.2.1 One Division per Cell

Since we want to understand the effects of multiple cell-cycles, we will have better insight if we first look at what happens when cells can undergo a single division. In this case, there will be a window of proliferation the length of cell-cycle, followed by a 10 hr window to allow the system to finish patterning.

#### Simulation Results

With each cell undergoing a single division, this results in the population number doubling, with a final total of 72 cells. Due to each cell starting at a different phase of its cycle, each cell divides individually. Each simulation therefore has a unique order in which the cells divide, which causes the final arrangement of cells to change, and in turn, the distribution of different cell types.

An overview of results for each set of model parameters and initial conditions is summarised in the Table 4.1.

| $n_s$ | Initial Conditions | ~ 6hr Cell-cycle | | ~ 10hr Cell-cycle | | ~ 16hr Cell-cycle | |
|---|---|---|---|---|---|---|---|
| | | Time to Switch Range | PF Cell Number | Time to Switch Range | PF Cell Number | Time to Switch Range | PF Cell Number |
| 2 | A | 16.3 - 19.1 | 18.95 | 17.22 - 20.64 | 19.25 | 17.03 - 22.28 | 17.55 |
| | B | 17.41 - 21.75 | 18.5 | 16.61 - 20.96 | 18.75 | 18.03 0 22.66 | 17.45 |
| 3 | A | 10.1 - 13.02 | 18.55 | 10.18 - 12.38 | 17.85 | 10.29 - 17.89 | 17.75 |
| | B | 13.14 - 17.05 | 18.25 | 13.52 - 17.43 | 18.45 | 13.56 - 18.03 | 17.75 |
| 4 | A | 8.42 - 10.48 | 18 | 7.98 - 12.39 | 17.9 | 7.96 - 18.21 | 16.5 |
| | B | 12.74 - 15.38 | 18.2 | 13.37 - 16.85 | 17.35 | 13.26 - 19.775 | 16.95 |

Table 4.1: Range of switching times and final proportion of PF cells for the system (4.0.1) using parameters (4.0.2) with various $n_s$, and initial conditions given by (4.0.3). For each choice of $n_s$ and initial conditions, we run simulations with cell-cycle lengths of ~ 6, ~ 10, ~ 16 hours.
The number of PF cells is the mean final number of PF cells over 100 simulations, and the Time to Switch range is the mean range of switching times for PF cells over 100 simulations.

In comparison to a fixed lattice of cells, an adaptive irregular array causes a lower number of cells to adopt the Primary Fate, and a greater variability in the number of Primary Fate [PF] cells between simulations with the same initial conditions and parameter values.

1 **An irregular lattice of cells will have a lower proportion of Primary Fate cells than a regular lattice of cells.**

If we compare the PF proportions from Section 4.1, the non-proliferating regular lattice always has a greater proportion of PF cells. However, this is expected from the results of the larger populations in the previous Chapter. For a $6 \times 6$ array with periodic boundary conditions, obtaining a perfect period-3 pattern is more likely than a imperfect period-3 pattern. Larger arrays are more capable of starting to pattern in multiple locations, which consequently increases the likelihood of defects in the pattern, lowering the proportion of PF cells.

If we have a fixed array of 72 cells with periodic boundary conditions, the cells can be arranged as either $9 \times 8$, $12 \times 6$, or $3 \times 24$ arrays, in order for every cell to have 6 distinct

neighbours. For 200 runs of each arrangement, we find a consistent PF proportion, with a mean of 0.287 cells ($\sim 20.7$ per 72) overall.

Comparing these PF proportions with the results from Table 4.1, we find that there is always a lower number of PF cells for an irregular arrangement of cells. This may also be a result of the interplay between cells patterning and proliferating, but we will come back to this.

2 **For a system starting with initial conditions B, global synchronous oscillations in the states of the cells are robust to proliferation.**

Every simulation with initial conditions B displays uninterrupted oscillations (stable for $n_s \geq 3$, decaying for $n_s = 2$) for all cell-cycle lengths, with the states of the cells continuing to oscillate in synchrony even after undergoing a division. We have shown this oscillatory behaviour when $n_s = 3$ in Figure 4.2

The initial conditions of new daughter cells are the state of the mother cell at division, plus an equal and opposite random perturbation of magnitude $10^{-2}$ for each daughter cell. This causes a slight asymmetric division, and ensures conservation principles are respected.

This is not strictly based on biological evidence, as stem cell populations tend to have symmetric divisions, which create two new stem cells, or asymmetric divisions, which create a stem cell and a differentiated cell. The divisions we use would technically fall under the symmetric category, as daughter cells do have nearly homogeneous states, but we do not have divisions where the initial states of the daughter cells would class them as different cell-types. However, we are not using cell divisions as the mechanism for fate determination. For the purposes of these simulations, this method is favourable, as cell-fate determination is still controlled by Notch signalling.

Since this perturbation is of the same order of magnitude as the variability between the initial population, and all neighbouring cells are still oscillating in phase, together this ensures the daughter cells continue the oscillatory dynamics.

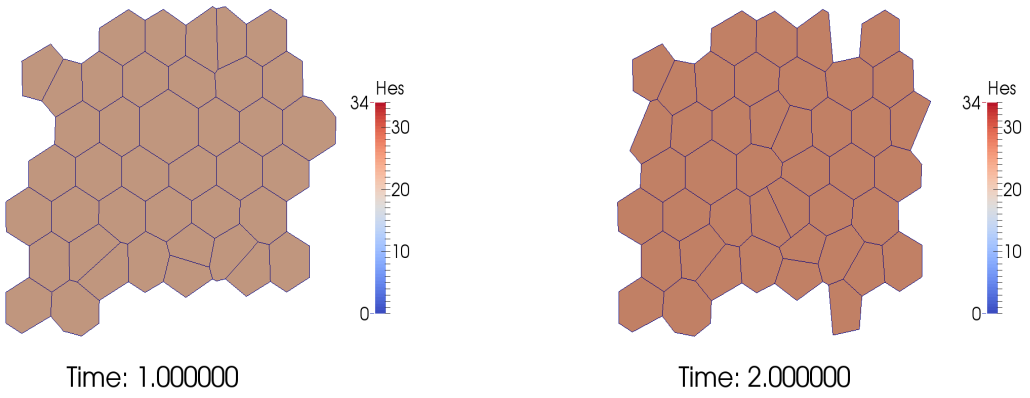


(a)




(b)

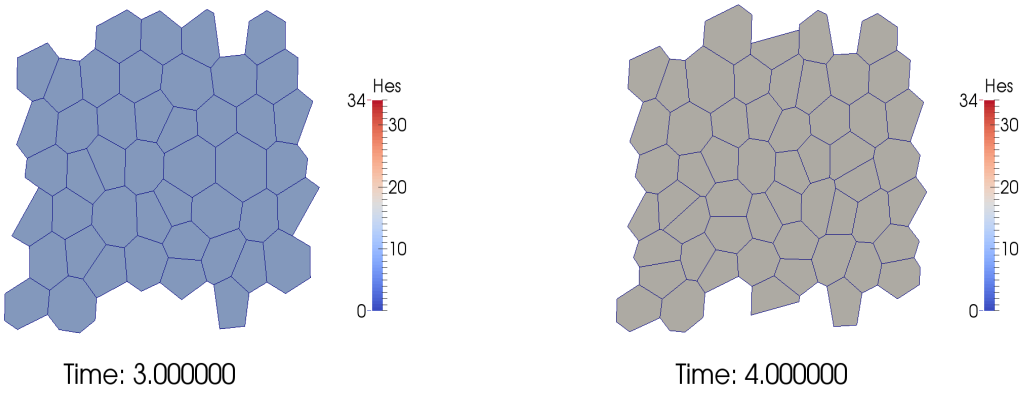


(c)




(d)

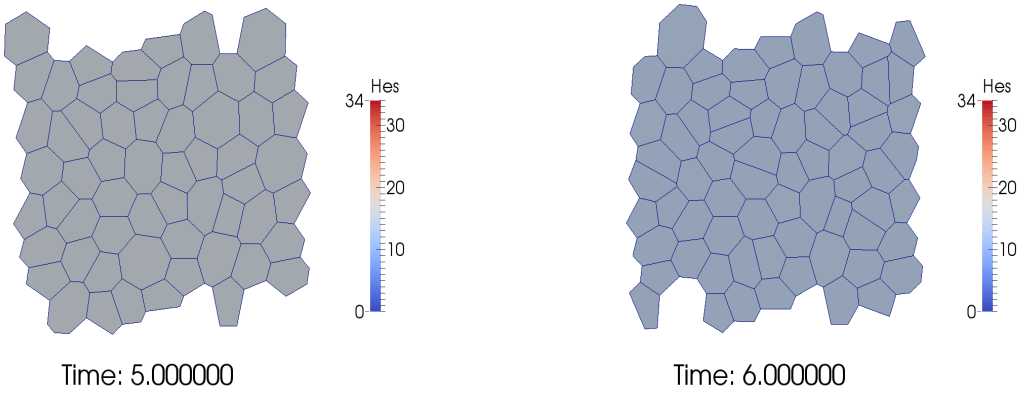


(e)




(f)

Figure 4.2: Snapshots of the system (4.0.1) for the first six hours, illustrating each cell's Hes activity. We have used parameters (4.0.2) and initial conditions B from (4.0.3). We observe global in-phase oscillations throughout the population robust to cell proliferation, until the cells begin to determine their fates. This can be observed via the global, synchronous changes in the levels of Hes activity.

3 **For a population of 72 cells, the number of Primary Fate cells will be higher when there are free boundary conditions instead of periodic boundary conditions.**

When we do not have periodic boundary conditions, cells on the boundary have fewer neighbours than the inner cells, as they are no longer connected to the cells on the opposite boundary. For this reason it is more likely that the pattern will emerge on a boundary, potentially from multiple locations.

We find that the numbers of PF cells increase to means of 21.25, 20.5 and 18.95, corresponding to the cell-cycle lengths ~ 6, ~ 10, and ~ 16 hr, respectively. Again, this also suggests there is an effect on the number of PF cells by the cell-cycle length. An example of the final pattern of cell-types when there are either periodic boundary conditions or non-periodic boundary conditions is shown in Figure 4.3.

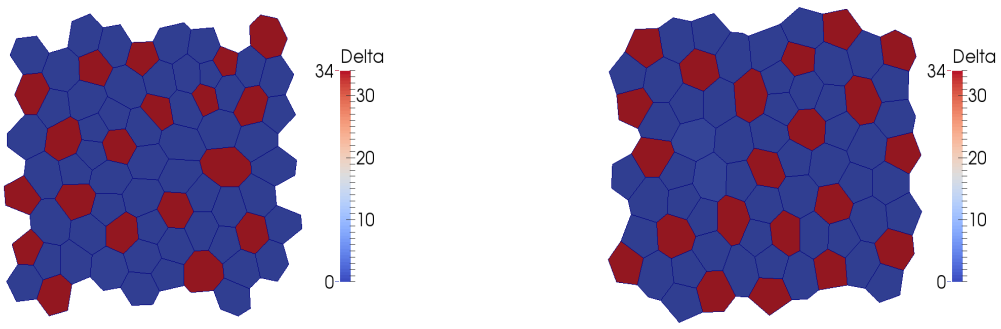


(a) (b)

Figure 4.3: Final distribution of cell types for the system (4.0.1) using parameters (4.0.2), with: (a) periodic boundary conditions; (b) free boundary conditions.
Generally, the proportion of PF cells is higher when using free boundary conditions, with a greater number of PF cells being able to form on the boundary, as illustrated here.

4 **An increase in population size and cell irregularity causes a larger range of Time to Switch for Primary Fate cells.**

From the first set of simulations with no proliferation, we observed coherent patterning, with the mean range of switching times only 0.753 hr.

The previous Matlab simulations tell us that an increase in population sizes causes the TtS range to increase, which we have further verified for a fixed population of 72 cells on a regular $12 \times 6$ hexagonal lattice. From 20 simulations for each parameter choice, we find the mean range increases to 1.71 hr.

However, these simulations show a more significant increase. We find that for each cell-cycle length, there is a mean range of switching times of 3.19hr, 3.63 hr, and 6.45 hr,

respectively. This does suggest irregularity in the array causes an increase in the range of switching times, but it is evident that the cell-cycle length is a big contributing factor to this increase.

5 **The cell-cycle length can affect both temporal dynamics and the ratio of different cell-fates.**

**i** If the cell-cycle length is less than the emergence time of PF cells, the initial switching times and range of switching times are similar for each run of the model. The range increases from the simulations in Section 4.1, but this is primarily due to a larger population and cell irregularity throughout the lattice. There may be a slight delay in the emergence of PF cells in comparison to simulations with no proliferation, but again, this is a feature of the irregularity of the array, rather than the specific length of the cell cycle.

**ii** If the cell-cycle length is greater than the emergence time of PF cells, signalling becomes less coherent, there are fluctuations in the number of PF cells, and the range increases dramatically. This can be seen for various parameters and initial conditions, and is most evident for the simulations with a cell-cycle length of ~ 16 hr and $n_s = 3$ or 4.

This leads to the main result of this Section, which will be important for the following cases:

**Proposition 4.2.1.** *The greater the cell-cycle length is compared to the mean TtS of the system, the greater the effect the cell-cycle length has on the system's temporal dynamics.*

If a cell adopts Primary Fate prior to its division, this will cause fluctuations in the number of PF cells. A cell who has adopted the PF and then divides will become 2 PF cells momentarily, but due to the inhibitory nature of the signalling, they will quickly return to uncommitted cells, before one potentially returns to being a PF cell. If multiple cells do this prior to division, the PF levels will continue to fluctuate until the end of the proliferative period.

Additionally, if the final cells to divide are already PF cells, we see a much slower commitment rate than normal, which causes the increased range in switching times. This is because there are now 2 cells both capable of becoming a PF cell, but are surrounded by non-PF cells, resulting in both daughter cells 'fighting' over who will retain PF.

Also, these results suggest that the more cells capable of committing to PF before division, there will be a fewer final number of PF cells. However, this is inconclusive from each cell only dividing once, and we will address this again when cells continue proliferating.

### 4.2.2 Multiple Cell Divisions

After just a single division per cell followed by a period of 'static' signalling, we have seen that the length of the cells' cell-cycles can affect the dynamics of the population, especially for 'interacting' timescales for division and decision-making.

We now want to increase the proliferative period to 4 rounds of division.

Again, we are interested in how the cell-cycle length can affect the balance between proliferation and differentiation, but now we want to study how this balance changes throughout proliferation.

We saw from the single-division simulations that the dynamics differ from a static population when the cell-cycle length is greater than the emergence time of PF cells, since this increases the probability of a cell becoming a PF cell before undergoing division. This causes fluctuations in the PF numbers, generally resulting in a final lower proportion of PF cells, with a much broader range of switching times.

For these simulations we will only use the parameters

$$n_s = 4,\ n_2 = 2,\ n_g = 3, \quad \mu = 0.03, \quad \theta_s = \theta_2 = \theta_g = 0.2/\mu. \tag{4.2.1}$$

These allow for the fastest switching times when using initial conditions A, and cause the states of the cells to oscillate when using initial conditions B.

By keeping the parameters fixed and only changing the cell-cycle length, we should be able to make a clear statement on whether changing the cell-cycle length can affect the balance of cell-types, both during proliferation and after.

In Sections 4.1 and 4.2.1 PF cells were defined similarly to the previous chapter; a cell becomes a PF cell when its Delta level exceeds 80% of the maximum Delta level. However, it is more appropriate to define a PF cell as a cell who has reached the required Delta level, but then remains above this threshold for a given duration.

Therefore, we will redefine a Primary Fate cell, and also introduce a new preliminary term.

**Definition 4.2.1.** A Potential Primary Fate [PPF] cell is any cell who has a Delta level which exceeds 80% of the maximum Delta level, such that cell $i$ is a PPF cell if

$$D_i > 0.8 \times \max(D_i) \equiv \frac{0.8}{0.03} = 26.667,$$

where $\max(D_i) = 1/\mu$.

**Definition 4.2.2.** Commitment Time [CT] is the duration a cell must remain as a PPF cell before committing to being a PF cell:

$$CT \equiv 0.5\text{hr}.$$

We have used half an hour as our commitment time as this ensures that any oscillations which may exceed the PF threshold do not cause the cell to commit prematurely, and only

when they have actually switched from an uncommitted state. Details of the sensitivity to this choice are given in the discussion at the end of this chapter.

**Definition 4.2.3.** A Primary Fate [PF] cell has a Delta level great than 80% than the maximum Delta level, and does so for half an hour. Cell $i$ is a PF cell if:

$$D_i(t+T) > \frac{0.8}{0.03},\ \forall T \in [0, CT].$$

Over multiple divisions, the population will grow significantly, but the space in which the cells can exist is finite. This is true for both periodic and non-periodic boundary conditions.

We know that during proliferation the cells grow before dividing, which has a knock-on effect on the size of neighbouring cells, causing them to shrink. In this scenario, it is now possible for cells to be removed from the population entirely.

This is a feature ubiquitous to vertex models called a T2 swap, which causes a cell to be removed from the array if its size is lower than a given threshold, which results in a more regular cell size throughout the tissue, and ensures that no cell intersections occur [74].

Following on from Section 4.2.1 we will address the following questions:

1. How do oscillations in the states of the cells behave through multiple cycles of division?

2. What is the ratio of cell-types at the end of each cycle, and at the end of the simulation? How does this ratio change with the cell-cycle length?

3. What differences do we see between PPF and PF numbers, and how does this change with the cell-cycle length?

4. With cells still dividing regardless of whether they are PF cells or not, this will cause fluctuations in the PF numbers. If we want to know

   (a) How to have the biggest PF ratio per cycle;

   (b) How to have the biggest PF ratio at the end of the simulation;

   what temporal interactions between cell-cell kinetics and cell-cycle length do we need in each case?

We are aware that this method of patterning is not biologically viable, since cells becoming Primary Fate cells will stop proliferating and differentiate. However, we will look at examples of this in the following sections, and use this section as a indicator of how different time scales interact over a longer duration.

## Simulation Results

We will cover the main results of these simulations by answering the preceding questions, and include any additional results which are of importance.

**i** Oscillations in the states of the cells are independent of cell division, provided the daughter cells' initial conditions only differ from one another with a magnitude similar to the initial population's initial conditions.

Although robust to division, if the variables continue to oscillate during proliferation this causes the emergence of PPF cells to be delayed, in comparison to when there is just a single cell division per cell.

For example, in Section 4.2.1 we saw PF cells (PPF cells in this scenario) emerge at ~ 13 hours for initial conditions B and any cell-cycle length, but when the cells now continue to proliferate, we only begin to see PPF cells at ~ 15 hours for the same initial conditions.

Additionally, we find that for initial conditions A there is no noticeable change to when the first PPF cells appear. This further supports the earlier statement that oscillations in the states of the cells in a proliferating population delay the onset of patterning.

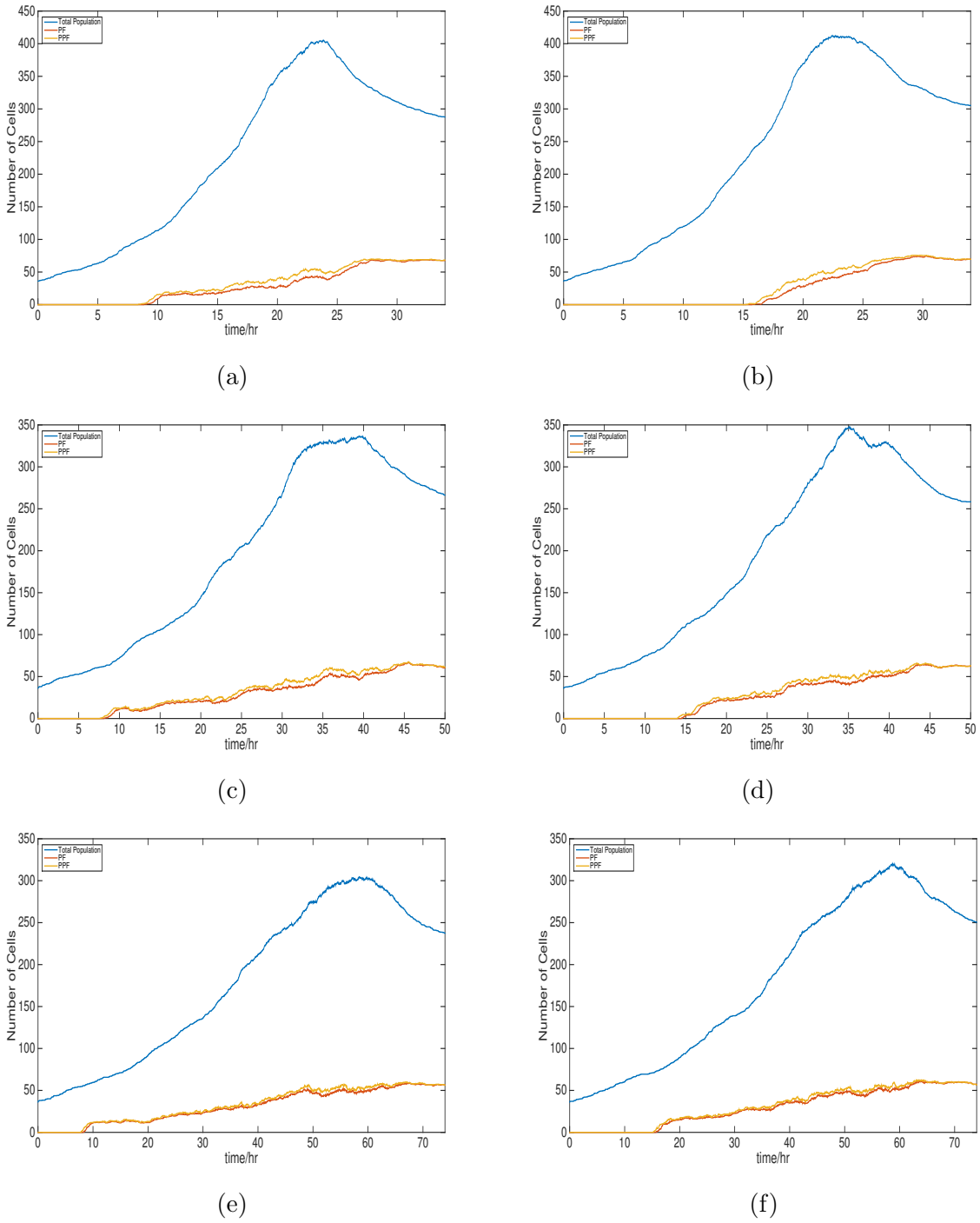


Figure 4.4: Population levels and Primary Fate levels over time for the system (4.0.1) using parameters (4.2.1), initial conditions from (4.0.3) and various cell-cycle lengths. Each simulation runs for for rounds of proliferation, followed by a 10 hour non-proliferative window for the system to establish a final pattern of cell types.
(a) Cell cycle of ~6 hours, initial conditions A; (b) Cell cycle of ~6 hours, initial conditions B; (c) Cell cycle of ~10 hours, initial conditions A; (d) Cell cycle of ~10 hours, initial conditions B; (e) Cell cycle of ~16 hours, initial conditions A; (f) Cell cycle of ~16 hours, initial conditions B.

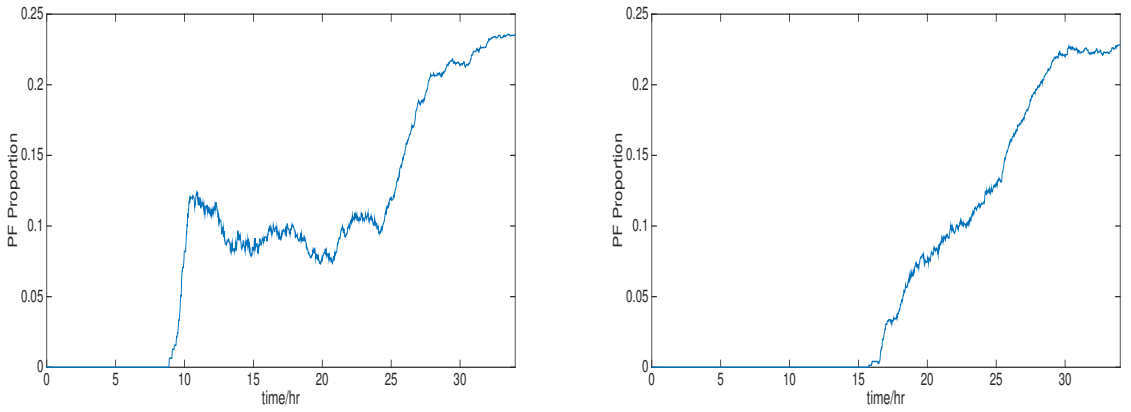


(a)




(b)

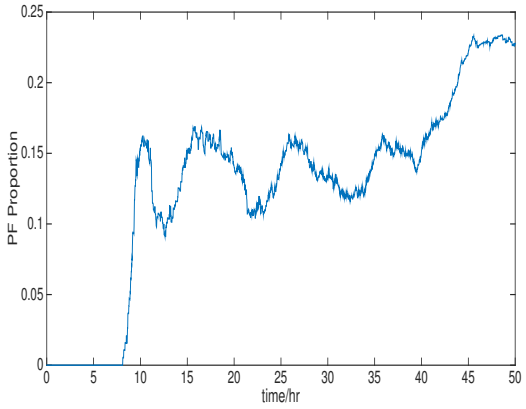


(c)

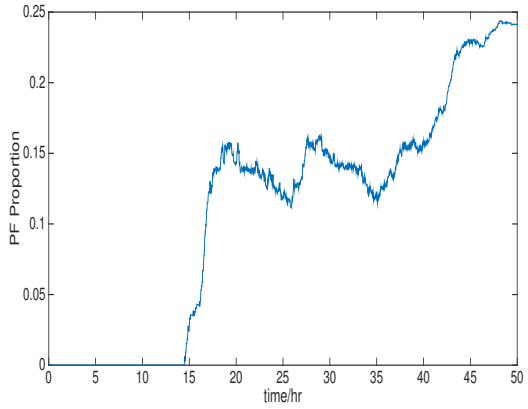


(d)

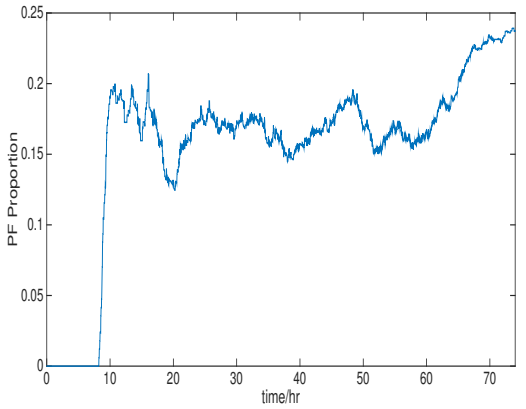


(e)

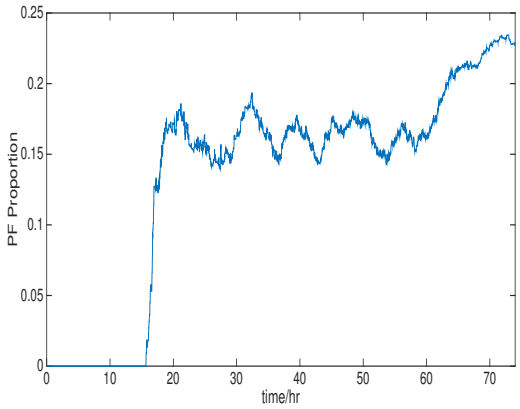


(f)

Figure 4.5: Proportion of PF cells over time for the system (4.0.1) using parameters (4.2.1), initial conditions from (4.0.3) and various cell-cycle lengths.
(a) Cell cycle of ~6 hours, initial conditions A; (b) Cell cycle of ~6 hours, initial conditions B; (c) Cell cycle of ~10 hours, initial conditions A; (d) Cell cycle of ~10 hours, initial conditions B; (e) Cell cycle of ~16 hours, initial conditions A; (f) Cell cycle of ~16 hours, initial conditions B.

**ii** The ratio of different cell types through the simulations depend on both the system's initial conditions and the lengths of the cells' cell-cycles

As we stated for a single division, the system's temporal dynamics can depend on whether the emergence of PF cells occurs before or after the population has finished dividing. We see these characteristic behaviours again, now prevalent over several cycles.

For example, when the cell-cycle length is ~ 6 hours, both sets of initial conditions have emergence times greater than the cell-cycle length, and for initial conditions B, the emergence time of PF cells is over double the cell-cycle length.

Since the rate of division is greater than the decision-making times, this causes continuous fluctuations in the number of PF cells, with no real discernible pattern being formed until the cells stop proliferating. This is illustrated in Figure 4.6.

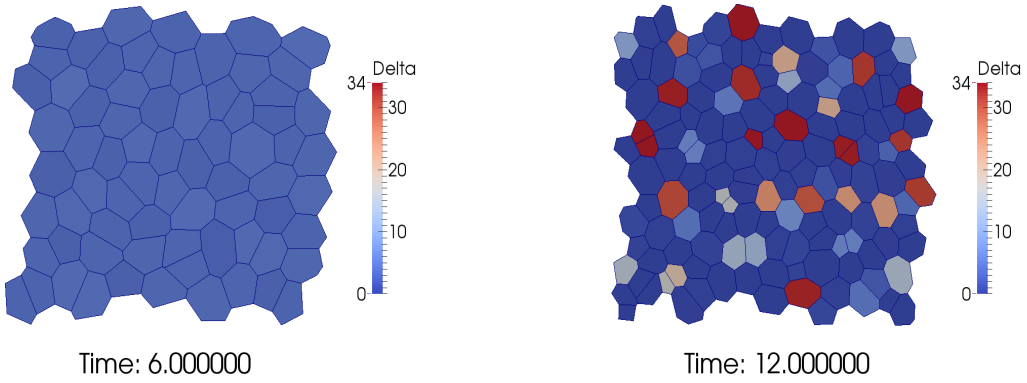


(a)




(b)

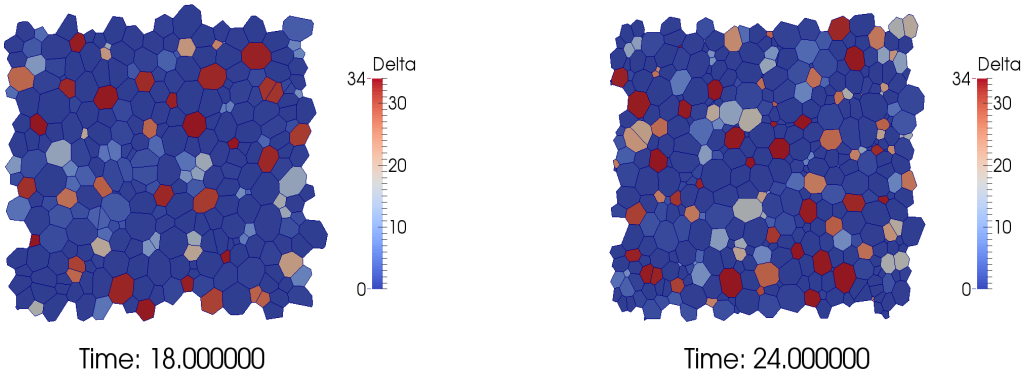


(c)




(d)

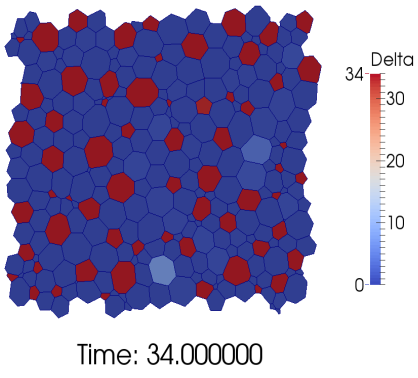


(e)

Figure 4.6: Snapshots of the system (4.0.1) showing the cells' Delta levels at the end of each proliferative window, and at the end of the simulation (34 hours). We have used parameters (4.2.1), initial conditions A from (4.0.3) and a cell-cycle length of ~6 hours. No discernible pattern can be seen until after proliferation has finished, as seen in (e).

**Cell-cycle of ~ 6 hours**

With respect to the proportion of PF cells in the population, we find that each set of initial conditions gives different results. For initial conditions A, PF cells begin to appear during the second cycle, but once the third cycle starts and cells begin to divide again, this causes the proportion to drop. This process repeats, with the PF proportion showing very little increase during each cycle.

For initial conditions B, we find the PF proportion changes in a different manner. Due to the population being considerably larger before PF cells begin to emerge, the proportion shows a more gradual increase, only reaching similar values to initial conditions A during the fourth cycle of division.

In both cases, the PF proportion shows the biggest increase after proliferation. As we can see from Figures 4.5 (a), (b), this corresponds to cells now being able to signal to neighbours with fewer interruptions, whilst the total population is diminishing due to T2 swaps.

**Cell-cycle of ~ 10 hours**

In this case, the emergence times of PF cells fall either side of the cell-cycle length for each set of initial conditions, but unlike when using a cell-cycle of ~ 6 hours, the proportion of PF cells is much closer when comparing each set of initial conditions .

If we look at Figure 4.5 (c), (d), we see that for both sets of initial conditions, the proportion of PF cells initially rises to ~ 15% of the population, followed by a decrease, and increase throughout the following cycle. This cyclic behaviour is representative of the population initially increasing, followed by the PF cells being reestablished for that cycle, and continues until the cells stop proliferating at ~ 40 hours.

The proportion of PF cells can now now increase without such fluctuations, again due to uninterrupted signalling and a diminishing population.

**Cell-cycle of ~ 16 hours**

The emergence of PF cells now falls approximately half way through the first cycle for initial conditions A, and at the end end of the first cycle for initial conditions B. For initial conditions A, the proportion of PF cells reaches 20% of the population during the first cycle, and similarly to the single-division simulations, a well-formed pattern is established during the cycle.

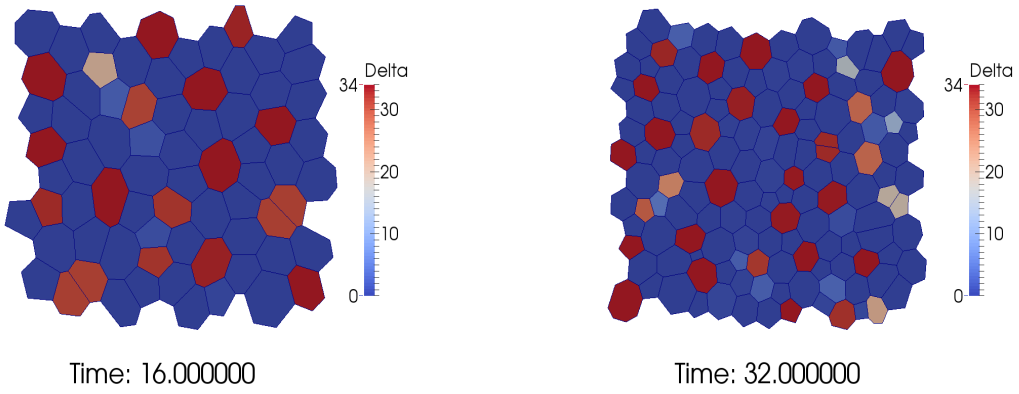


(a)




(b)

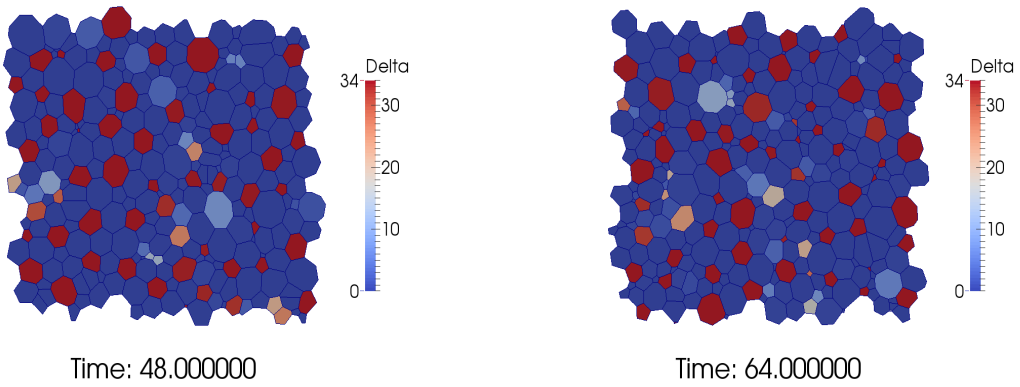


(c)




(d)

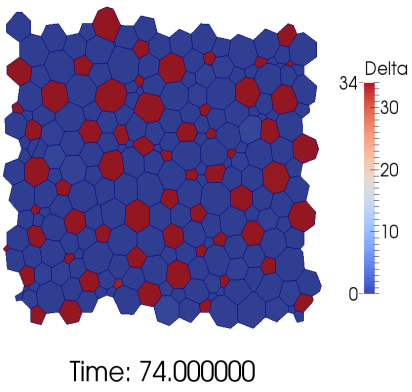


(e)

Figure 4.7: Snapshots of the system (4.0.1) showing the cells' Delta levels at the end of each proliferative window, and at the end of the simulation (74 hours). We have used parameters (4.2.1), initial conditions A from (4.0.3) and a cell-cycle length of ~16 hours. Since the emergence of new PF cells happens at a faster rate than proliferation, a distinct pattern of cell-types can be observed each cycle.

For initial conditions B, similar behaviour is observed in the proportion of PF cells, whilst Figures 4.4 (e) and (f) show how similar the PF cell numbers are for each set of initial conditions.

However, for both sets of initial conditions, the rate of decision-making is faster than the rate of division, which means a coherent pattern is formed during every cycle. This is demonstrated in Figure 4.7. But similar to the previous simulations, this causes some cells to become a PF cell before that cycle's division. In comparison to a cell-cycle length of ~ 10 hours, we now observe greater fluctuations in the proportion of PF cells.

Again, the proportion of PF cells increases once proliferation has finished, albeit less so than when cells have a shorter cell-cycle.

**iii** Fluctuations in the number of PPF and PF cells decrease when the cell-cycle length is increased.

As we have seen, a longer cell-cycle allows for a more coherent pattern of cell types to be formed each cycle, and if coherence increases, fluctuations generally decrease.

Be that as it may, the discrepancy between the number of PPF cells and PF cells increases during proliferation, but the discrepancy decreases as the cell-cycle length is increased. Again, it is easier for a PPF cell to become a PF cell due to fewer interruptions in the signalling.

**iv** As we have seen from Figure 4.5, which shows the proportion of PF cells in the population, the interaction of different time scales can have clear effects on the balance of different cell types.

(a) If we want the largest proportion of PF cells for each cycle, then a longer cell-cycle is required. The greater the cell-cycle length is in comparison to the emergence time of PF cells, the easier it is for the system to form a coherent pattern each cycle.

The same holds true for the number of PF cells; the longer the cell-cycle, the greater the number of PF cells at the end of every cycle.

(b) To have the largest proportion of PF cells at the end of simulation, the cell-cycle length has little effect, with the final proportion being ~ 23% in every case.

However, if we consider the number of PF cells, then a shorter cell-cycle length will produce a greater number of PF cells by the end of the simulation.

This is due to the non-proliferative 10-hour window at the end of the simulation. As we have observed, the maximum population is greatest for a smaller cell-cycle length, which results in more cells being available to become PF cells during this final window.

## 4.3 Including Differentiation for a Spatial Pattern

Now we have seen how the system behaves over several cycles of division, we now want to implement differentiation.

Until now, if a cell met the condition for becoming a PF cell, it did not act differently to the rest of the population, and still continued to divide. The simulations in Section 4.2.2 have given a good indication on how the time scales of division and decision-making interact, but now we want to introduce a different behaviour for those who become PF cells, to establish they have differentiated.

Instead of PF cells continuing to divide with the rest of the population, they will now exit their proliferative stage and stop dividing. The remainder of the population will continue to proliferate, and the final pattern is now built in stages throughout the simulation.

Following on from the previous Sections, we will address the following questions:

1. How does a spatial pattern form in a proliferative population?
2. For a given cell-cycle length, do the initial conditions affect the pattern throughout the simulation?
3. How does the cell-cycle length affect patterning over each cell-cycle, and the final pattern of cell-fates?

### Simulation Results

**i** The final pattern of cell types is now a gradual process, with the pattern forming in a clearer, more coherent manner throughout the simulation.

Due to cells exiting the proliferative phase, this causes a fewer number of cells to divide during the next cycle, resulting in a lower maximum population in comparison to the last set of simulations .

Also, there is now a spatial restriction for generating new PF cells. Enough non-PF cells must divide before any are capable of adopting the primary fate, since a cell can only become a PF cell when not in contact with any other PF cells.

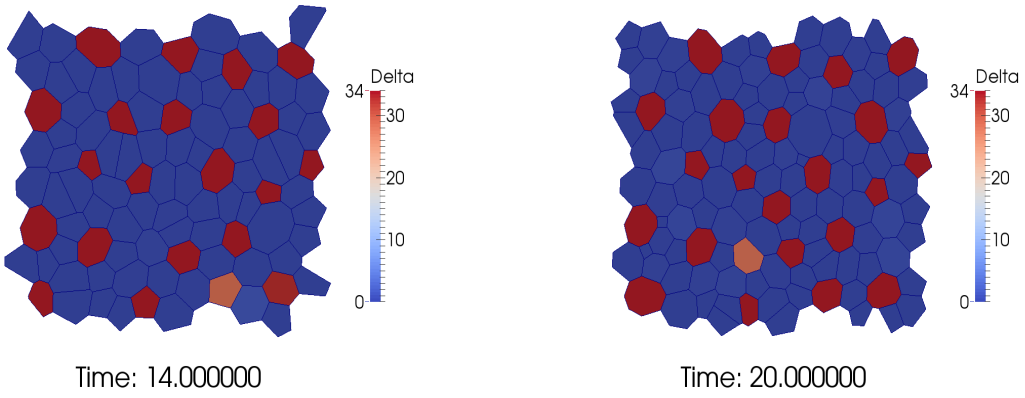


(a) (b)

Figure 4.8: Snapshots of the system (4.0.1) showing the cell's Delta levels at (a) 14 hours; (b) 20 hours. We have used parameters (4.2.1), initial conditions A from (4.0.3) and a cell-cycle length of ~10 hours.
Since PF cells now stop proliferating and remain in the tissue, we only see one new PF cell form in this window of time, due to spatial restrictions and the rate of proliferation.

**ii** Initial conditions A and B have different effects on the system for a given cell-cycle length.

**Cell-cycle of ~ 6 hours**

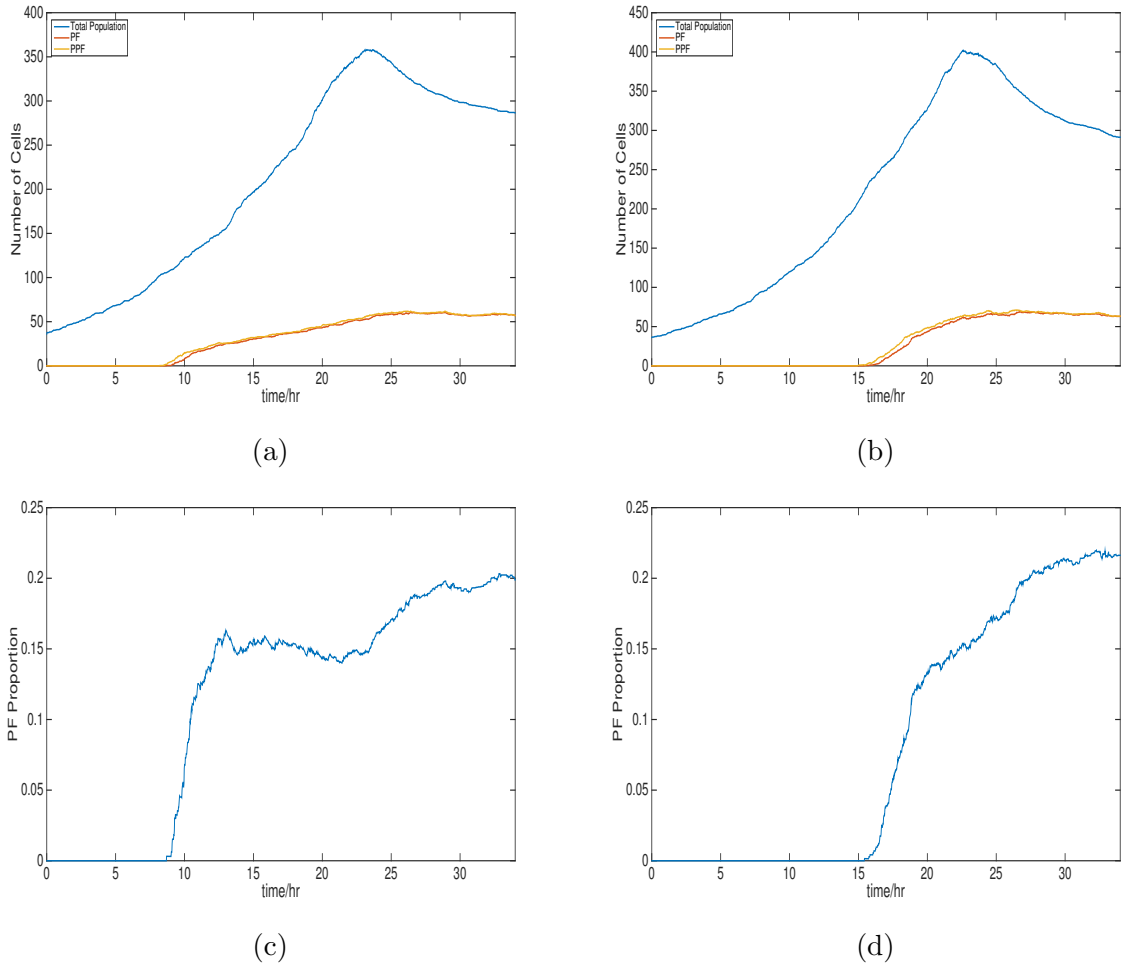


Figure 4.9: Population levels and PF proportions over time for the system (4.0.1) using parameters (4.2.1), initial conditions from (4.0.3) and a cell-cycle length of ~6 hours. (a) Population levels when using initial conditions A; (b) Populations levels when using initial conditions B; (c) Proportion of PF cells when using initial conditions A; (d) Proportion of PF cells when using initial conditions B.

When the cell-cycle is ~ 6 hours, there is again a noticeable difference in dynamics for each set of initial conditions.

From Figure 4.9 we find that the population number, and number of PPF and PF cells behave similarly to the previous simulations, but with less fluctuation in the PPF and PF numbers.

Due to PF cells emerging during the second cycle for initial conditions A, and the third cycle for initial conditions B, this causes the total populations to differ, with the maximum populations having a difference of ~ 45.

The proportions of PF cells are also similar in form to previous simulations, but there are fewer drops in the proportion throughout the simulation for initial conditions A, with the proportion remaining between 0.14 and 0.16 during proliferation.

For initial conditions B, we see the same gradual increase in the proportion of PF cells, also showing similar values to initial conditions A during the fourth cycle.

There is no longer the large increase in proportion of PF cells after proliferation has finished. We do still see an increase, but this is primarily due to the removal of cells, rather than extra PF cells forming, as was the case previously.

**Cell-cycle of ~ 10 hours**

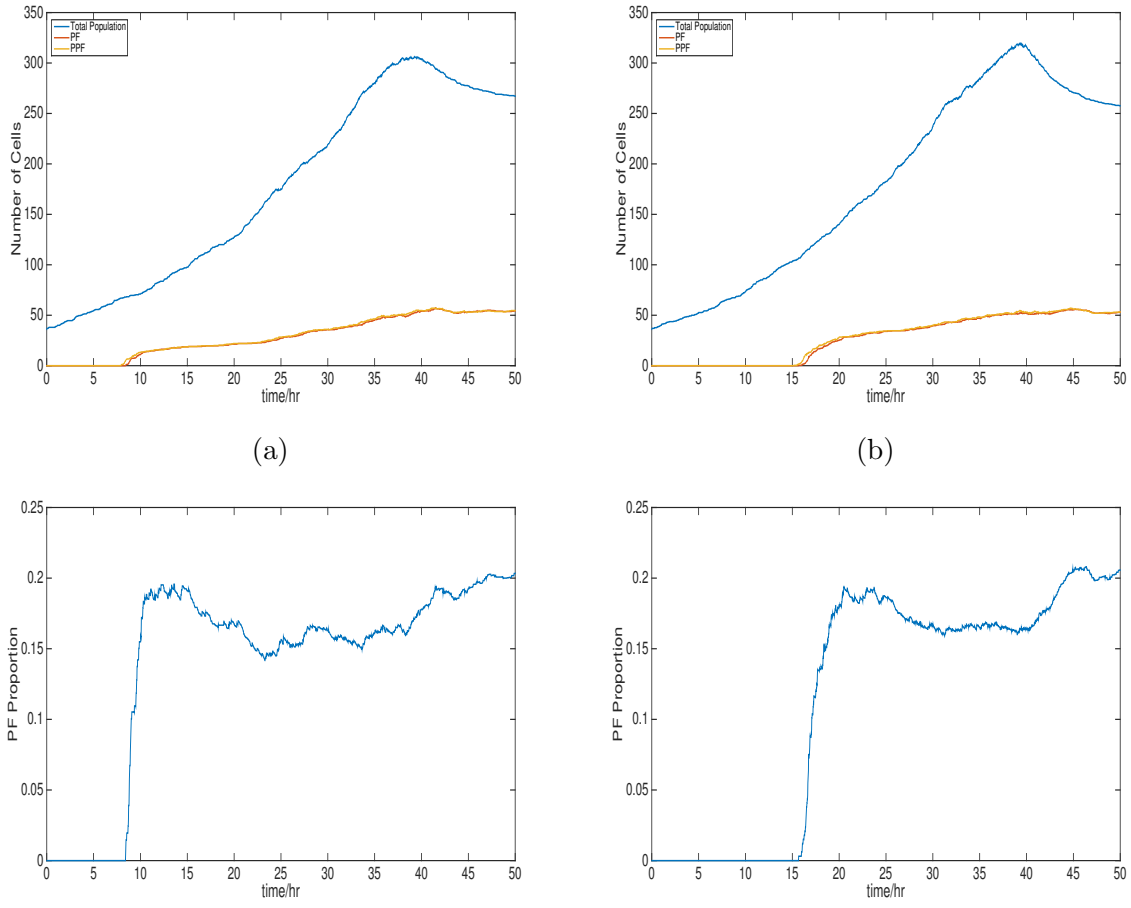


Figure 4.10: Population levels and PF proportions over time for the system (4.0.1) using parameters (4.2.1), initial conditions from (4.0.3) and a cell-cycle length of ~10 hours. (a) Population levels when using initial conditions A; (b) Populations levels when using initial conditions B; (c) Proportion of PF cells when using initial conditions A; (d) Proportion of PF cells when using initial conditions B.

For a cell-cycle of ~ 10 hours, we now see a difference between the sets of initial conditions which was not previously present.

If we look at the numbers of PPF and PF cells for each set of initial conditions, initial conditions B have a consistently higher number of PF cells until the end of proliferation,

by which point they are equivalent. The PF numbers also remain similar for the final 10 hours of the simulation.

Unlike with a cell-cycle of ~ 6 hours, there is very little difference between the maximum population numbers for each set of initial conditions.

Comparing the proportion of PF cells for each set of initial conditions, we find that they do behave similarly to each other. However, it is no longer of the form we saw in Section 4.2.2. In both cases, there is a fast rise to ~ 20% of the population once they begin to emerge, but for the remainder of the proliferative period there are no longer cyclic fluctuations. Instead, there is now a slow overall decrease until cell division has finished. For either set of initial conditions, the proportion does increase again, but only back up to ~ 20%. This is shown in Figure 4.10.

**Cell-cycle of ~ 16 hours**

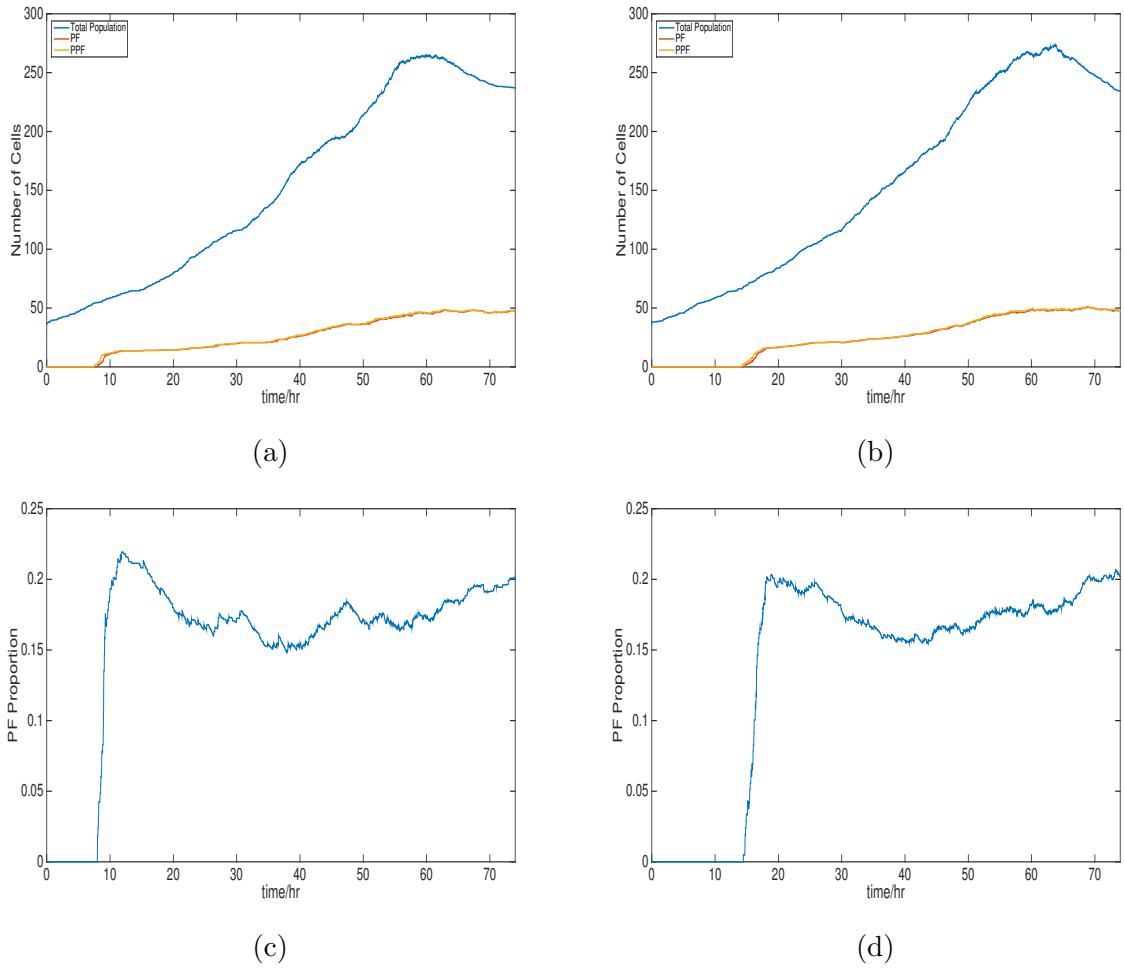


Figure 4.11: Population levels and PF proportions over time for the system (4.0.1) using parameters (4.2.1), initial conditions from (4.0.3) and a cell-cycle length of ~16 hours. (a) Population levels when using initial conditions A; (b) Populations levels when using initial conditions B; (c) Proportion of PF cells when using initial conditions A; (d) Proportion of PF cells when using initial conditions B.

For cells with a cell-cycle of ~ 16 hours, the system displays similar behaviours as when the cell-cycle is ~ 10hours. There is even less discrepancy between PPF and PF numbers, and during each cycle there exists a period where the PPF and PF numbers are equal with no fluctuations, corresponding to the formation of a coherent pattern. Fluctuations are only visible from ~ 50 hours, and as we can see in Figure 4.12, this matches with when PF cells begin to be removed from the population.

The proportion of PF cells also shows similar behaviour to when there is a cell-cycle of ~ 10 hours. There is an initial rise to ~ 21% when cells start to commit to PF, but we again see a decrease until ~ 40 hours, followed by a gradual increase back to ~ 20%.

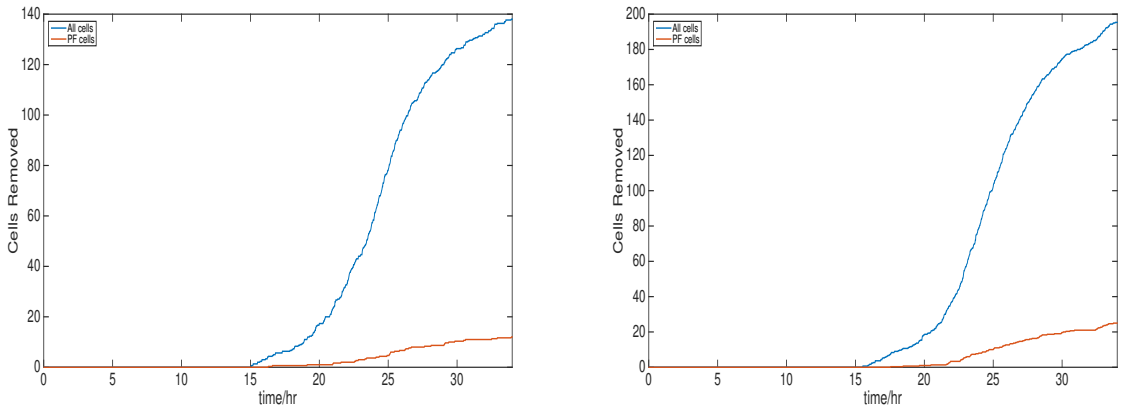


(a)




(b)

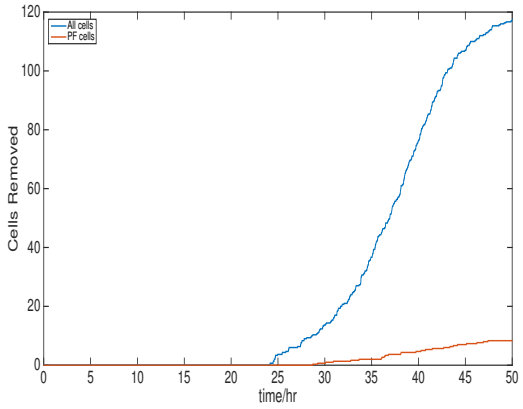


(c)

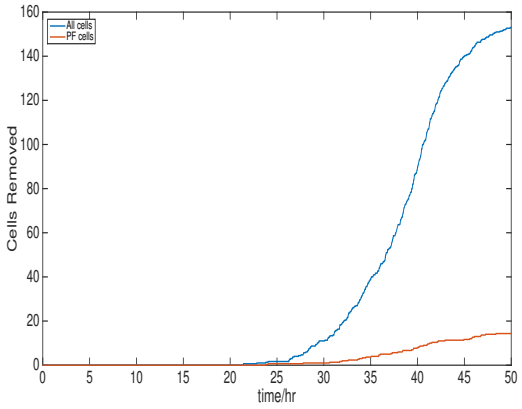


(d)

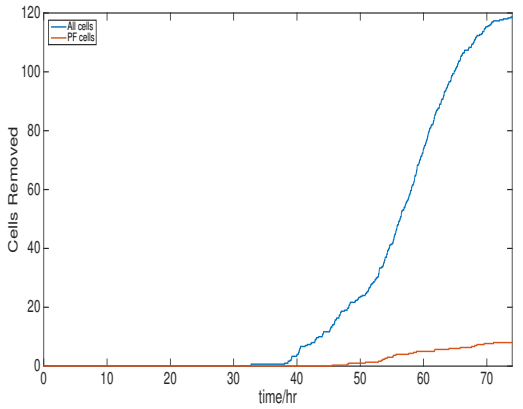


(e)

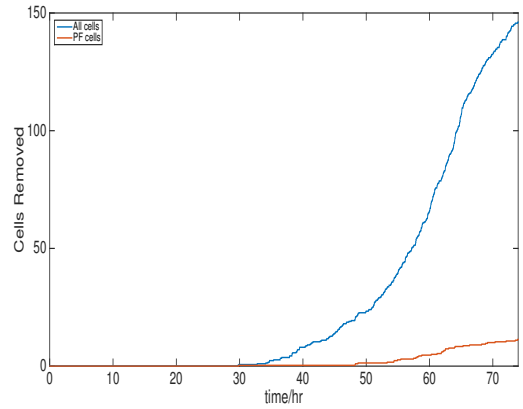


(f)

Figure 4.12: Number of cells removed over time for the system (4.0.1) using parameters (4.2.1), initial conditions (4.0.3) and various cell-cycle lengths.
(a) Cell cycle of ~6 hours, initial conditions A; (b) Cell cycle of ~6 hours, initial conditions B; (c) Cell cycle of ~10 hours, initial conditions A; (d) Cell cycle of ~10 hours, initial conditions B; (e) Cell cycle of ~16 hours, initial conditions A; (f) Cell cycle of ~16 hours, initial conditions B.

- For each cell-cycle length, the number of removed cells is always less than the corresponding simulation from Section 4.2.2. Now, this is to be expected with fewer cells dividing at the end of each cycle, but there is now a clear difference in removal numbers between each set of initial conditions for a given cell-cycle length.

  Additionally, in comparison to the simulations from Section 4.2.2, which had a similar number of cells removed independent of the system's initial conditions or cell-cycle length, we now find that the number of cells removed depends on both of these.

  As the length of the cell-cycle is increased, fewer cells get removed from the population and the difference in removal numbers between initial conditions A and B decreases. This is for both the total number of cells, and PF cells specifically.

  There are always more cells removed when using initial conditions B in comparison to initial conditions A, which is a consequence of the difference in the initial switching times for PF cells between each set of initial conditions. The system patterns faster when using initial conditions A, causing fewer cells to divide during the next cycle. Due to fewer cells in the population, fewer cells get removed.

**iii** In the previous simulations, if the cell-cycle length was less than the emergence time of PF cells, PF cells did not appear until the second or third cycle, depending on the system's initial conditions. If the cell-cycle length was greater than the emergence of PF cells, a coherent pattern of cell types could be reformed each cycle.

For this type of patterning, we are only concerned with the final proportion of PF cells. As we saw before, there is very little difference in the final proportion of PF cells when changing the cell-cycle length or the initial conditions, but if we use initial conditions B and the cells have a cycle length of ~ 6 hours, the final proportion of PF cells is 22%, where, for the other conditions it falls between 19-21%.

The same is also true for the final number of PF cells. For a cell-cycle length of ~ 6 hours, there will be more PF cells at the end of the simulation in comparison to the longer cycle lengths.

So, to generate either the highest proportion, or number, of PF cells, it is better to have a cell-cycle length less than the emergence time of PF cells, and initial conditions B to increase this difference.

Even though there are no PF cells until the third cycle, the population is much larger by this point. There is now less spatial restriction for the propagation of the pattern, allowing a greater proportion to become PF cells.

- The greater the proportion of PF cells formed during a cycle restricts the number of cells who continue to proliferate, and in turn the number of new PF cells which can be formed. Therefore, when forming a spatial pattern over multiple cycles of

division in this way, it is more effective for the population of the system to increase by as much as possible each cycle, rather than have the most PF cells form.

### 4.3.1 Implementing Differentiation with Delamination

For these simulations, we want to change how differentiated cells behave. Instead of modelling the formation of a spatial pattern, let us now consider a system in which differentiated cells leave the population through delamination.

This type of patterning is used throughout the development of neural crest cells in vertebrate embryos, and the development of mammalian inner ear, to name a couple [17,42].

To model this behaviour, we will again prevent PF cells from proliferating, but rather than remain in the tissue of cells, they will now leave the population. To implement PF cells delaminating from the population, PF cells have a new target area of zero. Since cells in the array usually have equivalent target areas to ensure evenly sized cells, changing a cell's target area to zero allows the cell to shrink gradually before disappearing from the tissue, without leaving a void in the tissue. This is favourable for maintaining mechanical equilibrium throughout the tissue, and provides a more realistic abstract of cell extrusion from an epithelial tissue in comparison to cells simply vanishing from the population.

For this alternative type of patterning, the focus is now on how many PF cells are removed from the population, as opposed to the proportion of PF cells within the population.

For the previous simulations, we have only been concerned with the remaining population of cells, and simply acknowledged how the number of removed cells is dependent on the cell-cycle length and initial conditions of the system.

In this case, cells are now being removed intentionally in addition to those who are removed via T2 swaps. However, we can assume that any PF cell being removed is intentional, and only non-PF cells are removed due to T2 swaps.

For consistency, we will be using the same model parameters and initial conditions as Sections 4.2.2 and 4.3, where each simulation consists of 4 rounds of cell divisions followed by a non-proliferative 10 hour window of cell-cell signalling.

From these simulations, we want to answer the following questions:

1. For each cell-cycle length, how do the numbers of PF cells change throughout the simulation, in terms of the number of removed PF cells, and remaining PF cells?

2. What length of cell-cycle is most effective if:

   (a) We want the most PF cells to leave the array each cycle?

   (b) We want the most PF cells to leave the array in total?

## Simulation Results

In this section we refer to the number of PF cells that have delaminated from the tissue and who are still in the population. For each choice of cell-cycle, we have carried out 100 simulations, so the mean number of delaminated cells, or the mean size of the population might not be an integer cell number. To avoid confusion, we have used the mean values in the results tables, but in the text we have rounded to the nearest integer.

Figure 4.13 below demonstrates PF cells shrinking, representative of them delaminating out of the tissue.

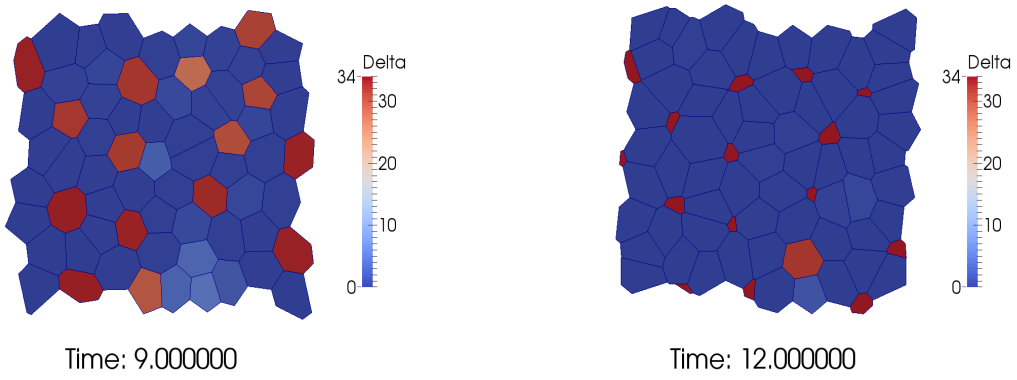


(a) (b)

Figure 4.13: Snapshots of the system (4.0.1) at 9 hours and 12 hours, illustrating the cells' Delta activity and PF cells delaminating from the population. We have used parameters (4.2.1) and initial conditions A from (4.0.3).
We can clearly see cells begin to shrink once they have become PF cells. This is representative of these differentiated cells leaving the tissue.

**Cell-cycle of ~ 6 hours**

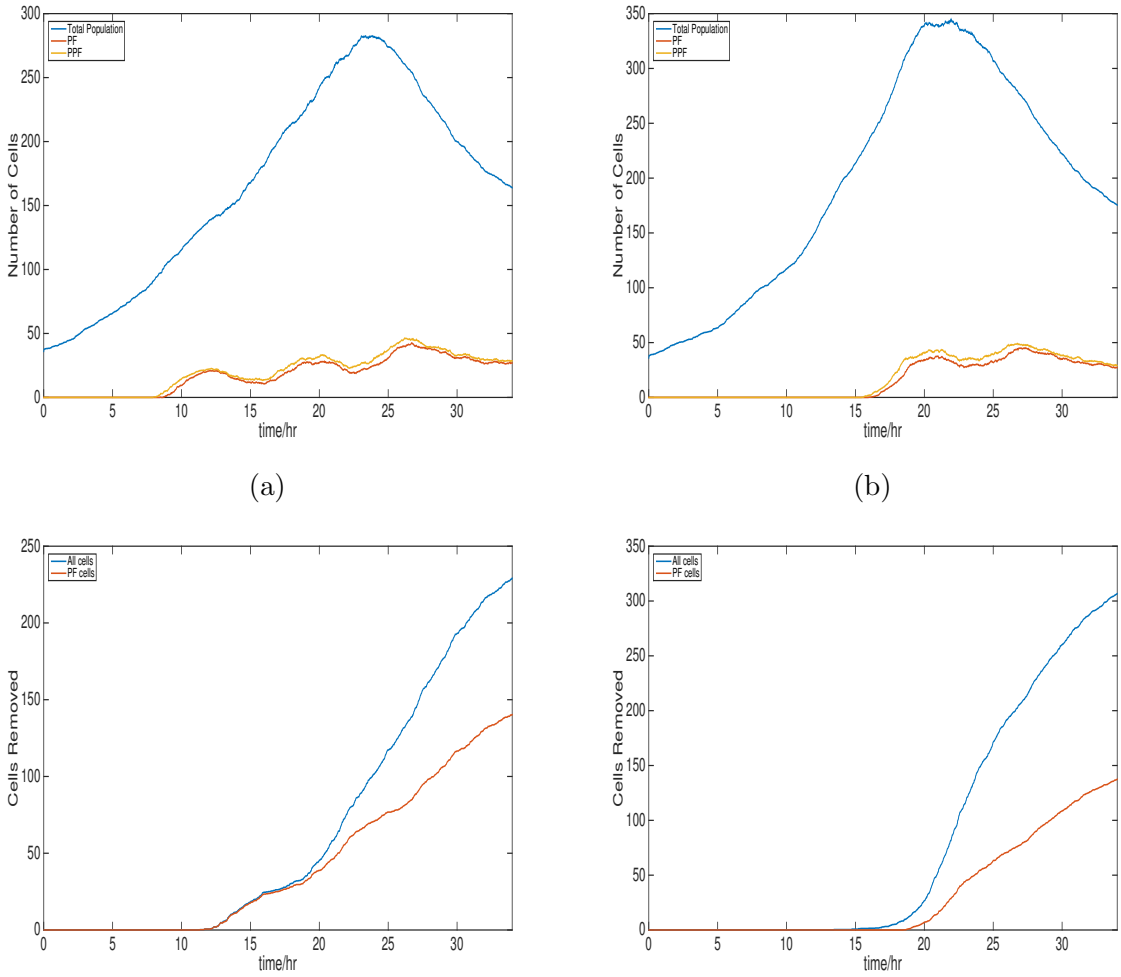


Figure 4.14: Population levels and removal numbers over time for the system (4.0.1), using parameters (4.2.1), initial conditions from (4.0.3) and a cell-cycle length of ~6 hours. (a) Population levels when using initial conditions A; (b) Population levels when using initial conditions B; (c) Number of cells removed when using initial conditions A; (d) Number of cells removed when using initial conditions B.

| Number of Delaminated PF Cells | | | | | | |
|---|---|---|---|---|---|---|
| Initial Conditions | Cycle 1 | Cycle 2 | Cycle 3 | Cycle 4 | No Proliferation | Total |
| A | 0 | 0.6 | 27.6 | 42.6 | 69.4 | 140.2 |
| B | 0 | 0 | 0 | 54.4 | 83.2 | 137.6 |

Table 4.2: Mean number of delaminated PF cells for the system (4.0.1) using parameters (4.2.1), initial conditions from (4.0.3) and a cell-cycle length of ~6 hours.
With the rate of proliferation being faster than cellular decision-making, we see very few PF cells removed during the first two cycles (three for initial conditions B), with the majority being removed during the final non-proliferative window.

When we look at the how the PF numbers still in the population vary throughout the simulation, there is now a cyclic nature to their values.

For initial conditions A, there are three distinct cycles of growth and decay. The first two occur during proliferation, with the third during the final 10 hour window. PF cells start to delaminate just before the second cell-cycle has finished (~ 12 hours), and by the end of the third cycle 28 PF cells have delaminated. The total number of removed cells is 30, so there have only been 2 non-PF cells removed via T2 swaps.

During the fourth cycle and the final window there are a much higher number of non-PF cells being removed, evident by the growing difference in the removal numbers in Figure 4.14 (c) By the end of the simulation there have been 140 PF cells which have delaminated from the tissue, and an additional 89 non-PF cells from T2 swaps.

If we look at the rate at which PF cells are removed, we observe a periodic behaviour, which corresponds to the cyclic behaviour observed in the remaining number of PF cells. A peak in the remaining PF numbers is immediately followed by a steep removal rate, and a trough in the remaining PF numbers is followed by a shallower removal rate. Simply put, there is a greater rate of delamination when there are more PF cells available to delaminate. The final population consists 164 cells, 27 of which are PF cells.

For initial conditions B, the same cyclic behaviour is seen, but due to PF cells emerging later, it is observed a cycle later, with less prominence.

PF cells do not start delaminating until 18.5 hours, but the final removal number is 137, indicating a greater rate of removal in comparison to the initial conditions A. Non-PF cells start to leave the population at the end of the second cell-cycle before delamination starts, and due to a higher population, more cells are being removed due to T2 swaps.

The final population consists of 175 cells, 27 of which are PF cells.

**Cell-cycle of ~ 10 hours**

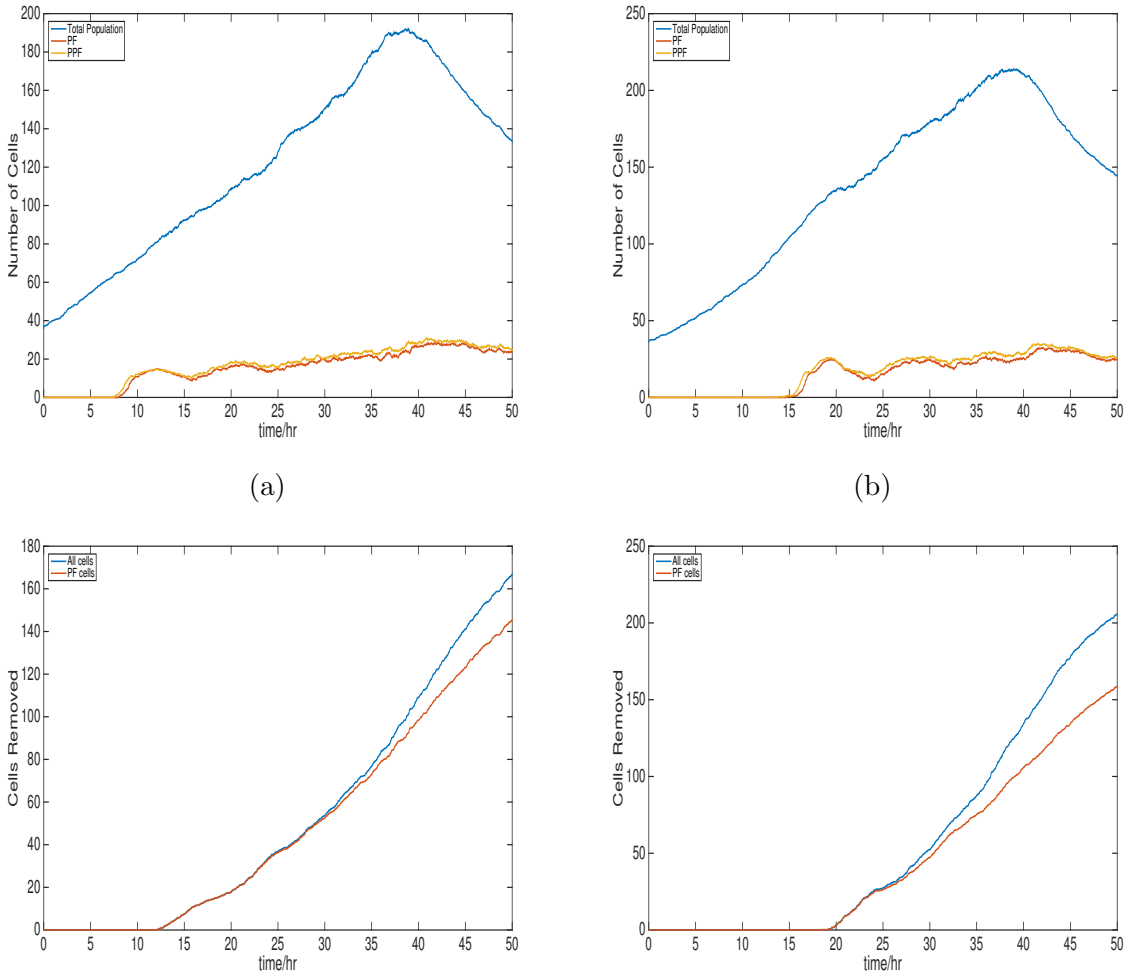


Figure 4.15: Population levels and removal numbers over time for the system (4.0.1), using parameters (4.2.1), initial conditions from (4.0.3) and a cell-cycle length of ~10 hours. (a) Population levels when using initial conditions A; (b) Population levels when using initial conditions B; (c) Number of cells removed when using initial conditions A; (d) Number of cells removed when using initial conditions B.

| Number of Delaminated PF Cells | | | | | | |
|---|---|---|---|---|---|---|
| Initial Conditions | Cycle 1 | Cycle 2 | Cycle 3 | Cycle 4 | No Proliferation | Total |
| A | 0 | 17.8 | 34.6 | 46 | 47 | 145.4 |
| B | 0 | 3.2 | 44 | 58.8 | 52.6 | 158.6 |

Table 4.3: Mean number of delaminated PF cells for the system (4.0.1) using parameters (4.2.1), initial conditions from (4.0.3) and a cell-cycle length of ~10 hours.
With the timescales of proliferation and fate determination in a similar range, we see more PF cells delaminate earlier, with the total number removed greater than when using a smaller cell-cycle.

The cyclic fluctuation in the number of PF cells in the population we observed for a cell-cycle of ~ 6 hours is less prevalent now, especially for initial conditions A. It is present initially, but as the population grows, the number of PF cells in the population shows a more linear increase. This continues until the end of proliferation, at which point the number of PF cells starts to decline.

In comparison to the shorter cell-cycle length, there are always fewer PF cells in the remaining population.

The number of cells removed throughout each cell cycle, and at the end of the simulation can be seen in Figure 4.15 (c), (d) and are summarised in the above Table.

For each initial condition, the number of remaining PF cells at the end of the simulation are 25 for initial conditions A, and 26 for initial conditions B.

**Cell-cycle of ~ 16 hours**

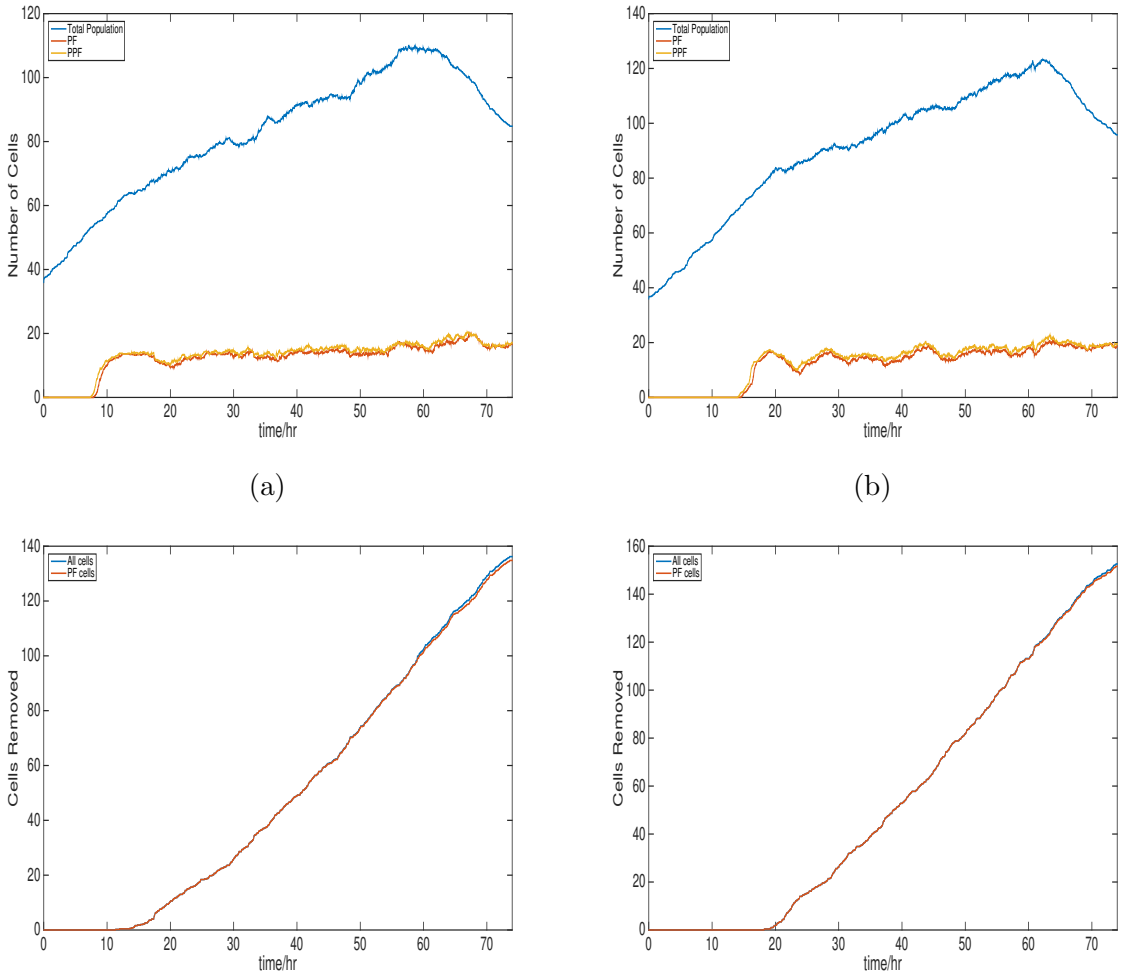


Figure 4.16: Population levels and removal numbers over time for the system (4.0.1), using parameters (4.2.1), initial conditions from (4.0.3) and a cell-cycle length of ~16 hours. (a) Population levels when using initial conditions A; (b) Population levels when using initial conditions B; (c) Number of cells removed when using initial conditions A; (d) Number of cells removed when using initial conditions B.

| Number of Delaminated PF Cells | | | | | | |
|---|---|---|---|---|---|---|
| Initial Conditions | Cycle 1 | Cycle 2 | Cycle 3 | Cycle 4 | No Proliferation | Total |
| A | 2.6 | 27.8 | 37.4 | 44.2 | 22.8 | 134.8 |
| B | 0 | 32.2 | 45.6 | 48.6 | 25.2 | 151.6 |

Table 4.4: Mean number of delaminated PF cells for the system (4.0.1) using parameters (4.2.1), initial conditions from (4.0.3) and a cell-cycle length of ~16 hours.
With fate determination happening quicker than the rate of proliferation, PF cells start to delaminate sooner still, with a more consistent delamination rate. However, this causes a lower number to leave during the final non-proliferative window, resulting in a lower total number of delaminated PF cells, in comparison to a cell-cycle length of ~10 hours.

For initial conditions A, the cyclic fluctuations in PF numbers are even less prominent. Throughout proliferation there is a slight overall increase, but there is very little change in the number of PF cells in the population. There are more smaller fluctuations however, which suggests that there is a constant exchange of PF cells delaminating and new PF cells being made.

For initial conditions B, there does actually seem to be a clearer cyclic behaviour in PF numbers, but due to the increase in the cell-cycle length, the number of cycles has increased.

Again, the number of current PF cells is always less than when there is a cell-cycle length of ~ 10 hours.

The number of cells removed throughout each cell cycle, and at the end of the simulation can be seen in Figure 4.16 (c), (d), and are summarised in the above Table.

For each initial condition, the number of remaining PF cells at the end of the simulation are 17 for initial conditions A, and 20 for initial conditions B.

A general point from these simulations is that the population grows slower after ~ 11 hours as the length of the cell-cycle is increased, which causes the maximum population to decrease as a function of the cell-cycle length.

The difference in the maximum population between initial conditions A and B also decreases as a function of the cell-cycle length, which is due to a smaller difference in the population numbers when PF cells begin to emerge.

**ii (a)** If we want the most PF cells to delaminate each cycle, there is no clear choice for which cell-cycle to use.

Unlike the previous cases, it is unclear which cell-cycle length to choose, as none provide the highest number of PF removals for every cycle.

In some cases, such as a cell-cycle length of ~ 6 hours using either set of initial conditions, there are very few removals of PF cells in the first two cycles, but then the number removed during the last 10 hours is much greater than other cases. Conversely, if there are a large number of PF cells removed during the first couple of cycles, such at when the cell-cycle length is ~ 16 hours, this causes the total population to diminish quicker, resulting in much fewer leaving during the final 10 hours.

**ii (b)** If we want the most PF cells to delaminate in total, for a given set of initial conditions, a cell-cycle of ~ 10 hours gives the best, and most consistent results.

Again, this balance comes down to the interplay between the length of the cell-cycle, and the emergence times of PF cells. If the emergence time is much less than the cell-cycle length, such as when we use initial conditions B and a cell-cycle of ~ 16 hours, then it is possible to remove too many PF cells too early, resulting in fewer cells being able to become PF cells later on.

If the emergence time is much greater than the cell-cycle length, it may be that too few cells get removed initially. Even though there is now a larger population going into the last cycle and 10 hour window, the system cannot generate, and remove, PF cells at a fast enough rate.

For this type of patterning, it seems the best balance between proliferation and differentiation is achieved when the cell-cycle is ~ 10 hours. The emergence times of PF cells falls either side of the cell-cycle length for each initial condition, but the differences are much less than for the other cell-cycles.

This provides a good compromise; we want to be able to have a consistent number of PF cells being removed each cycle, but not so many that it depletes the population too heavily.

## 4.4 Discussion

### 4.4.1 Summary of Results

In this chapter we have used a vertex model to create a system of proliferating cells governed by lateral inhibition. The aim has been to explore the dynamics of a system forming a pattern of alternate cell-types on a growing population, and the interplay of timescales between cell-cell kinetics and the rate of proliferation.

We have shown that, even when there is only a single division per cell, the variability in the number of neighbours each cell has at any given time reduces the coherency of signalling throughout the population. This causes an increase for the time taken for PF cells to begin emerging, and reduces the proportion of PF cells in comparison to a non-proliferating population.

The lower proportion of PF cells is expected; since cell divisions cause irregularities in the arrangement of the population, this can lower the maximum possible number of PF cells. Furthermore, if the patterning rate is faster than the rate of proliferation, this can introduce spatial restrictions for where new PF cells can form. This results in a further decrease in the proportion of PF cells. These results are summarised in Table 4.1.

By then increasing the number of divisions each cell undergoes, we have investigated how changing the cell-cycle length and initial conditions can affect the number of PF cells formed, the transient dynamics, and the ability to form a discernible pattern.

We find that, when the cell-cycle length is shorter than the rate at which PF cells emerge, it is difficult for the system to establish a well-defined pattern of cell-types. This is due to the cellular fluctuations in position, number of neighbours, and the coherency in the signals received from regularly changing neighbours.

When the cell-cycle length is longer than the rate at which PF cells emerge, there is less fluctuation in the number of neighbours each cell has, and in the coherency of the signals received from neighbouring cells. With a slower rate of proliferation, cell signalling is interrupted less, and a well-defined pattern of cell-types can be formed during each round of proliferation. These results are illustrated clearly by Figures 4.6 and 4.7.

Furthermore, when initial conditions are chosen such that the initial population displays transient oscillations in their cell states, these oscillatory dynamics are robust to proliferation, provided each pair of daughter cells have states relatively similar to each other and the neighbouring population. This is demonstrated in Figure 4.2.

When oscillations are present in a proliferating population, they cause a delay to the emergence of PF cells in comparison to a static population, with cell divisions appearing to cause the population to remain in a state of homogeneity for longer.

By then introducing differentiation, whereby PF cells now stop proliferating, and using

the cell-cycle length as a control parameter, we have shown that the cell-cycle length has a direct effect on the proportion of PF cells both during and at the end of the simulations.

When implementing differentiation such that PF cells stop proliferating and remain in the tissue, the final pattern is a gradual process. Again, the rate at which differentiated cells form is dependent on the cell-cycle length. When the cell-cycle length is shorter than the rate of differentiation, the formation of PF cells is regular, with the proportion of PF cells in the population steadily increasing, and reaching a maximum only at the end of the simulations. This is seen clearly in Figure 4.9(d).

As the cell-cycle length is increased, such that the rate of fate commitment becomes quicker than proliferation, a well-defined pattern is formed during the first round of proliferation. However, with differentiated cells remaining in the tissue, no new differentiated cells can form until there is space; enough cells must first divide until there are cells free from direct contact with existing differentiated cells. This causes the PF proportion to reach a maximum during the first round of proliferation and then fluctuate during each cycle, only reaching a similar proportion at the end of the simulation. This can be seen in Figure 4.11(d).

If the aim of this system is to create as many PF cells as possible, it is better to have a faster rate of proliferation to differentiation. This causes a larger population before patterning begins, and there are no spatial restrictions for forming new PF cells. But, if the aim of this system is to produce a regular amount of PF cells over time, it is better to have similar rates of proliferation and differentiation. This allows PF cells to form during the first round of proliferation, and the population increases fast enough for a steady formation of new PF cells.

Lastly, we implemented differentiation through delamination, such that once a cell has differentiated, it gradually leaves the tissue. This is a different means of pattern formation to what we have previously focused on; here we are interested in the rate at which differentiated cells form and leave the population, as opposed to the formation of a spatial pattern of alternate cell-types.

We found that although varying the cell-cycle length causes different removal rates throughout the simulation, there is no clear choice for an optimum cell-cycle length to ensure a consistent removal rate. For a short cell cycle, no cells delaminate until midway through the simulation, and for a long cell cycle, a much larger proportion of the population leave early on, depleting the number of remaining cells. The effect of lengthening the cell cycle on PF cell formation and delamination is illustrated by Figures 4.14, 4.15, and 4.16, and summarised in Tables 4.2, 4.3 and 4.4.

If the rate at which cells delaminate is of less importance, and we simply want as many delaminated PF cells as possible, this is achieved when the rate of differentiation and proliferation are of a similar length. This allows a steady proportion of differentiated cells to delaminate each cycle, but not so much that the population is depleted.

### 4.4.2 Model Implementation

To model our proliferating cell population on a growing lattice, we had to specify certain behaviours and mechanics for the model.

To implement cell divisions, we assigned cell-cycle lengths from a Gamma distribution, and chose parameters such that all cells' cycles were in a 2-hour window centred around the chosen cell-cycle length. Each cell in the initial population started at a randomly chosen phase of their cell cycle, such that cell divisions happened one at a time, rather than collectively. New daughter cells were also given a cell-cycle length from a Gamma distribution, which stopped them dividing simultaneously.

We implemented a period of growth over the last hour of each cell's cycle, such that the target area of the cell doubled. This is to represent the growth during the G1 phase of the cell cycle. This allowed daughter cells to be of a similar size as the neighbouring cells, since the cell divisions split the cells into equal areas.

Cell division was implemented by choosing an angle of mitosis, which was in the direction of the shortest axis through the cell's centroid. It has been shown that the choice of the angle of division can have a significant effect on the resulting epithelial sheet topology, particularly on the frequency of hexagonal cells in the tissue [92].

To check the effects of this in our model, we ran some simulations with a specific angle of division for each cell. This did cause less irregularity throughout the lattice during the first round of proliferation, but due to the mechanical forces between cells to regulate their sizes, very little difference could be seen in the final topologies.

Additionally, we ran some simulations in which the growth window was varied from one hour to the duration of the cell cycle, as well as simulations where there was no cell growth prior to division. Altering the growth window did introduce some minor topological differences, but this did not affect the overall signalling between cells. This is supported by [93], who show that provided the order of growth is greater than the mechanical relaxation time of the tissue, the exact implementation of cell growth is of less importance.

Similarly, removing all cell growth causes a topological difference, with daughter cells being half the size of undivided cells, but as simulations progress and the population increases, the final state of the tissue shows little difference to the simulations with cell growth prior to division. Again, this does *not* affect the balance of cell types or the temporal dynamics of the intercellular signalling.

Furthermore, our focus has not been on the topology of the tissue, but rather the distribution of alternate cell types. We find that the balance of cell types and the rate of fate determination is robust to the specific mechanics of cell growth and division.

Commitment Time, as defined in Section 4.2.2, was chosen as half an hour. This was chosen because it stopped any cells who exhibited initial transients in their levels of Delta activity which exceeded the PF threshold from prematurely becoming PF cells. We only

want cells to become a PF cell if the state of the cell is explicitly moving to the steady state associated with high Delta levels.

If there is no minimum time restriction for a cell to be a PF cell, we find that the number of PF cells fluctuates more throughout the simulations in Section 4.2.2, where there is no behavioural change for PF cells. But, the general balance of cell types is unaffected.

By increasing Commitment Time, this delays the emergence of PF cells, creates a larger discrepancy between PPF and PF cell numbers, and causes the proportion of PF cells to decrease at the end of each proliferative window. This is most obvious when using the shortest cell-cycle length, and has less effect as the cell-cycle length is increased. Unsurprisingly if Commitment Time is significantly increased, the final proportion of PF cells will decrease.

This choice has not been based on biological evidence, but as we have stated, it is to ensure a cell does not inadvertently become a PF cell because of an initial transient.

### 4.4.3 Conclusions

This chapter has given novel insight into how signalling via lateral inhibition behaves for a proliferating population. To address the initially proposed questions, we have found that some of the dynamics observed for a static population, such as transient oscillations, are robust to cell divisions, but introducing cell divisions causes interrupted signalling between neighbouring cells, resulting in slower patterning throughout the population. Additionally, cell divisions introduce irregularity in the the size and arrangement of the cells, and as this is a gradual process, rather than an initial feature of the simulations as seen previously in [82], this causes a smaller proportion of PF cells to form during the simulations.

With regard to the interaction of timescales between cell-cell kinetics and biological processes, we have found that the rate of proliferation has a clear effect on the patterning potential of the system. When the rate of proliferation is faster than patterning, formation of differentiated cells is delayed due to interrupted signalling, and a pattern can only be formed after proliferation has finished. Alternatively, when patterning is faster than proliferation, PF cells can form when the population is still small, and a distinctive pattern is formed gradually. However, if patterning is much faster than proliferation, and differentiation is implemented by cell removal, the population can be depleted too quickly. For a population to maintain a balance between proliferative and differentiated cells, we find this achieved best when the timescales are in a similar range.

Comparing the findings to current literature, these support existing results well. It has been shown experimentally that in a population of neuroepithelial cells, when the length of G1, and consequently the cell cycle, is increased, this changes the balance between proliferative and differentiated cells, resulting in premature neurogenesis [62,65].

The results also support a recent study of both experiments and mathematical modelling for a growing tissue governed by Delta-Notch signalling, in which differentiated cells remain in the tissue. They show that there is a fine balance between proliferation and differentiation for gradual pattern formation, and when the rate of patterning quickens (represented by a longer cell-cycle length in our simulations), premature patterning occurs throughout the tissue, leading to the formation of excess differentiated cells [83].

Possible means of model validation for this chapter may be possible via a culture system of stem cells, or a synthetic model, similar to [94]. As we said in the discussion of the previous chapter, if the system is capable of demonstrating oscillatory dynamics, we could use Time to Switch as a means of model validation.

Looking back at Figure 3.72(b), there are two distinct regimes for Time to Switch as a function of $\chi$. We have Time to Switch behave as a decreasing function until $\chi = 0.06$, and then a very slowly increasing function for $\chi > 0.06$. If we were to introduce a Notch inhibitor into the cell culture, this would have the effect of lowering the feedback strength $\chi$. If this caused Time to Switch to increase, sensitive to the change in $\chi$ then the system would be in the regime to the left of $\chi = 0.06$, and if Time to Switch were to slightly decrease, we would be in the regime to the right of $\chi$. For a proliferating population, If Time to Switch were to increase, we would see fewer cells differentiate in a given time window, and if it were to decrease, we would see more cells differentiate in a given time window.

However, it must be stressed that the models of switching presented here are inspired by Delta-Notch mediated lateral inhibition, but ultimately, they are generic theoretical models of bistable switches. In fact, these would be just as applicable to other processes involving positive feedback and nearest neighbour interactions, provided the assumptions we have made are still satisfied.

# Chapter 5

# Summary and Conclusions

The aim of this research project has been to provide a theoretical study for modelling cell-fate decision-making in populations of cells governed by lateral inhibition. The work has been motivated by previous theoretical models of pattern formation via lateral inhibition.

Although the Notch pathway has been discussed and referenced throughout this study, we want to reiterate that the results presented here are *not* specific to Delta-Notch signalling, but can be applied to other processes involving positive feedback and juxtacrine signalling, provided the mechanics satisfy the assumptions we have made.

In Chapter 2 we were able to show that systems governed by ODEs are able to have a Hopf bifurcation, provided there are at least three components in each cell. This holds for systems of two cells, as well as larger populations, independent of the arrangement of the cell population. Furthermore, this bifurcation does not depend on the presence of a time delay in the intercellular signal between neighbouring cells.

In Chapter 3 we then showed that, for cells with nearly equivalent initial conditions, when the conditions for a Hopf bifurcation from linear stability analysis were met, oscillations during cell-fate determination were observed in the states of the cells. Therefore, transient oscillatory dynamics are not a unique feature of models with time delays [50,51,70], but they do require a minimum of three components per cell.

From [63], it is shown that for an $n$-component loop governed by negative regulatory functions, there are either stable oscillations if $n$ is odd, or transient oscillations followed by bistability if $n$ is even. Now, this is expected from what we understand about positive and negative feedback loops, but it gives insight into what we have observed.

For a 2-cell system, signalling is driven by a double-negative (positive) feedback loop, but due to the symmetry of our models, there exists a subspace of the system, the Surface of Equivalence, which is governed by a negative feedback loop. Therefore, if there are at least three components per cell, or a time delay, there can exist a stable periodic orbit in this subspace. If the state of the system starts near this subspace, for some initial conditions we will see in-phase oscillations in the states of the cells whilst the state of the system approaches one of the two final steady states.

This idea is important, and could be applied to numerous other systems which possess a similar symmetry. Regardless of the overall complexity of the regulatory logic, studying this equivalence subspace can provide a lot of information about the system, without having to analyse the full system.

In Chapter 2 we also presented a method of analysing larger populations using a reduction of dimensionality. By assuming the final pattern of cell types, we proposed a means of analysing each cell type, rather than each cell. This allowed us to carry out linear stability analysis and give conditions for when switching would be possible.

As predicted by the linear stability analysis and supported numerically in Chapter 3, when there is a lower proportion of PF cells in the final pattern, the feedback strength required for switching is greater. This supports results by [48, 91], who have shown that cells on a hexagonal lattice require a greater feedback strength between neighbouring cells for switching from homogeneity, with a slower rate of switching.

From analysis in Chapter 2 and the supporting numerical results, we have also shown that there can exist a part of parameter space which allows the conditions for a Hopf bifurcation to be met, but not for switching. It is therefore possible for a system governed by lateral inhibition to display stable in-phase oscillations, without the existence of other steady states.

In Chapter 3 we looked at the global dynamics of the systems presented in Chapter 2. We found the potential dynamics of a system are dependent on the number of components per cell, and the choice of initial conditions.

If the state of the system starts in the vicinity of the HSS, then regardless of the number of components per cell or the inclusion of a time delay, switching is a fast, coherent process, with a small range of switching times throughout the population. Furthermore, linear stability analysis provides a highly accurate prediction for the rate at which cells switch from homogeneity. This holds not just at the HSS where the analysis was carried out, but continues until the vicinity of the system's final state.

However, if the state of the system starts with the same level of homogeneity, but away from the HSS, there can exist uniform oscillations throughout the population. Their presence causes slower, more varied switching times, and Time to Switch is no longer a continuously decreasing function of the feedback strength, $\chi$. This is shown in [50,51] for systems with a time delay, but we have shown explicitly that it is true for any system of this form if oscillatory dynamics are present.

We were able to illustrate that the dynamics observed for systems governed by ODEs or DDEs are qualitatively equivalent, but we find that the patterning rate is reduced by the presence of a time delay. This supports previous studies [50,51], who find that the

inclusion of a time delay causes a slower rate of patterning.

This comparison could be useful for future modelling work as it could allow more complex models to be simplified via time delays, without losing the range of potential dynamics. Then, by knowing how the results would be quantitatively different to the original model, such as the growth rate of perturbations, it may be possible to give predictions for how the original model would behave, both spatially and temporally. This is similar to the approach used in [51].

In Chapter 4, we used a vertex dynamics model to create a system of proliferating cells governed by lateral inhibition, and explore the dynamics of pattern formation for a growing population, and the interplay of timescales between cell-cell kinetics and the rate of proliferation.

We were able to show that some of the dynamics observed in Chapter 3 for a static population, such as global transient oscillations prior to switching, were robust to cell divisions, but other behaviours, such as coherent signalling, was interrupted by cell divisions. This resulted in a slower emergence of Primary Fate cells, and a more sporadic pattern formation.

Due to the irregularity of the cell size and arrangement in the tissue due to cell divisions, patterning was much more of a gradual process, which resulted in a lower proportion of differentiated cell in comparison to a static population.

In terms of the interplay of timescales for differentiation and proliferation, there was a distinct difference in the system's pattern-forming potential when the rate of proliferation was adjusted. When the rate of proliferation was faster than differentiation, formation of differentiated cells was delayed as a consequence of less coherent signalling, and a pattern of alternate cell types could only be formed later in the simulation, when the population was larger and cell signalling was interrupted less.

When the rate of differentiation was faster than proliferation however, differentiated cells were able to form when the population was still relatively small, and patterning was a more gradual process. Additionally, if differentiated cells also left the tissue, when differentiation was faster than proliferation this caused too many cells to leave the population during the first rounds of proliferation. This depleted the population, causing fewer differentiated cells to be able to form, and delaminate later in the simulation.

Overall, this project has been a success. Using theoretical models adapted from Collier *et al.* [48], we have been able to build on their findings, address some previous limitations, and provide cases where new dynamics can be observed. Furthermore, we have taken an adapted Collier model for lateral inhibition and implemented it into a proliferating population, and explored how cell-fate determination behaves with the inclusion of other biological processes.

Referring back to our initial questions in Section 1.3, we have been able to successfully

address each of them.

We find that oscillatory dynamics in the levels of Notch and Delta activity are not only possible with the inclusion of a time delay, but can be achieved by the inclusion of an intermediate component in each cell.

Provided there are at least three components per cell, the system is capable of having a Hopf bifurcation, and for a range of initial conditions, this results in in-phase oscillations prior to the system reaching its final state. This is demonstrated in Section 3.1.2.

Although this is a simple mathematical result, as far as we are aware, this is novel for published literature for models of lateral inhibition governed by ODEs. It may be such dynamics have been seen previously, such as in [55] where a more complex model is used, but the focus was on the steady states, rather than the transient dynamics.

For systems which can display oscillatory dynamics during decision making, we find this causes a temporal increase in the time taken for cells to reach their final state.

From our numerical studies throughout Chapter 3, we showed that the relationship between Time to Switch and $\chi$ was altered when oscillatory dynamics were present. Time to Switch is a continuously decreasing function of $\chi$ in the absence of oscillations, but when they are present, Time to Switch begins to increase with $\chi$.

This observed temporal increase is due to the existence of an attractive periodic orbit in the Surface of Equivalence, which becomes more stable to perturbations as $\chi$ increases.

This supports work in current literature [50,51,52], in which the presence of oscillations causes a significant increase in the time take for the system to reach a final pattern.

By using a numerical approach from Floquet theory, we have additionally been able to find an approximate estimation for the patterning rate when there are oscillatory dynamics. We will continue to explore this, with the aim of providing an accurate means of determining Time to Switch or patterning rate, and a simple application of Floquet analysis.

We have found that cellular dynamics are affected by the geometry of the population.

By investigating systems on different geometries, governed by the same differential equations, we find that the dynamics can be dependent on both geometry and the number of components in a cell.

For all systems capable of producing a period-2 pattern, the conditions for when switching is possible are always the same, but when increasing the complexity of the geometry - determined by the number of direct neighbours each cell has - the mean Time to Switch in the population increases, in addition to the range of switching times.

For populations on a hexagonal array, there is a lower proportion of Primary Fate cells in the final pattern cell types, and as we show in Section 2.3.1, when the proportion of PF cells decreases, a greater feedback strength is required for switching. The mean Time to Switch is further increased, and due to the increased complexity from having six

neighbours, the range of switching times also increases.

This supports findings in [48, 91], who both determine a greater feedback strength is required for switching, and patterning happens at a much slower rate.

A novel result from linear stability analysis is that for cells on a hexagonal lattice, provided there are enough components per cell, or a large enough time delay, there exists some parameter space in which stable, global, in-phase oscillations can occur before the conditions for switching are met.

We have continued to explore this behaviour. We show in the discussion of Chapter 2 that if the proportion of Primary Fate cells is further decreased due to an irregular lattice, for example, we expect an even greater required feedback strength before switching can occur, and a larger parameter space for the existence of stable oscillations. We want to determine the accuracy of this analysis, as it could provide a means of finding the pattern-forming potential for a system displaying little to no periodicity in the final pattern of cell types.

In a proliferating population of cells governed by lateral inhibition, there is a distinct effect on pattern formation and cell differentiation when we alter the rate of proliferation. When proliferation happens faster than cell-fate determination, formation of differentiated cells is delayed, due to interrupted signalling, and a coherent pattern takes significantly longer to form.

Alternatively, if pattern formation is faster than the rate of proliferation, differentiated cells are able to form quickly, and spatial pattern formation is more of a gradual process. If differentiated cells also leave the tissue however, when the rate of differentiation is greater than proliferation this can cause too many cells to leave the tissue early on, depleting the population.

These results fit nicely with current literature, where it has been shown that varying the length of the cell cycle will cause a change to the balance of proliferative and differentiated cells. It has been shown experimentally [62, 65], and mathematically in [83], who find that if the cell cycle is lengthened too much, this causes too many cells to differentiate prematurely, disrupting successful development.

In terms of future research, we wish to further explore models for lateral inhibition, but increase their complexity. As we have seen, it only takes one extra component in a cell to change the potential temporal dynamics of the system, and from preliminary investigation, by including intracellular feedback loops, far more exciting dynamics are possible.

By using this simple models as a basis, we will explore how the behaviours are affected when additional functions are included in regulation. What happens if components can self-regulate? How do intracellular dynamics and intercellular signalling interact?

We also plan to continue research on multi-level modelling. This study has highlighted

the importance of modelling across different biological levels, and although it is quite straightforward in comparison to other more powerful models, it has indicated that behaviours observed in a static environment may not translate when other processes are at play.

Thank you for reading.

# Chapter 6

# References


1. Alberts, Bruce et al. Molecular Biology Of The Cell. New York: Garland Science, 2002.

2. Cooper, Geoffrey M and Robert E Hausman. The Cell. Washington, D.C.: ASM Press, 2007.

3. Stelling, Jrg et al. "Robustness Of Cellular Functions". Cell 118.6 (2004): 675-685.

4. Balzsi, Gbor, Alexander van Oudenaarden, and James J. Collins. "Cellular Decision Making And Biological Noise: From Microbes To Mammals". Cell 144.6 (2011): 910-925.

5. MacLean, A. L., P. D. W. Kirk, and M. P. H. Stumpf. "Cellular Population Dynamics Control The Robustness Of The Stem Cell Niche". Biology Open 4.11 (2015): 1420-1426.

6. Pontarotti, Pierre. Evolutionary Biology - Concepts, Molecular And Morphological Evolution. Berlin, Heidelberg: Springer-Verlag Berlin Heidelberg, 2010.

7. Evans, Nicholas D. et al. "Epithelial Mechanobiology, Skin Wound Healing, And The Stem Cell Niche". Journal of the Mechanical Behavior of Biomedical Materials 28 (2013): 397-409.

8. de Jong, Hidde. "Modeling And Simulation Of Genetic Regulatory Systems: A Literature Review". Journal of Computational Biology 9.1 (2002): 67-103.

9. Mitrophanov, Alexander, Y., Groisman, E. "Positive Feedback In Cellular Control Systems". Bioessays 30.6 (2008): 542-555.

10. Tyson, John J, Katherine C Chen, Bela Novak. "Sniffers, Buzzers, Toggles And Blinkers: Dynamics Of Regulatory And Signaling Pathways In The Cell". Current Opinion in Cell Biology 15.2 (2003): 221-231.

11. Tyson, J. J et al. “Biological Switches And Clocks”. Journal of The Royal Society, Interface 5 (2008): S1-S8.

12. Mayr, Otto. “The Origins Of Feedback Control”. Sci Am 223.4 (1970): 110-118.

13. Hartman, B. H., T. A. Reh, and O. Bermingham-McDonogh. “Notch Signaling Specifies Prosensory Domains Via Lateral Induction In The Developing Mammalian Inner Ear”. Proceedings of the National Academy of Sciences 107.36 (2010): 15792-15797.

14. Saravanamuthu, Senthil S., Chun Y. Gao, and Peggy S. Zelenka. “Notch Signaling Is Required For Lateral Induction Of Jagged1 During FGF-Induced Lens Fiber Differentiation”. Developmental Biology 332.1 (2009): 166-176.

15. Siekmann, Arndt F. and Nathan D. Lawson. “Notch Signalling And The Regulation Of Angiogenesis”. Cell Adhesion & Migration 1.2 (2007): 104-105.

16. Sainson, Richard C. A. and Adrian L. Harris. “Regulation Of Angiogenesis By Homotypic And Heterotypic Notch Signalling In Endothelial Cells And Pericytes: From Basic Research To Potential Therapies”. Angiogenesis 11.1 (2008): 41-51.

17. Urabn, Noelia and Fransois Guillemot. “Neurogenesis In The Embryonic And Adult Brain: Same Regulators, Different Roles”. Frontiers in Cellular Neuroscience 8 (2014): 396.

18. Imayoshi, I. et al. “Essential Roles Of Notch Signaling In Maintenance Of Neural Stem Cells In Developing And Adult Brains”. Journal of Neuroscience 30.9 (2010): 3489-3498.

19. Crosnier, C. “Delta-Notch Signalling Controls Commitment To A Secretory Fate In The Zebrafish Intestine”. Development 132.5 (2005): 1093-1104.

20. Savage, Natasha Saint and Wolfgang Schmidt. “From Priming To Plasticity: The Changing Fate Of Rhizodermic Cells”. Bioessays 30.1 (2007): 75-81.

21. Freeman, M. “Feedback control of intercellular signalling in development”. Nature 408 (2000): 313-319.

22. Trotta, Laura, Eric Bullinger, and Rodolphe Sepulchre. “Global Analysis Of Dynamical Decision-Making Models Through Local Computation Around The Hidden Saddle”. PLoS ONE 7.3 (2012): e33110.

23. Owen, Markus R. and Jonathan A. Sherratt. “Mathematical Modelling Of Juxtacrine Cell Signalling”. Mathematical Biosciences 153.2 (1998): 125-150.

24. N. Monk, J. Sheratt, M. Owen. "Spatiotemporal patterning in models of juxtacrine intercellular signalling with feedback." P. Maini, H. Othmer (Eds.), Mathematical Models for Biological Pattern Formation, Springer, Berlin (2000), 65-192

25. Li, Weihan *et al.* "Switching Between Oscillations And Homeostasis In Competing Negative And Positive Feedback Motifs". Journal of Theoretical Biology 307 (2012): 205-210.

26. Harris, Sandra L and Arnold J Levine. "The P53 Pathway: Positive And Negative Feedback Loops". Oncogene 24.17 (2005): 2899-2908.

27. Goodwin, Brian C. "Oscillatory Behavior In Enzymatic Control Processes". Advances in Enzyme Regulation 3 (1965): 425-437.

28. Griffith, J.S. "Mathematics Of Cellular Control Processes I. Negative Feedback To One Gene". Journal of Theoretical Biology 20.2 (1968): 202-208.

29. Gonze, Didier and Wassim Abou-Jaoud. "The Goodwin Model: Behind The Hill Function". PLoS ONE 8.8 (2013): e69573.

30. Elowitz M, Leibler S: "A synthetic oscillatory network of transcriptional regulators". J Biol Chem 274 (1999): 6074-6079.

31. Andersson, E. R., R. Sandberg, and U. Lendahl. "Notch Signaling: Simplicity In Design, Versatility In Function". Development 138.17 (2011): 3593-3612.

32. Latasa, Maria Jesus, Elsa Cisneros, and Jose Maria Frade. "Cell Cycle Control Of Notch Signaling And The Functional Regionalization Of The Neuroepithelium During Vertebrate Neurogenesis". Int. J. Dev. Biol. 53.7 (2009): 895-908.

33. Gazave, Eve *et al.* "Origin And Evolution Of The Notch Signalling Pathway: An Overview From Eukaryotic Genomes". BMC Evol Biol 9.1 (2009): 249.

34. Lewis, J., Hanisch, A., Holder, M. "Notch Signaling, The Segmentation Clock, And The Patterning Of Vertebrate Somites". Journal of Biology 8.4 (2009): 44.

35. Oates, A. C., L. G. Morelli, and S. Ares. "Patterning Embryos With Oscillations: Structure, Function And Dynamics Of The Vertebrate Segmentation Clock". Development 139.4 (2012): 625-639.

36. Shimojo, Hiromi, Toshiyuki Ohtsuka, and Ryoichiro Kageyama. "Oscillations In Notch Signaling Regulate Maintenance Of Neural Progenitors". Neuron 58.1 (2008): 52-64.

37. Okamura, Y. and Y. Saga. "Notch Signaling Is Required For The Maintenance Of Enteric Neural Crest Progenitors". Development 135.21 (2008): 3555-3565.

38. Beatus, Paul and Urban Lendahl. "Notch And Neurogenesis". J. Neurosci. Res. 54.2 (1998): 125-136.

39. "Notch Activity Key To The Link Between Angiogenesis And Osteogensis". IBMS BoneKey 11 (2014): 591.

40. Guruharsha, K. G., Mark W. Kankel, and Spyros Artavanis-Tsakonas. "The Notch Signalling System: Recent Insights Into The Complexity Of A Conserved Pathway". Nat Rev Genet 13.9 (2012): 654-666.

41. Kopan, Raphael and Ma. Xenia G. Ilagan. "The Canonical Notch Signaling Pathway: Unfolding The Activation Mechanism". Cell 137.2 (2009): 216-233.

42. D'Souza B, Meloty-Kapella L, Weinmaster G. "Canonical and non-canonical Notch ligands". Curr Top Dev Biol 92 (2010): 73-129.

43. D'Souza, B., Meloty-Kapella, L., Weinmaster, G. "Canonical and non-canonical Notch ligands". Curr Top Dev Biol 92 (2010): 73-129.

44. Hartman, B. H., T. A. Reh, and O. Bermingham-McDonogh. "Notch Signaling Specifies Prosensory Domains Via Lateral Induction In The Developing Mammalian Inner Ear". Proceedings of the National Academy of Sciences 107.36 (2010): 15792-15797.

45. Tanimoto, M. *et al.* "Origin Of Inner Ear Hair Cells: Morphological And Functional Differentiation From Ciliary Cells Into Hair Cells In Zebrafish Inner Ear". Journal of Neuroscience 31.10 (2011): 3784-3794.

46. Wahi, Kanu, Matthew S. Bochter, and Susan E. Cole. "The Many Roles Of Notch Signaling During Vertebrate Somitogenesis". Seminars in Cell & Developmental Biology 49 (2016): 68-75.

47. Miguel Maroto, Robert A. Bone, J. Kim Dale. "Somitogenesis". Development 139 (2012): 2453-2456.

48. Collier, Joanne R. *et al.* "Pattern Formation By Lateral Inhibition With Feedback: A Mathematical Model Of Delta-Notch Intercellular Signalling". Journal of Theoretical Biology 183.4 (1996): 429-446.

49. Collier J. (1997) "Spatial and Propagating Patterns in Emryology". PhD Thesis. University of Oxford.

50. Veflingstad, Siren R., Erik Plahte, and Nicholas A.M. Monk. "Effect Of Time Delay On Pattern Formation: Competition Between Homogenisation And Patterning". Physica D: Nonlinear Phenomena 207.3-4 (2005): 254-271.

51. Momiji, Hiroshi and Nicholas A. M. Monk. “Oscillatory Notch-Pathway Activity In A Delay Model Of Neuronal Differentiation”. Physical Review E 80.2 (2009).

52. Glass D.S., Jin X.,Riedel-Kruse I.H. “Signaling delays preclude defects in lateral inhibition patterning”. Phys. Rev. Lett. 116, 128102 (2016).

53. Owen M. “Lateral induction by juxtacrine signaling is a new mechanism for pattern formation”. Dev Biol 217 (2000): 54-61.

54. Cohen, M., B. Baum, and M. Miodownik. “The Importance Of Structured Noise In The Generation Of Self-Organizing Tissue Patterns Through Contact-Mediated Cell-Cell Signalling”. Journal of The Royal Society Interface 8.59 (2010): 787-798.

55. Meir, Eli *et al.* “Robustness, Flexibility, And The Role Of Lateral Inhibition In The Neurogenic Network”. Current Biology 12.10 (2002): 778-786.

56. Webb S., Owen M. “Intra-membrane ligand diffusion and cell shape modulate juxtacrine patterning”. J Theor Biol 230 (2004): 99-117.

57. Sprinzak, David *et al.* “Cis-Interactions Between Notch And Delta Generate Mutually Exclusive Signalling States”. Nature 465.7294 (2010): 86-90.

58. Formosa-Jordan, Pau and Marta Ibaes. “Competition In Notch Signaling With Cis Enriches Cell Fate Decisions”. PLoS ONE 9.4 (2014): e95744.

59. Erneux, T. “Applied Delay Differential Equations”. New York, NY: Springer-Verlag, 2009.

60. Strogatz, Steven H. Nonlinear Dynamics And Chaos. Cambridge, MA: Westview Press, 2000.

61. Seirin Lee, Sungrim. “Lateral Inhibition-Induced Pattern Formation Controlled By The Size And Geometry Of The Cell”. Journal of Theoretical Biology 404 (2016): 51-65.

62. Calegari, F. “An Inhibition Of Cyclin-Dependent Kinases That Lengthens, But Does Not Arrest, Neuroepithelial Cell Cycle Induces Premature Neurogenesis”. Journal of Cell Science 116.24 (2003): 4947-4955.

63. Strelkowa, N. and M. Barahona. “Switchable Genetic Oscillator Operating In Quasi-Stable Mode”. Journal of The Royal Society Interface 7.48 (2010): 1071-1082.

64. Julian, Lisa M. *et al.* “Formula G1: Cell Cycle In The Driver’s Seat Of Stem Cell Fate Determination”. BioEssays 38.4 (2016): 325-332.

65. Lange, Christian and Federico Calegari. “Cdks And Cyclins Link G 1 Length And Differentiation Of Embryonic, Neural And Hematopoietic Stem Cells”. Cell Cycle 9.10 (2010): 1893-1900.

66. Mallet-Paret J., Smith H. “The Poincare -Bendixson Theorem for Monotone Cyclic Feedback Systems”. Journal of Dynamics and Differential Equations 2.4 (1990): 367-421.

67. Mallet-Paret J., Sell G. “The Poincare-Bendixson Theorem for Monotone Cyclic Feedback Systems with Delay”. Journal of Differential Equations 125 (1996): 441-489.

68. Hirata, H. *et al.* “Oscillatory expression of the bHLH factor Hes1 regulated by a negative feedback loop”. Science 298 (2002): 840-843.

69. Monk, N. “Oscillatory Expression of Hes1, p53, and NF-$\kappa$B Driven by Transcriptional Time Delays”. Current Biology 13.16 (2003): 1409-1413.

70. Lewis, J. “Autoinhibition with Transcriptional Delay: A Simple Mechanism for the Zebrafish Somitogenesis Oscillator”. Current Biology 13.16 (2003): 1398-1408.

71. Cvitanovi, P., Artuso, R.,Mainieri, R., Tanner, G., Vattay, G. “Chaos: Classical and Quantum”. Niels Bohr Institute, Copenhagen, 2005, http://ChaosBook.org.

72. Simmendinger, C., Wunderlin, A., Pelster, A. “Analytical approach for the Floquet theory of delay differential equations”. Physical Review E 59.5 (1999): 5344-5353.

73. Luzyanina, T., Engelborghs, K. “Computing Floquet Multipliers for Functional Differential Equations”. Int. J. Bifurcation Chaos 12.12 (2002): 2977-2989.

74. Fletcher, A.G., Osborne, J.M., Gavaghan, D.J., *et al.* “Implementing vertex dynamics models of cell populations in biology within a consistent computational framework”. Prog. Biophys. Mol. Biol., 113 (2013): 299-326.

75. Cohen, M., Georgiou, M., Stevenson, N.L., Miodownik, M., Baum, B. “Dynamic Filopodia Transmit Intermittent Delta-Notch Signaling to Drive Pattern Refinement during Lateral Inhibition”. Developmental Cell 19.1 (2010): 78 - 89.

76. Frankfort, B.J., Mardon, G. “R8 development in the drosophila eye: a paradigm for neural selection and differentiation”. Development 129 (2002): 1295-1306.

77. Crowe, R., Henrique, D., Ish-Horowicz, D., Niswander, L. “A new role for notch and delta in cell fate decisions: patterning the feather array”. Development 125 (1998): 767-775.

78. Neves, J., Abell, G., Petrovic, J., Giraldez, F. “Patterning and cell fate in the inner ear: a case for notch in the chicken embryo”. Dev Growth Differ 55(1) (2012): 96-112.

79. Jiang, Y. J., Aerne, B. L., Smithers, L., Haddon, C., Ish-Horowicz D., Lewis, J. “Notch signalling and the synchronization of the somite segmentation clock”. Nature 408 (2000): 475-479.

80. Riedel-Kruse, I. H., Muller, C., Oates, A. C. “Synchrony dynamics during initiation, failure, and rescue of the segmentation clock”. Science 317 (2007): 1911-1915.

81. Kageyama, R., Ohtsuka, T., Kobayashi, T. “Roles of Hes genes in neural development”. Develop. Growth Differ. 50 (2008): S97-S103.

82. Formosa-Jordan, P., Sprinzak, D. “Modeling notch signaling: A practical tutorial”. Methods in Molecular Biology 1187 (2014): 285-310.

83. Hunter, G.L., Hadjivasiliou, Z., Bonin, H., He, L., Perrimon, N., Charras, G., Baum, B. “Coordinated control of Notch/Delta signalling and cell cycle progression drives lateral inhibition-mediated tissue patterning”. Development 143 (2016): 2305-2310.

84. Osborne, J., Fletcher, A., Pitt-Francis, J., Maini, P., Gavaghan, D. “Comparing individual-based approaches to modelling the self-organization of multicellular tissues”. Plos Comp. Bio. (2017): 10.1371.

85. Hester, SD., Belmonte, JM., Gens, JS., Clendenon, SG., Glazier, JA. “A Multi-cell, Multi-scale Model of Vertebrate Segmentation and Somite Formation”. PLoS Comput Biol. (2011): 7:e1002155.

86. Pin, C., Watson, A.J., Carding, S.R. “Modelling the Spatio-Temporal Cell Dynamics Reveals Novel Insights on Cell Differentiation and Proliferation in the Small Intestinal Crypt”. PLoS One, 7 (2012): p. e37115.

87. Fletcher, A., Murray, P., Maini, P. “Multiscale modelling of intestinal crypt organization and carcinogenesis”. Math. Mod. Meth. Appl. Sci. 25 (2015):2563-2585.

88. Sancho, R., Cremona, CA., Behrens, A. “Stem cell and progenitor fate in the mammalian intestine: notch and lateral inhibition in homeostasis and disease”. EMBO Rep. (2015): 16:571-81.

89. Walker, DC., Georgopoulos, N., Southgate, J. “From pathway to population - a multiscale model of juxtacrine EGFR-MAPK signalling”. BMC Syst Biol. Vol.2, (2008): http:/www.biomedcentral.com1752-0509/2/102.

90. Bellman, R., Cooke, K.L. “Differential-Difference Equations”. Academic Press, London, 1963.

91. Webb, S., Owen, M. “Oscillations and patterns in spatially discrete models for developmental intercellular signalling”. Journal of Math. Bio. 48.4, (2004): 444-476.

92. Fletcher, AG., Osterfield, M., Baker, RE., Shvartsman, SY. “Vertex Models of Epithelial Morphogenesis”. Biophysical Journal 106.11 (2014):2291-2304.

93. Kursawe, J., Baker, R., Fletcher, A. “Impact of implementation choices on quantitative predictions of cell-based computational models”. bioRxiv 092924; doi: https://doi.org/10.1101/092924.

94. Matsuda, M., Koga, M., Woltjen, K., Nishida, E., Ebisuya, M. “Synthetic lateral inhibition governs cell-type bifurcation with robust ratios”. Nature Communications, 6, 6195, 2015.

# Appendices

# Appendix A

This appendix is to provide evidence to support our claim in Section 1.6 that for a given delay differential equation, if we use a range of $\Phi(t)$ to describe the initial conditions of the system in the range $[-\tau, 0]$, then $X(t) \to ke^{\lambda t}$ for large $t$.

Consider the equation

$$\dot{X} = -X + \gamma X(t-1). \tag{A.0.1}$$

Following the steps of Section 1.6, the characteristic equation for A.0.1 is given by

$$\lambda + 1 = \gamma e^{-\lambda}. \tag{A.0.2}$$

If $\gamma > 1$, there exists a solution $\lambda \in \mathbb{R}^+$, and if $\gamma < 1$, then $\mathrm{Re}(\lambda) < 0$ for all solutions of A.0.2.

In our simulations, we choose $\gamma = 2$, and $\gamma = 0.5$, and find that, when numerically solving the characteristic equation (A.0.2) we find the corresponding $\lambda$ solutions to be $\lambda = 0.3748$ and $\lambda = -0.3149$. When plotting $\log(X)(t)$ for a range of $\Phi(t)$, we find that $X(t) \to ke^{\lambda t}$ for large $t$ for all choices of $\Phi(t)$. This is illustrated in Figure A.1.

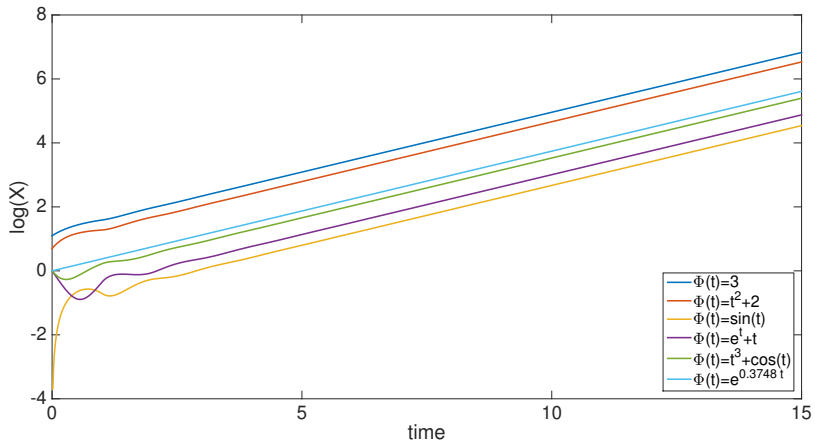


(a)

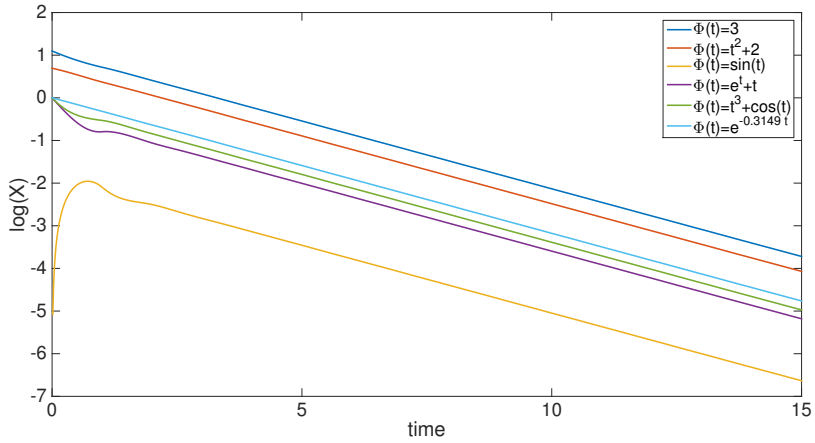


(b)

Figure A.1: $\log(X)(t)$ with various $\Phi(t)$. (a) $\gamma = 2$, and $\lambda$, the gradient of $\log(X)(t)$, is positive, and holds for all $\Phi(t)$. (b) $\gamma = 0.5$, and $\lambda$, the gradient of $\log(X)(t)$, is negative, and holds for all $\Phi(t)$.